DESIGN CONSTRAINTS FOR GAS-LIQUID CATALYTIC MICROREACTORS

A THESIS SUBMITTED TO
THE GRADUATE SCHOOL OF NATURAL AND APPLIED SCIENCES
OF
MIDDLE EAST TECHNICAL UNIVERSITY

BY

NECİP BERKER ÜNER

IN PARTIAL FULFILLMENT OF THE REQUIREMENTS
FOR
THE DEGREE OF MASTER OF SCIENCE
IN
CHEMICAL ENGINEERING

AUGUST 2014

Approval of the thesis:

DESIGN CONSTRAINTS FOR GAS-LIQUID CATALYTIC MICROREACTORS

submitted by **NECİP BERKER ÜNER** in partial fulfillment of the requirements for the degree of **Master of Science in Chemical Engineering Department, Middle East Technical University** by,

Prof. Dr. Canan Özgen _____
Dean, Graduate School of **Natural and Applied Sciences**

Prof. Dr. Halil Kalıpçılar _____
Head of Department, **Chemical Engineering**

Prof. Dr. Deniz Üner _____
Supervisor, **Chemical Engineering Dept., METU**

Assist. Prof. Dr. Ertuğrul Erkoç _____
Co-supervisor, **Chemical Eng. Dept., Bursa Tech. Uni.**

Examining Committee Members:

Assist. Prof. Dr. Erhan Bat _____
Chemical Engineering Dept., METU

Prof. Dr. Deniz Üner _____
Chemical Engineering Dept., METU

Assist. Prof. Dr. Ertuğrul Erkoç _____
Chemical Engineering Dept., Bursa Technical University

Prof. Dr. Erdoğan Alper _____
Chemical Engineering Dept., Hacettepe University

Assoc. Prof. Dr. Almıla Güvenç Yazıcıoğlu _____
Mechanical Engineering Dept., METU

Date: 25.08.2014

I hereby declare that all information in this document has been obtained and presented in accordance with academic rules and ethical conduct. I also declare that, as required by these rules and conduct, I have fully cited and referenced all material and results that are not original to this work.

Name, Last name: Necip Berker ÜNER

Signature :

ABSTRACT

DESIGN CONSTRAINTS FOR GAS-LIQUID CATALYTIC MICROREACTORS

ÜNER, Necip Berker

M. S. Department of Chemical Engineering

Supervisor: Prof. Dr. Deniz ÜNER

Co Supervisor: Assist. Prof. Dr. Ertuğrul ERKOÇ

August 2014, 220 pages

Microreactors are a promising class of chemical reactors, which can provide high conversion, selectivity, heat-mass transfer rates and safety in production. They can accommodate gas-liquid or gas-liquid-solid reactions very well. The aim of this study is to present some new mass transfer and kinetics oriented physical phenomena and operation strategies that can emerge in multiphase microreactors, which are usually overlooked in macroscale reactors.

The first example is demonstrated experimentally by absorbing NO into ferrous sulfate solutions with help of a novel contactor. It is observed that when the liquid layer is almost stagnant with respect to the gas flow, Marangoni convection currents occur upon gas absorption. These are dimmed by adding chemical reactants to the liquid, but then a surface poisoning effect may occur, which decreases uptake rates

significantly. In addition to this homogeneous reaction-diffusion example, the applicability of classical mass transfer theories to finite films is questioned and quantitative limitations are given for the use of penetration theory for gas-liquid mass transfer in thin films. The saturation-depletion limits for contact times are also provided. A general solution for diffusion into a flowing liquid film with n^{th} order reaction is presented, in order to demonstrate the effects of velocity field on mass transfer rates.

As a gas-liquid-solid example, low-temperature Fischer-Tropsch synthesis is investigated. Effectiveness factors for diffusion with negative order reaction are presented. Conceptual periodic operation of Fischer-Tropsch synthesis is discussed and a model for Taylor flow is generated. Analogous to the homogeneous reaction part, a general solution of mass transfer to a flowing liquid film with surface reaction is presented, whereby the reaction initiation times are deduced for any flow field in the film.

Keywords: gas-liquid mass transfer, microreactors, NO absorption, Fischer-Tropsch synthesis, periodic operation, Taylor flow, diffusion-reaction problems.

ÖZ

GAZ-SIVI KATALİTİK MİKROREAKTÖRLER İÇİN TASARIM KOŞULLARI

ÜNER, Necip Berker

Yüksek Lisans, Kimya Mühendisliği Bölümü

Tez Yöneticisi: Prof. Dr. Deniz ÜNER

Ortak Tez Yöneticisi: Assist. Prof. Dr. Ertuğrul ERKOÇ

Ağustos 2014, 220 sayfa

Mikroreaktörler yüksek çevrim, seçimlilik, ısı-kütle iletim hızları ve güvenlikleri nedeniyle gelecek vaad eden kimyasal reaktörler olarak görülmektedirler. Gaz-sıvı ya da gaz-sıvı-katı reaksiyonlarını oldukça başarılı bir şekilde gerçekleştirdikleri kanıtlanmıştır. Bu çalışmanın amacı makro boyutlardaki reaktörlerde ihmal edilen, fakat mikroreaktörlerde üzerinde düşünülmesi gerekilen kütle aktarımı ve reaksiyon kinetiği çerçevesinde bir takım yeni fiziksel olayları ve işletim stratejilerini sunmaktır.

Ilk örnek olarak, NO'nun demir sülfat çözeltilerine yeni bir temas ünitesi ile deneysel emilimi verilmiştir. Üzerinden akan gaza göre neredeyse durağan bir sıvıda gaz emilimi nedeniyle Marangoni konvektif akımları oluşabileceği gözlemlenmiştir. Emilim hızını arttırması beklentisiyle eklenen kimyasalların, yüzeyi

zehirleyebileceği ve aktarım hızlarını ciddi anlamda düşürebileceği gösterilmiştir. Bu homojen reaksiyon-difüzyon örneğine ek olarak, klasik gaz-sıvı kütle aktarımı kuramlarının sonlu sıvı filmlerinde geçerlilikleri tartışılmış ve penetrasyon kuramının kullanımı için bir takım sayısal sınırlar belirlenmiştir. İnce filmler için doyma ve tükenme sınırları da verilmiştir. Ayrıca akan sıvı filmlerine n'nci dereceden reaksiyonlu kütle aktarımı için genel bir çözüm sunulmuş ve film içindeki hız profillerinin kütle aktarımına nasıl etki edebileceği gösterilmiştir.

Sonrasında, bir gaz-sıvı-katı reaksiyon sistemi olarak Fischer-Tropsch sentezi incelenmiştir. Eksi mertebeden yüzey reaksiyonları için etkenlilik katsayıları sunulmuştur. Kavramsal olarak Fischer-Tropsch sentezinin çevrimsel işletimde yürütülmesi tartışılmış ve buna ithafen Taylor akış modeli uygun görülmüştür. Bu akışla ilgili olarak bir de matematiksel model oluşturulmuştur. Son olarak, homojen reaksiyonlarda olduğu gibi akan sıvı filmlerine kütle aktarımı ve akabinde herhangi bir yüzey reaksiyonu için genel bir çözüm sunularak reaksiyonun başlama zamanlarının film içerisindeki hız profiline bağlılığı gösterilmiştir.

Anahtar Kelimeler: gaz-sıvı kütle aktarımı, mikroreaktörler, NO emilimi, Fischer-Tropsch sentezi, çevrimsel işletim, difüzyon-reaksiyon problemleri.

though I'm offering

a rose to a goat

or vice versa

to all the things that we wait for

and to all the things that we calculate

and equate to something

but come up wrong in the end.

ACKNOWLEDGEMENTS

In the course of three years of this thesis, many people have provided generous support and guidance to me. First of all, I would like to present my gratitude to my supervisor and mentor Deniz Üner, for her never ending motivation, patience and unbounded tolerance. I am grateful for the times of intense discussions and all the knowledge she shared with me. Without her, not only this thesis, many of the things in my life would not have happened.

I would also to like to present my gratitude for my co-supervisor Ertuğrul Erkoç for introducing me the world of computational fluid dynamics and for all the guidance and criticism. I'm also obliged for one of the most beautiful months of my life I've spent in Dresden Technical University, which had been very enlightening.

I'm indebted to İsmail Tosun for presenting me the power of mathematics, and to Nevin Selçuk, for helping me to develop my code writing skills and for the experiences she shared with me. I feel obliged to Erdoğan Alper for discussions on mass transfer and for his support on the topic, and to İbrahim Bayar for his invaluable help on the NO_x analysis setup. The inspiring discussion made with Edward L. Cussler is also gratefully acknowledged. In addition, TÜBİTAK INTEN-C project for providing the computational resources and METU CC for software support are thankfully acknowledged.

I want to thank my dear friends and CACTUS research group members, Güvenç Oğulgönen, İbrahim Bayar, Atalay Çalışan, Nevzat Can Aksu, Mustafa Yasin Aslan and Cihan Ateş for all the times we shared; from experiments and courses, to kebaps and friendship, which form pretty much a life on their own. I also want to thank my office mates Burcu Gökbudak, Halime Gül Zerze and Berrak Erkmen for being great company; and to all C-Block residents of METU ChE as well.

I spent unforgettable times with my beloved friends Barış Çakmakçı, Emre Akın and Şermin Özlem Turhan when making music. Sometimes music ripped me off from thesis work, but it eventually sent me back to studying, with more enthusiasm than before. Güneş Kortel, Erinç Odabaş, Canberk Hacıbaloğlu, Gökçen Tek, İpek Kahraman, Sedat Anar, Ferhat Çaylı, Tayfun Şakalakoğlu, Çağrı Ulusoy, İlayda Başaran, Can Karacadağlı, Ercan Elidemir and Tunç Durmaz have all contributed to this thesis in indirect, subtle and musical ways.

With my house mate Hüseyincan Eryılmaz, we spent good times together. It is always good to have a life-long friend nearby.

Finally; my dad, my mom, my sister, my brother and my beautiful niece Zeynep; your existence is a force to move on. Still, I'm only able to say a mere thank you for the limitless love you give. I too love you with all my heart.

TABLE OF CONTENTS

LIST OF TABLES

TABLES

LIST OF FIGURES

FIGURES

LIST OF SYMBOLS

A_S	Cross section area (m^2)
b	Stoichiometric coefficient
b_S	Slip length (m)
C	Concentration (mol/m^3)
$\bar{C}$	Average concentration (mol/m^3)
C^*	Equilibrium interfacial concentration (mol/m^3)
C_b	Bulk concentration (mol/m^3)
C_i	Interfacial concentration (mol/m^3)
C_0	Initial concentration (mol/m^3)
D	Diffusivity (m^2/s)
E	Enhancement factor
E_a	Activation energy (J/mol)
E_i	Enhancement factor for an instantaneous reaction
g	Gravitational acceleration (m/s^2)
h	General convective heat or mass transfer coefficient (W/m^2K or m/s)
H	Henry's constant ($mol/m^3 \cdot Pa$)
H_c	Mean curvature (m^{-1})
k	Reaction rate constant (various dimensions)
k"	Surface reaction rate constant (various dimensions)
k_G	Gas phase mass transfer coefficient (m/s)
k_L	Liquid phase mass transfer coefficient (m/s)
$\bar{k}_L$	Average liquid phase mass transfer coefficient (m/s)
$\bar{k}'_L$	Average liquid phase mass transfer coefficient for physical absorption (m/s)
k_S	Interfacial resistance coefficient, linear (m/s)
K_G	Overall mass transfer coefficient base on the gas phase ($mol/m^2s \cdot Pa$)
K_S	Interfacial resistance coefficient, nonlinear (mol/m^2s)
L	Axial (Film, bubble, compartment) length (m)

L_c	Characteristic length (m)
M	Molecular weight (g/mol)
n	Reaction order
n	Normal vector
$\dot{n}$	Molar flow rate (mol/s)
n_a	Amounts absorbed (mol/m^2)
$\hat{n}_a$	Dimensionless amounts absorbed
N	Flux (mol/m^{2}s)
$\overline{N}$	Average Flux (mol/m^{2}s)
P	Partial pressure (Pa)
P^{∞}	Partial pressure in the bulk gas phase (Pa)
P_i	Partial pressure above the interface (Pa)
R	Radius (m)
R_g	Gas constant (J/mol·K)
s	Surface renewal rate (1/s)
t'	Clock time (s)
t	Exposure (or contact) time (s)
t_e	Exhaustion time (s)
t_d	Depletion time (s)
t_r	Time to reach the surface (s)
T	Temperature (K)
T_i	Interfacial temperature (K)
u	Dimensionless concentration, C/C^*
v	Velocity (m/s)
$\bar{v}$	Average velocity (m/s)
v_i	Interfacial velocity (m/s)
$\dot{V}$	Volumetric flow rate (m^3/s)
W	Width (m)
W_S	Width of free surface (m)

Greek symbols

α	Condensation coefficient
γ	Diffusivity ratio
δ	Film thickness (m)
δ_p	Penetration thickness (m)
$\hat{\delta}$	Dimensionless penetration thickness
η	Effectiveness factor
θ	Contact angle, °
λ	Mean free path (m) and $\Lambda/\sqrt{2(2n+1)}$
μ	Viscosity (Pa·s)
ν	Stoichiometric coefficient
ξ	Dimensionless diffusion length, x/L_c
$\boldsymbol{\pi}$	Stress tensor
ρ	Density (kg/m^3)
σ	Surface tension (N/m)
τ	Dimensionless time (same with Fo)
τ_i	Interfacial shear (N/m^2)
Φ	Age distribution function & Heaviside function
∇	Gradient operator
$\boldsymbol{\nabla_s}$	Surface gradient operator

Dimensionless groups

Bi	Biot number, hL_c/D
Bo	Bond number, $\Delta\rho g{L_c}^2/\sigma$
Ca	Capillary number, $\mu\bar{v}/\sigma$
Fr	Froude number, $v/\sqrt{gL_c}$
Ga	Galilei number, $\rho^2 g{L_c}^3/\mu^2$
Da	Damköhler number, $kC^{*n-1}t$
Da^{II}	Second Damköhler number, $k''L_c/D$

Fo	Fourier number (same with τ), Dt/L_c^2
Ka	Kapitza number, $\sigma(\rho/g\mu^4)^{0.33}$
Kn	Knudsen number, λ/L_c
M_H	Hatta modulus, $\pi k C_{B_0} t/4$, for PT
Re	Reynolds number, $L_c\bar{v}\rho/\mu$
Sh	Sherwood number, $k_L\delta/D$
We	Weber number, $\rho\bar{v}^2 L_c/\sigma$
β	Dimensionless time for interfacial saturation
β_T	Prater Modulus,
γ_e	Arrhenius number, E_a/RT_s
γ_S	Saturation-reaction number, $C^*\sqrt{kD}/K_S$
Λ	Thiele modulus, $\sqrt{k\delta^2 C^{*n-1}/D}$

Abbreviations

ADF	Age distribution function
AIBM	Approximate integral balance method
CAS	Computer algebra system
CFD	Computational fluid dynamics
CPI	Chemical process industries
FEM	Finite element method
FFMR	Falling film microreactor
FT	Film theory
FTS	Fischer-Tropsch synthesis
HAA	Hikita-Asai approximation
IMBE	Integral mass balance equation
LHHW	Langmuir-Hinshelwood-Hougen-Watson
NR	Newton-Raphson
MOL	Method of lines
ODE	Ordinary differential equation

PDE	Partial differential equation
PT	Penetration theory
RET	Random eddy theory
SRT	Statistical rate theory
SuRT	Surface renewal theory

CHAPTER 1

INTRODUCTION

Synthesis of commodities, many specialty chemicals and production of devices that implement physicochemical phenomena are continuously and increasingly demanded by the world. Such chemical operations should be run in well designed and well understood reactors that work in the most economical way. This principle constitutes the discipline of chemical reactor engineering (CRE), whose foundations lie on the fields of chemical kinetics, thermodynamics, fluid mechanics and heat-mass transfer. Although the basic principles of these fields are very well established, their interaction is usually quite complex, nonlinear and sometimes chaotic. Along with the difficulties in measuring physical properties accurately, the coupling of the fields mentioned above forms one of the main difficulties in chemical engineering, which creates problems in quantitative and qualitative analysis. This eventually hinders a priori design. A priori design is the dream of each chemical engineer, since its accomplishment would mean a leap in the development of chemical industry where at the same the design costs would be reduced significantly.

The difficult procedure of reactor engineering still leads to active research. The complicated forms of interacting physics bring many variables to control and measure, thus the types of reactors and relevant designs branch widely. So in a reactor design project, a change in any parameter may change the whole design.

1.1. Common Practices in the Industry

Reactors can be generally defined as hydrodynamic systems containing dispersed reactants. A chemical reactor may contain a gas, liquid, gas-liquid, liquid-liquid, gas-solid, liquid-solid or a gas-liquid-solid system. Yet more, now even new reactors containing an assisting plasma phase are being considered [1].

Gas-solid and gas-liquid-solid operations embrace very important processes like the Fischer-Tropsch synthesis (FTS), dimethyl ether synthesis (DME) and ammonia production. This fact actually shows the importance of the common solid phase, which usually means the science of catalysis. On the other hand, gas-liquid reactions also have significant importance. Besides synthesis, like the reaction of liquid water with nitrogen tetroxide to obtain nitric acid, there is a huge list of operations focused on reactive separation, like carbon dioxide capture in amine solutions or NO_x absorption in acidic liquors. In such processes, the gas and liquid phases may include some diluted reactants and a solvent (or a certain excess feed of a reactant), or they can be concentrated mixtures. Analysis and accomplishment of such processes form the heart of the chemical process industries (CPI).

Generally, CPI operates with very large reactors. Attaining required mixedness in terms of temperature levels (also in terms of concentration in some cases) becomes hard in large reactors. Temperature nonuniformities result in hot spots, which usually reduce selectivity and/or conversion. Another complexity is the amount and structure of dispersion. In multiphase systems like gas-liquid or gas-liquid-solid systems, chaotic multiphase flow patterns, sensitive even to the minor changes in reactor geometry are common. One may add other complications to this, like interfacial mass transfer, turbulence, radiative heat transfer for high temperature synthesis and complex surface reactions. The common practice in designing such complex phenomena is to scale-up from lab scale experiments, where the molecular-scale discoveries are made, through pilot scale and finally to industrial scale in a rapid processing, safe, economical and environmentally benign manner [2]. Although logical and systematic, this is an expensive methodology. The heuristics developed with help of prior design experiences is commonly employed for reactor design in CPI.

1.2. The Concept of Miniaturization in Chemical Reaction Engineering

It was the end of 90's that the miniaturization concept entered the world of CRE. The idea is due to Feynman and dates back to 1960 [3]. In his paper, Feynman had ideas of quickly dissipating the heat generated in a very small lubrication device. He claimed that the heat generated by friction and viscous dissipation would escape away very rapidly due to the small size of the device. In fact, it is this logic that builds the bridge between miniaturization and CRE. If the reactor is very small in both diameter and length, than the heat generated via reactions will be conducted very fast and mass diffusion occurs very rapidly when compared to reactor dimensions. This enables to use the well applied theory of diffusional transport and to eliminate hot spots.

With already developed tools of micro-manufacturing like silicon micromachining, flow channels were etched on polymer, silica or elastomeric plates in the late 90's, with polydimethylsiloxane (PDMS) becoming one of the most popular substrates. The result was lab-on-chip (LOC) devices [4], which are a combination of process units on a millimetric scale. This means a 1000 fold decrease in reactor size (see Figure 1). Besides the LOC devices, there were also the monoliths. Existing monolithic reactor technology of catalytic converters is already applied to commercial catalytic gas-solid reactions [5, 6]. The mm-sized channels gave birth to variations the μm scale. Fluid phenomena in such channels are called as microfluidics, and reactors in microfluidic domains are called as microreactors.

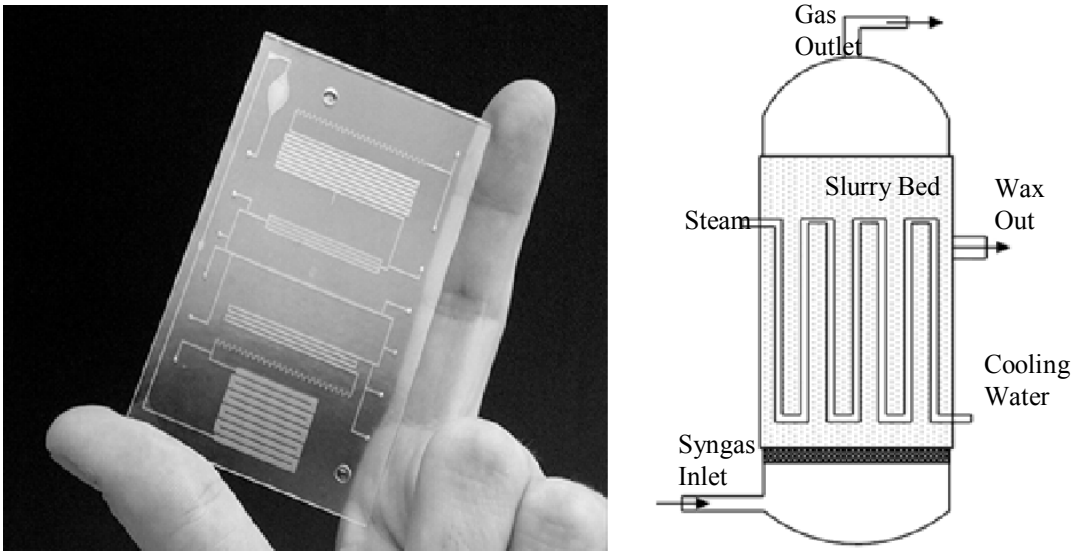

Figure 1. A lab on a chip device [7] and a schematic for the slurry bubble column.

1.3. Transport Processes in Small Scale

To exemplify, on may analyze mass transport in microfluidic flows where the classical continuum convection-diffusion equation is adequate for modelling purposes. For a single species in a dilute system with constant diffusivity, the equation can be given as:

$$\frac{\partial C}{\partial t'} + \mathbf{v} \cdot \nabla C = D\nabla^2 C + r(C) \tag{1}$$

C is concentration, t' is time,D is diffusivity[1], $\mathbf{v}$ is the velocity field vector and r is the reaction rate expression. Upon ignoring the convection and reaction terms, non-dimensionalization in 1-D with $\xi = x/L_c$ yields:

$$\frac{\partial C}{\partial \tau} = \frac{\partial^2 C}{\partial \xi^2} \tag{2}$$

where L_c is the characteristic length of the system and the new time variable τ is the dimensionless time, or Fourier number:

$$\tau = Fo = \frac{Dt'}{{L_c}^2} \tag{3}$$

[1] D~10^{-8}-10^{-10} m^2/s for soluble gases in liquids and ~10^{-5} m^2/s in a gaseous mixture.

Such a simplification in analysis is used to solve in many transient diffusion problems in stagnant media. The Fourier number represents the ratio of diffusion time to storage capacity. In classical reactor design, Fo is usually low, depicting large storage or short contact times. This is utilized by the assuming the geometry of analysis as semi-infinite. The time t' is the clock time, but in gas-liquid mass transfer analysis, the exposure time, t, can replace it.

A priori knowledge about the relative magnitude of convective and diffusive transport rates is also helpful in design and prediction. The comparison of transport rates are given by the Biot number:

$$\mathrm{Bi} = \frac{hL_c}{D} \tag{4}$$

where h is a general heat or mass convective transfer coefficient. For small Bi numbers, the mathematical problem can be reduced to a purely convective one. But for large Bi numbers, the diffusive problem must also be included in mathematical analysis.

1.4. Use of Microreactors in Synthesis and Devices

Microchannels and microfluidics are employed in many subjects of research, in terms of synthesis, analysis[2], sensors and energy production. Though the development of the latter two is mainly falls under the huge literature of MEMS research, it has been demonstrated that sensors can easily be implemented into microchemical processes for effective control [8]. Focusing on synthesis and analysis, the continuous microfluidic microreactor is already accepted by many chemists as the replacement for batch reactors for fast, hazardous and highly exothermic reactions [9, 10], for which microreactors can provide safe and efficient synthesis. In addition, microreactors are also implemented into industrial manufacturing of pharmaceuticals and fine chemicals [11, 12]. The small volumes needed for a micro-analysis system are also found very valuable by the bio-medical scientist due to their huge savings on chemicals and samples [13].

[2] Also called μTAS: micro total analysis systems.

As examples, microreactors are applied to liquid-liquid multiphase synthesis and separation[3] of carbamates where hazardous azides and isocyanates occur [14]. The liquid-liquid synthesis scenarios are enhanced with the accomplishment of the Aldol reaction and alkylations [15]. As gas-liquid-solid reactions, using washcoated microchannels operating in gas-liquid multiphase flow, extensive forms of hydrogenation reactions are accomplished by Kobayashi et al. [16]. Novel processes like hydrogen production for portable electronics and polymerase chain reactions have also been demonstrated [17].

In the perspective of the chemical engineer, the schemes for synthesis should be feasibly translated into mass production if needed. This brings out the need for understanding the gas-liquid multiphase flow patterns. For closed conduits, flow regime maps can be used, which can be found for many kinds of flow configurations. Examples for microfluidic flow patterns in closed conduits are given below in Figure 2. As a free surface multiphase contactor, the falling film microreactor (FFMR) of IMM[4] is given as an example in Figure 3.

The more ordered structure of slug, annular and film flow patterns are amenable to analysis and they have very large interfacial areas, around 25000 m^2/m^3, where in a typical bubble column it is around 200 m^2/m^3 [17]. Table 1 presents a detailed comparison between micro- and conventional reactors. The liquid side mass transfer coefficients, k_L, and interfacial areas per unit volume, a, are given and combined for the total mass transfer coefficient k_La.

[3] Running such operations in microreactors are now being called as micro-unit operations (MUO).
[4] Mainz Institute of Microtechnology, recently acquired by the Fraunhofer Society in 2014.

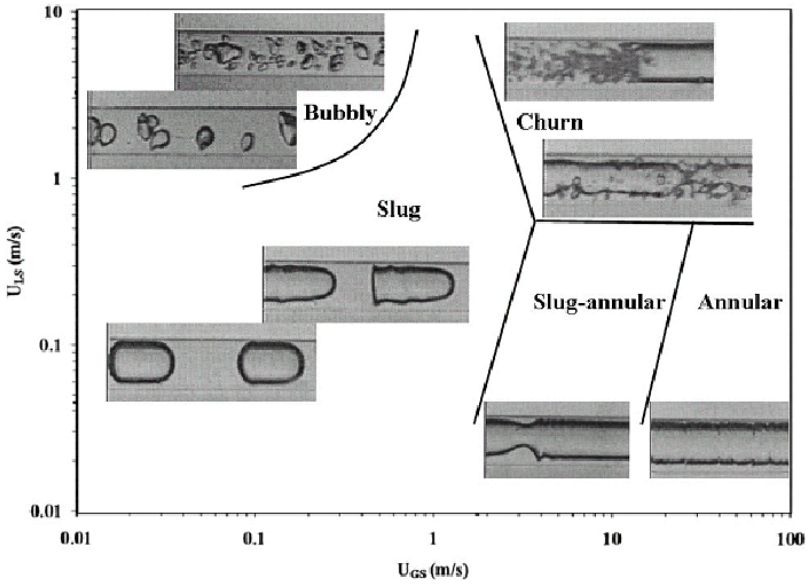

Figure 2. Flow patterns for air-water flow in a 1mm diameter circular tube based on superficial liquid and gas velocities. Taken from [18], used with permission of Wiley&Sons.

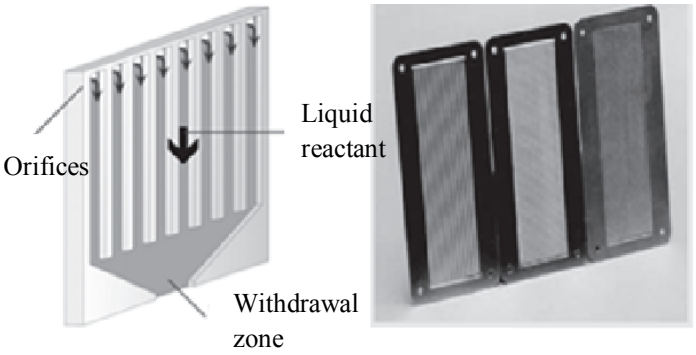

Figure 3. The IMM FFMR. Left: a schematic for flow in slots. Right: FFMR plates containing the slots for liquid flow, [19].

Table 1. Microreactors compared with conventional reactors in gas-liquid mass transfer performance (adapted from Yue et al. [20])

Type of Contactor	$k_L \cdot 10^5$ (m/s)	a (m^2/m^3)	$k_L a \cdot 10^3$ (s^{-1})
Bubble columns	10-40	50-600	0.5-24
Taylor-Couette Flow reactor	9-20	200-1200	3-21
Impinging jet absorbers	29-66	90-2050	2.5-122
Packed columns, concurrent	4-60	10-1700	0.04-102
Packed columns, counter-current	4-20	10-350	0.04-7
Spray column	12-19	75-170	1.5-2.2
Static mixers	100-450	100-1000	10-250
Stirred tank	0.3-80	100-2000	3-40
Tube reactors, horizontal & coiled	10-100	50-700	0.5-70
Tube reactors, vertical	20-50	100-2000	2-100
Gas-liquid microchannel	40-160	3400-9000	30-2100

From the table, it can be seen that the interfacial areas in microreactors may be 10 to 100 times greater than an average macroscale reactor. Such high interfacial areas lead to the occurrence of very thin fluid films. The distinctive feature of such films is the capillary effect; therefore the complications led by surface tension cannot be neglected. Buoyancy effects diminish, and gravity effects almost vanish in horizontal flows. In addition to Reynolds number Re, which gives the ratio of inertial forces to viscous forces, new dimensionless numbers, such as the Bond number[5] (Bo), the Weber number (We) and the capillary number (Ca) also take role in flow characterization. Although not related with surface tension effects, the definition Froude number (Fr) is also given below along with the abovementioned numbers, since it is important for free surface flows. It characterizes gravitational waves in shallow open channel flows.

$$\mathrm{Bo} = \frac{\Delta\rho g {L_c}^2}{\sigma} = \frac{\text{gravity forces}}{\text{surface forces}}, \qquad \mathrm{We} = \frac{\rho \bar{v}^2 L_c}{\sigma} = \frac{\text{inertial}}{\text{surface forces}}$$

$$\mathrm{Ca} = \frac{\mu \bar{v}}{\sigma} = \frac{\text{viscous forces}}{\text{surface forces}}, \qquad \mathrm{Fr} = \frac{v}{\sqrt{g \frac{A_S}{W_S}}} = \frac{\text{characteristic velocity}}{\text{gravitational wave velocity}} \tag{5}$$

[5] Also called as the Eötvos number, abbreviated as Eö.

In the definition of capillary number, μ and $\bar{v}$ (at the entrance) can be related to the gas phase or the liquid phase. Phase averaging is also possible. Note that for single phase flows, $\mathrm{Re} = \mathrm{We}/\mathrm{Ca}$. Some descriptive operating parameters and dimensionless numbers are given for the FFMR in Table 2. The Fourier number convention will be explained in Section 4.2 in detail.

Figure 4. Top: Bubbles visualized in Taylor flow. Bottom: Schematics for the circulations in liquid slugs. Taken from [21], used with permission of Wiley&Sons.

All the three ordered flow types noted before have many advantages, but slug flow is the most unique. For slug flow in microchannels, rigorous circulations may occur in both the bubble and the liquid slug. Such flows are called as Taylor flow, named after G.I. Taylor, due to his experiments for determining the film thickness between the lateral surface of the bubble and the wall [22]. Besides the expected circulations inside the bubbles, Taylor also predicted the possible existence and shape of the circulations in the liquid slug. Such circulations mean mixing and the existence of the thin liquid layer signals effective applications of gas-liquid-solid reactions for a washcoated channel, since diffusion through the film would be very fast. A photograph of Taylor flow is given in Figure 4, along with the numerical solution of the liquid circulation patterns

The FFMR seems to be the easiest to analyze and simulate, since very stable interfaces can be obtained. Annular flow has the highest interfacial area, and its near-turbulent gas core gives the best gas-phase mixing. This flow setup is actually the one used by Kobayashi and his co-workers for various hydrogenation reactions [16]. On the overall, since the behavior of the gas-liquid interface is known, this would

ease predicting the mass transfer rates a priori. Furthermore, by knowing the effects of diffusion well, more realistic kinetic studies may be performed for distinguishing the reaction mechanisms.

Table 2. Data for the FFMR. Calculations are performed for the narrowest reaction plate, $W \times d = 300 \times 100\mu m$, by taking $D = 3 \cdot 10^{-9} m^2/s$, $\delta = 50\mu m$ and by using the physical properties of air and water at 20°C.

FFMR Specifications [19]		**Derived Data**	**Formula**	**Magnitude**
Reaction channel length (L)	7.6 cm	Average velocity in a slot:	$\bar{v} = \dot{V}/nW\delta$	0.04 m/s
Reaction channel width (W) and depth (d)	300x100 µm 600x200 µm 1200x400 µm	Peclet number:	$Pe = \bar{v}L/D$	$1.1 \cdot 10^{6}$
Number of slots (n)	64, 32 ,16	Reynolds number:	$Re = \left(\frac{4\delta W}{2\delta + W}\right)\frac{\bar{v}\rho}{\mu}$	4.4
Flow rate ($\dot{V}$)	$1.4 \cdot 10^{-8}$ - $4.2 \cdot 10^{-7}$ m^3/s	Nusselt Film thickness	$\delta = \left(\frac{3\dot{V}\mu}{\rho g}\right)^{0.33}$	$2.4 \cdot 10^{-3}$ m
Residence time	0.8-20 s	Fourier number	$Fo = \frac{Dt}{\delta^2} = \frac{2DL}{3\bar{v}\delta^2}$	1.4
Measured liquid film thickness (δ)	25-100 µm	Capillary number	$Ca = \frac{\mu_L \bar{v}}{\sigma}$	$6.1 \cdot 10^{-4}$
Interfacial area	up to 20000 m^2/m^3	Weber number	$We = \frac{\rho \bar{v}^2 \delta}{\sigma}$	$1.3 \cdot 10^{-3}$
Operation temp. - pressure	180 to 300°C, 10 to 20 bar	Bond number	$Bo = \frac{\Delta \rho g \delta^2}{\sigma}$	$3.4 \cdot 10^{-4}$

The advantages of microreactors should be used effectively for large scale synthesis and analysis. Since microreactors are numbered up instead of scaling, their large scale production depends on the distributor design only. For example, the FFMR plates shown in Figure 3 can be stacked to increase production capacity. Such stacked devices are already made commercial [19]. The stability and the uniformity of multiphase flow patterns in such designs are deemed to be important in synthesis, consequently there is now a growing literature on multiphase flow regulation and

control [23]. However, multiphase flow systems are very complex to analyze analytically. This brings out the importance of computational fluid dynamics (CFD), where robust numerical schemes are used to solve the Navier-Stokes equations in both phases. In addition to these, a new understanding of the mass transport phenomena is necessary since the thin liquid films would get saturated or depleted in terms of reactants (or diffusants). Furthermore, the knowledge on temperature distribution and heat effects in stacked microreactors is not matured yet, but they seem to be important, even though the microreactors theoretically dissipate much better than commercial ones.

Considering gas-liquid reactions in microfluidic domains, CO_2 absorption in water and NaOH solutions is the most frequently studied reaction [24, 25, 26]. There are many important applications for gas-liquid reactions such as absorption of chlorine in alkaline solutions for the synthesis of hypochlorites, oxygen absorption to fermentation liquors in bio-engineering uses and absorption of hydrogen for removing the sulfur from petroleum fractions [27]. Process intensification via miniaturization in such gas-liquid systems and their feasibility is yet unknown. The same seems to be valid for gas-liquid-solid reactions or liquid-liquid contact operations also. As Kashid et al. assert [28], the information of the characterization of fluid-fluid mass transfer and reaction is not enough, although there have been a lot of demonstrations. In contrast, pure gas-solid reactions are an exception, since their applicability is already well studied in monolithic channels.

On the overall, microreactors seem to have a potential for significant mass transfer intensification and increased control over product selectivity and conversion. This is mainly due to the regular flow patterns that allow tuning the multiphase contact times. In addition, the removal of falsifications due to mass transfer limitations should allow a better basis for kinetic studies thus the hypotheses on reaction mechanisms may be tested on a more neutral ground. In terms of synthesis, there are doubts whether microreactors will be successful in general. Dudukovic [29] argues that after 2 decades of research, microreactors are not well implemented in chemical technology, although they are inexpensive to produce and they have significant power saving features [28].

1.5. Scope of the Thesis

In this thesis, gas-liquid-solid microreactor design in terms of mass transfer and chemical reaction is investigated in two levels of complexity. First, the gas-liquid mass transfer setup with homogeneous reaction is studied experimentally via NO_x absorption in ferrous sulfate solutions. Although the experimental setup is in centimeter scale, the aim is to present the behavior of gas absorption to almost stagnant fluids, which do not possess any mixing agents, like in many microfluidic contactors. Then, the applicability limits of penetration theory type models in microfluidic domains, with or without chemical reactions, were demonstrated mathematically. Quantitative limits are given for the critical contact times after which saturation or depletion of reactants arise in the liquid film. A general approximate analytical solution is provided to account for the effects of the velocity field on mass transfer and fast n^{th} order chemical reaction.

Secondly, the gas-liquid-solid system is treated with Fischer-Tropsch synthesis (FTS) as the test reaction. First, the gas-liquid mass transfer rates of reactants, H_2 and CO are investigated. Then, effectiveness factors for diffusion with general order power law type surface reaction are given to see the regions of multiplicities in reactions with a surface poisoning species. Since FTS is such a reaction, a conceptual periodic operation scheme is suggested to enhance the reaction rates, where reactants are periodically fed to the liquid film. The periodical behavior of the reaction-diffusion system is then investigated numerically, with employing chemically consistent kinetics that includes more complexity. A model of Taylor flow for FTS is suggested and formulated, in order to test the feasibility of employing such periodic microfluidic flow fields for increasing the reaction rates and tuning selectivities. Finally, similar to the work done for homogeneous reactions, a general treatment of gas absorption into flowing liquid films in presence of heterogeneous reactions is presented. The necessary contact times to initiate a heterogeneous reaction in a flowing liquid film are provided by demonstrating the effects of the velocity field in the film.

CHAPTER 2

LITERATURE REVIEW

In this section, first the theories of interfacial mass transport are summarized. The theories are actually models, which try to simplify complex combinations of diffusion, reaction and hydrodynamics. Then, the connections between the theories and current microfluidic contactors are given. Finally, supplementary material on diffusion and hydrodynamics is provided for aid in modeling mass transfer with chemical reaction, along with some information on Fischer-Tropsch synthesis.

2.1. Film Theory (FT)

The first systematic theoretical approach to interfacial mass transfer is due to Whitman in 1923 [30]. As a footnote in his classic paper, he added:

"Few subjects are creating more interest both theoretically and practically than gas absorption. For years entirely empirical in its applications and even yet preponderantly so, there have been developed several theories that seem to shed some light on its mechanism. This paper clears up some fog around the potential factor. It will contribute in helping to put this unit process on a substantial basis. One of slogans should perhaps be: "No more monstrosities as absorption towers!" No more of the old formula: "Let's make it a foot bigger in diameter and 5 feet higher just for good luck.""

It seems that the empirical approach has been embraced by chemical engineers as a primary chemical engineering design procedure after 50 years [31]. After 90 years, the empiricism has become the main material in standard mass transfer text books [32]. Although the complexity of standard unit operations on mass transfer prevented Whitman to reach his aim, his work has generated a large literature on mass transfer, and on its interplay with chemical reactions and hydrodynamics.

In his theory, Whitman simply considered turbulent gas and liquid phases contacted along a straight interface. He assumed that stagnant films exist at both sides of the interface. This is the main assumption of FT.

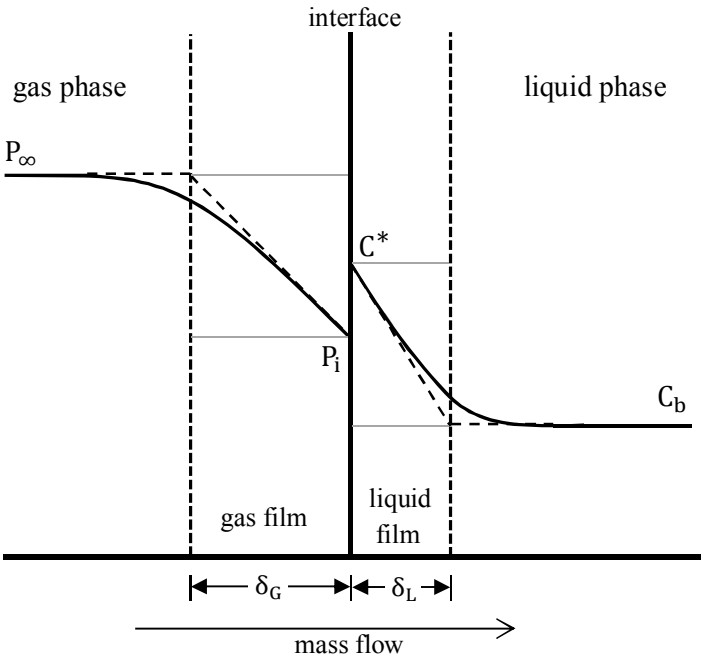

Figure 5. Schematic of FT.

Considering physical absorption, FT can be summarized with the following equation which describes the flux of a single species across the interface:

$$N = k_G(P^\infty - P_i) = k_L(C^* - C_b) \quad (6)$$

Here, k_G and k_L are the mass transfer coefficients for gas and liquid phases, respectively. P^∞ is the partial pressure of the diffusing species in the bulk gas phase, P_i is the vapor pressure of the gas dissolved in the liquid. C^* is the interfacial

concentration and C_b is the concentration in the bulk liquid. Both sides of Equation-(6) express a linearized driving force for mass transfer, as can be seen from Figure 5. When compared with Fick's law, mass transfer coefficients can be expressed as

$$k_G = \frac{D_G H}{\delta_G}, \qquad k_L = \frac{D_L}{\delta_L} \tag{7}$$

Subscripts define gas and liquid phases respectively. Thus, mass transfer rate is directly proportional to diffusivity. If the solution is dilute, as it usually would be for O_2 or CO_2 absorption in water, one may employ Henry's law;

$$C^* = HP_i \tag{8}$$

otherwise interfacial concentration would then be a nonlinear function of P_i and should be obtained from vapor-liquid equilibrium data. By using Equation-(8) in Equation-(6), one can eliminate P_i and C^*:

$$N = \frac{1}{\frac{1}{k_G} + \frac{1}{Hk_L}}(P^\infty - C_b/H) = K_G(P^\infty - C_b/H) \tag{9}$$

The denominator indicates the compound resistance, which is validated experimentally [33]. The result is the overall mass transfer coefficient, given by K_G. For very soluble gases, it is likely that mass transfer will be governed by gaseous diffusion only, as can be derived from the right hand side of Equation-(9) by keeping H as very large. Conversely, for low solubilities, the main resistance is in the liquid phase, hence one may use directly:

$$N = k_L(C^* - C_b) \tag{10}$$

Another useful methodology is to use the Sherwood number, which is related to the Biot number:

$$Sh = \frac{k_L \delta}{D} \tag{11}$$

After the development of FT, the theory is tested by blowing gas over stirred pots extensively and results are presented in the Absorption Symposium of ACS [34, 35, 36]. However, the scatter on the absorption rate data was quite wide due to the differences in contactor design, mixing and unstable interfaces. These arguments still apply to the use of FT in stirred contactors, where the fictitious film thickness δ is

merely a fitting parameter for each system and for each set of operating conditions. It is interesting to note that in the discussion section of Whitman's extension paper of FT [34], the possible large amounts of gas uptake rate by a bubble rising through a liquid is punctuated. This argument formed the experimental basis of penetration theory, and can be seen as a signal for the future use of Taylor bubbles in gas absorption.

FT is extended by Hatta by incorporating first order reactions [37] and substantially by van Krevelen and Hoftijzer [38], who considered second order reactions in an approximate, but valid manner. The theory for second order reactions will be given in Section 2.8.3.

In order to rationalize gas-liquid mass transfer and kinetics experimentation, Levenspiel and Godfrey [39] introduced the double-stirred contactor, even though primitive variants were used by Whitman and Davis before [40]. A wireframe sketch is given by Figure 6. The contactor may have baffles liquid and gas sections. The gas section operates in continuous mode and the liquid section can operate both in batch and continuous mode, depending on the rates of mass transfer. An important feature is the plates placed on the interface, which have a distinct number of holes of small size. This effectively stabilizes the interface for certain range of stirring speeds, in the same time gives an exactly known interfacial area. Levenspiel and Godfrey divided the case of mass transfer with second order bimolecular reaction into 8 regimes in terms of the magnitude of reaction velocity. They proposed an experimental plan for distinguishing kinetic regimes.

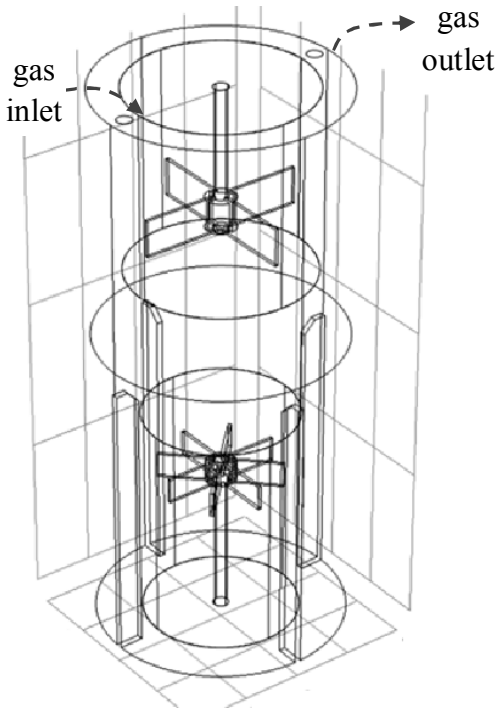

Figure 6. Sketch of a double stirred contactor. Liquid side is baffled and operated in batch mode. The interfacial plate is not shown.

Although their experimental rationale was systematic and logical, they found increasing mass transfer coefficients with increasing rotating speeds, even during the maximum rotation speeds that the contactor can allow without any interfacial rupture. This is an example of the difficulties of tuning mass transfer devices with a stirring apparatus. Later users provided small amounts of surfactants to the liquid phase to stabilize the interface during higher stirrer speeds [41, 42, 43]. However, it is known that surfactants effectively suppress mass transfer [44] by forming additional resistive layers on the interface. In liquid-liquid cases, 4-to-5 fold decrease is possible even if surfactant amounts on the order of 10 ppm are added [45].

Nevertheless, the device has been found to be useful for many regimes of mass transfer, especially where sole diffusion reigns. Tamir and Merchuk [46] adopted it for measuring diffusivities of evaporated liquids, by making use of the film-penetration theory, which is explained in Section 2.4.1. The contactor has been modified for the applications in liquid-liquid extraction. Al-Dahhan and Wicks [47] provides a survey of such contactors.

The kinetic regimes used by Levenspiel and Godfrey form the basis of the use of FT with chemical reactions. An extensive review is provided by Doraiswamy [48].

FT needs bulk phases and steady gradients in order to be effective in modelling mass transfer with chemical reaction. Bulk phases are absent in microfluidic contactors. In addition, a distinct (usually not negligible) transient period, in terms of the development of concentration boundary layers, is expected to exist in microreactors. This is not accounted in FT, since a steady model of diffusion is accounted. This may mean physically that the initial transient region is very short for FT or conversely, based on the definition of Fourier number, FT would work for long contact times. So, one may then say that FT is for large Fo only [49]. Hence, the use of film theory may only contribute to construction of new correlations for some special micro-contacting designs, where mass transfer coefficients should be fitted to a large range of parameter data of Hohydrodynamics and equipment geometry.

2.2. Penetration Theory (PT)

Unlike the film model, the penetration model stems from an unsteady physical scheme. Considering a stagnant liquid layer beside a gas phase, the simplification of Equation-(1) to Equation-(2) can be reprised[6]. The resulting unsteady diffusion equation with the following conditions define the penetration theory:

$$\frac{\partial C}{\partial t'} = D\frac{\partial^2 C}{\partial x^2} \qquad \begin{aligned} &\text{at } t' = 0,\ \ C = C_0 \\ &\text{at } x = 0,\ \ C = C^* \\ &\text{as } x \to \infty,\ \ C \to 0 \end{aligned} \qquad (12)$$

However, PT is much more general than the stagnant layer case and it can be applied to flowing films also. Consider diffusion into a broad vertically falling laminar film, where the film is steady. So for this case, one may write the differential equation for the transport of a dilute species by cancelling the unsteady and reaction terms in Equation-(1). If the flow is unidirectional, say it is along the z-axis, then the velocity profile comes from the classical analysis of Nusselt [50]. Eventually, the convection-diffusion equation becomes:

[6] The cancellation of the velocity terms can be interpreted as the product of perpendicular concentration gradient and parallel flow velocity, thus yielding zero.

$$v_i\left[1-\left(\frac{x}{\delta}\right)^2\right]\frac{\partial C}{\partial z}=D\frac{\partial^2 C}{\partial x^2} \qquad (13)$$

The equation above neglects axial dispersion, convective flux through the interface (moderate solubility), interfacial shear, waves, surface tension and wetting effects. v_i is the maximum velocity, or in general, the interfacial velocity. Nusselt's analysis is discussed in Section 460.

For short contact times, the solute will not penetrate much into the liquid; hence the local flow velocity will be around v_i. This simplifies Equation-(13) into:

$$v_i\frac{\partial C}{\partial z}=D\frac{\partial^2 C}{\partial x^2}$$

The above equation can be put in a more practical form by employing the transformation $t=z/v_i$, which is the exposure time. Thus, the model can be formulated with its boundary conditions as:

$$\frac{\partial C}{\partial t}=D\frac{\partial^2 C}{\partial x^2} \qquad \begin{array}{l} \text{at } t=0,\ C=C_0 \\ \text{at } x=0,\ C=C^* \\ \text{as } x\to\infty,\ C\to 0 \end{array} \qquad (15)$$

which is the same with Equation-(12). The model is steady in terms of clock time, but unsteady in terms of exposure time. The stagnant formulation is an unsteady model and 1-D in space. However, this exposure time-based formulation is 2D in space.

It assumes an initially loaded and infinitely large liquid phase. At the interface, the equilibrium is reached instantly upon contact. This model is suggested by Higbie [51] in 1935. The solution of the PDE is a classic and it provides valuable information:

$$\frac{C-C_0}{C^*-C_0}=\operatorname{erfc}\left(\frac{x}{2\sqrt{Dt}}\right) \qquad (16)$$

where erf(x) and erfc(x) are the error and complimentary error functions:

$$\operatorname{erfc}(x)=1-\operatorname{erf}(x)=\frac{2}{\sqrt{\pi}}\int_0^x e^{-u^2}du \qquad (17)$$

One may calculate the surface flux for the instantaneous rate of absorption:

$$N = -D\frac{\partial C}{\partial x}\Big|_{x=0} = (C^* - C_0)\sqrt{\frac{D}{\pi t}} \tag{18}$$

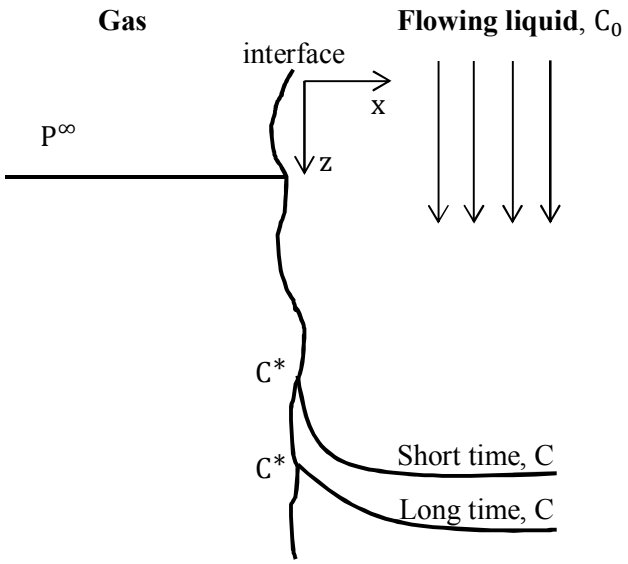

Figure 7: Schematic of PT [52].

Note that initially the absorption rate is infinite. The amount absorbed is expressed as:

$$n_a = \int_0^t N dt = 2(C^* - C_0)\sqrt{\frac{Dt}{\pi}} \tag{19}$$

The average rate absorption per unit area then can be calculated easily:

$$\bar{N} = \frac{n_a}{t_{exp}} = 2(C^* - C_0)\sqrt{\frac{D}{\pi t_{exp}}} = \bar{k}_L(C^* - C_0) \tag{20}$$

The above expression yields the average mass transfer coefficient: $\bar{k}_L = 2\sqrt{D/\pi t}$. Configurationally, it depends on $D^{0.5}$, in contrast to FT's linear first order dependence.

Since the model incorporates unsteady state diffusion, by looking at the magnitude Fo one can determine the effect of boundaries on mass transfer. One may arbitrarily define the position where $(C - C_0)/(C^* - C_0) = 0.005$ as the penetration thickness [53], $x = \delta_p$. Using Equation-(16):

$$\delta_p \cong 4\sqrt{Dt} \qquad (21)$$

Since the model assumes an infinite liquid layer, the penetration thickness should not surpass the actual thickness δ of the finite layer. Note that δ is also the characteristic length of the system. Thus Equation-(21) also brings a limitation in Fo:

$$Fo = \frac{Dt}{\delta^2} = \frac{DL}{\delta^2 v_i} < 0.06 \qquad (22)$$

Furthermore, taking the time derivative of δ_p gives the spreading velocity as $2\sqrt{D/t}$. This shows that the Fickian perspective gives an initially infinite spreading velocity. Therefore for $t > 0$, the concentration is non-zero everywhere on $0 < x < \infty$. Physically this is wrong and this erroneous behavior is overcome by hyperbolic diffusion formulations [54]. So when penetration fronts are important in diffusion problems, the Fickian theory may only provide approximate results. Still, in microdomains, using the Fickian formulation seems to be appropriate.

So consequently, PT is for low Fo (short contact times), in contrast to the film model. For non-quiescent fluids, the Fo limit is actually lower than as given in Equation-(22), since at sufficiently high Fo, the solute leaves the fluid layer that is flowing approximately with v_i. This will also decrease the uptake. The reason is that the fluid layers away from the surface usually flow slower than the interfacial elements, if there is a wall nearby. These layers sweep the diffusing molecules slower and slower as the solute approaches to the wall. Thus, in such a confined system with sufficiently long contact times, or high Fo, PT will over predict the uptake rates. Furthermore, when the diffusants reach the wall, the lack of a bulk phase and the finiteness of the liquid film will result in additional errors.

Higbie performed his experiments by absorbing CO_2, in form of long bubbles, to water in narrow pipes. He measured the film thickness and the length of the bubble for his calculations. Using his data at 25°C; $D = 1.93 \cdot 10^{-9}$ m^2/s, $\delta = 0.14$ mm and a maximum of $t = 0.1s$, one finds $Fo \cong 0.01$, which is below the limit given by Equation-(22).

Though usually such cases prevail in the industry, in the context of microreactors and microfluidics, the limit can be easily surpassed. The contacting devices may ensure very thin film thicknesses and relatively long residence times simultaneously. As an

example, one may use the operation data for the IMM FFMR [19]. By using the average exposure time $t = 2L/3\bar{v}$ [7] and film thickness data given as 16s and 50μm by Table 2 respectively, one finds $Fo = 0.9$ if diffusivity of CO_2 is kept as the same. This result indicates that, in microfluidic setups, the liquid film can easily get saturated in terms of the diffusant. The saturation effect also occurs in macrosystems, but in longer contact times. An example is the wetted wall column. Johnstone and Pigford [55] provided a series solution to Equation-(13) for high Fo, with the third boundary condition of the Equation set-(15) replaced as $\partial C/\partial x = 0$ at $x = \delta$:

$$\frac{C^* - \bar{C}}{C^* - C_0} = 0.7857e^{-5.1213Fo} + 0.1001e^{-39.318Fo} + 0.7857e^{-105.64Fo} + \cdots \quad (23)$$

where $\bar{C}$ is the average concentration at z. By comparing the solution with numerical solutions, it can be seen that the solution is valid for $Fo > 0.5$, and terms other than the first are negligible. For $Fo = 0.5$, Equation-(23) indicate about 90% saturation for the finite film. Thus, the film is almost saturated in physical absorption for higher Fo.

When a gas-phase resistance is present, one should replace the second boundary condition with $-D\,\partial C/\partial x = (k_G/H)(C^* - C_i)$. Here C_i is the interfacial concentration that is not in equilibrium with the gas phase. To determine whether a resistance exists, one can check the Biot number, as given in Equation-(4) (The convective transfer coefficient h is replaced with k_G/H). The methodology is given by Table 3.

Note that for small Bi, gradients in the film vanish. This case is frequently observed in microdomains [56], since δ is small. It is important to note that PT does not have a static characteristic length. It was also discussed that for a working PT, $\delta_p < \delta$. These eventually suggest that PT cannot predict lumped capacitance at any time.

[7] This expression is related with Nusselt's analysis and given in Section 0.

Table 3. Biot number – gas phase resistance relationship with appropriate boundary conditions [53].

Case	Physical Explanation	Boundary Conditions
$\mathrm{Bi} > 40$	almost no resistance exists on the gas-side.	Dirichlet type, $C = C^*$
$0.1 < \mathrm{Bi} < 40$	a significant gas-side resistance exists.	Neumann type, with $-D\,\partial C/\partial x = h(C^* - C_i)$
$\mathrm{Bi} < 0.1$	lumped capacitance maybe applied, all gradients in the film are neglected.	No spatial BC's, the problem turns into a ODE

After Higbie, Danckwerts solved the case of PT for a first order reaction [57].

$$\frac{C}{C^*} = \frac{1}{2}\exp\left(-\sqrt{\frac{k}{D}}x\right)\mathrm{erfc}\left[\left(\frac{x}{2\sqrt{Dt}} - \sqrt{kt}\right)\right] + \frac{1}{2}\exp\left(\sqrt{\frac{k}{D}}x\right)\mathrm{erfc}\left[\left(\frac{x}{2\sqrt{Dt}} + \sqrt{kt}\right)\right] \quad (24)$$

Though complicated, the asymptotes of this solution for high and low Damköhler numbers, $\mathrm{Da} = kC^{*^{n-1}}t$, provided the basic equations for determining diffusivity, solubility and reaction rate constant in wetted wall columns or laminar jets. Number "n" is the reaction order, and is equal to one in Danckwerts' solution. However, unlike the physical absorption case, Danckwerts' solution does not allow an explicit relation for the penetration thickness, therefore for the transient stage; it cannot set a limit for the applicability of the penetration model for given combinations for Fo and Da numbers. These numbers are important and can be combined into a single critical parameter for ease in further analysis: the Thiele modulus with a general reaction of order n.

$$\Lambda = \sqrt{\frac{\mathrm{Da}}{\mathrm{Fo}}} = \sqrt{\frac{kC^{*^{n-1}}t}{Dt/\delta^2}} = \sqrt{\frac{k\delta^2 C^{*^{n-1}}}{D}} \quad (25)$$

2.3. Surface Renewal Theory (SuRT)

In FT, Whitman knew that accepting the existence of stagnant films nearby the interface was a serious oversimplification. On the existence of such films he noted that "actually no such demarcation exists." The fictitious existence of stagnant layers near the interface have been defended by many next generations and kept in later theories, such as the surface rejuvenation. The general judgment was that eddies of turbulence did not reach the interface completely. This was rigorously discussed in the 50's [58, 59], since experiments gave conflicting results. Years later, direct numerical simulations established [60] that surface elements constantly get replaced by eddies.

In 1951, Danckwerts [61] introduced a more general model that considers the effects of eddies of the turbulent bulk phase on gas absorption. He assumed that eddies continuously sweep the gas-liquid surface, thereby bringing fresh liquid patches to the surface and replacing the old patches that contain diffused amounts of solute during their existence on the surface. The life time of the patches on the surface is denoted as the age of the patch. Danckwerts considered a nonuniform age distribution among the patches. This distribution depends on the surface renewal rate, "s". This is the sole parameter of the model. Figure 8 presents the idea of surface renewal theory.

Considering random renewal, but constant "s" in time, a normalized exponential distribution is obtained:

$$\Phi(t') = se^{-st'}, \qquad \int_0^\infty \Phi(t')\,dt' = 1 \tag{26}$$

From probabilistic view, the age distribution function (ADF) $\Phi(t)$ can be regarded as a probability density function. Upon sampling an amount of interfacial area, it gives the probability of finding a surface patch with age t. With Equation-(26), one may use any surface flux expression to get the average absorption rates predicted by SuRT. The flux expressions can be obtained from solutions of the diffusion equation with various boundary conditions; such as constant surface concentration (PT), gas

phase or interfacial resistance[8]; and cases of diffusion with chemical reaction by using the following equation:

$$\bar{N} = \int_0^\infty \Phi(t')N(t')\,dt' = s\int_0^\infty e^{-st'}Ndt' \qquad (27)$$

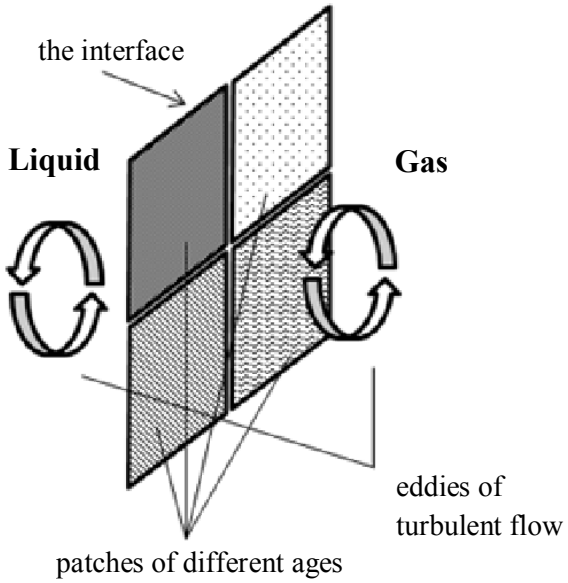

Figure 8: Schematic for SuRT.

In essence, the theory considers the patches as stagnant pieces of liquid, thereby allowing many solutions of the diffusion equation to be adapted. Furthermore, the above equation physically means the expected value or the first moment of surface flux. Mathematically, it is the Laplace transform of N. The simplest example can be given by applying the instantaneous surface flux predicted by PT (Equation-(18)):

$$\bar{N} = \sqrt{Ds}(C^* - C_0) \qquad (28)$$

Equation-(28) defines $\bar{k}_L = \sqrt{Ds}$ for SuRT.

Some of the results are quite interesting. For example for a gas phase resistance, a solution for N can be obtained via solving the Equation-(15) with the second

[8] Though usually expressed in the same matematical form, physically they are very different. Interfacial resistance concept is discussed in detail below.

boundary condition replaced with $-D\,\partial C/\partial x = (k_G/H)(C^* - C)$ at $x = 0$, and substituting its surface flux to Equation-(27) leads to:

$$\overline{N} = \frac{C^* - C_0}{\frac{1}{\sqrt{Ds}} + \frac{H}{k_G}} \tag{29}$$

which is surprisingly equivalent to the formulation given by film theory (i.e. combination of resistances, Equation-(9)), obtained from a very different route.

The SuRT has another connection with PT. Since PT can also be described by systematic renewal (constant renewal time), its distribution function can be given as:

$$\Phi(t) = \begin{cases} \frac{1}{t}, & 0 \le t' \le t \\ 0, & t' > t \end{cases} \tag{30}$$

Applying Equation-(27) with the uniform distribution given above, one obtains Equation-(20).

2.4. Unifications and Modifications for FT, PT and SuRT

In a period of 10 years after the accomplishment of SuRT, many modifications and corrections are made to the three main theories of interfacial mass transfer. Some attempts on the unification of these theories are also provided.

2.4.1. Film-Penetration Theory (FPT)

Toor and Marchello [62] formed unification between FT and PT. The theory lies on modifying the system described by Equation-(15) by dragging the boundary condition at infinity to a finite film thickness δ. For short times, the diffusant will obey the physics of PT and for long times, i.e. when the diffusant reaches δ; the physics of film theory is approached. At $x = \delta$, bulk concentration of the diffusant or the reaction rate in the bulk phase will prevail as boundary conditions. A schematic is given by Figure 9.

The theory suggests a smooth variation of the exponent "n" of diffusivity from 0.5 to 1. Although many experiments give "n" between those values, FPT is found to be qualitatively erroneous in terms of exponent's approach to 1 in some cases [63].

The theory provides important knowledge about the basis of the basic mass transfer theories. By considering a Higbie distribution and a standard Danckwerts distribution, the authors show that for all Fo numbers, the average transfer rates do not differ much. This is shown in Figure 10.

Later Huang and Kuo [64] added first order reaction into FPT. They also showed that the unknown parameters, s and δ, can be united into the Hatta modulus,

$$M_H = \frac{kD}{\bar{k}_L'^{\,2}} \qquad (31)$$

thereby converting FPT into a one parameter model. Here, $\bar{k}_L'$ represents the average physical mass transfer coefficient and it can be determined for many systems using film or penetration theory. Once $\bar{k}_L'$ is known, one can determine the chemical mass transfer coefficient, by using an enhancement factor expression, which is explained is Section 2.8.2. Like the asymptotic behavior of Toor and Marchello's FPT, their equation of FPT with chemical reaction approached to the solutions of Hatta [37] for film theory and to Danckwerts' solution as given with Equation-$\frac{C}{C^*} = \frac{1}{2}\exp\left(-\sqrt{\frac{k}{D}}x\right)\mathrm{erfc}\left[\left(\frac{x}{2\sqrt{Dt}} - \sqrt{kt}\right)\right] + \frac{1}{2}\exp\left(\sqrt{\frac{k}{D}}x\right)\mathrm{erfc}\left[\left(\frac{x}{2\sqrt{Dt}} + \sqrt{kt}\right)\right]$ (24).

For physical absorption, Huang and Kuo note that that the exponent of diffusivity may have values lower than 0.5 based on experimental data. From their equations, it can be seen that it is impossible to derive an exponent smaller than 0.5. This indicates the existence of an interfacial resistance; in such a case it should be regarded as an alternative and additive resistance. This fact will be detailed in Section 2.5. A realistic example of estimating s and δ as functions of Reynolds number is given by Brusset et al. [65].

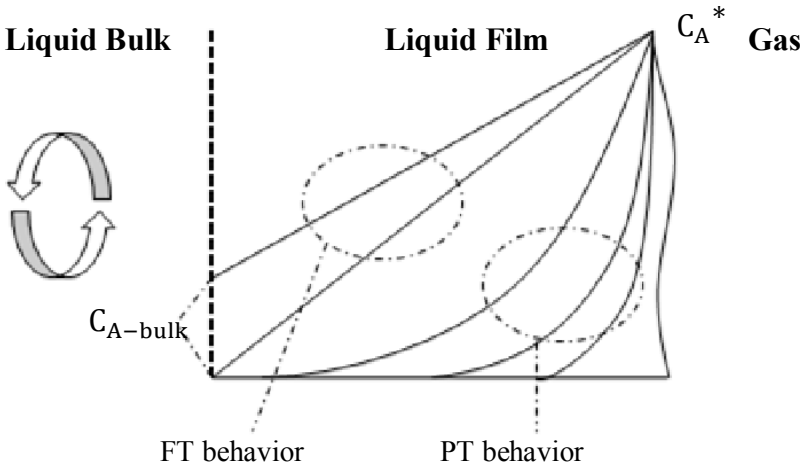

Figure 9: Schematic of FPT.

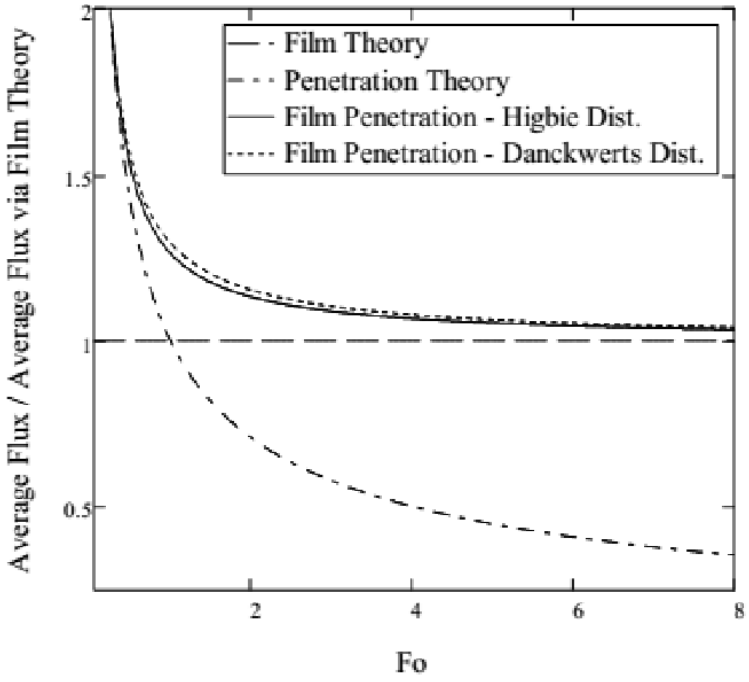

Figure 10. Equivalence of Higbie and Danckwerts ADFs. At low Fo, FPT approaches to PT and at high Fo it approaches to FT asymptotically.

Since now mass transfer with first order reaction is considered, it is clear that upon the establishment of steady-state, FT and PT may behave the same. It is shown by Lightfoot [66, 67] that for the same $\bar{k}'_L$ (or the Sherwood number), FT and PT behave almost the same at steady-state when a bulk phase is present. In other words, this means that one may always select a δ value for FT to conform to the results of PT.

This result is important, since it simply explains the practicality of FT, in terms of being a one parameter model and providing simple expressions at the same time. During any case with sufficiently fast kinetics in comparison to the contact times, and with the presence of a liquid bulk, FT can be useful tool.

From FT to FPT, it is always assumed that the concentrations of the bulk phases do not change. This assumption would induce serious errors for long times, and also for short times considering dilute gas bubbles. The remedy is mathematically possible, and by using PT, the finite capacity tank is treated by Gill and Nunge [68], and the depleting bubble problem is solved by Estrin and Schmidt [69], albeit solutions become complex in these cases.

2.4.2. Surface Rejuvenation and the Random Eddy Theory (RET)

In 1955, Danckwerts and Andrew [70] discussed that the SuRT should by modified in many cases like absorption processes in trickle beds, by changing the amount of surface renewal to certain extent. That is, mixing does not provide complete replenishment after each contact point. Instead, eddies sweep away some of the diffused solute at random times, but their approach distance to the interface is constant. That is, in their model called as surface rejuvenation, they accepted that eddies does not reach the surface. Alper [71] showed that in packed columns, surface rejuvenation is more realistic than complete surface renewal. Later on, Harriott [63] modified this theory, by simulating a physical absorption situation where eddies arrived at the surface layer at random times and approached in random distances to the interface. He chose fit this randomness to a gamma distribution

$$f(t', \alpha, \beta) = \frac{t'^{\alpha-1} e^{-t'/\beta}}{\beta^{\alpha}\Gamma(\alpha)} \qquad (32)$$

since $f(t, \alpha > 1, \beta)$ provides zero probability for an eddy to completely reach the surface, but it can come infinitesimally close to it. For $\alpha = 1$, the distribution function simplifies to Equation-(26). The idea of random eddy theory is illustrated in Figure 11.

Successful matches between many cases of mass transfer with a bulk phase, even to turbulent pipe flow scenarios were reported. The main result is that the approach distance is a vital parameter. Even when the average approach distance is constant, eddies that get closer to the interface enhance mass transfer much more in the overall. Thus, the standard deviation from the mean approach distance also affects mass transfer. This also provides a smooth transition of the diffusivity exponent from 0.5 to 1 upon wider contact time distributions. RET can be seen as the first computational and probabilistic model, but its success can also interpreted as a result of its 3-parameter nature.

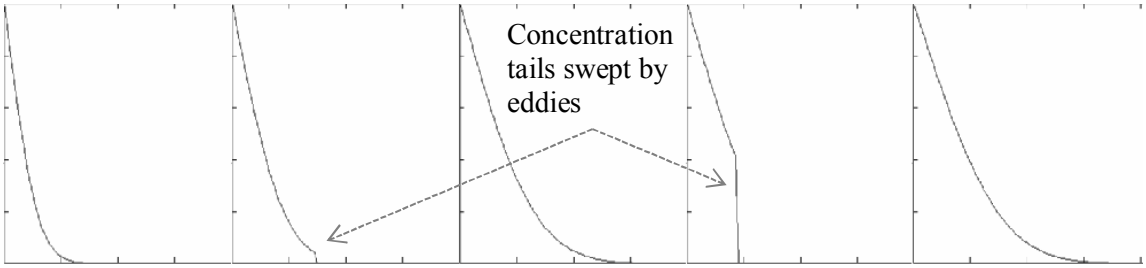

Figure 11. Concentration profiles in time for physical absorption, truncated after swept by the eddies of RET.

2.5. Interfacial Resistance and Statistical Rate Theory (SRT)

In his experiments, Higbie observed a mismatch between values predicted via his penetration formulation and his measured uptake values at very short contact times, on the order of 0.1 s. He assumed that the surface saturates exponentially with time. The rate constant for saturation is arbitrarily chosen to fit the data. The qualitative fit introduces a new parameter which is not substantiated by any theory. Nevertheless, the interfacial resistance concept was born.

Following this perspective, in presence of a resistance at the interface, rigorous mixing should affect the transport rates adversely if contact times are too short. Furthermore, the resistance also refutes the existence of the classical age distribution function of SuRT (Equation-(26)). The distribution claims that the most probable

surface age is zero, which is unlikely. Since interfacial resistance can also be thought as an initial time of reduced transfer, by analogy one can say that the surface elements are not considerably taken away by eddies at very short times, since then almost no mass transfer would occur.

The interfacial resistance concept is incorporated to the SuRT by Perlmutter [72]. He replaced s with $1/\tau$, and interpreted it as the surface residence time. With this move, he showed that the classical surface age distribution is the same with the washout function of a perfect CSTR in residence time distribution (RTD) theory (see [52] for the basic concepts). By using Zwietering's formula on eddy RTD and eddy age frequency [73], he established a connection between SuRT and RTD. Thereby he considered multiple capacitances (washout function of two CSTR's in series) and dead volume (washout function of a PFR followed by a CSTR or vice versa) models to enhance SuRT's ADFs. With such models, interfacial resistance is taken into account and for long contact times, the Higbie distribution given by Equation-(30) is approached by both models. Though physically meaningful, Perlmutter's convention increased the number of unknown parameters in the problem herewith decreasing the ease of the use of his model.

Upon Higbie's insights on interfacial resistance, Danckwerts [74] tried to apply the kinetic theory of absorption developed by Miyamoto [75, 76]. The theory uses a Maxwellian distribution of velocity on both sides of the interface, and assumes only that a certain fraction of molecules, which have enough kinetic energy, can pass through it. The theory yields an FT-like expression:

$$N_A = k_S(C^* - C_i) \tag{33}$$

where

$$k_S = \frac{\alpha}{H\sqrt{2\pi R_g T M}} \tag{34}$$

M is molecular weight and α is the condensation (or evaporation) coefficient or the probability that the molecule passes through the potential created by surface tension at the interface. Equation-(34) is sometimes called as Hertz-Knudsen equation and it determines the collision frequency on a flat line. Although the theory is of fundamental essence, it still possesses the unknown parameter α, which changes for

each gas-liquid-solute system. Moreover, Danckwerts failed to fit this kinetic model to Higbie's data. This created suspicion about the existence of interfacial resistance and validity of Higbie's results. Upon more unconformable results on the existence of interfacial resistance in laminar jet experiments (see Figure 12), Toor [77] noted that evolution of boundary layers near the surface of the laminar jet can create a falsified resistance to mass transfer. If there is acceleration in the surface layer, then the contact time becomes longer and averaged transfer rates decreases. He showed that upon assuming a surface velocity for a laminar jet falling along x direction in form of Px^n , where $-1 < n < 1$ [9], the age distribution functions can have a similar form with the gamma distribution used in random eddy theory, thereby designating a resistance-like response. The mathematics of the idea was established by Scriven and Pigford [78, 79], who along with Raimondi and Toor [80] carried out carefully designed experiments for CO_2 and O_2 absorption in water, concluding that interfacial resistance is very small for slightly soluble gases. However, interfacial resistance is found to exist for soluble gases, for liquid-liquid organic pairs [81], for mediums with trace amounts of ions are present [82] and where the fluxes are high when the contact times are short.

Later, Coughlin [83] re-analyzed the kinetic formulation and showed that the interface also may not be in thermal equilibrium due to the heat liberated in adsorption on to liquid surface, or due to the heat of condensation in a two phase single substance case. He emphasized that heat and diffusion equations must be strongly coupled, but he failed to fit his theory to experimental data also. He added that in some cases the condensation coefficient changes with experimental conditions. This eventually suggests that the kinetic formulation is incomplete. Nevertheless, the Hertz-Knudsen theory has an established place in the field of evaporation of pure substances. For water, a broad literature and data for α exists [84].

[9] $n = 1/4$ would approximately resemble a laminar jet and $n = 1/2$ would describe free fall. P is the perimeter of the jet.

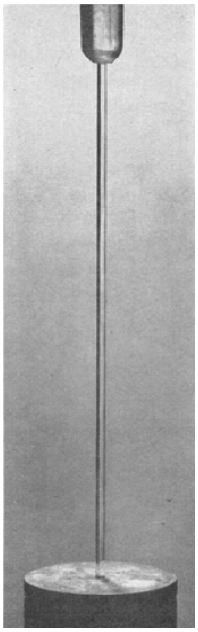

Figure 12: The laminar jet. Taken from [79], used with permission of Wiley&Sons.

The developments on interfacial resistance took a step forward when Ward [85] created statistical rate theory. He created a new boundary condition for interfacial mass transfer where adsorption from gas phase on the liquid surface is a negative first order process and desorption into the gas phase is of straight first order, leading to:

$$N_A = K_S\left(\frac{C^*}{C_i} - \frac{C_i}{C^*}\right) \tag{35}$$

with

$$K_S = \frac{P_B{}^{vap} C_B P_A}{H\sqrt{2\pi R_g T M}} \tag{36}$$

Note that K_S is similar with k_S of kinetic formulation. B denotes the solvent phase substance. The transfer rate is dependent of the solvent's vapor pressure also. In case of water, C_B is usually around 55.2 molar. SRT suggests the existence of a surface phase and a bulk phase, into which solutes are transported. For long times, $C_i \rightarrow C^*$, so the surface and the neighboring layer of the bulk phase reaches equilibrium concentrations. The theory is the most fundamental and comprehensive on interfacial mass transfer, since it does not have any fitting parameters. Later, Ward et al. [86] verified the theory by finding molecular distributions in each phase with

Boltzmann's microstates entropy approach and calculated the transition probability from a perturbation analysis of the Schrödinger equation, eventually leading to the same expressions given by Equation-(35) and (36). Applications of bubble growth, nondissociative and dissociative adsorption are also given [87, 88, 89]. Since it is based on adsorption-desorption dynamics, SRT has become a theoretical tool for analyzing adsorption-desorption kinetics both on solids and liquids.

The mathematical solution of the diffusion problem with equation-(36) as the boundary condition is given by Tao [90] in terms of a series sum of iterated integrals of the complimentary error function. Since the solution was complex and not always analytic[10], the interfacial concentration is approximated by Gupta and Sridhar [91] with a simpler equation:

$$\frac{C_i}{C^*} = \sqrt{1 - \exp(\beta^2)\mathrm{erfc}(\beta)}\ , \qquad \text{with } \beta = \frac{K_S}{C^*}\sqrt{\frac{t}{D}} \qquad (37)$$

It can be seen that as time increases, η increases and C_i tends to C^*. Authors show that, for $K_S > 10^{-5}$ mol/cm^{2}s, Tao's solution is almost the standard PT solution (Equation-(16)). They also provide saturation times for oxygen, carbon dioxide and hydrogen in water as 0.0124[11], 0.0054 and 0.0043 seconds respectively, which are calculated from Equations (36) and (37). Although the times are short, it is speculated that under high surface renewal conditions, interfacial resistance may lead to erroneous measurements. That is, experimental values for D and kinetic rate constants will be measured higher than normal, if PT is used directly. Thus, for the general application of the instant equilibrium boundary condition, one should now the saturation time. The most practical tool is Equation-(37), which is in implicit form.

Although interfacial resistance is found to be low for general macroscale equipment, it is possible that negating effect may exist, or the models may lump their existence. In the presence of surfactants it is almost undebatable that a significant resistance

[10] i.e. the series does not always converge.

[11] Toor and Raimondi's [49] saturation time is much lower. When calculated, it comes as 0.002 seconds, but experimental errors should have a huge impact on this result, and also their BC is linear (See Appendix E).

forms on the interface [44, 92]. The resistance effects in micro-contactors are not demonstrated yet.

2.6. Boundary Layer Solutions

Boundary layer theory is a very well developed area of transport phenomena and it has a huge number of applications. The theory can explicitly answer to many problems in terms of heat and mass transfer coefficients, including cases with developing velocity and temperature fields [93] and also can encompass arbitrary surface reactions [94] or slow homogeneous reactions [95]. However, due to narrowly confined geometries of microfluidics, velocity profiles in liquid flow develop almost instantly along the channel when compared to the concentration profiles[12]. In addition, confined geometries are not suitable for boundary layer solutions, which are naturally solved in semi-infinite domains. To see the length of the developing region, one may use the following empirical equation [96] for approximating the order of entrance length for laminar flow in a cylindrical microtube:

$$L_{ent} = 0.035\, d\, Re \qquad (38)$$

Typically, the diameter $d \sim 1$ mm and $Re \sim 10^2$, then L_{ent} comes out around 3 mm. This can be considered as a short distance when compared to the axial length of many microchannels, which are usually few centimeters long. Therefore boundary layer solutions may not be useful for analyzing microfluidic cases. For mass transport, they can only be used when the predicted boundary layer thickness is small when compared to characteristic diffusion length, but Akiyama [97] proves that PT already gives the same results in such a case. Under such conditions, curvature may be neglected[13], then PT will also give results obtained from using potential flow models [98].

[12] This is due to the Schmidt number, $Sc = Pe/Re = \nu/D$. For liquid flows, it is about 100-1000.
[13] For bubbles and drops for example.

2.7. Mass Transfer Theories Applied to Microcontactors

Many of the above explained theories are used to analyze and quantify mass transfer in microcontactors, but with limited success. It seems that use FT in microcontactors is already disregarded due to its 1-D nature [28]. The developments done under PT with or without chemical reaction seem to be especially valuable for micro-milli contactors since it is a 2-D model. Many of microfluidic contacting systems would hardly be modelled at steady-state in terms of the exposure time (the methodology presented in Section 2.1 is followed here), since a certain transient period would be present at the short times. Exposure, which might be cut off before or after the concentration profiles have settled, depends on the design of the device and hydrodynamics. Furthermore, for irreversible bimolecular reactions, a steady-state does not exist in the absence of a bulk phase, apart from complete saturation and depletion in terms of the reactants.

In terms of physical absorption, the inadequacy of PT for long contact times was known long before [99]. However, with the great number of successful applications in stirred tanks and bubble columns during 60's and 70's, the essence of the limitations seems to be overlooked. Recently, under the context of microfluidic applications, questions on the applicability of PT have been re-emerged. As explained above, for sufficiently large Fourier numbers PT can over predict the uptake rate in physical absorption. This over prediction of PT has been enunciated by Sobieszuk et al. [18] during the experiments involving the physical absorption of carbon dioxide into water in FFMR's. In addition, Haase et al. [100] reported the same effect for flow over singly packed microspheres in a cylindrical microchannel, on which a dissolution process[14] occurs. For short contact times, PT is successively employed in Taylor flow scenarios by van Baten and Krishna (numerical) [101] and Vandu et al. (experimental) [102]. Albeit for longer contact times, i.e. for smaller bubble velocities or long bubbles, saturation effects are observed. These results bring out the importance of a saturation criterion. In a short communication, Pohorecki [103] formulated some rough limits for effective use of Taylor flow in physical

[14] Dissolution may also be modelled with PT.

absorption, instantaneous reaction and surface reactions. He considered the contact time as:

$$t = \frac{L_B}{v_B} \tag{39}$$

where L_b is the bubble length and v_B is the bubble velocity, as shown in Figure 13.

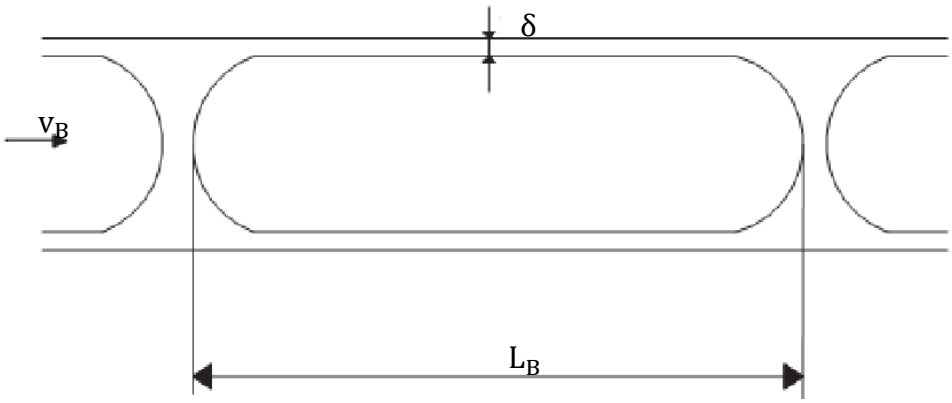

Figure 13. A schematic of Taylor flow.

The author simply suggested that the maximum uptake rate will be equal to the one predicted by PT (Equation-(19)):

$$\delta {C_A}^* = 2{C_A}^* \sqrt{\frac{D_A t_e}{\pi}} \tag{40}$$

where the saturation-exhaustion time t_e can be given as:

$$t_e = \frac{\pi}{4}\frac{\delta^2}{D_A} = 0.77\frac{\delta^2}{D_A} \tag{41}$$

Following the same path for an instantaneous reaction of $A + bB \rightarrow P$, considering A as the absorbed reactant and B is fluid phase reactant of initial presence, the depletion of B can be given as:

$$\delta C_{B_0} = 2bE_i{C_A}^* \sqrt{\frac{D_A t_d}{\pi}} \tag{42}$$

C_{B_0} is the initial concentration of B in the film, E_i is the enhancement factor for an instantaneous reaction, to be given by Equation- (58). But here, he somewhat oversimplified it as:

$$E_i \approx \frac{C_{B_0}}{bC_A^*}\sqrt{\frac{D_B}{D_A}} \tag{43}$$

to yield the neat result:

$$t_d = \frac{\pi}{4}\frac{\delta^2}{D_B} \tag{44}$$

Equation-(44) is the minimum time for depletion when a second order bimolecular reaction occurs in the film. Since $t \ll t_e$ and $t \ll t_d$, Pohorecki concluded that

$$Fo = \frac{L_B D}{v_B \delta^2} \ll 1 \tag{45}$$

where D is D_A for saturation upon physical absorption and D_B for liquid reactant depletion. For a heterogeneous reaction, the reverse criterion $Fo \gg 1$ should hold, since the diffusant must reach the catalytic wall and accumulate there well, in order to allow kinetically controlled synthesis.

Van Elk et al. [104] ran a numerical study of gas absorption in confined films. They considered physical absorption, absorption with first order reaction and second order bimolecular reaction in a laminar film. The reason of their investigation was to investigate the limits of PT in packed absorbers. The limits of PT were demonstrated qualitatively. Yue et al. [105] have run a similar numerical study for first and second order reactions in plug flow, but this time, they approached the problems from the perspective of microfluidic mass transfer.

In addition to the theories and their applications explained above, simpler engineering approaches are also applied to microcontactors when measuring mass transfer rates. The most important of them is to define an overall mass transfer coefficient. If mass transfer resistance lies in only one of the phases, then one can assume one of the phases as a plug flow unit:

$$\frac{dC}{d\tau} = k_L a(C^* - C) \tag{46}$$

τ is the mean residence or contact time and $k_L a$ is the volumetric mass transfer coefficient with a as the specific interfacial area. By accepting the above formula, velocity and dispersion effects are implemented into $k_L a$. If the resistance lies in both phases, an alternate derivation involving the hold-ups are necessary [28]. Integration of Equation-(46) gives:

$$k_L a = \frac{1}{\tau} \ln\left(\frac{C^* - C_{in}}{C^* - C_{out}}\right) \tag{47}$$

This simple equation can be used directly to determine $k_L a$ from experimental measurements. However, since volumetric flow rates are low, offline measuring methods, like sampling some of the biphasic mixture, subjecting it to phase separation and then to chemical analysis; cannot be applied well. This is due to the combined effects of short residence times and small amounts of material in microcontactors [28]. In aid of this situation, online mass transfer measurement techniques have been developed. A pH based light induced fluorescence (LIF) method has been recently applied during nitration of urea in a silicon microreactor [106].

Alongside with mass transfer coefficient analysis based on PT and on the overall, some other modelling approaches are also implemented. As examples, Su et al. [107] implemented surface renewal concept to micropacked beds for a liquid-liquid water-kerosene system and Mhiri et al. [108] used the classical number of transfer units (NTU) concept in an FFMR for the treatment of chlorinated volatile organic compounds.

In summary, the methods of attack to model and quantify mass transfer in microcontactors vary to a great degree. The generic mass transfer models may be useful in modelling microreactors; however they are only suitable for some restricted cases More detailed and reliable models, whose solutions are also practical to use, seem to be necessary. As Kashid et al. [28] demonstrates, the measured data and model predictions in microfluidic mass transfer does not seem to match. In general, experiments lead to a very wide scatter of volumetric mass transfer coefficients. As an example, the data for mass transfer in air-water Taylor flow is given in Figure 14. In Figure 15, insufficient modeling via PT and FT is demonstrated for CO_2 absorption in an FFMR.

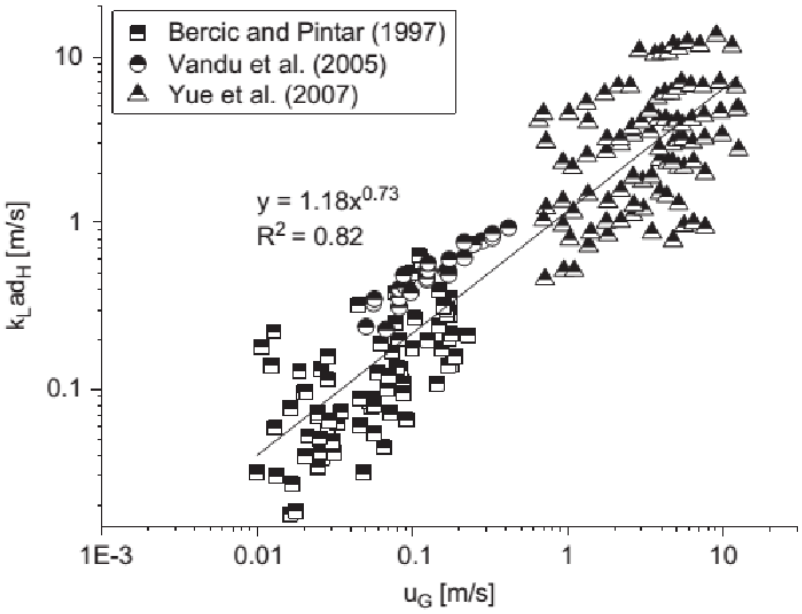

Figure 14. Variation of $k_L ad_H$ with gas velocity in Taylor flow. Taken from Kashid et al. [28], used with permission of Elsevier.

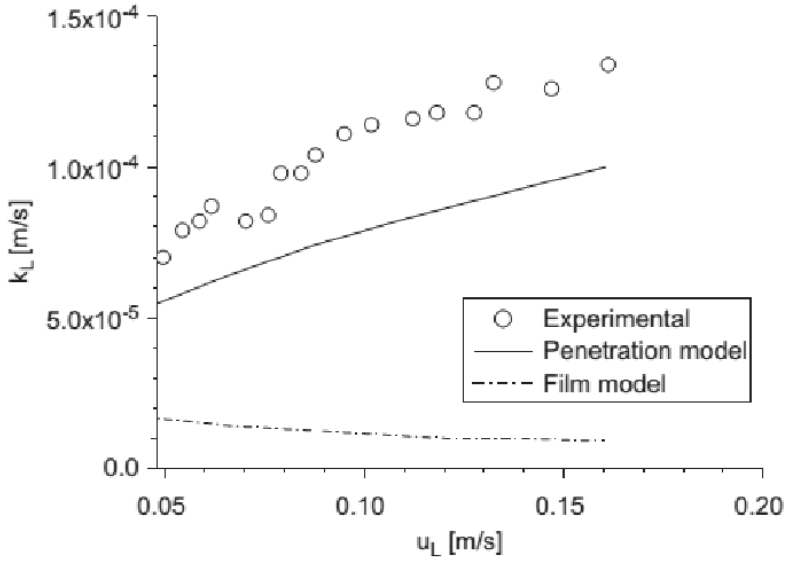

Figure 15. Comparison of experimental results for liquid phase mass transfer coefficients with FT and PT predictions in an FFMR. Taken from Kashid et al. [28], used with permission of Elsevier.

2.8. Additional Tools of Transport Phenomena

2.8.1. The Hikita-Asai Approximation (HAA)

In 1964, without showing any proof, Hikita and Asai [109] developed linearized formulas to accommodate m^{th}-n^{th} order reactions in FT and PT as an extension to van Kravelen and Hoftijzer's work [38]. Their linearization of the pseudo n^{th} order reaction in PT was especially successful. For the nonlinear source term, they used:

$$kC^n \cong \frac{2}{n+1} kC^{*n-1} C = k_{HAA} C \qquad (48)$$

(24) for any order, provided that $n > -1$. The approximation is very accurate; maximum is error is about 2%. 26 years later, Asai [110] completed the basis of the approximation and generalized it for reversible reactions in FT. He considers a reactive absorption case in a liquid film where the gas phase resistance is neglected, therefore on the interface $C = C^*$ and the on the boundary neighboring the liquid bulk $C = C_b$. Considering an nth order reaction kC^n, he integrates the nonlinear steady-state reaction-diffusion equation once to obtain fluxes at each boundary. Then upon linearizing the reaction rate as $kC^n = aC + b$ and solving the linearized reaction-diffusion equation, he finds the values of a and b by the using the exact description of fluxes at the boundaries and an enhancement factor expression that is valid for fast reactions. Upon setting $C_b = 0$, b comes out as zero and the linearization given in Equation-(48) is obtained. b is non-zero when there is equilibrium due to a reversible reaction in the bulk, that is $C_b \neq 0$.

Although the linearization is made in steady-state; it is very accurate in transient cases as well. In other words, even if the linearization is derived for FT, it can also be used safely in PT, with zero concentration at the propagation front.

2.8.2. Effectiveness and Enhancement Factors

The number or variation of reaction-diffusion problems is almost infinitely many. Reasons for this is the number of parameters, various rate forms and some nonlinearly relationships; like the Arrhenius equation for the rate constant; and

concentration, temperature or gradient dependent [111] nature of the physical properties. In practical analysis, many of the effects leading to variable parameters may be neglected if operation conditions allow. If so, two factors can be used for practical computations. For gas-solid reactions, the effectiveness factor [112]:

$$\eta = \frac{\text{average reaction rate}}{\text{reaction rate at the surface}} \tag{49}$$

and for gas-liquid reactions, the enhancement factor [38] :

$$E = \frac{\text{absorption rate with chemical reaction}}{\text{absorption rate without chemical reaction}} \tag{50}$$

are introduced[15]. The effectiveness factor for first order reactions can be found in many textbooks [113]. It is used for steady-state analysis, and can also be extended to gas-liquid reactions by using the film theory [114].On the other hand, enhancement factor can also be used for both steady and unsteady-state analysis by using FT and PT respectively.

A general effectiveness factor expression for any rate expression and with variable diffusivity[16] is given by Bischoff [115]

$$\eta = \frac{\sqrt{2}}{\delta r(C^*)}\left[\int_{C_\delta}^{C^*} D(C)r(C)dC\right]^{1/2} \tag{51}$$

The concentration at the wall, C_δ, must be solved from an implicit equation to use this expression. However, at relatively high rates, it may be almost zero. Then a "dead core" occurs. In such a case, the above integral can be evaluated much simply by setting $C_\delta = 0$. Formation of a dead core is important in catalysis and it is strictly unwanted, since the catalyst in the dead core is wasted. This phenomenon is related to gas-liquid mass transfer with chemical reaction, where a portion of a liquid film is used in gas absorption at all.

Following the steps of Bischoff, a general expression for enhancement factor at steady-state can be given as:

[15] The absorption rates are usually time averaged. Thus, the definition of E can also be given as the ratio $\bar{k}_L/\bar{k}'_L$, or as the ratios of the amounts absorbed (n_a) under physical and chemical absorption.
[16] Useful for reactions with volume change.

$$E = \frac{2D}{k_L(C^* - C_b)} \int_{C_b}^{C^*} r(C)dC \qquad (52)$$

D is assumed as constant and C_b is the concentration in the bulk, which is usually known. In unsteady state, one may provide a general expression by using the HAA in CC∗=12exp−kDxerfcx2Dt−kt⁄12expkDxerfcx2Dt+kt (24) and with use of Equation-(18) for the denominator of Equation-(50):

$$E = \left[\sqrt{M_n} + \frac{\pi}{8\sqrt{M_n}}\right] \mathrm{erf}\left(\frac{2\sqrt{M_n}}{\sqrt{\pi}}\right) + \frac{1}{2}\exp\left(-\frac{4M_n}{\pi}\right), \sqrt{M_n} = \sqrt{\frac{2\pi}{n+1} k C^{*n-1} t} \qquad (53)$$

However, general expressions for E in finite films, for mass transfer with arbitrary homogeneous reactions and for non-plug flow velocity fields cannot be provided analytically. Yue and his co-workers has published a series of four papers, in which they considered instantaneous reactions in plug flow [116], first and second order reactions in plug [105] and laminar film flows [117] and in the presence of gas-phase resistance [118]. For finite films and over an extensive parameter space, they provided correlations for E, by matching the numerical results with the empirically modified forms of the relations given by Danckwerts [57] and Hikita and Asai [109] for PT.

2.8.3. Second Order Reactions

In the perspective of FT, the first approximate solution to the equation set:

$$\begin{matrix} D_A \frac{dC_A}{dx} = kC_A C_B & \text{at } x = 0, \ C_A = C_A^* & \text{at } x = \delta, \ C_A = 0 \\ D_B \frac{dC_B}{dx} = bkC_A C_B & \text{at } x = 0, \ dC_B/dx = 0 & \text{at } x = \delta, \ C_B = C_{B_0} \end{matrix} \qquad (54)$$

was provided by van Krevelen and Hoftijzer [38] in terms of an approximate and implicit relation for the enhancement factor:

$$E = \frac{\sqrt{M_H}\sqrt{1 - (E-1)\frac{D_A b C_A^*}{D_B C_{B_0}}}}{\tanh\left[\sqrt{M_H}\sqrt{1 - (E-1)\frac{D_A b C_A^*}{D_B C_{B_0}}}\right]} \qquad (55)$$

where $M_H = kC_{B_0}D_A/\bar{k}_L'^2$ is the Hatta modulus (a modified version of Equation-(31)). Also, the enhancement factor for an instantaneous reaction is given as:

$$E_i = 1 + \frac{D_B C_{B_0} H_A}{bD_A P_{A_i}} = 1 + \frac{D_B C_{B_0}}{bD_A C_A^*} \tag{56}$$

In view of PT, the equations for reaction-diffusion form the following system:

$$\begin{aligned} &\frac{\partial C_A}{\partial t} = D_A \frac{\partial^2 C_A}{\partial x^2} - kC_A C_B \qquad \text{at } x = 0,\ C_A = C_A^* \qquad \text{as } x \to \infty,\ C_A = 0 \\ &\frac{\partial C_B}{\partial t} = D_B \frac{\partial^2 C_B}{\partial x^2} - bkC_A C_B \qquad \text{at } x = 0,\ \partial C_B/\partial x = 0 \quad \text{as } x \to \infty,\ C_B = C_{B_0} \\ &\qquad\qquad \text{at } t = 0, \qquad C_A = 0 \ \&\ C_B = C_{B_0} \end{aligned} \tag{57}$$

Like Equations-(54), Equations-(57) form a nonlinear set and need a numerical solution. Danckwerts [119] provided an exact solution for the instantaneous case, which is an upper limit of absorption intensification. He also provided the enhancement factor for this case. His complicated and implicit expression for enhancement factor is later simplified and accepted as [120]:

$$E_i \cong \sqrt{\frac{D_A}{D_B}} + \frac{C_{B_0}}{bC_A^*}\sqrt{\frac{D_B}{D_A}} \tag{58}$$

for relatively large E_i. Numerical solutions are then provided by Perry and Pigford[17] [121] and Brian et. al. [122, 123]. The main result was that van Kravelen and Hoftijzer's expression (Equation-(55)) was accurate within 8% percent for FT, and in addition, E for PT can be represented by a modified and still implicit form of Equation-(55):

$$E = \frac{\sqrt{M_H \frac{E_i - E}{E_i - 1}}}{\tanh\left[\sqrt{M_H \frac{E_i - E}{E_i - 1}}\right]} \tag{59}$$

[17] It is interesting to note that the analog computer used by Perry and Pigford needed hours for a solution. However with a dual core mediocre laptop and a CAS, solving Equations-(5757) takes a couple of seconds, which shows a speed improvement about 60000 times. This linearly corresponds to getting 1000 times faster every year.

with the modified Hatta modulus $M_H = \pi k C_{B_0} t/4$ [18] within 20% error. The error is assumed as acceptable, and the parameter space was divided into five kinetic regimes as given by Table 4 below [120]. The E vs.M_H plot is reproduced in Figure 16.

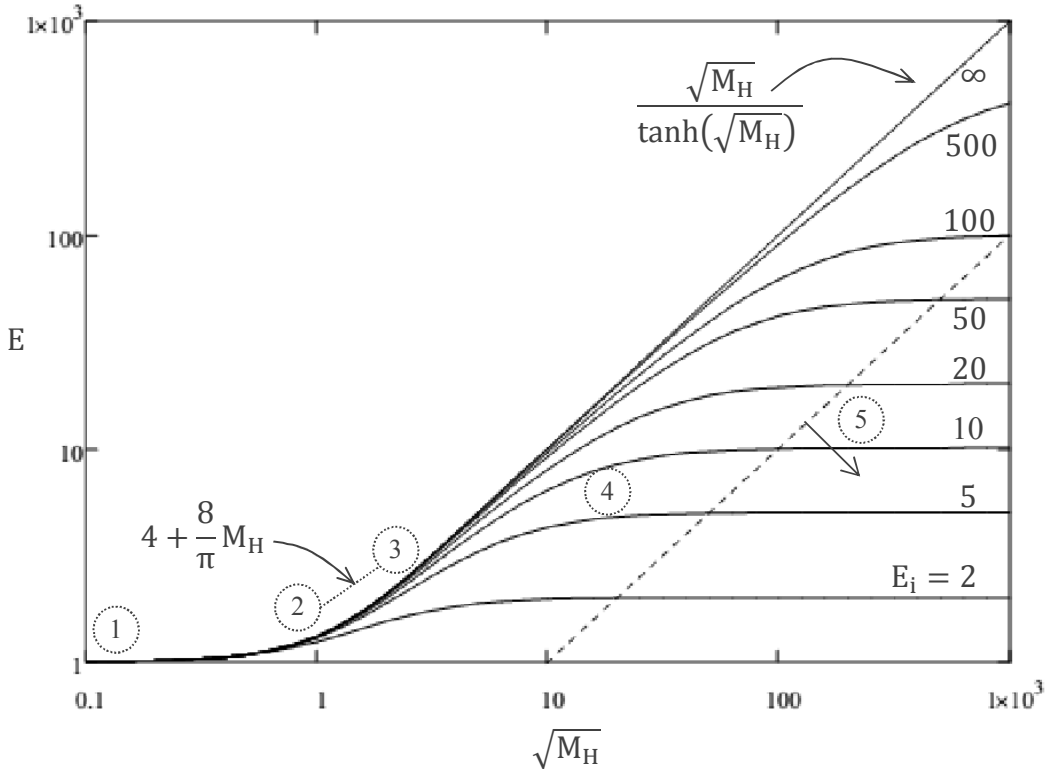

Figure 16. The enhancement factor versus Hatta number for a second order bimolecular reaction in PT. Adapted from [124] and [125].

Some additional approximate numerical limits can be provided for M_H. For example for the second regime, $\sqrt{M_H} < 0.5E_i$, for the third regime$\sqrt{M_H} > 3$ and $\sqrt{M_H} > 0.5E_i$ for the fifth regime. These expressions are based on FT but found to be valid for PT also.

[18] Very similar to M_n given in Equation-(53).

Table 4. Reaction regimes for second order bimolecular reaction [120].

Case		Regime	Approach for determining E
1	$\sqrt{M_H} \ll 1$, $E \approx 1$	Slow reaction	Employ physical absorption solutions.
2	$\sqrt{M_H} \ll E_i$	Pseudo-first order	Use Equation-(53).
3	$1 \ll \sqrt{M_H} \ll E_i$, $E \cong \sqrt{M_H}$	Fast-pseudo first order	Use Equation-(53) and (58).
4	$\sqrt{M_H} \sim E_i$	Intermediate	Use numerical solutions, E vs $\sqrt{M_H}$ plots or approximate equations.
5	$\sqrt{M_H} \gg E_i$, $E \approx E_i$	Instantaneous	Use Equation-(58).

2.8.4. Nusselt Theory

For a falling film on an infinitely wide vertical plate, Nusselt's analysis [50, 96] yield the following expression between film thickness and volumetric flow rate:

$$\delta = \left(\frac{3\dot{V}\mu}{\rho g}\right)^{0.33} \tag{60}$$

The surrounding gas is assumed to be stagnant and the shear on the liquid interface is assumed to be zero. Such conditions yield the velocity field given in Equation-(13) and the interfacial velocity is comes out as:

$$v_i = \frac{\rho g h}{\mu^2} \tag{61}$$

which is also the maximum velocity in the film. The average velocity is given as $\bar{v} = 2v_i/3$. When exposure time is defined with average velocity, $t = z/\bar{v} = 3z/2v_i$, the Fo number used in Table 2 and in footnote 7 is obtained.

For the effects of slip and shear on the velocity profile, see Appendix-D.

2.8.5. Stability in Stratified Flow

Normally, the general boundary condition between two fluids would be the jump condition on stress [126], which can be given as:

$$\mathbf{n} \cdot [\boldsymbol{\pi}_I - \boldsymbol{\pi}_2] = 2H_c\sigma\mathbf{n} - \boldsymbol{\nabla}_s\sigma \qquad (62)$$

$\mathbf{n}$ is the normal vector, $\boldsymbol{\pi}$ denote the stress tensor in each fluid, H_c is the mean curvature of the interface and $\boldsymbol{\nabla}_s$ is the surface gradient operator, which can also be given as $\boldsymbol{\nabla} - \mathbf{n}(\mathbf{n} \cdot \boldsymbol{\nabla})$. For equilibrium interfaces H_c is a constant, but for a transient case, it changes with the unsteady stress fields of both phases in a very complicated manner. This is due to the perpendicular components of the velocity vectors that almost always exist during the flow of two superposed fluids with different viscosities in parallel shear flow [127]. When sufficient disturbance is applied, instability may give birth to bubbles or drops. However, surface tension can suppress this instability if [128]:

$$(v_1 - v_2)^2 < 2\sqrt{g\sigma(\rho_1 - \rho_2)}\,\frac{\rho_1 + \rho_2}{\rho_1\rho_2} \qquad (63)$$

This unstable nature is called as the Kelvin-Helmholtz instability. For gas-liquid flows, flows are usually stable in microfluidic applications. However, for liquid-liquid flow, instability may be seen in micro-scales. Research for flow stabilization has been done by many workers in the field and these are summarized by Günther and Jensen [129]. In microfluidics, even a complete elimination of waves during stratified flow is shown to be possible.

2.8.6. Falling Film Reactors

Stratified flow configurations have been used by chemical engineers in macrocontactors for many years. But the complications that occur during the analysis at the gas-liquid interface is usually avoided. Since Equation-(62) needs computational resources for non-stagnant interfaces, one may simplify it by

neglecting the curvature and surface tension regarding a completely parallel flow. This leads to equivalent tangential shear stresses at the interface:

$$\tau_{t_1} = \tau_{t_2} = \tau_i \tag{64}$$

The interfacial shear τ_i is well studied and correlated for macroscale gas-liquid stratified flows with a large range of Re numbers [130, 131]. For low liquid phase Re, the interfacial shear is usually equivalent to that of single phase gas flow over a smooth wall [132]. It is expected that this would also be the case in microfluidics, also for liquid-liquid flows, when slip between the phases is negligible. Theoretically slip effects are expected to increase the thickness of falling films, but no demonstration has been given. On the other hand, the expected shear thinning is found to be negligible for gas velocities up to 15m/s in wetted wall reactors [133], but this effect for micro-liquid falling film and neighboring gas-flow is not well investigated. Equation-(60) can be modified to accommodate neighboring gas flow in an empirical manner:

$$\delta = \left(\frac{\mu}{\rho^2 g}\right)^{0.33} A\, {Re_L}^B \tag{65}$$

For $A = 0.909$ and $B = 0.33$ Equation-(65) becomes equivalent to Equation-(60).

Note that, there should be a limiting value of δ for each flow setup and operational parameters, unlike the zero asymptote predicted by Equations (60) and (65). This so called minimum wetting thickness has been studied both theoretically and experimentally for large plates. The existence of incomplete wetting and dry patches, and also the adverse effect of flooding under high flow rates have been demonstrated for an FFMR by Zhang et al. [134]. In view of a falling film reactor, dry patches reduce productivity; lead to lower heat transfer surfaces for exothermic reactions (sulfonations and ethoxylations are examples), may produce unwanted reactions at gas-liquid-solid contact line and may cause corrosion due to direct gas-solid contact; for example for operations involving H_2S. Although the theories for minimum wetting thickness in partially confined slots (like the one in an FFMR plate) have not developed yet, a simple equation for the minimum Re for a vertical falling film on an infinitely wide plate should be provided here [133]:

$$Re_{min} = 0.148[Ka(1 - \cos\theta)]^{0.6} \tag{66}$$

θ is the contact angle and Ka is the Kapitza number, used for characterizing falling film flows under gravity:

$$\mathrm{Ka} = \sigma\left(\frac{\rho}{g\mu^4}\right)^{0.33} \tag{67}$$

2.8.7. Slip Flow

One of the new phenomena that emerged under microfluidics is boundary slip. Instead of the classical no-slip boundary condition on a fluid-solid interface, a more general the slip boundary condition[19] is proposed [135]:

$$\underbrace{\text{at } x = 0, \quad v_z = 0}_{\text{no}-\text{slip}} \longrightarrow \underbrace{\text{at } x = 0, \quad v_z = v_{int} - b_s \frac{dv_z}{dx}}_{\text{slip}} \tag{68}$$

Both the slip and the no-slip boundary conditions stem from observational studies. The slip length b_s leads to a non-zero velocity on the interface. This is schematically shown by Figure 17. v_{int} is added to account for a moving interface. For gases, the occurrence of slip flow is determined by Knudsen number:

$$\mathrm{Kn} = \frac{\lambda}{L_c} \tag{69}$$

where λ is the mean free path[20] and L_c is the characteristic axial length of the flow duct. For $\mathrm{Kn} < 10^{-2}$ continuum approximation is valid. For $10^{-2} < \mathrm{Kn} < 10^{-1}$ slip flow occurs. The interval $10^{-1} < \mathrm{Kn} < 3$ is called as the transitional regime and for $\mathrm{Kn} > 3$ is the free molecular flow reigns [56]. Slip effects reduce frictional drag and usually increase flow rates.

From the kinetic theory of gases, for dilute gases, the slip length is theoretically given as $b_s \cong 1.15\,\lambda$ [136]. On the other hand, for liquids, the absence of a developed molecular theory and an indicator like Kn, complicate the accountancies of slip in liquid flows. The only theoretical tool is molecular dynamics (MD). From

[19] This is an example for the generality of Neumann BC's, since as b_s goes to zero; the no-slip BC (Dirichlet BC) is obtained. Similar case occurs for mass transfer with gas-phase or interfacial resistance.

[20] For a dilute gas, $\lambda = k_B T/\sqrt{2}\pi d^2 P$ from kinetic theory. k_B is Boltzmann's constant, d is the molecular diameter.

MD simulations [137] and experiments [138], it is proved that slip effects are usually insignificant in liquid flow down to the length scales of 100 nm. This scale is out of the range of microfluidics, and related to the domain of extended nanospace.

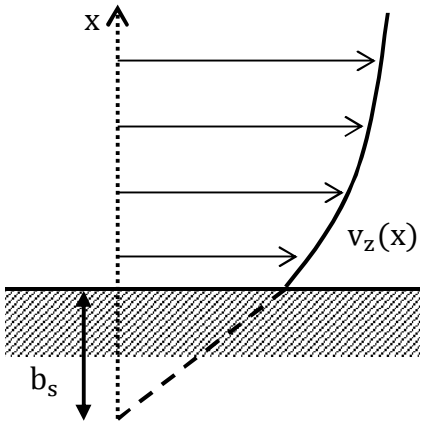

Figure 17: Boundary slip.

However, caution must be exercised with such numbers. For example slip-lengths on the order of 100 nm have been measured on superhydrophobic surfaces [139]. Further slip may be induced when ridges (also called as grooves) are etched on channel walls, similar to the ones used by Daniello et al. [140] (Figure 18). Due to the stagnant fluids in the ridges, the overall shear stress on the wall decreases. Upon the initial feed of liquid, the ridges are usually filled with air. In this initial period, the slip has its highest value[21]. After a certain time, air dissolves in the flowing liquid, and it is eventually replaced by the flowing liquid. This reduces the slip on the overall, but the values of b are still much higher than the ones obtained from superhydrophobic coatings[22]. The slip lengths due to such stagnant pockets can be a few micrometers [139]. For thin films, this may be a considerable magnitude. Considering Taylor flow, since the liquid film that surrounds the bubbles has a thickness of 5-50 μm (depending on the Ca number) [141], ridges may affect the flow characteristics in terms of wall slip, as long as the width and depth of the ridges are not larger than film thickness.

[21] This is condition is called as the Cassie state, where wetting is incomplete. Later transition into complete wetting occurs and this state is called as the Wenzel state.
[22] Drag reduction via microridges occur naturally on the microscopically rough skin of large fishes [257].

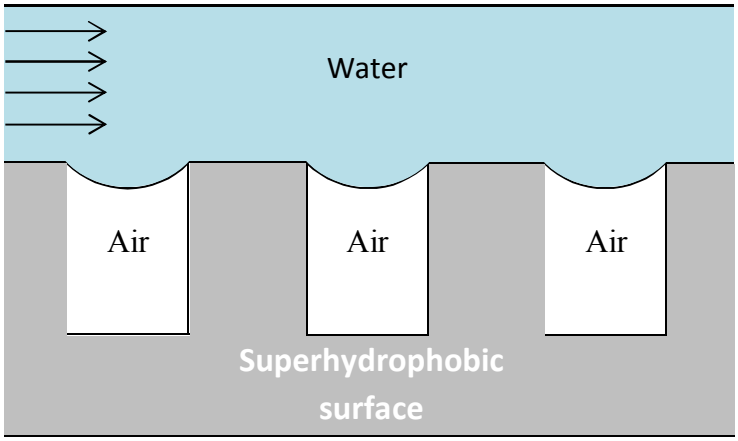

Figure 18. Slip via flow over air pockets and superhydrophobic surfaces, adapted from [140].

The ridges are also important in the context of mixing, since they may induce small scale currents which would enhance mass transfer. This is an old modification that has been done for many kinds of reactors and separators [142], but in the microfluidic domain, ridges provide slip also. Such in-channel mixing structures are proved to be effective in microreactors. An example is shown by Rebrov et al. [143] during catalytic oxidation of octanal by oxygen, where liquid side mass transfer coefficients increased 1.2-1.3 times when compared to the experiments of Zhang et. al. in which the same reactor setup is used, but without ridges [24]. IMM's FFMR has such staggered-herringbone micro-grooves of 160μm width in its slots [19].

2.9. Effects of Non-Flat Interfaces on Gas Absorption

It is a fact that surface waves almost always occur during the flow liquids in contact with another liquid [127]. By many experiments, it has been shown waves enhance mass (or heat) transfer. This is not due to the increase in surface area, on the contrary, due to the additional convective fields below wave crests, and the thinning that occur in wave troughs [144]. Upon rigorous disturbance at the surface, secondary convection cells may occur below the crests, which are called as "roll waves" [145]. It has been found that adjoint gas flow smoothes the wave profiles, but

decreased gas flow and increasing viscosity makes the waves more regular, albeit with steeper fronts. However, one may say that the frequency and the velocity of waves do not get influenced much by gas flow, when gas velocities above the surface are smaller than 10m/s [133]. This should apply to many cases in microfluidics with two-phase flow, but not to annular flows (see Figure 2) since gas velocities may be much higher [146].

It is interesting to note that the simple Nusselt theory given by Equation-(60) have been found to provide the mean film thickness in wavy flow very accurately, only with about 1% underprediction. Equation-(60) can be used safely up to Reynolds numbers of 1600 [147].

Since the fluid mechanics of wave inception and wavy flows are quite complicated, mass transfer in such cases is much more difficult to analyze. Several attempts have been performed by Ruckenstein [148], Javdani [149] and Ishimi et al. [150] for pre-set sinusoidal wave profiles. Explicit relations for mass transfer coefficients are obtained but they usually complicated and apply only to short penetration distances. Howard and Lightfoot [151] created the surface stretch theory, which includes a very detailed mathematical description of waves. The theory can be applied to any wave shape and also can treat circulatory motion under a wave crest or a finite layer. However, for such complicated cases, numerical calculations are necessary. Nevertheless, the theory is well suited for periodically varying interfaces, especially for large oscillating bubbles, where the mass transfer coefficients can be given in a simple form [152]. Bubbles should be considered as large, since internal gradients and circulations inside the bubble must be neglected. This is possible if there is almost turbulence in the core of the bubble. In the context of microfluidics and Taylor flow, the circulations inside the bubbles are not negligible in terms of hydrodynamics, but whether the circulations affect mass transfer significantly or not seems to be an unanswered question.

When wave forms are complex, empirical correlations for mass transfer can be used. For $\mathrm{Re} < 300$, an example can be given as [133]:

$$\mathrm{Sh} = \mathrm{A}\,\mathrm{Re}^{\mathrm{B}}\,\mathrm{Sc}^{\mathrm{C}}$$
$$\mathrm{A} = \frac{0.1025}{\mathrm{Ga}^{1.05}}, \qquad \mathrm{B} = 0.73, \qquad \mathrm{C} = 0.5 \tag{70}$$

Ga is the Galilei number. In strictly confined geometries of microfluidics, the approaches above seem to be insufficient for modeling hydrodynamics and mass transfer. Instead of trying to adapt these theoretical developments, one may accommodate CFD with ease and apply it for a great number of cases. The Volume of Fluid (VOF) and the Level Set (LS) numerical schemes have been used to model many cases of multiphase flows and they had been incorporated into commercial CFD solvers. In the computations involving these schemes, Navier-Stokes equations are solved for both phases and the interface is tracked either with VOF, LS or both. Both schemes have their advantages and disadvantages. For example VOF is better as mass conservation, but LS provides more accurate interfaces. Coupled VOF and LS is more robust, but such simulations need large computing times.

CFD solutions involving VOF or LS have been presented for multiphase flows in microreactors, for example Ho et al. [153] provided solutions for the IMM FFMR and Gupta et al. [154] used CFD to analyze Taylor flow. Some volume fraction contours for these VOF simulations are given by Figure 19 and Figure 20.

Although they can resolve complicated phenomena, multiphase flow simulations need serious computational resources. It has been demonstrated that mass transfer can be coupled with VOF [155] or LS [156] algorithms. These applications are even more costly, and the general numerical methodologies are not yet implemented into commercial solvers. The difficulty of comparing numerical results with experiments is another important issue in this case. One simplification for numerical computation may be solving for the velocity field first and then averaging it over time to obtain a time-averaged interface shape. Then this field may be implemented for a mass transfer study [157]. However, since transient currents and interface shapes would enhance and mass transfer nonlinearly, such an application may not be accurate in terms of mass transport rates. For flow fields with alternating phases like Taylor flow, such a simplification is not even possible.

Since computation times for the CFD resolution of multiphase flows are long, further simplifications are applied in order simulate the flow in a practical manner and rapid

manner. For example for Taylor flow, one of the approaches is to move the wall of the microconduit in simulations, instead of feeding the gas into a liquid stream (Figure 20), as it would be in reality. This eliminates the relatively difficult bubble formation step. This step is replaced by methodology where an initial ellipsoidal shape is drawn for the bubble. During the simulation, bubble obtains its familiar Taylor bubble shape in time. Such simulations have been performed [158, 159] and they demonstrated vivid circulations both in the Taylor bubbles and in the liquid slug. However, by inspecting the governing dimensionless numbers, one sees that the moving wall simulations are governed by Ca only, and interjector-fed simulations are governed by Ca and We numbers. Thus, their validity and the strict existence of liquid slug vortices are also questionable.

An extensive review of mass transfer into wavy film flows is given by Sisoev et.al from a non-CFD perspective [160]. CFD applications are summarized by Wörner [161].

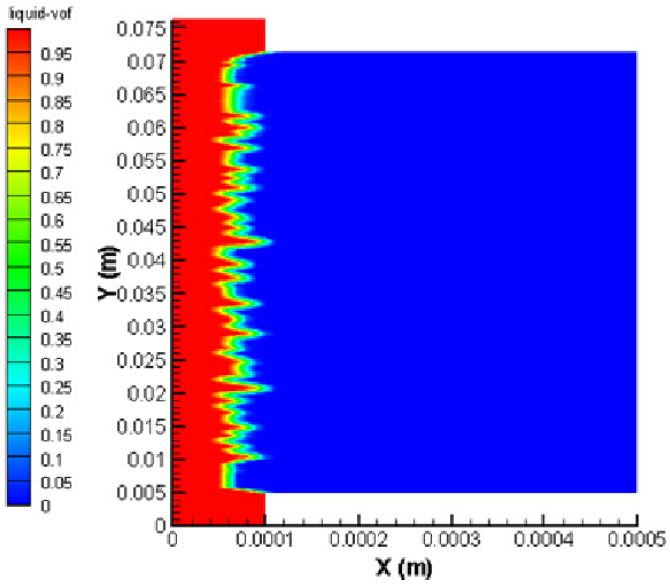

Figure 19. Volume fractions of liquid (red) and gas (blue) in an FFMR. Significant wave formation is predicted by CFD. From [153], used with permission of Elsevier.

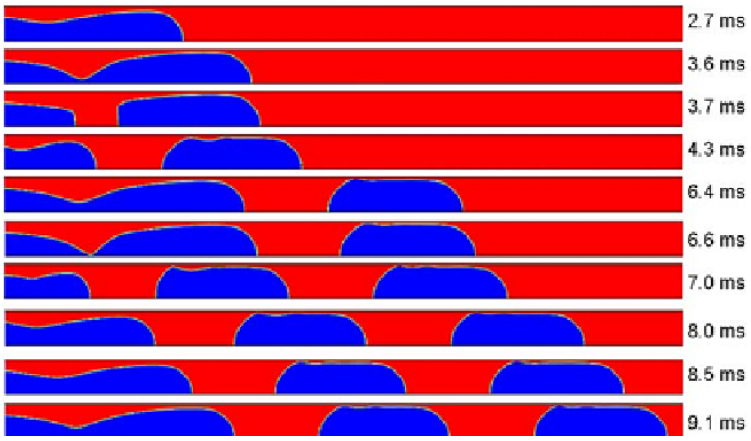

Figure 20. Taylor bubbles in a capillary, split into two from its symmetry axis. The flow is resolved to the lubricating film by using a very fine mesh. Note that even in such small scales, small waves still propagate on the perimeter of bubbles. From [154], used with permission of Elsevier.

2.10. Fischer-Tropsch Synthesis

Fischer-Tropsch (FTS) is an important coal/natural gas-to-liquids technology, where synthetic fuels like higher hydrocarbons can be generated from syngas, i.e. CO-H_2 mixture, over a catalyst, according to the following descriptive reaction

$$(2n + 1)\,H_2 + n\,CO \rightarrow C_nH_{2n+2} + n\,H_2O \qquad (71)$$

The chemistry and engineering of the synthesis is being studied for about 80 years, with still alive prospects of a leap in its technological implementation. The process is of great importance, since it is one of the main technologies to produce crude oil when oil reserves begin to deplete or oil gets expensive.

2.10.1. Kinetics

For FTS, one may use iron, cobalt or ruthenium catalysts. In case of iron catalysts the water-gas shift reaction, which produces H_2 and CO_2, also takes place. The process is usually performed at pressures range of 0.5-2.5 MPa and at a temperature range of 200-300 ℃ for the so-called low temperature synthesis. A general mechanism for FTS proposed by Kellner and Bell [162] is given by Equations-(72). The mechanism of the reaction is based on the formation of methyl groups on the surface, growing by coupling with adsorbed methylene (or carbine) to larger carbon chains, while simultaneously terminating into desorbed linear α-olefins and paraffins. The probability of growth is denoted by α, and called as the chain growth probability. Since the FTS is actually a polymerization reaction, an Anderson-Schulz-Flory distribution emerges, which limits the selectivity to a certain range of products. Both α and the olefin-to-paraffin ratio (OPR) depends on the nature of the catalyst and on the characteristics of operation. Since higher hydrocarbons are aimed for the production of commodity fuels, like diesel for example, conversion and selectivity must be both high. This brings along many difficulties in FTS reactor design.

$$
\begin{aligned}
&H_2 + 2* \rightarrow 2\,H* \\
&CO + * \rightarrow CO* \\
&CO* + * \rightarrow C* + O* \\
&C* + H* \rightarrow CH* + * \\
&CH* + H* \rightarrow CH_2* + * \\
&O* + H* \rightarrow OH* + * \\
&OH* + H* \rightarrow H_2O + 2* \\
&CH_2* + H* \rightarrow CH_3* + * \\
&CH_3* + H* \rightarrow CH_4 + 2* \\
&R_n* + CH_2* \rightarrow R_{n+1}* + * \\
&R_n* + H* \rightarrow P_n + 2* \\
&R_n* \leftrightarrow O_n + H* \\
&R_2* \leftrightarrow O_2 + H*
\end{aligned}
\tag{72}
$$

At high temperatures and high H_2/CO feed ratios, termination is favored, leading to shorter chain hydrocarbons. Conversely, low H_2/CO feed ratios result in high selectivity towards olefins. It is also known that CO has a strong poisoning effect that heavily decreases conversion, especially on the cobalt catalyst.. Unlike paraffins, the termination step of olefins is reversible, thus OPR decreases as chain length increases. Since longer chain olefins form the basis of many chemicals and untreated low octane number gasoline, low OPR ratios might not be desirable [163].

Although the reaction mechanism is very complex, very simple empirical rate equations are proposed after validating them in a certain range of operation. For example Post et. al. [164] proposed a very simple first order rate with respect to CO for iron and cobalt based catalysts:

$$-r_{CO} = k_{CO} C_{CO} = -\frac{1}{2} r_{H_2} = \frac{1}{2} k_{H_2} C_{H_2} \tag{73}$$

which represents severe diffusion limitations in the liquid filled pores for particle sizes greater than 1mm. The expression is valid for CO conversions up to 60% [165]. Considering Langmuir-Hinshelwood-Hougen-Watson (LHHW) kinetics, Yates and Satterfield [166] fitted their experimental data best to:

$$-r_{H_2+CO} = \frac{a P_{H_2} P_{CO}}{(1 + b P_{CO})^2} \tag{74}$$

where a and b are temperature dependent parameters:

$$a = 8.8533 \cdot 10^{-3} \exp\left[4494.14\left(\frac{1}{493.15} - \frac{1}{T}\right)\right]$$
$$b = 2.226 \exp\exp\left[-8236\left(\frac{1}{493.15} - \frac{1}{T}\right)\right] \quad (75)$$

Dixit and Tavlarides [167] also arrived to the same rate expression upon testing their experimental data to a large class of LHHW models. Yates and Satterfield's model have seen a large acceptance and used in many model studies, including monolithic reactors [168].

The FTS is an exothermal process. Various activation energies are reported in the literature, generally it is between 120-170 kj/mol for iron and cobalt catalysts. Activation energies for methane synthesis on ruthenium are given on Table 5. Activation energy for ruthenium catalysts is much lower than the ones provided by iron and cobalt catalysts. The rightmost column presents the reaction orders with respect to H_2 and CO, for a general power law fit. Zimmerman and Bukur provides a similar table for iron based FTS [169].

Table 5. Activation energies and apparent reaction orders for ruthenium catalyzed FTS.

	Activation Energy (kj/mol)	Catalyst	Reactions Orders w.r.t. H_2 , CO
Dalla Betta et. al. [170]	24	1.5 % Ru/Al_2O_3	1.8, -1.1
Vannice [171]	24.2	5 % Ru/Al_2O_3	1.6, -0.6
Ekerdt and Bell [172]	24.1	5 % Ru/SiO_2	1.5, -0.6
Kellner and Bell [162]	28.2	1 % Ru/Al_2O_3	1.35, -0.99

2.10.2. Reactors and Modelling

From its invention in 1920's by Franz Fischer and Hans Tropsch, the FTS reactor has been continuously studied both experimentally and computationally to improve fuel yields. For a summary on conventional reactors, one may see de Deugd et.al. [163]. In terms of modelling and computation, new reactors and operations are being investigated in parallel with catalysis research. With the ascension of CFD and numerical methods, modelling studies have blossomed. In the Table 6 recent modelling studies, their anatomy and aims are given.

Table 6. Recent modeling studies of FTS synthesis in novel reactors

Work	Geometry & Setup	Kinetics	Heat-Mass Transfer	Notes, Aims/Accomplishment
de Deugd et. al. (2003) [258]	1D Rectangular channel, steady state, pseudohomogeneous.	Equation-(74), CoMgO catalyst, coated with finite thickness. 1-D diffusion reaction in the catalyst.	Overall mass transfer coefficients, heat transfer only in the liquid phase.	No results on selectivity and chain growth. The recycle ratios are investigated.
Bradford et. al. (2005) [259]	There is not much about a model, except pressure drop expressions.	None.	None.	Various properties of Co/Al_2O_3 catalysts are given. It is found that catalyst thickness is a critical parameter since it greatly enhances production.
Pangarkar et. al. (2009) [260]	2D species and energy equation with radial and axial diffusion contributions. Steady state and pseudohomogeneous, Athena Visual Studio®.	Equation-(74), Co/Al_2O_3 and $Co–ZrO_2$ catalysts.	Overall mass transfer coefficients, heat transfer only in the liquid. The value for the mass tr. coef. is not given.	The heat distribution and its effect on production and selectivity is observed for different structured packings with different conductivities, d_H's and porosities.
Vervloet et. al. (2009) [261]	Fluid flow is simulated inside a randomly packed catalyst with Lattice Boltzmann Method.	None.	None.	Ps.hom. models are found to be inaccurate for structured packings. Fluid flow simulations show that there are strict regions of channeling in such packings.

Table 6 cont'd. Recent modeling studies of FTS synthesis in novel reactors

Cao et. al. (2009) [262]	3D pseudohomogeneous heat and mass transfer in COMSOL.	Not given	3D flow equations are coupled with catalyst temperature and mass balance	Biot number justification and convective heat- mass transfer coefficients are not given. Smaller catalyst particles and higher pressures give lower methane selectivity and higher α. High H2/CO ratios increase CO conversion.
Visconti et. al. (2011) [263]	2D pseudohomogeneous heat and mass transfer.	Irreversible power law regressed from previous kinetic work, Co/Al_2O_3.	Overall transfer coefficients obtained from Graetz solutions in rectangular channels.	It is shown that low temperature FTS synthesis is feasible in monoliths with almost isothermal operation and negligible pressure drop.
N. Hooshyar et. al. (2012) [264]	1D pseudohomogeneous gas-liquid two-phase heat and mass transfer.	Equation-(74), catalyst not given.	Slurry bubble columns and multi-tubular fixed beds are compared.	Effect of axial dispersion on C_{5+} production is demonstrated. Reducing dispersion effects increase C_{5+} yield.
Hösükoğlu et. al. (2012) [265]	2D heat conduction, Brinkman equations and gaseous flow, liquid is absent, COMSOL.	The all components hydrocracking model of Pellegrini et. al. [266].	Concentration profiles are assumed to be continuous at the porous interface.	Although there is axial dispersion, Danckwerts' BC's [52] are not used. The effect of the thickness and heat conductivity of the monolith walls of conversion and selectivity is investigated.
Gümüşlü and Avcı (2012) [266]	Same with the one above.	Wang et. al.'s [267]model and data for a Fe-Cu-K catalyst.	Same with the one above.	The effects of coolant flow rates and etched grooves on walls of monolith channels are investigated.
Vervloet et. al. (2013) [267]	1D heat tr. with length correction, in place of the erroneous ps.hom. model.	None.	Nu estimated experimentally.	Considering closed cross-flow structure packing elements, an intelligent improvement has been done, without using detailed CFD models.

CHAPTER 3

MATERIALS AND METHODS

3.1. Gas-Liquid Reaction Experiments

In the first part of this study, gas-liquid reactions are studied experimentally and theoretically. For the gas-liquid reaction system, nitric oxide absorption in liquid phase is chosen due to availability of experimental facilities.

For NO absorption, the following setup given in Figure 21 is used. NO-N_2 mixture is drawn from a 100ppm tank (Linde) and dry air is drawn from ambient air. These gases are carefully mixed in 1:14 proportion with help of Teledyne 200 Series flow controllers. The mixed gas is then sent to the contactor. The details of the setup are given elsewhere [173].

A novel but simple contactor is manufactured from glass, which would allow a stratified gas-liquid contact with negligible amount of wave formation on the surface. A photo is given in Figure 22. The liquid side is in batch mode and gas flows over it. Liquid circulation is possible via a slow peristaltic pump. The contactor has a length of 15 cm and a diameter of 3 cm. The gas enters the contact region from the upper half of the cylindrical contactor; flowing in a truncated cylindrical geometry of 0.5 cm height. The rest of the contactor is filled with liquid of 8.2 mL volume.

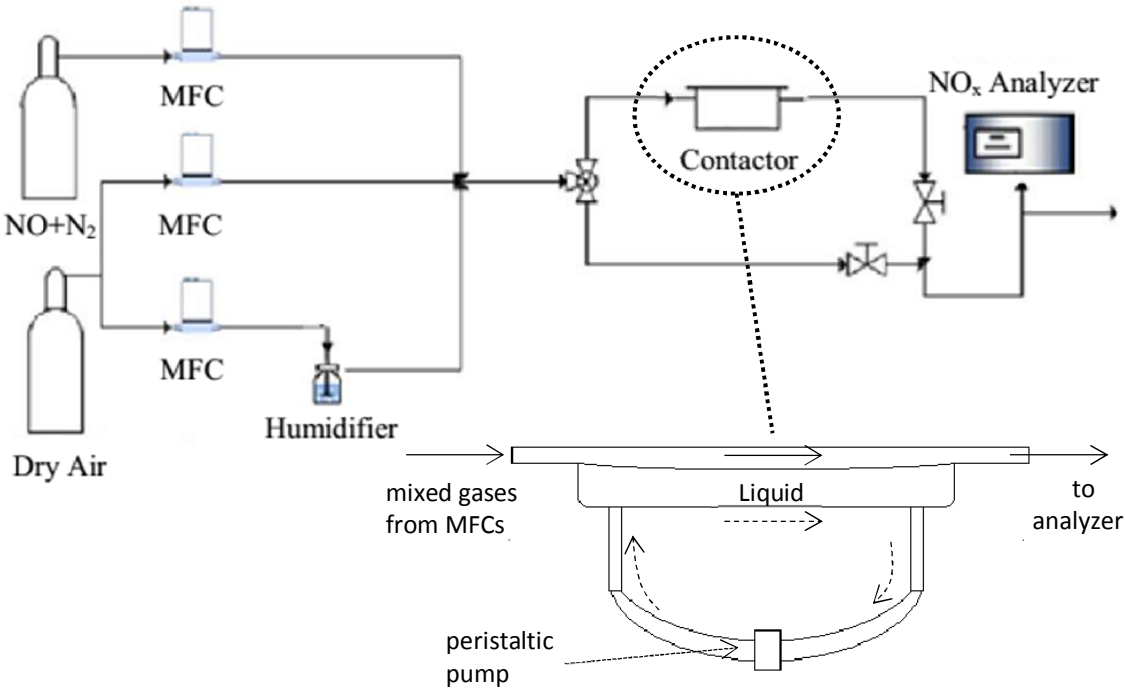

Figure 21. NO_x analyzer setup, adapted from [173].

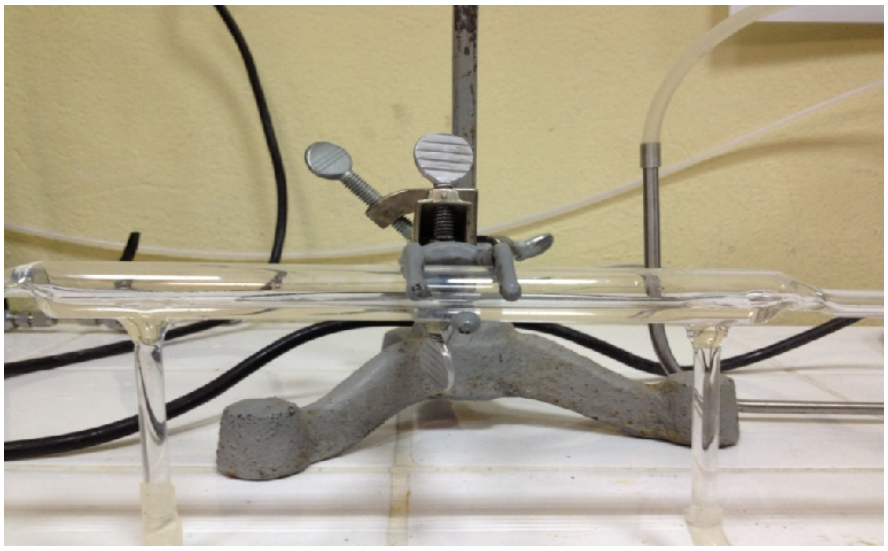

Figure 22. The gas-liquid contactor for NO_x absorption.

The outlet gas is analyzed by the online chemiluminescence NO_x analyzer (Thermo Scientific Model42i). The device can detect NO, NO_2 and NO_x amounts. The analyzer reacts NO with ozone to produce a characteristic luminescence with an

intensity that is almost linearly proportional to NO concentration. This process forms excited NO_2 molecules, according to the following reactions:

$$NO + O_3 \rightarrow NO_2^* + O_2$$

$$NO_2^* \rightarrow NO_2 + h_c v$$

The second reaction is the process of reaching an equilibrium state via chemiluminescence, where h_c is Planck's constant and v is frequency. Therefore, light energy is emitted. The emission may also be induced by collision with another molecule. The luminescence is detected by a photomultiplier tube inside the reaction chamber.

A schematic is given for the NO_x analyzer in Figure 23. The device draws dry air to generate ozone, which is required for the chemiluminescent reaction. The main inlet that the sample flows through is followed by a solenoid valve. The valve selects the operation mode. In the NO_x mode, molybdenum based NO_2-to-NO converter heats up the sample to about 325°C, so that NO_2 is converted to NO.

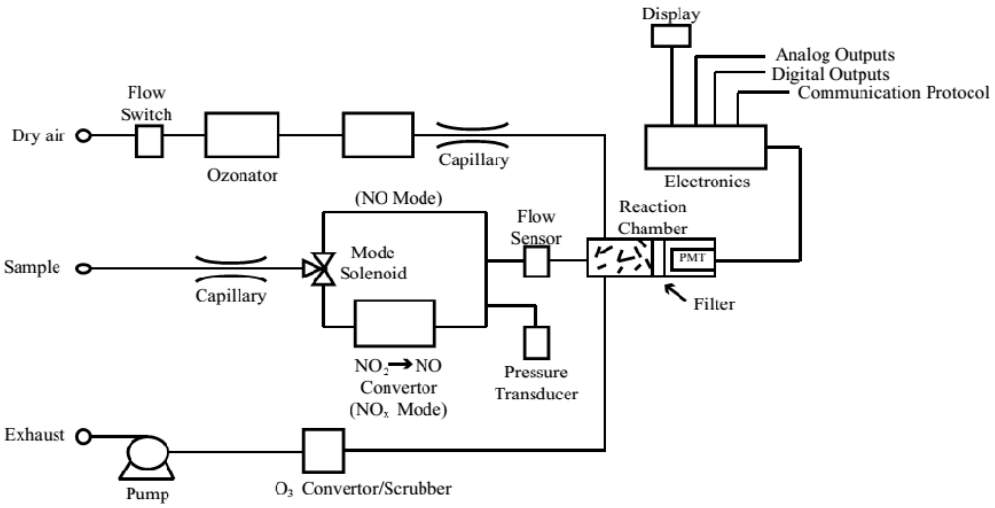

Figure 23. Interior setup of Thermo Scientific Model42i NO_x analyzer [173].

3.2. Mathematical Models and Methods

3.2.1. The Approximate Integral Balance Method (AIBM)

The approximate integral method is an approximate analytical method for partial differential equations (PDE). It dates back to von Karman and Pohlhausen [93, 174], who used the method for solving boundary layer problems. Among mechanical engineers, the method is also known as the heat balance integral method (HBIM) or Goodman's approximate integral method. The method can handle linear or nonlinear problems and reduces the PDE into an ordinary differential equation (ODE) [175]. Its mathematical basis and manipulations are fairly simple.

First, the method aims to choose a polynomial profile which fulfills the boundary conditions. The selected profile is then tuned to satisfy the spatially integrated version of the PDE, but it does not satisfy the original equation. For propagation problems, where semi-infinite geometries may be assumed, the spatial integration has the boundaries 0 and a proposed penetration thickness, which propagates in time. Beyond the penetration thickness, there is no variation and no material flow. For fixed domains, the penetration thickness is constant, but values at the boundaries may change. For simplicity, propagation problems will be discussed here.

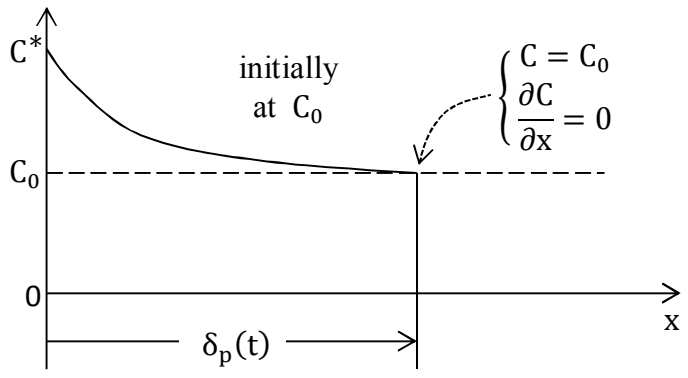

Figure 24. The penetration thickness concept in AIBM.

One may demonstrate a simple example by considering the equation set for PT. Integration of the PDE from 0 to $\delta_p(t)$[23] [176] yields:

$$\int_0^{\delta_p(t)} \frac{\partial C}{\partial t} dx = D \frac{\partial C}{\partial x}\Big|_{x=\delta_p(t)} - D \frac{\partial C}{\partial x}\Big|_{x=0} \tag{76}$$

where the first term on the right hand side is considered to be zero since there is no flow into the outer layer of the penetration thickness, as discussed above. By using Leibnitz's rule:

$$\frac{d}{dt}\int_{a(t)}^{b(t)} f(x,t)dx = \int_{a(t)}^{b(t)} \frac{\partial f(x,t)}{\partial t} dx + f[b(t),t]\frac{db}{dt} - f[a(t),t]\frac{da}{dt} \tag{77}$$

the derivative at left hand side can be taken out:

$$\frac{d}{dt}\int_0^{\delta_p(t)} C\, dx = \int_0^{\delta_p(t)} \frac{\partial C}{\partial t} dx + \frac{d\delta_p(t)}{dt} C_{\delta_p(t)} \tag{78}$$

From Figure 24, $C_{\delta_p(t)} = C_0$. Again for simplicity, assume that C_0 is zero for now. C_0 can always be normalized to be equal to zero, if initial distributions are uniform. This is also possible if the problem is linear and an initial steady state distribution exists[24] [177]. Letting $\theta = \int_0^{\delta_p(t)} C\, dx$:

$$-D\frac{\partial C}{\partial x}\Big|_{x=0} = \frac{d}{dt}\theta \tag{79}$$

Now that if a polynomial function of x that satisfies the boundary conditions is selected for the concentration profile, the above equation yields an ODE for the penetration thickness $\delta_p(t)$. As can be seen from Figure 24, $\delta_p(t)$ is present in boundary conditions, therefore it will also be present in the concentration profile. Integrating the ODE completes the AIBM solution. $\delta_p(t)$ adds the time dependent behavior to the polynomial profile. The complete example is given in Appendix-G with additional notes on the accuracy and use of AIBM.

[23] A variant is to integrate two times. This way is called as the refined integral method (RIM) or double integral method (DIM). Accuracy can be improved slightly in some cases.

[24] This is done by defining a deviation concentration $C_{dev} = C - C_{steadystate}$ and solving for C_{dev}.

3.2.2. Method of Lines (MOL)

MOL is a numerical method for solving parabolic or hyperbolic PDEs. It is one of the methods that transform boundary value problems (BVP) into initial value problems (IVP) [178]. Considering a simple 1-D diffusion problem with specified concentrations at both ends, one may discretize the spatial derivative with a finite difference formula. For example, by using a 3 point central difference formula, the nodal values of concentration can be expressed as:

$$\frac{\partial C_j(t)}{\partial t} = \frac{D}{\Delta x^2}\left[C_{j-1}(t) - 2C_j(t) + C_{j+1}(t)\right], \qquad 1 \le j \le N+1 \quad (80)$$

Considering L as the thickness as the domain, the grid size is given as $\Delta x = L/(N+1)$ with N as the number of intervals. The above equation is now a set IVP-ODEs. In matrix form:

$$\mathbf{C'} = \mathbf{MC} + \mathbf{S} \quad (81)$$

where $\mathbf{M}$ is the coefficient matrix and $\mathbf{S}$ is the source vector. This system can be solved by many seasoned ODE solvers, such as Runge-Kutta (RK) variants. The advantage of MOL over finite differences (FD) is that these solvers can be employed to get a quite correct transient behavior and stability in terms of time integration can be assured. For hyperbolic problems, specific integrators like the Runge-Kutta-Nyström method [179] might be employed.

Mathcad®[25], which has an internal MOL solver, is used for solving simple parabolic differential equations. Mathcad can employ five point differences, which are 4^{th} order accurate [180]. Time integration pattern is black box, but since the system of equations is solved recursively, the application of a backward differentiation formula (BDF) is probable. The solver is found to be quite robust, fast and practical. For most cases, the solver is found to handle nonlinear equations. However, for nonlinear BC's of the second or third kinds with large transfer coefficients, significant artificial diffusion is detected. In such a case, time steps are taken smaller. A representative screen is given on Figure 25.

[25] Mathcad is a trademark of PTC Inc.

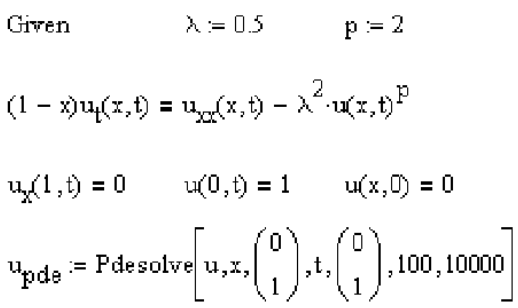

Figure 25. Mathcad screen for the MOL solution of the PDE representing diffusion with second order reaction in Couette flow.

3.2.3. Shooting Method

Shooting method is a way to convert BVP-ODEs into IVP-ODEs. After obtaining an IVP one may again employ RK solvers to get the solution. Assume that y is the solution of a general nonlinear second order ODE with the boundary conditions:

$$y(a) = A\,, \qquad y(b) = B \tag{82}$$

There should be an α, such that the boundary condition

$$y'(a) = \alpha \tag{83}$$

would also give the same result instead of the Dirichlet boundary condition as $x = b$. Assuming y as a function of α , as well as x, one may show the conformity by [181]:

$$f(\alpha) = y(\alpha, b) - B = 0 \tag{84}$$

One may try to solve this equation with Newton-Raphson method:

$$\alpha_{i+1} = \alpha_i - \frac{f(\alpha_i)}{f'(\alpha_i)} \tag{85}$$

Since function f is not known, one should use a backward finite-difference formula for $f'(\alpha_i)$:

$$f'(\alpha_i) = \frac{f(\alpha_{i-1}) - f(\alpha_i)}{\alpha_{i-1} - \alpha_i} \tag{86}$$

Newton-Raphson method modified by Equation-(86) is called as the secant method [182]. Then Equation-(85) becomes:

$$\alpha_{i+1} = \alpha_i - \frac{(\alpha_{i-1} - \alpha_i)[y(\alpha_i, b) - B]}{[y(\alpha_{i-1}, b) - y(\alpha_i, b)]} \qquad (87)$$

Thus with two initial guesses, α can be found by iterating Equation-(87). When α is obtained, then the problem becomes an IVP, so that it can easily be solved by RK integrators. A Mathcad screen is provided in Figure 26.

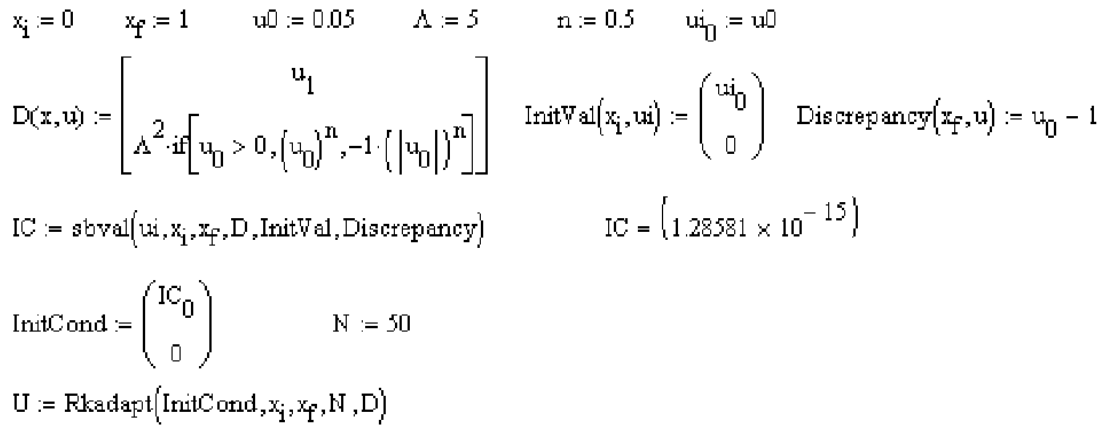

Figure 26. Mathcad screen for the solution of the steady-state diffusion-reaction problem with fractional order kinetics. First, the shooting method is applied, then this is followed by adaptive Runge-Kutta integration.

Mathcad is used for most of the calculations except the more complicated numerical solutions, which are provided by COMSOL®[26]. Mathcad is found to be fast, dynamic and time saving during repetitive tasks and trial-error. Since the program allows code writing and involves a symbolic solver, it can be used an all-around mathematical tool. In the text where it is noted that a computer algebra system (CAS) has been used, it points out to Mathcad usage. The integrals and equations that come up in the analytical parts of this study was evaluated and plotted with the program.

[26] Formerly FemLAB, Comsol Multiphysics is a trademark of COMSOL Inc.

3.2.4. Finite Element Method and COMSOL

The finite element method (FEM) is a widely used numerical method to solve general forms of partial differential equations of arbitrary geometries. It has two formulations: The Ritz method and the Galerkin method. Ritz method is the predecessor of Galerkin method, and it is usually preferred for structural problems. Here, Galerkin method will be summarized, since it is more general and it has been incorporated into various commercial solvers, like COMSOL, to handle fluid flow, heat and mass transfer, electrical and acoustical problems.

It seems mandatory to select a specific function to exemplify the method. Consider the linear three dimensional diffusion-reaction equation of the general form:

$$\begin{aligned} 0 &= \nabla(\mathrm{D}(\mathrm{x},\mathrm{y},\mathrm{z})\nabla\mathrm{C}) - \mathrm{kC}\,, \qquad \text{on R} \\ \mathrm{C} &= \mathrm{a}(\mathrm{x},\mathrm{y},\mathrm{z}), \qquad \text{on } \partial\mathrm{R}_1 \\ \mathrm{D}\frac{\partial \mathrm{C}}{\partial \mathrm{n}} &= -\mathrm{p}(\mathrm{x},\mathrm{y},\mathrm{z})\mathrm{C} + \mathrm{q}(\mathrm{x},\mathrm{y},\mathrm{z}), \qquad \text{on } \partial\mathrm{R}_2 \end{aligned} \tag{88}$$

where R is the region that the equation is to be solved on, $\partial \mathrm{C}/\partial \mathrm{n}$ is the directional derivative in the direction of the normal vector of the boundary $\partial\mathrm{R}_2$. The other part of the boundary is $\partial\mathrm{R}_1$, on which a Dirichlet boundary condition is given. Now one multiplies the equation with a *trial function* Ξ (or shape element) which is so selected to be zero on $\partial\mathrm{R}_1$:

$$\iiint_{\mathrm{R}} [\nabla(\mathrm{D}(\mathrm{x},\mathrm{y},\mathrm{z})\nabla\mathrm{C}) - \mathrm{kC}]\Xi \,\mathrm{dxdydz} + \iint_{\partial\mathrm{R}_2} \left[-\mathrm{D}\frac{\partial \mathrm{C}}{\partial \mathrm{n}} - \mathrm{pC} + \mathrm{q}\right]\Xi \,\mathrm{dA} = \text{Residual} \tag{89}$$

After applying the divergence theorem and some vector calculus, if the following form of a solution is assumed:

$$\tilde{\mathrm{C}}(\mathrm{x},\mathrm{y},\mathrm{z}) = \Omega(\mathrm{x},\mathrm{y},\mathrm{z}) + \sum_{\mathrm{i}=1}^{\mathrm{M}} \mathrm{b}_{\mathrm{i}}\, \Xi_{\mathrm{i}}(\mathrm{x},\mathrm{y},\mathrm{z}) \tag{90}$$

one can obtain the equation:

$$\iiint_{\mathrm{R}} \left[\left(\mathrm{D}\nabla\tilde{\mathbf{C}}\right)\nabla\Xi_{\mathrm{i}} - \mathrm{k}\tilde{\mathrm{C}}\Xi_{\mathrm{i}}\right]\mathrm{dxdydz} + \iint_{\partial\mathrm{R}_2} \left[-\mathrm{p}\tilde{\mathrm{C}}\Xi_{\mathrm{i}} + \mathrm{q}\Xi_{\mathrm{i}}\right]\mathrm{dA} = \text{Residual} \tag{91}$$

The above equation is called as the weak formulation and $\tilde{\mathrm{C}}$ is the weak solution. $\tilde{\mathrm{C}}$ is so found that the residual is minimized [181]. If it is zero, then the solution is exact.

COMSOL is a general PDE solver. It uses FEM and works according to the principles as summarized above [183]. However, for stability, convergence and accuracy many more mathematical complications are involved in the solvers.

COMSOL is an all-in-one numerical analysis package. That is, it includes the classical trio of pre-processing, solver and post-processing tools within. The pre-processing step involves the geometry constructor which is based on a CAD system. After drawing the geometry, one may define the boundary conditions, volume sources or necessary multiphysics couplings. Before solving the equations, the geometry must be meshed. Meshing is quite simple, triangular or quadrilateral cells can be selected. After meshing, the equations become ready to be solved. COMSOL has physics based solvers. By using them, COMSOL adapts to the type of problem by automatically arranging its solver scheme. On the other hand, one may directly use the kernel of the program to solve general types of PDEs and ODEs and manipulate the library of solvers manually. Adding various details like moving boundaries and sensitivity analysis is possible. However, without the physics packages, solving specialized equations like the Navier-Stokes may not be possible.

After the problem is solved, the remaining step is post-processing. This step involves the representation of results in form of plots and animations.

To run a numerical model with COMSOL, one may follow the general pathway as outlined below:

1. Select the dimensions of the geometry and then select the physics to be solved if specialized physics packages are available. If not, use the kernel.
2. Select the solver type. This may be a steady-state (stationary) solver or a transient solver.
3. Draw the geometry. Avoid the unnecessary details. Always use the symmetry if it is available in the geometry; this would save considerable time.
4. Define the boundary conditions and sources, and if there is, the initial conditions[27]. If the boundary conditions are time dependent, avoid sharp

[27] Even for steady-state solver, initial conditions appear. These work as initial guesses and may improve convergence, if appropriately selected.

changes and smoothen the functions if such variations are existent. Such sharp variable dependency may exist in physical properties.

5. Construct the mesh. A denser mesh is necessary to resolve the regions with steep gradients. If a quadrilateral mesh is used, its aspect ratio must be carefully arranged. For example, for boundary layers, very thin and long elements can be placed near the wall where the flow is always in the direction of the longer edges. This would capture the gradient very well. But if cross flow to such elements occur, these meshes give physically wrong results due to numerical diffusion.
6. Solve the equations. If a transient solver is selected, then adjust the time step to be taken by the solver. Even when the time steps are specified, COMSOL takes free steps in between to enhance accuracy by default. It can also take larger time steps if convergence is fast. Such a solver may not suitable to every problem. For a linear diffusion problem the decay the steady-state is exponential and the free behavior of the solver may speed up convergence. But for periodic steady-states that involve relatively sharp changes between each state, the solver is not suitable.
7. Plot the results or extract the data. Check mesh independency by reducing cell sizes. Reduce the absolute and relative errors (tolerances) to see if the solution is sufficiently accurate. Higher order trial functions can also be selected to establish the validity of the solution. If there is experimental data or an exact solution to a similar case, the numerical solution should always be validated.
8. If solution is to be reprised with different parameters, optimize the accuracy with respect to computing time.

The possibilities with COMSOL seem to be almost limitless, only that the limits emerge as computing times. Various couplings between species transport, heat transfer and fluid flow are possible. The program is also quite flexible in the sense that it allows almost any kind of user-defined functions for entering detailed boundary conditions or additional PDEs in general. The user-defined functions do not need to be written with a language and no compilations are necessary. All is embedded into the graphical user interface. For more complicated simulations, one

may interoperate COMSOL with Matlab®[28] to provide the necessary programming features.

COMSOL is relatively less black box than most software, since many of its solver features are transparent. Still, a source code is not available.

[28] Matlab is a trademark of Mathworks Inc.

CHAPTER 4

RESULTS AND DISCUSSION

4.1. Gas-Liquid Systems

4.1.1. NO Absorption in Ferrous Sulfate Solutions

The aim of this section is to experiment gas absorption on almost stagnant liquid layers. Such layers exist in microreactors, for example in FFMR's, when the liquid flow rates are much lower than gas flow rates [26]. Since the gravitational flow of the liquid film is slow, the film is almost stagnant with respect to the gas flowing above it and thereby the gas drags the liquid along.

NO uptake rates can be monitored online with the available NO_x analyzer. NO absorption has also an established literature, in terms of mass transfer and kinetics [184]. Various inorganic and organic materials, such as ferrous sulfate ($FeSO_4$) ions [41] and iron-EDTA complexes [185] have been included in water in past studies and enhanced absorption rates are observed. In this work, $FeSO_4$ are added to water, yielding the reaction [184]:

$$NO + Fe^{2+} \rightleftharpoons FeNO^{2+} \quad (92)$$

Like Hikita et. al. [41], 0.17 M H_2SO_4 is added to the stock solution of $FeSO_4$, which is 0.5 M, in order to prevent the oxidation of iron ions. After diluted with air and

saturated with water, the feed gas mixture consisted 7300-7350 ppb NO. Gas flow rate is 0.8 lt/min.

Initially, the NO mixture bypassed the contactor and sent straight to the NO_x analyzer. When the device calibrated itself, two two-way valves are simultaneously switched and the gas mixture is fed to the contactor. The analyzer sampled and reported the NO amounts at time periods of 10s.

In addition to the ferrous-acidic solution of 0.5 M, absorption into pure and tap water is also tested. Results of the experiments are given on Figure 27.

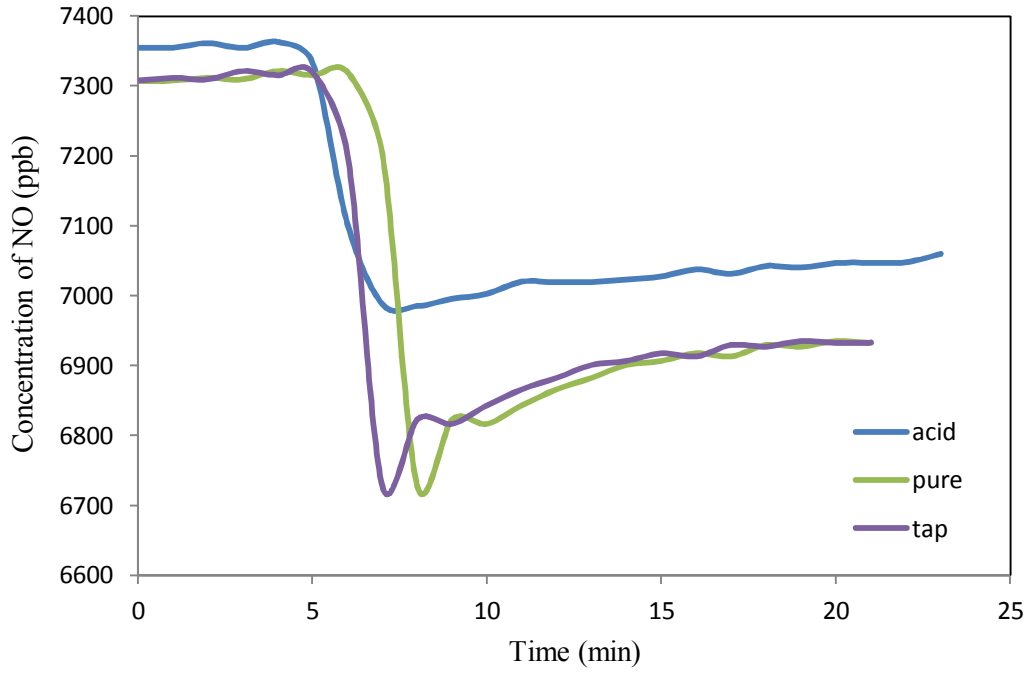

Figure 27. Time trend of NO concentration at the outlet of the contactor.

All of the liquids lead to a very sharp drop of NO concentration in the gas stream when valves are switched. Gas phase concentration time trends corresponding to pure and tap water are very similar. They both show broad oscillations (with an initial period on the order of several minutes), which may have attributed to convection currents induced by absorption and reaction. Interestingly, the ferrous

acidic solution leads to lower absorption rates. The oscillations also seem to be suppressed.

The reason for such a decrease in uptake rates may arise from interfacial turbulence. The existence of interfacial turbulence during CO_2 absorption was demonstrated long ago by Danckwerts [186]. When a gas is absorbed, density stratifications may occur, and these may lead to significant cellular convection patterns in the liquid. Another possibility is the variation of surface tension over the interface due to the differences in composition, that occur during absorption. These may lead to Marangoni effects. However, determining the exact mechanism seems to be difficult.

In macrocontactors like wetted walls and packed columns, it has been found that interfacial turbulence increases mass transfer rates [187]. However, there is also experimental data on near quiescent fluids, where mass transfer is hindered [188]. On thinner films supplied by laminar jets and falling films, such inhibitory effects are also observed. [189, 190]. It is proposed that a stagnant layer comprising ions form on the interface. Ions usually stem out of reactions, for example in the absorption of CO_2 with monoethanolamine (MEA) solutions:

$$CO_2 + 2RNH_2 \rightarrow RNHCOO^- + RNH_3^+$$

It has before said that the presence of ions may lead to an interfacial resistance. In addition, if the surface tension of this layer is larger than in the bulk, then cellular convections are enhanced. But if they are low, the currents will be slightly damped, leading to larger residence times on the surface. This prolonged surface layer would then be saturated with the gas and reactant; thereby uptake rates decrease. In another perspective, one may also say that the effective diffusivity is concentration dependent, and changes near the interface. Measurement of the surface tension of the stagnant layer is found to be quite difficult, and cannot be accomplished by standard methods [186].

Recently, such surface poisoning is also observed in FFMR's [191]. The addition of NaOH to water for CO_2 capture resulted in lower liquid side mass transfer coefficients than in absorption to pure water. The results have been attributed to Marangoni effects.

So the reason for the oscillations for runs made with pure and tap water may be the interfacial turbulence, which occurs in form of slow convection currents. The currents are slow since the period of oscillations are on the order of minutes. For the liquid containing ferrous sulfate solutions, the behavior may result by a poisoning effect due to the forming $FeNO^{2+}$ ions on the interface. These ions may be clinging on interface and forming the reckoned stagnant layer, thereby slowing absorption and diffusion. This effect seems to be analogous to the effect provided by surface-active substances during mass transfer [44]. . Furthermore, the reduced uptake rates in the acidic solution may be due to heat effects. It is possible that the absorbed gases may desorb when the interface gets heated by the enthalpy of absorption. The acidic solution would be a better conductor of heat; hence if the oscillations are due to heat effects, they would be suppressed in the acidic solution.

The similar effects observed in FFMR's may be due to the same mechanisms proposed above. If this is so, microreactors can have significant disadvantage in multiphase synthesis and separation when compared to macrocontactors, which usually have constant mixing effects due to stirring, complex flow geometry (like packed beds) or flow instabilities (like waves on a wetted-wall column) that possibly lead to breakage of such stagnant surface layers. However, in order to exactly determine the mechanism of the absorption and its importance in microsystems, more experiments with smaller and isothermal contactors seem to be necessary.

4.1.2. Limits of Penetration Theory

In the previous section a significant phenomenon in mass transfer is given experimentally. Beginning from this section, the study will follow a mathematical basis. On analytical grounds, the aim of this section is to describe the limits of penetration theory and film saturation-depletion in a quantitative manner. It might be considered as an extension to Pohorecki's [103], van Elk et al.'s [104] and Yue et al.'s work [192].

In addition to physical absorption, PT with chemical reaction can theoretically be used both for the steady and the transient stages depending on Fo and Λ. High Fo

numbers decreases Λ, since $\Lambda = \sqrt{\mathrm{Da}/\mathrm{Fo}}$. Then this would indicate a relatively slow reaction, thin film or fast diffusion. Based on this judgments, high Fo and low Λ, both point out a possible saturation in a finite film. To find the transition period to saturation, one can calculate the time to reach the wall via the approximate penetration thickness concept, as given by Equation-(21) for plug flow. However, Equation-(21) is only valid for physical absorption and in the presence of reaction, such limits are not readily apparent.

In this section, the use of Thiele modulus is encouraged, since in a finite medium, mass transfer with homogeneous chemical reaction is essentially very similar with solid-gas kinetics in a porous catalyst, except for the velocity profiles in the film. Also the criteria given in Table 4 might provide additional errors to the effects of finiteness.

The number of PT based models is huge and a large class of gas-liquid reaction cases has been complied by Doraiswamy and Sharma [193], which includes real applications from gas purification to synthesis of specialty chemicals. Therefore, for systems with small characteristic lengths for diffusion, one may want to know whether one can use the PT type analytical solutions, in order to utilize the literature.

Hereby, some special cases of the convection-diffusion equation will be analyzed:

$$\mathrm{v_z}(\mathrm{x},\mathrm{z})\frac{\partial \mathrm{C_A}}{\partial \mathrm{z}} = \mathrm{D_A}\frac{\partial^2 \mathrm{C_A}}{\partial \mathrm{x}^2} - \mathrm{r}\left(\mathrm{C_A}, \mathrm{C_{i_{i\neq A}}}\right), \qquad \mathrm{i} = \mathrm{B},\mathrm{C},\mathrm{D}\ldots \qquad (93)$$

Equation-(93) is an enhanced version of Equation-(13). It includes a general reaction and velocity field terms; and neglects gas-liquid interfacial dynamics by assuming a flat and stationary interface. Axial dispersion is not accounted for since Péclet numbers are usually large (see Table 2 as an example).

The reaction term $\mathrm{r}\left(\mathrm{C_A}, \mathrm{C_{i_{i\neq A}}}\right)$ will be taken as zero for physical absorption, and then as $\mathrm{kC_A^n}$, indicating a pseudo $\mathrm{n^{th}}$ order reaction[29]. This would be the case for gases reacting with pure fluids, like hydrogenation or ethoxylations reactions [28]. NO absorption in pure water presented in the previous section is also an example. However, for gases reacting with soluble compounds that are present in the liquid,

[29] The reaction rate constant k can also be given as $\mathrm{k_2 C_{B_0}}$ is this case.

bimolecular reactions would occur. For a second order bimolecular reaction with the rate equation $r(C_A, C_{i_{i\neq A}}) = k_2 C_A C_B$, Danckwerts [57] qualitatively showed that if $kC^*t < 1$, the system behaves approximately as a pseudo-first order reaction-diffusion case. This would indicate low solubility, relatively low contact times[30] or slow reactions. In terms of E_i and $\sqrt{M}$, this would correspond to the 2nd and 3rd regimes given in Table 3. For fast reactions, high C_{B_0} seems to be needed to avoid depletion of the reactant B and to enhance reaction rates.

What is defended here is that for bimolecular reactions, the pseudo order approximation does not depend on the finiteness on the liquid film. Thus, as long as it holds for a bimolecular second order reaction, then the Hikita-Asai approximation (HAA) can be employed to a certain degree, and the effects of saturation and the effects of velocity profiles will provide the main errors when PT models are used.

Although simple, PT for physical absorption will be treated first, since its limits are not given in a quantitative manner by van Elk et al [104]. The existence of interfacial resistance is also omitted in this section. The analysis is not completely specific to gas-liquid mass transfer, but also can be employed to relevant fields involving mass transfer accompanied by chemical reactions.

4.1.2.1. Limits of Penetration Theory for Physical Absorption

Instead of tracking the penetration thickness, which does not have a distinct value, one may track the changes at the surface flux and compare this with the exact solution. This is more rational, since for a certain period, the surface flux does not change much, even when the solute reaches to the wall and accumulates there [104]. This means that PT may be applicable with a small error for a period after $\delta_p = \delta$. Considering the amounts absorbed, PT should be accurate enough for Fourier numbers well above 0.1. Thus, one may calculate the amounts absorbed via Equation-(19), and compare with the results obtained from the numerical solutions of the following non-dimensional problem:

[30] This does not directly indicate that Fo is low.

$$f(\xi)\frac{\partial u}{\partial \tau} = \frac{\partial^2 u}{\partial \xi^2} \qquad \begin{array}{ll} \text{at } \tau = 0, & u = 0 \\ \text{at } \xi = 0, & u = 1 \\ \text{at } \xi = 1, & \partial u/\partial \xi = 0 \end{array} \qquad (94)$$

The function $f(\xi)$ denotes the velocity field and it is taken as 1, $1 - a\xi$ and $1 - \xi^2$ representing plug flow (or a quiescent fluid), generalized Couette flow and film flow (see Appendix-D). For the sake of completeness, an analytical solution for generalized Couette flow is also provided with its eigenvalues. All of the solutions, surface flux and absorbed amount expressions for these cases are given in Appendix-A. The comparison of the amounts absorbed is given below in Figure 28, as plots of relative percent error. It is important to note that the curves are universal, since no parameters are involved except the coordinate axes.

The simple Couette flow ($a = 1$) yields the lowest limits, use of PT in this case results in about 10% error when $Fo \cong 0.1$, but quickly rises to 50% around $Fo \cong 0.4$. At such Fo numbers, the error when compared to plug flow is less than 10%. The error with respect to film flow lies in between these values. The behavior of generalized Couette flow can also be discussed on these results. As $a \to 0$, the error curve for generalized Couette flow will tend to the red curve of plug flow, as can be seen from the dotted and dashed-dot green lines representing Couette flow with $a = 0.5$ and $a = 0.2$ respectively. The initial errors are due to the flow field near the interface, and the errors that accumulate sharply for long times are due to saturation. From the red line for plug flow, it can be seen that the limit based on the penetration thickness, as given by Equation (22), is too stringent. Thus, PT solutions can be used for $Fo < 0.7$ within 10% error for a finite film in plug flow. In general, it may be said that for monotonically decreasing flow profiles (like the ones used here), the limits decrease as the average velocity decreases. For the profiles considered here, PT can be said to be valid for $Fo < 0.3$. If instantaneous surface fluxes were considered, limits would then be much lower for all flow fields.

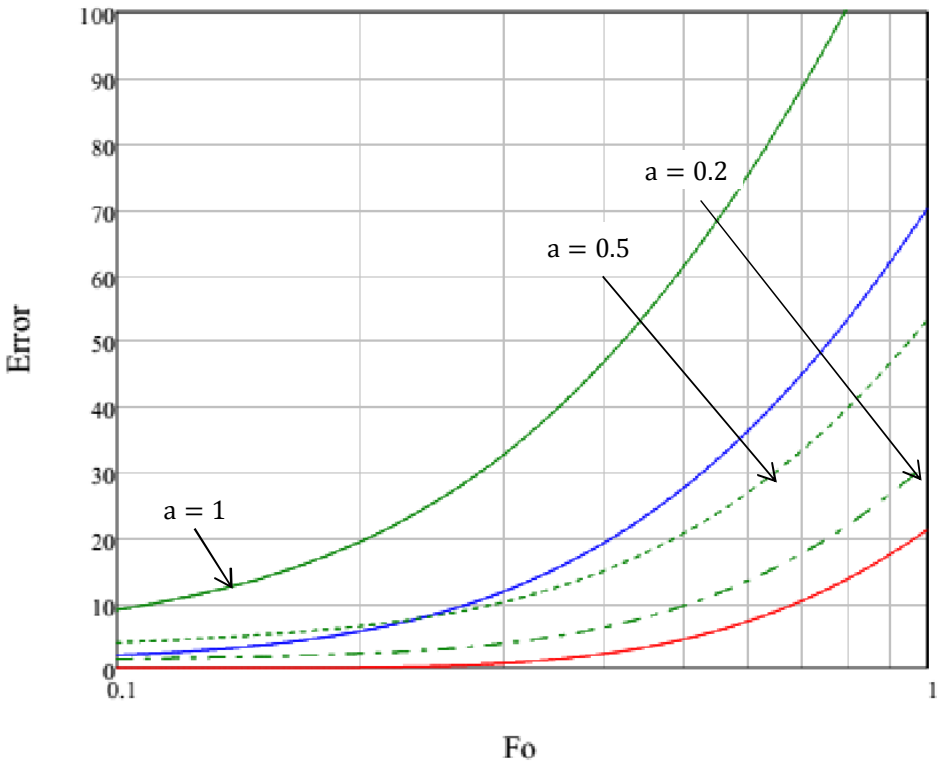

Figure 28. Relative percent errors between surface fluxes predicted by PT and the exact solutions for diffusion into a finite flowing film. Green: Couette flow, blue: film flow, red: plug flow.

4.1.2.2. Effect of Velocity Fields on Reactive Absorption

The effect of a velocity field to mass transfer is a complicated topic, and many analyses have been performed. However, Gottifredi et.al. [194] have provided a useful insight on the applicability of the PT in flow conditions. Considering the field as $v_z(x)$ only and with a first order reaction, they normalized Equation-(93) in a different way and expanded the velocity term with a Taylor series:

$$\left(1+\frac{\varepsilon_1}{\Lambda}\xi^*+\frac{\varepsilon_2}{\Lambda^2}\xi^{*2}+\cdots\right)\frac{\partial u}{\partial \tau}=\frac{\partial^2 u}{\partial \xi^{*2}}-u \qquad (95)$$

where

$$\varepsilon_1=\delta\frac{(dv/dx)|_{x=0}}{v_i};\ \varepsilon_2=\frac{\delta^2}{2}\frac{(dv/dx)|_{x=0}}{v_i};\ \tau=\frac{kz}{v_i};\ \xi^*=\frac{x}{\delta}\Lambda \qquad (96)$$

v_i is the interfacial velocity. The series expansion is valid as long as v_i is not close to zero and the penetration depth is not very far away. The resulting PDE is linear and superposed functions in the brackets immediately suggest a solution of the form:

$$u = u^0(\xi^*, \tau) + \frac{1}{\Lambda}u^1(\xi^*, \tau) + \frac{1}{\Lambda^2}u^2(\xi^*, \tau) + \cdots \qquad (97)$$

Replacing this into the original form of Equation-(93) generates a series of PDE's. The first one is:

$$\frac{\partial u^0}{\partial \tau} = \frac{\partial^2 u^0}{\partial \xi^{*2}} - u^0 \qquad (98)$$

and it is equivalent to Equation-$\frac{C}{C^*} = \frac{1}{2}\exp\left(-\sqrt{\frac{k}{D}}x\right)\operatorname{erfc}\left[\left(\frac{x}{2\sqrt{Dt}} - \sqrt{kt}\right)\right] + \frac{1}{2}\exp\left(\sqrt{\frac{k}{D}}x\right)\operatorname{erfc}\left[\left(\frac{x}{2\sqrt{Dt}} + \sqrt{kt}\right)\right]$ (24) given by Danckwerts. The other PDE's which stem from other terms with higher superscripts does not have known solutions, but from Equation-(97) one may easily say that PT is a first approximation to Equation-(95) with an error of the order of $1/\Lambda$.. To demonstrate the validity of this reasoning, PT can be tested along numerical solutions, in combination with the HAA to accommodate higher reaction orders. Hence Equation-(48) can be incorporated into Equation-$\frac{C}{C^*} = \frac{1}{2}\exp\left(-\sqrt{\frac{k}{D}}x\right)\operatorname{erfc}\left[\left(\frac{x}{2\sqrt{Dt}} - \sqrt{kt}\right)\right] + \frac{1}{2}\exp\left(\sqrt{\frac{k}{D}}x\right)\operatorname{erfc}\left[\left(\frac{x}{2\sqrt{Dt}} + \sqrt{kt}\right)\right]$ (24), then the dimensionless surface flux expression can be obtained.

$$-\left.\frac{\partial u}{\partial \xi}\right|_{\xi=0} = \Lambda\sqrt{\frac{2}{n+1}}\operatorname{erf}\left(\Lambda\sqrt{\frac{2\tau}{n+1}}\right) + \frac{1}{\sqrt{\pi\tau}}\exp\left(-\Lambda^2\frac{2\tau}{n+1}\right) \qquad (99)$$

This expression is compared with the numerical solutions of the problem solved with MOL:

$$f(\xi)\frac{\partial u}{\partial \tau} = \frac{\partial^2 u}{\partial \xi^2} - \Lambda^2 u^n \qquad \begin{aligned} &\text{at } \tau = 0\,, \quad u = 0 \\ &\text{at } \xi = 0\,, \quad u = 1 \\ &\text{as } \xi = 1\,, \quad \partial u/\partial \xi = 0 \end{aligned} \qquad (100)$$

$f(\xi)$ is taken as $(1-\xi)$ and $(1-\xi^2) + S(1-\xi)$. These represent Couette flow and film flow with shear, as can be seen from Appendix-D. The parameter S signifies the magnitude of the shear at the interface and it is taken as -0.2, representing counter

current contacting. The surface flux is obtained via a five-point central difference formula [180]:

$$-\left.\frac{\partial u}{\partial \xi}\right|_{\xi=0} \cong -\frac{-25u(0,\tau)+48u(\Delta\xi,\tau)-36u(2\Delta\xi,\tau)+16u(3\Delta\xi,\tau)-3u(4\Delta\xi,\tau)}{12\Delta\xi} \quad (101)$$

$\Delta\xi$ is the grid size, it is taken as 0.01. The comparisons and relative absolute percent errors are given in Figure 29.

The results show that PT with HAA gives the correct trend, but there is always an error in short contact times. It is observed that if the velocity increases away from the interface, then error increases significantly, as can be seen in the example of shear flow with counter-current shear. But when the interfacial velocity is the maximum, as for simple Couette flow, errors are very small. Since the system will eventually tend to the same steady-state independent of the flow profile, which is determined by Λ and the reaction rate expression, errors decrease substantially as concentration profiles settle. For larger Λ, errors vanish faster. It seems that these errors can be neglected for many cases for non-marginal flow patterns, since they decay very fast on the overall. This can be seen from the green and blue dotted lines on the right hand graphs of Figure 29.

However, an exception to this rule may emerge when the reaction rate term leads to a multiple steady states, hence the approach path to steady state may affect the final state. In the context of gas-liquid reactions, the possibility of such a case seems to be vague, in contrast of the highly non-isothermal systems or LHHW kinetics in gas-solid reactions.

Aside from all these, one can say that absorption with reaction is more suitable for the applications of PT than physical absorption in flowing films, since for long times, the reactants may not reach to the wall due to chemical reaction, and upon the settlement of steady-state, velocity effects vanish. However, the red lines with low Λ have an error that increases monotonously in both flow scenarios. This is due to finiteness of the system. In these cases, film starts to saturate with the reactant. This effect will be discussed below.

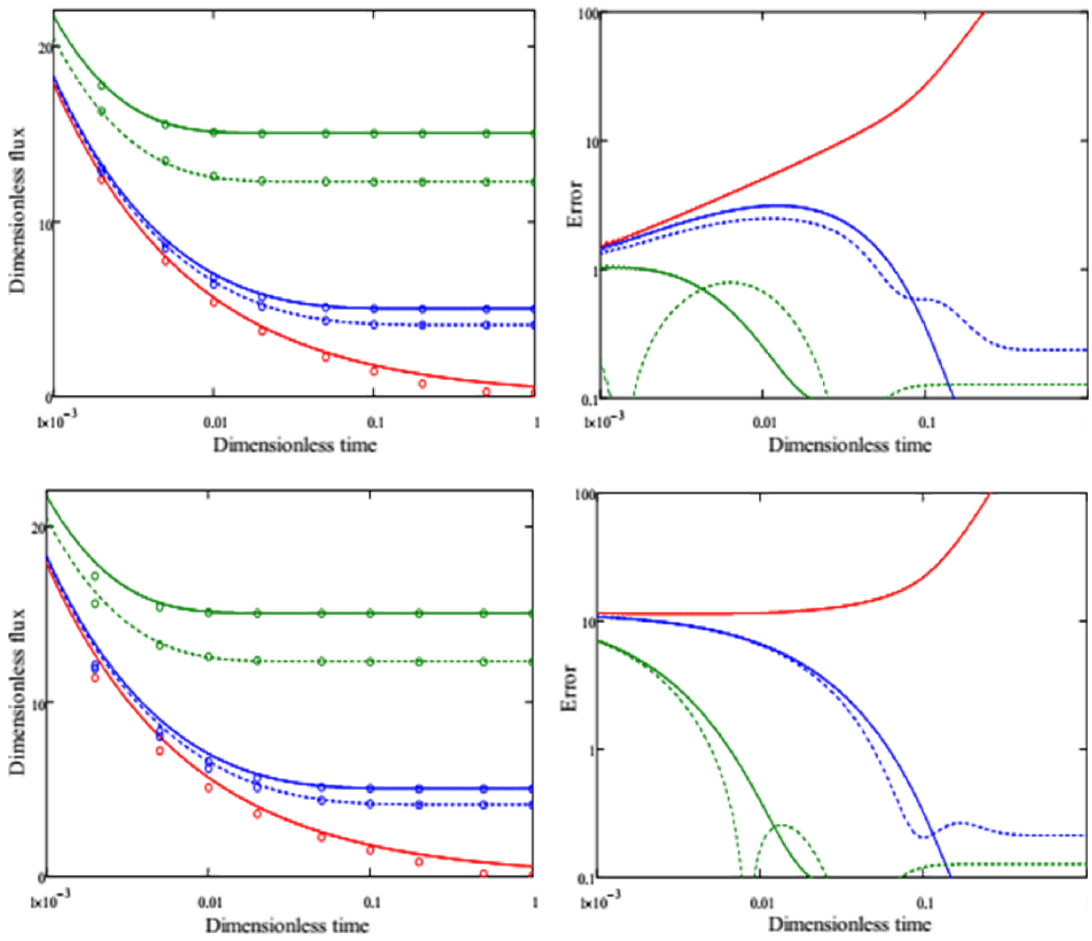

Figure 29. Red: $\Lambda = 0.1$; blue: $\Lambda = 5$; green: $\Lambda = 15$. Dots: numerical solutions; straight and dotted lines: results predicted by Equation-(99). Straight lines: first order reaction; dotted lines: second order reaction.

4.1.2.3. The Finite Film and the Critical Moduli

To investigate the limits of PT with respect to finiteness one may investigate the steady-state case of Equation-(93). If the exact steady-state flux matches HAA within acceptable error, then relatively simple PT models can be used. With pseudo n^{th} order kinetics, the steady and nondimensional from of Equation-(93) yields:

$$\frac{d^2u}{d\xi^2} = \Lambda^2 u^n \qquad \begin{matrix} \text{at } \xi = 1, & u = 1 \\ \text{at } \xi = 0, & du/d\xi = 0 \end{matrix} \qquad (102)$$

The coordinate system is reversed. This move is done for ease in analysis. Mehta and Aris [195] treated the above nonlinear problem as steady-state reaction-diffusion in catalyst slabs and obtained solutions describing the behavior of Thiele modulus and effectiveness factors. They used the convention $u(\xi = 0) = u_0$ as the concentration at the symmetry axis, which happens to be a wall in gas-liquid reactions, and obtained an expression of Λ in terms of u_0 and n. Their result indicates that wall concentrations are never zero when $n > 1$. For $n < 0$ there exist multiplicities since there are two wall concentrations, one of them is very low and the other is very high, for a single value of Λ. The multiplicity become especially severe for $n < -1$ and a distinct maximum for Λ emerges. Beyond this value, no steady solution exists. Since the HAA can account for $n > -1$ only and such low orders in gas-liquid reactions are very unlikely[31], the analysis will not include $n \leq -1$. For an almost clean liquid the approach to the steady state will also end up with the smaller u_0, most probably.

The results explained above stem from the following equations. The solutions for $n = -1$ and $n \leq -1$ are not given.

$$\Lambda = \sqrt{\frac{2}{n+1}}\, {u_0}^{-(n-1)/2}\, (1 - {u_0}^{n+1})^{0.5}\, F(0.5\,, 0.5 + q\,; 1.5\,; 1 - {u_0}^{n+1}), \qquad n > 1 \qquad (103)$$

$$\Lambda = \sqrt{\frac{2}{n+1}}\, (1 - {u_0}^{n+1})^{0.5}\, F(1\,, 1 - q\,; 1.5\,; 1 - {u_0}^{n+1}), \qquad |n| < 1 \qquad (104)$$

$F(a, b; c; d)$ is the hypergeometric function and $q = 1 / (n + 1)$. As $n \to 1$ Equations (103) and (104) become equivalent. The mathematical details and a brief re-derivation of Mehta and Aris' solutions are given in Appendix-B. The solution is used by many authors, for example Kulkarni and Doraiswamy [196] adopted and modified the solution methodology for the presence of a bulk phase. Recently York et al. [197] used the material for analyzing dead cores in catalyst particles. That is, in some cases, when Λ is great enough, there appears a significant dead region on the interval $0 < \xi < \xi_0$, with $(du/d\xi)_{\xi=\xi_0} = 0$ and $0 < \xi_0 < 1$. The same rationale can be used for gas-liquid reactions of pseudo orders and an unused part of the film may appear. Also for bimolecular reactions, this rationale is applicable as long as the pseudo-order approximation holds. For fractional orders, $0 < n < 1$, the dead region

[31] A possibility may be exothermic homogenous catalysis.

is exact, that is, there exists a ξ_0 where concentration is exactly zero. However, for higher orders the concentrations drop to very small values but are never zero. The exact analysis corresponding to the work of Mehta and Aris [195] on fractional orders is given in Appendix-B. For higher orders, the conditions for the emergence of an unused film are discussed in Section 4.1.4.1. The unused film happens in reality and Rebrov et al.'s work [143] can be given as an example. In their experimental FFMR study coupled with simulations, they have found during the homogeneous catalysis of octanal to octanoic acid by molecular oxygen that oxygen front only surpasses about 10% of their film of 70 μm thickness. In addition, they deduce the reaction as fast-pseudo first order. So, if numbering up of reaction plates is considered under these conditions, this would mean that around 80% of the liquid volume would be wasted. Rebrov et al. punctuates that their FFMR works in a mass transfer controlled regime. If elimination of mass transfer resistances is the ultimate aim of microreactors, then such cases of microreactor operation seem to be quite away from it.

To demonstrate the validity of HAA with respect to the finiteness of the system, one may select a tolerable error and then compare the surface fluxes given by the exact solution and the HAA. The exact steady solution gives the surface flux as:

$$N_E = \left.\frac{du}{d\xi}\right|_{\xi = 1} = \Lambda \sqrt{\frac{2}{n+1}}\,(1 - {u_0}^{n+1})^{0.5} \qquad (105)$$

As $\tau \to 0$, Equation-(99) tends to:

$$N_{HAA} = \Lambda \sqrt{\frac{2}{n+1}} \qquad (106)$$

As expected, due to the semi-infinite assumption, the HAA expression is equivalent to the exact solution when u_0 is zero. One may now define the relative error:

$$Err = \frac{N_{HAA} - N_E}{N_E} = \frac{1 - \left(1 - {u_{0_c}}^{n+1}\right)^{0.5}}{\left(1 - {u_{0_c}}^{n+1}\right)^{0.5}} \qquad (107)$$

Solving for the critical u_{0_c} gives:

$$u_{0_c} = \left[1 - \left(\frac{1}{1+\mathrm{Err}}\right)^2\right]^{1/(n+1)} \tag{108}$$

Now, with a prescribed error, one may find u_{0_c} from Equation-(108), and then extract the critical Thiele modulus, Λ_c, from Equations (103) and (104). Elimination of u_{0_c} from these equations yields:

$$\Lambda_c = \sqrt{\frac{2}{n+1}}\left[1 - \left(\frac{1}{1+\mathrm{Err}}\right)^2\right]^{-\frac{(n-1)}{2(n+1)}}\left(\frac{1}{1+\mathrm{Err}}\right) \mathrm{F}\left(0.5\,,0.5+q\,;1.5\,;\left(\frac{1}{1+\mathrm{Err}}\right)^2\right) \tag{109}$$

$$\Lambda_c = \sqrt{\frac{2}{n+1}}\left(\frac{1}{1+\mathrm{Err}}\right) \mathrm{F}\left(1\,,1-q\,;1.5\,;\left(\frac{1}{1+\mathrm{Err}}\right)^2\right) \tag{110}$$

With Equations (109) and (110) one can now plot Λ_c versus reaction order. Figure 30 shows that low Λ_c can be tolerated, especially for low reaction orders.

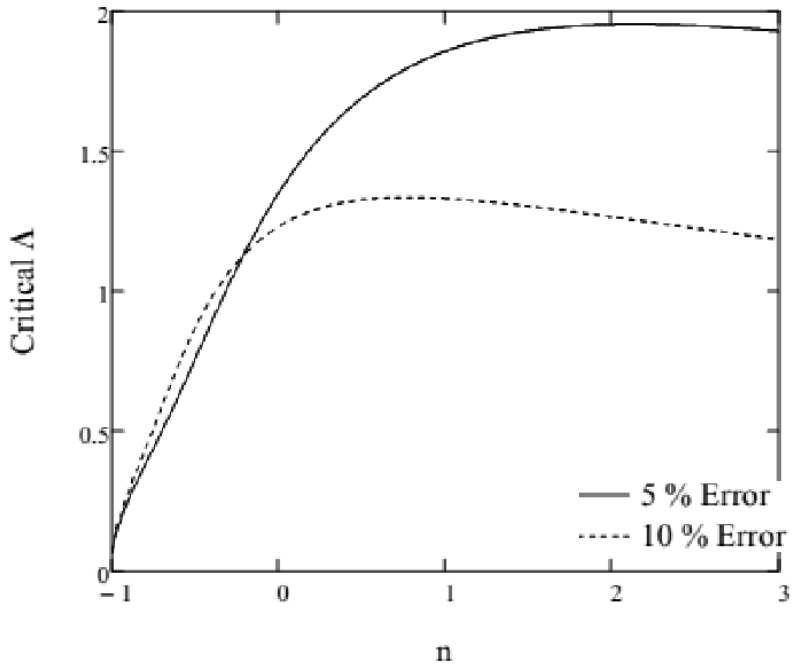

Figure 30. Λ_c for 5 % error (red) and 10 % error (blue) respectively.

For example, for errors smaller than 5 %, $\Lambda > 1.8$ is a must for a first order reaction, if PT is going to be used. This proves the nature of the deviation of the red error lines in Figure 29, since Λ was selected as 0.1 in that case. On the overall, one can say that

PT can be applicable for $\Lambda \gtrsim 1$ and $n \geq 0$, as long as the velocity field classification given in the previous subsection holds.

The resulting concentration profiles predicted by the numerical solution of Equation-(102) and HAA are given by Figure 31. It seems that under acceptable error limits, there are significant discrepancies. However, since the sufficiently accurate uptake rates are aimed to be calculated, the whole profile is not important, instead, the slope at the interface is of prime value. The numerical solutions to Equation-(102) are obtained via first transforming the problem into an initial value problem by applying the shooting method, then integrating numerically by an adaptive Runge-Kutta algorithm.

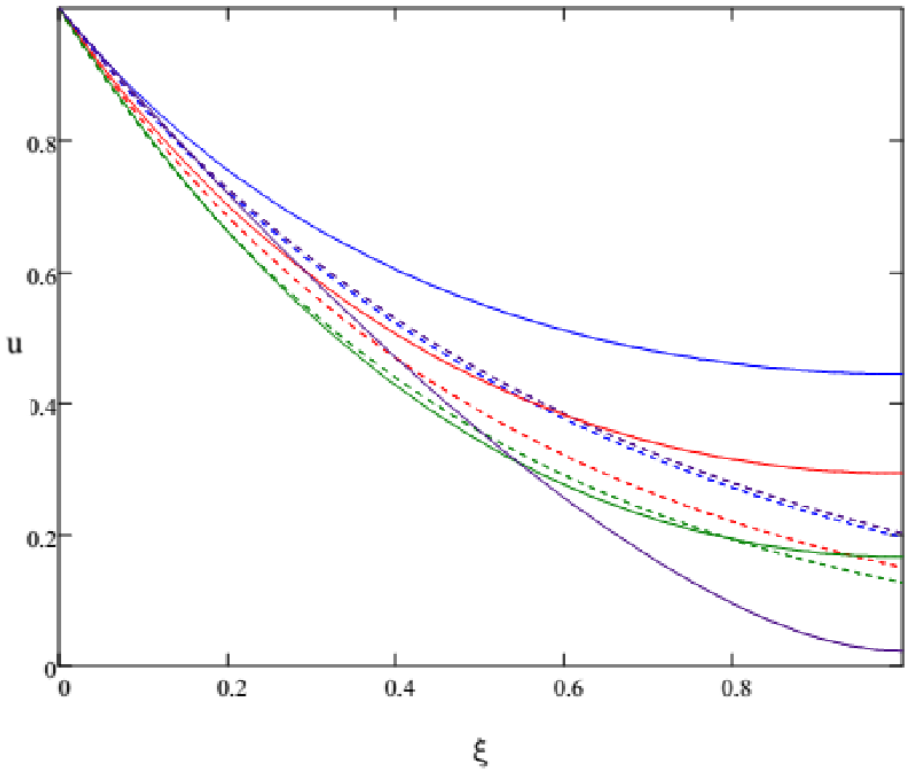

Figure 31. Concentration profiles calculated for different n at corresponding Λ_c: exact vs. approximate. Straight lines: numerical solution. Dotted lines: HAA solution. Red: $n = 1$, blue: $n = 2$, green: $n = 0.5$, purple: $n = -0.5$.

It is also important to note that HAA yields accurate results for fractional orders less than unity, whereas such cases may lead to instabilities in numerical solutions. Problems originate from the fast changes in the reaction rate near zero concentration.

This property leads to a distinct penetration front during the transient period, where the front concentration is exactly zero. The fractional order case may be encountered in homogeneous catalysis.

Although the hypergeometric function is embedded in many CAS, simple exact solutions can be used for $n = 0$ and 1. They are given in Appendix-B. Thiele [198] and Bischoff [115] provided solutions for $n = 2$ and various others, but these are also implicit and usually more complicated than Equations (103) and (104).

In addition, the effectiveness factor can be obtained when the surface flux is known:

$$\eta = \frac{\text{average rate}}{\text{maximum rate at surface conditions}} = \int_0^1 u^n \, d\xi = \frac{1}{\Lambda^2} \frac{du}{d\xi}\Big|_{\xi = 1} \qquad (111)$$

The plots of η has been given by Mehta and Aris [195, 199] in detail, which deliberately shows multiplicities and $\eta > 1$ for negative order reactions.

4.1.2.4. Slow Reactions

In Figure 30, the applicability limits are drawn for sufficiently fast reactions. These have Λ values that lie above the plots given in Figure 30. Therefore, the cases corresponding to such moduli can be accurately treated by HAA. For slower reactions, or generally for smaller Λ that lies beneath curves of Figure 30, HAA may still be useful. Up to a certain time, during which the accumulation at the wall is not so serious, HAA should give accurate uptake rates. That gives rise to a critical Fo number, Fo_c .

Finding Fo_c for any Λ that lies below the curves of Figure 30 and also for any reaction order is not a simple task and cannot be accomplished exactly. However, by numerical experiments, this case can be simplified and resolved with good accuracy.

First of all, from MOL solutions of Equation-(100) for plug flow can be provided for $0 < n < 3$ and $0 < \Lambda < \Lambda_c$. What immediately obtained is that for $\Lambda < 0.7$, the system almost behaves as physical absorption for all orders. Hence the Fo limits of PT for physical absorption should apply. When dealing with the effects of flow fields

it was noted that first and second order reactions behaved almost the same for low Λ, under any flow field. This is further expected from Figure 30, since for low errors, the n vs Λ_c curve is almost flat. Thus, one may represent the interval of orders $1 < n < 3$ as first order with good accuracy. Moving from here, one may solve Equation-(100) for plug flow and for the interval $\Lambda \in [0.7, \Lambda_c]$ corresponding to first order reaction. Then one can solve for the Fo_c when ratio of the fluxes between the numerical solution and the HAA are in a predefined error limit. The Λ interval is divided into eight and the error limit is assumed as 5 %. So for each Λ, one obtains a Fo_c . These then can be regressed, to give Fo_c as a function of Λ. For first order reaction:

$$Fo_c{}^{I} = 1.941 \cdot 10^{-3} \exp(2.78\Lambda) + 0.275 \qquad (112)$$

Since the interval $0 < n < 1$ behaves quite differently, as can be seen from Figure 30, a fit for zero order reaction is also accomplished.

$$Fo_c{}^{0} = 2.106 \cdot 10^{-3} \exp(6.4\Lambda) + 0.362 \qquad (113)$$

The parameter $1 - \mathcal{R}^2$, where $\mathcal{R}$ is the Pearson correlation coefficient, is smaller than 10^{-3} in both cases. The correlations show that the Fo_c increases exponentially with Λ.

To sum up, now one may say that if the velocity field is appropriate, slow reactions, i.e. $\Lambda < 0.7$, can be treated as physical absorption up to a certain exposure time. This exposure time is closely predicted by Figure 28 for different flow fields. For $\Lambda \gtrsim 1$, PT can provide acceptable prediction for all contact times. This leaves a narrow interval for Λ, which is not accessible by simple solutions.

4.1.2.5. Non-Isothermal Cases and Heat Coupling

The fractional, negative and high integer orders may emerge when heat transfer effects are lumped into the reaction term. At steady state, the dimensionless equations of heat and mass transfer

$$\begin{aligned} \Delta u &= \Lambda^2 r(u, v) \\ \Delta v &= -\beta_T \Lambda^2 r(u, v) \end{aligned} \qquad (114)$$

can be combined into a single equation of concentration only. Here β_T is the Prater modulus given as

$$\beta_T = \frac{(-\Delta H_{RXN})DC^*}{k_t T_s} \tag{115}$$

$\beta_T > 0$ denotes exothermic reaction. The modulus is on order of 10^{-2} for CO_2 absorption in concentrated NaOH solutions [200]. For gas-liquid reactions, it probably lies around such magnitudes.

Upon multiplying the upper equation with β and summing up the equations:

$$\begin{aligned} \Delta u &= \Lambda^2 f(u) \\ v &= \beta_T(1-u) + 1 \end{aligned} \tag{116}$$

This is valid only when Biot numbers are large. In order words, only BCs of the first kind are allowed. Otherwise, the formulation is not so simple [201]. For the n^{th} order reaction, the function $f(u)$ in Equation-(116), becomes:

$$f(u) = u^n \exp\left[\frac{\beta_T \gamma_e (1-u)}{1+\beta_T(1-u)}\right] \tag{117}$$

$\gamma_e = E_a/RT_s$ is the Arrhenius number. In some cases, the exponential term can be approximated with a function of the type u^m. This is first demonstrated by Mann and Clegg [202] for the absorption of chlorine in toluene. They experimentally found a reaction order of 5 due to lumping of heat effects.

If the power law approximation, $f(u) = u^{n+m}$, can be accomplished, the HAA can also be further utilized for non-isothermal conditions[32] [203]. This is especially possible when the factor $\beta_T\gamma_e$ is sufficiently low, and the reasons for this will be discussed. Fortunately, low $\beta_T\gamma_e$ values should be prevalent for many gas-liquid reactions. Actually, even for gas-solid reactions, β_T rarely exceeds 0.2 and γ_e is around 20 [204].

At significantly exothermic conditions, the form of the rate given by Equation-(117) can take values higher than one and holds a peak on $u \in [0,1]$. Thus, there occurs a theoretical need for a condition involving β_T, which would render $f(u)$ as

[32] The results achieved in steady-state is aimed to be applied to unsteady cases. This may seem inappropriate, but the derivation of HAA also lies on an analysis at steady-state.

monotonically increasing, because the power law approximating function is a monotonically increasing one. By using simple calculus, one may investigate the derivative of f(u), to explore the conditions for a peak to occur on the interval $u \in [0,1]$. The only term of $df(u)/du$ with possible alternating signs is the polynomial $u^2 - \left(2 + \gamma_e/n{\beta_T}^2 + 2/n\beta_T\right)u + (1 + 2/n\beta_T + 1/\beta_T)$. Equating this polynomial to zero and looking for roots is straight forward. The condition to be seeked is the one to keep the peak concentration out of the interval $[0,1]$. The analysis leads to a very neat result:

$$\beta_T \leq \frac{n}{\gamma_e} \tag{118}$$

If the above criterion holds, one may find the approximate m value from the equation:

$$\frac{d}{dm}\int_0^1 \left\{u^n \exp\left(\frac{\beta_T\gamma_e(1-u)}{1+\beta_T(1-u)}\right) - u^{n+m}\right\}^2 du = 0 \tag{119}$$

and it can be simplified into:

$$\int_0^1 u^{2n+m-1} \exp\left(\frac{\beta_T\gamma_e(1-u)}{1+\beta_T(1-u)}\right) du = \frac{1}{2(n+m)} \tag{120}$$

A close form solution of the integral in Equation-(120) is given by Tavera [205], but it is not simpler than the integral itself. However, a CAS can easily solve for m, by evaluating the integral numerically. Such a procedure is employed for obtaining m. As a test case, β_T is taken as 0.05 and -0.05 with $\gamma_e = 20$ and $n = 2$, which can be considered as significantly thermic. With these values, m is found to be -0.716 and 0.860. This results in new orders as 1.284 and 2.86. Exothermicity decreases the order, while endothermicity increases it.

Now one may test the modified HAA with numerical solutions. The nonlinearly coupled equations of heat and mass diffusion must be solved. The equations are nondimensionalized as given below:

$$\frac{\partial u}{\partial \tau} = \frac{\partial^2 u}{\partial \xi^2} - \Lambda^2 u^n \exp\left[-\gamma_e\left(\frac{1-v}{v}\right)\right] \qquad \begin{array}{lll} \text{at } \tau = 0 & & u = 0 \\ \text{at } \xi = 0 & & u = 1 \\ \text{at } \xi = 1 & & du/d\xi = 0 \end{array}$$

$$\frac{1}{Le}\frac{\partial v}{\partial \tau} = \frac{\partial^2 v}{\partial \xi^2} + \Lambda^2 \beta_T\, u^n \exp\left[-\gamma_e\left(\frac{1-v}{v}\right)\right] \qquad \begin{array}{lll} \text{at } \tau = 0 & & v = 1 \\ \text{at } \xi = 0 & & v = 1 \\ \text{at } \xi = 1 & & dv/d\xi = 0 \end{array} \qquad (121)$$

These are solved with MOL. $Le = \alpha/D$ is the Lewis number and it is taken as 10. For liquids, $\alpha \sim 10^{-7} - 10^{-8}$ usually. Since $D \sim 10^{-8} - 10^{-10}$, now the choice for the Lewis number can be justified. For $Le > 1$, which is likely, the results would be quite the same. The comparison of numerical and HAA solutions are displayed in Figure 32, Figure 33 and Figure 34. From Figure 32, it is evident that the steady-state temperature profile is almost flat. But this does not mean that temperature is ineffective on the concentration profile. Actually the slopes at the interface change significantly and the power law approximation captures this effect.

The deviation from the isothermal solution shows that thermal effects are significant. Figure 33 and Figure 34 can show this on a time basis, where the modified HAA closely approximates to the exact values of the surface flux, but the isothermal HAA does not. The errors rise to a few percent but they decay out to almost zero deviation. Note that the systematic error of the isothermal solution may lead to large errors in total uptake amounts. Although the power law approximation comes from a steady-state analysis, it is shown that its use in unsteady-analysis may be assumed as acceptable.

Non-isothermal behavior is observed in microreactors, for the FFMR, there exists a 20℃ difference between the side and bottom plates in Rebrov et al.'s study [143].

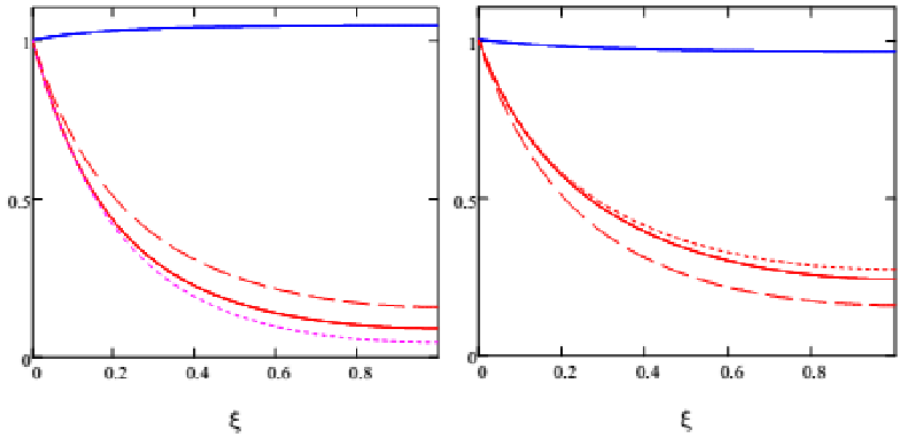

Figure 32. Results of MOL solutions for steady-state concentration (red) and temperature (blue) profiles for exothermic (left) and endothermic (right) cases. Straight line: non-isothermal; dotted line: power law approximation; dashed line: isothermal.

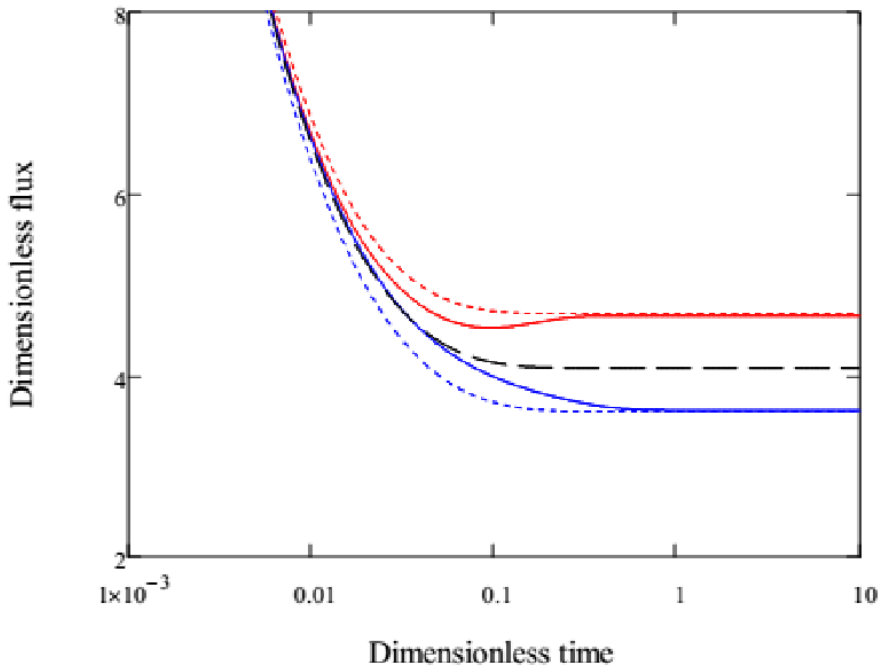

Figure 33. Dimensionless surface flux for exothermic (red) and endothermic (blue) cases. Straight lines: numerical solution; dotted lines: HAA with power law approximation. Dashed line is isothermal HAA.

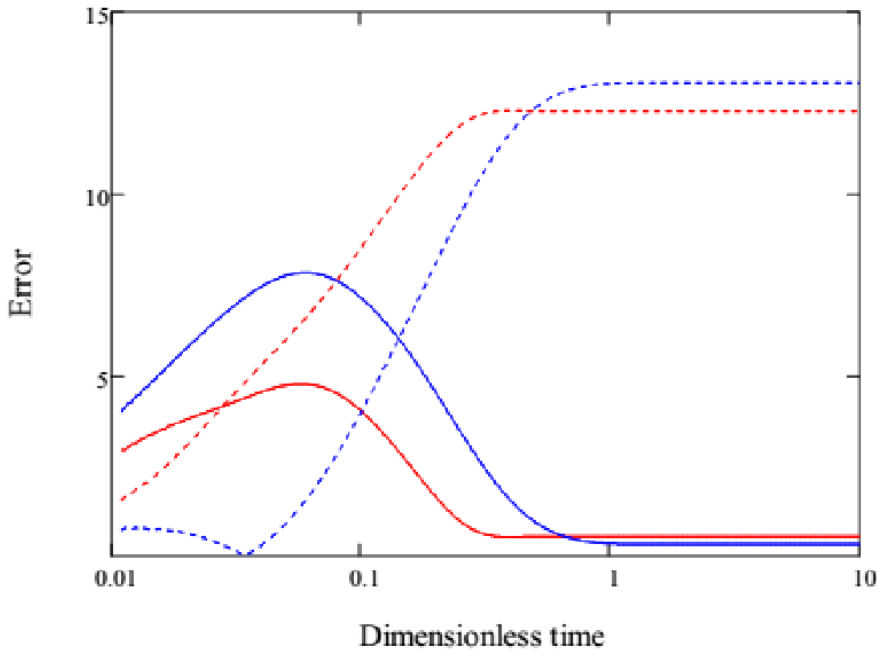

Figure 34. Relative percent errors for surface flux. Straight lines: HAA with power law approximation; dotted lines: isothermal HAA.

4.1.2.6. Gas-Phase Resistance, Complex and Second Order Reactions

In case of a significant gas-phase resistance, additional complications occur. Danckwerts [206] presents a solution for the uptake in the presence of first order reaction and linear resistance under isothermal conditions:

$$\frac{\partial u}{\partial \xi} = \frac{1}{1-(\Lambda/\mathrm{Bi})^2}\left\{\mathrm{erf}\left(\Lambda\sqrt{\tau}\right) + \frac{\mathrm{Bi}}{\Lambda}\,\mathrm{erfc}\left(\mathrm{Bi}\sqrt{\tau}\right)\exp[\tau(\mathrm{Bi}^2-\Lambda^2)] - \frac{\Lambda}{\mathrm{Bi}}\right\} \qquad (122)$$

But the HAA cannot be applied in this case, since the interfacial concentrations change with time. Algebraic complications do not allow the derivation of a new Hikita-Asai-like linearization also. If $n = 1$, then Equation-(122) can be used directly. Otherwise, this case does not have an analytical solution, unlike the no-resistance case. Mehta and Aris [199] also solved the ODE given by Equation-(102) with surface resistance, and established a connection between the solutions where $\mathrm{Bi} = k_g\delta/D$ is finite and $\mathrm{Bi} \to \infty$, which is the solution of the Equation-(102). Thus, the critical modulus found above for no resistance, can be translated into the case with a gas phase resistance, by using the following formula:

$$\Lambda_{cS} = \Lambda_c \left(1 + \frac{\Lambda_c \sqrt{\frac{2}{n+1}}}{Bi} \right)^{n-1/2} \qquad (123)$$

It can be seen from Equation-(123) that as Bi decreases, the tolerance limits for Λ widens, since the relative speed of internal transport increases with respect to the speed of interfacial transport. It is also clear that as $Bi \to 0$, $\Lambda_{cS} \to 0$ also. As expected, as Bi gets larger, $\Lambda_{cS} \to \Lambda_c$. If a variant of HAA with gas-phase resistance existed, then Equation-(123) would be utilized more effectively.

The reasoning developed above can be translated to some cases of complex reactions. If the slowest reacting (pseudo n^{th} order reaction) and the fastest diffusing absorbed substance does not accumulate on the wall and the velocity field beneath the interface does not have any maximums close to the surface, then PT combined with the HAA may be employed for many cases with acceptable error. These may involve non-isothermal cases with the utilization of the power law approximation. For parallel reactions, an explicit expression is available for the critical Thiele modulus:

$$\Lambda_{c_{eq}} = \sqrt{2} \sum_{n=1}^{N} \frac{\Lambda_i}{n_i + 1} \qquad (124)$$

However, for series reactions analysis gets complicated. The number of regimes and variations of the cases involving mass transfer with chemical reaction are very large, so that a general encapsulation is not possible. It is evident that the methodology also cannot be extended to second order reactions. Therefore, for systems which are not fit here, special methods of analysis are necessary.

4.1.3. Saturation-Depletion in Finite Films

4.1.3.1. Physical Absorption

The approximate analysis of Pohorecki [103], summarized by Equations-(39) to (45), can be put in an exact form. One may calculate the total uptake amounts for diffusion into plug, film and Couette flows, from:

$$n_a = \int_0^{t_{exp}} N dt \qquad (125)$$

then the time yielding 95% saturation can be extracted. The dimensionless surface flux expressions are provided in Appendix-A by Equations(A2), (A4) and

(A14). However, their use in an integral has been found to be erroneous. Since the uptake rates are maximized in the initial stages, series solutions are cannot capture it accurately, because their convergence for small times is very slow. Many additional terms are necessary to obtain accurate values. Therefore, the analysis is conducted numerically. The diffusion equations are solved by MOL, then the five point difference formula is employed for the surface flux (Equation-(101)). This formula is integrated by an adaptive quadrature embedded in Mathcad, and finally the numerical integral expression is solved for the Fo_S that gives 95% saturation. The results are given in Table 7. From the beginning, all the analysis was based on scaling the contact length with interfacial velocity to get the exposure time. One may also use average velocity for this purpose. The relevant saturation Fourier number is denoted as $Fo_S{}^a$ can be easily obtained by:

$$Fo_S{}^a = Fo_S{}^i \frac{v_{max}}{\bar{v}} \qquad (126)$$

In both film and Couette flow cases, $v_{max} = v_i$.

Table 7. Saturation Fourier numbers for diffusion into plug, film and Couette flow.

		$Fo_S{}^i$ (scaled wrt v_0)	$Fo_S{}^a$ (scaled wrt $\bar{v}$)
Plug Flow		1.13	1.13
Film Flow		0.54	0.81
Couette Flow	$a = 1$	0.35	0.69
	$a = 0.5$	0.72	0.96
	$a = 0.2$	0.95	1.05

The laminar film saturates much quicker than plug flow, almost in half-time. It seems that knowing the profile in the film is important when Fo is relatively high.

Considering Taylor bubbles, Pohorecki assumes that the surrounding film is in laminar or in plug flow, which does not make any difference in his analysis. However, if the film is in laminar flow, it will get saturated by a bubble of halved length when compared to a film flowing which is stagnant (or in plug flow). For cases involving physical absorption or slow reaction, approximating laminar flow with plug flow may induce serious error in calculations. Therefore, knowing the velocity field is indeed important. The analysis can similarly be extended to other flow profiles given in Appendix-D.

4.1.3.2. Absorption with Bimolecular Reaction

Pohorecki's result [103] for the minimum depletion time (Equation-(45)) in instantaneous reactions can also be put on more distinct grounds. Consider the system given in Equations- (57), but in a finite domain with no-flux BC's on $x = \delta$. Assuming equal diffusivities, multiplying the equation for species A with z and then subtracting it from the equation for B results in:

$$\frac{\partial p}{\partial t} = D\frac{\partial^2 p}{\partial x^2} \tag{127}$$

where $p = C_B - bC_A$, subject to the following BC's:

$$\text{at } x = 0,\ p = C_{B_i} - bC_A^*;\ \text{at } x = \delta,\ \frac{dp}{dx} = 0;\ \text{at } t = 0,\ p = C_{B_0} \tag{128}$$

This problem cannot be solved, since the interfacial concentration of B, C_{B_i}, is not known. However a companion problem can be solved, which can approximate to the exact case under some asymptotic conditions. So suppose a thin layer beneath the interface acts as a batch reactor. Since the concentration of A is always constant on the interface:

$$\frac{dC_{B_i}}{dt} = -bkC_A^{*m}C_{B_i} \tag{129}$$

Unlike Equations- (57), a more general m^{th} order reaction in terms of A is assumed. This condition immediately yields:

$$C_{B_i} = C_{B_0}\exp\left(-bkC_A^{*m}t\right) \tag{130}$$

For an instantaneous reaction, interface cannot be significantly fed by the diffusing B from deeper layers. Thus, B depletes according to the classical mass-action kinetics on the interface, its value with time given by Equation-(130). So for very fast reactions this assumption should almost be exact. On the other hand, for slow reactions in a thin layer of fluid, the concentration profile of B and A would almost be flat, thus the interfacial concentration of B would almost equal to the concentrations that lie deeper to the wall. In that case, the whole system acts as a batch reactor.

Note that, for C_{B_i} to not to change much, $bkC_A^{*m}t \ll 1$. This condition reduces to Danckwerts' pseudo first order criterion for $b = m = 1$. For FT, this criterion approximately takes the form for m-,n[th] order as [109]:

$$\sqrt{M} = \sqrt{\frac{2DkC_{B_0}{}^{n}C_A^{*m-1}}{(n+1)k_L{}^{2}}} > 3 \qquad (131)$$

which is also due to Hikita and Asai. So, one may re-write the boundary condition at the interface as:

$$\text{at } x = 0, \;\; p = C_{B_0}\exp\left(-bkC_A^{*m}t\right) - bC_A^{*} \qquad (132)$$

Now the problem is transformed into a linear PDE with a time-dependent boundary condition. One may employ Laplace transform, but its inversion would be difficult. However, by using Duhamel's integral the problem can be solved with ease [175]. The integral is given as:

$$\hat{p} = f(0)\theta(x,t) + \int_0^{\tau} \theta(x,t)\frac{df(\tau)}{d\tau}d\tau \qquad (133)$$

where function f is the time dependent boundary condition of the 1[st] kind at the wall. θ is the solution of the corresponding diffusion problem with a unit-step boundary condition instead of function f. The theory and the solution steps are given in Appendix-C. The final result is tested over large range of parameters, and seen to be very close to the exact numerical solution for long times, near the depletion of reactant B.

The solution is quite bulky, but it can be simplified, especially for the wall concentration. Similar to the criteria given by Table 3 and Equation-(131), one may develop three regimes with Thiele modulus:

$$\Lambda_S{}^2 = \frac{bkC_A^{*m}\delta^2}{D} \tag{134}$$

The regimes are given in Table 8, on which the reaction rates are compared with diffusion rates. Note that the table is quite similar with Table 3.

The simplified solution for the value of p at the wall can be given as:

$$\frac{\pi}{4}\varphi = \frac{E_i}{E_i - 1}\exp\left(-\frac{\pi^2}{4}Fo_D\right) + \exp\left(-\Lambda_S{}^2 Fo_D\right)\left(\frac{\pi}{4} - \frac{3.876\Lambda_S{}^2}{\pi^2}\right) \tag{135}$$

E_i is the enhancement factor for equal diffusivities:

$$E_i = 1 + \frac{C_{B_0}}{bC_A^*} \tag{136}$$

Table 8. Regimes for the depletion solution given by Equation-(135).

	Regime	Λ_s	Condition	φ
1	Reaction is very fast, hence B depletes before A starts to accumulate on the wall.	$10 \lessapprox \Lambda_S$	$p_{wall} = -0.01C_{B_0}$	$\frac{0.99 + 0.01E_i}{E_i - 1}$
2	Reaction is of moderate speed, hence B depletes while A accumulates on the wall.	$3 \lessapprox \Lambda_S \lessapprox 10$	$p_{wall} = -0.5zC_A^*$	$\frac{0.5}{E_i - 1}$
3	Reaction is slow, hence A significantly accumulates on the wall, then B depletes	$\Lambda_S \lessapprox 3$	$p_{wall} = -0.99zC_A^*$	$\frac{0.01}{E_i - 1}$
4	Reaction is very slow, concentration gradients almost vanish	$\Lambda_S \lessapprox 0.5$	-	-

Since the solution is implicit, the depletion Fourier number, Fo_D, must be solved for the governing regime. Regimes are implemented into the solution by parameter φ. The solved Fo_D usually gives the time at which 90-99 percent of B has been depleted. If both the depletion of B and the saturation of A is wanted, then regime 3 always works. In regime 4, one may simply approximate the depletion time with the batch reactor solution given in Equation-(130). For 90% depletion:

$$t_d = \frac{4.61}{bkC_A^{*m}} \tag{137}$$

The solution for regime 3 also works for this case.

Unequal diffusivities cannot be treated with this solution. For slow reactions, it is seen that unequal diffusivities have negligible effect on the depletion time. The laminar flow field does not seem to have any influence at all.

One can also provide a solution for the m^{th}-n^{th} order reaction Duhamel's integral, but it cannot be presented in a simple form.

4.1.4. Diffusion into a Flowing Film with Arbitrary Homogeneous Reaction

In section 4.1.2, it has been shown that sufficiently for fast reactions of pseudo-n^{th} order, the HAA can be used effectively. In addition, HAA can also be employed for slow reactions, if exposure times are sufficiently small. However, like any PT model, HAA does not it involves velocity field in its formulations. For flow fields where the interfacial velocity is a maximum, the results given by HAA are quite accurate. But for fields, in which a velocity maximum lies within the film, HAA significantly deviates from the exact result. In section 4.1.2.2, film flow with counter-current shear was given as an example. The aim of this section is to derive an alternative solution in place of the HAA, which can treat various flow fields, also with an n^{th} order reaction. The problem can be given as:

$$f(x)\frac{\partial C}{\partial t} = D\frac{\partial^2 C}{\partial x^2} - k\,r(C) \qquad \begin{array}{ll} \text{at } t = 0, & C = 0 \\ \text{at } x = 0, & C = C^* \\ \text{at } x = \delta, & \partial C/\partial x = 0 \end{array} \tag{138}$$

Initial concentration is taken as zero for simplicity. With $r(C)$, usually nonlinear forms are considered. The solution of Equation- (138) will be accomplished in an approximate sense, similar to HAA. Approximate integral balance method (AIBM) will be used to obtain the general solution. One may first nondimensionalize the problem:

$$f(\xi)\frac{\partial u}{\partial \tau} = \frac{\partial^2 u}{\partial \xi^2} - \Lambda^2 r(u) \qquad \begin{array}{ll} \text{at } \tau = 0, & u = 0 \\ \text{at } \xi = 0, & u = 1 \\ \text{at } \xi = 1, & \partial u/\partial \xi = 0 \end{array} \qquad (139)$$

First the straight alternative to HAA will be derived. Then incorporation of velocity fields will be considered. As explained by an example in section 3.2, AIBM solutions are mostly used for semi-infinite geometries. Therefore these two parts of analysis will be based on the cases where reaction is sufficiently fast, so that concentration fronts do not significantly reach the wall. However, in addition to these solutions, the AIBM will also be applied to a finite film, in the last part of the analysis, which would suit for slow reactions.

4.1.4.1. An Alternative Formulation to Hikita-Asai Approximation

The fundamentals of AIBM provided in section 3.2 can be directly applied: For $f(\xi) = 1$, the IMBE can be written as:

$$\int_0^{\hat{\delta}} \frac{\partial u}{\partial \tau} d\xi = \left.\frac{\partial u}{\partial \xi}\right|_{\xi=\hat{\delta}} - \left.\frac{\partial u}{\partial \xi}\right|_{\xi=0} - \Lambda^2 \int_0^{\hat{\delta}} r(u)\, d\xi \qquad (140)$$

where the first term on the right hand side is considered to be zero. Note that $\xi = x/\delta$ and $\hat{\delta} = \delta_p/\delta$. By using Leibnitz's rule, the derivative at left hand side can be taken out:

$$\int_0^{\hat{\delta}} \frac{\partial u}{\partial \tau} d\xi = \frac{d}{d\tau}\int_0^{\hat{\delta}} u d\xi \qquad (141)$$

Letting $\varphi = \int_0^{\hat{\delta}} f(u)\, d\xi$:

$$-\left.\frac{\partial u}{\partial \xi}\right|_{\xi=0} - \Lambda^2 \varphi = \frac{d}{d\tau}\int_0^{\hat{\delta}} u\, d\xi \tag{142}$$

Assuming a second order polynomial for the concentration profile,

$$u = a + b\xi + c\xi^2 \tag{143}$$

the constants can be found by applying the following boundary conditions:

$$\begin{aligned} &\text{at } \xi = 0 && u = 1 \\ &\text{at } \xi = \hat{\delta} && u \cong 0 \\ &\text{at } \xi = \hat{\delta} && du/d\xi \cong 0 \end{aligned} \tag{144}$$

which results in:

$$\begin{gathered} a = 1, \qquad b = \frac{-2}{\delta}, \qquad c = \frac{1}{\delta^2} \\ u = \left(1 - \frac{\xi}{\hat{\delta}}\right)^2 \end{gathered} \tag{145}$$

The concentration profile can be substituted into Equation-(142), to obtain:

$$\frac{d\hat{\delta}}{dt} = \frac{6 - 3\Lambda^2 \hat{\delta}\varphi}{\hat{\delta}} \tag{146}$$

This ODE has the initial condition $\delta(0) = 0$. For some forms of φ, the ODE may be integrated analytically. However, the reaction rate expression in φ, must be composed of the absorbed component only. Therefore, pseudo order reactions are most general that can be treated with the AIBM formulation. So, for a pseudo n^{th} order reaction

$$\varphi = \int_0^{\hat{\delta}} u^n d\xi = \frac{\hat{\delta}}{2n+1} \tag{147}$$

and with $u_0 = 0$, the ODE can be solved to give the expression for the penetration thickness. For $n > -0.5$:

$$\hat{\delta} = \frac{\sqrt{2(2n+1)}}{\Lambda}\left[1 - \exp\left(-\frac{6\Lambda^2\tau}{2n+1}\right)\right]^{1/2} \tag{148}$$

One may use higher order polynomials, but then additional constants must be evaluated by using derived boundary conditions. For each term of the m^{th} order polynomial one may use:

$$\text{at } \xi = \hat{\delta}, \qquad \frac{d^{m-1}u}{d\xi^{m-1}} \cong 0 \tag{149}$$

Thus, a result for arbitrary polynomial order can be obtained by using the binomial Analysis yields:

$$u = \left(1 - \frac{\xi}{\hat{\delta}}\right)^m \tag{150}$$

$$\hat{\delta} = \frac{\sqrt{m(mn+1)}}{\Lambda}\left[1 - \exp\left(-\frac{2(m+1)\Lambda^2\tau}{mn+1}\right)\right]^{1/2} \tag{151}$$

and

$$-\left.\frac{du}{d\xi}\right|_{\xi=0} = \frac{m}{\hat{\delta}} \tag{152}$$

It has been observed that the quadratic profile works as the best. It captures the surface flux quite well, and on its penetration front, $C/C^* \approx 0.01$ which is a suitable value. Profiles which combine exponential functions with polynomials are also checked for accuracy, for example:

$$\begin{gathered} u = \left(1 - \frac{\xi}{\hat{\delta}}\right)^m \exp\left(-\frac{\xi}{\hat{\delta}}\right) \\ u = \left(1 - \frac{\xi}{\hat{\delta}}\right)^m \exp\left[\left(1 - \frac{\xi}{\hat{\delta}}\right)^{m+1} - 1\right] \end{gathered} \tag{153}$$

These satisfy the boundary conditions, but they cannot give an explicit expression for $\hat{\delta}$ when $n \neq 1$. In addition they are not as accurate as the quadratic profile in terms of surface flux predictions. Therefore, these profiles are discarded. The solution given by Equation-(148) was first given by Tarzia [207] in the context of heat transfer with absorption. However, his main interests were focused on the mathematical behavior of the solution. Here, much more additional information will be extracted from Equation-(148).

First, the surface flux may be given explicitly as:

$$-\left.\frac{du}{d\xi}\right|_{\xi=0} = \frac{2}{\hat{\delta}} = \Lambda\sqrt{\frac{2}{(2n+1)}}\left[1 - \exp\left(-\frac{6\Lambda^2}{2n+1}\tau\right)\right]^{-1/2} \tag{154}$$

Then penetration thickness may be investigated. For large times, δ tends to a constant value, giving the steady state penetration thickness as:

$$\hat{\delta}_{\infty} = \frac{\sqrt{2(2n+1)}}{\Lambda} = \frac{1}{\lambda} \tag{155}$$

If $\hat{\delta}_{\infty} < 1$, then the concentration front does not reach the surface. Thus, for the applicability of this semi-infinite AIBM solution, the criterion below emerges:

$$\Lambda \geq \sqrt{2(2n+1)} \tag{156}$$

Otherwise, accumulation on the wall is initiated. λ will be used in the second part of the analysis.

Note that if the above criterion holds, a part of the film will be unused. If a stacked setup of microfilms is considered (stacked FFMR is an example), then the unused liquid film will be wasted and has to be recycled back to the reactor to decrease excess loss of the liquid solution. This constitutes a constraint for efficient production and Equation-(155) forms an upper limit for the liquid flow rate. The lower limit was discussed to be the flow rate associated with the minimum wetting thickness, in Section 2.8.6. For gravitational flows, expressions like Equation-(66) may be used, but under the shear effects of the gaseous phase, suitable expressions may not exist. It is important to punctuate that this discussion does not apply to fast second-order bimolecular reactions.

One may utilize the condition given by Equation-(156) further. When it does not hold, then one may extract the time to reach the wall from Equation-(148). By setting $\hat{\delta} = 1$ and solving for τ yields:

$$\tau_r = \frac{2n+1}{6\Lambda^2} \ln\left(\frac{4n+2}{4n+2-\Lambda^2}\right) \tag{157}$$

It is observed that the flux expression provided by the AIBM is initially positively erroneous, but just with a few percent. However, once steady-state begins to settle, static errors are noted. At this point AIBM yields smaller steady-state fluxes. The reason for this is that the solution tends to a wrong steady-state. This can be easily mended. Since AIBM predicts with positive deviation, one may find the time when it equals to the steady-state flux given by Equation-(106). The result is:

$$\tau_S = \frac{2n+1}{6\Lambda^2} \ln\left(\frac{2n+1}{n}\right), \qquad \hat{\delta}_S = \frac{\sqrt{2(n+1)}}{\Lambda} \tag{158}$$

This amendment needs $n \geq 0$. Finally, one can calculate the amounts absorbed approximately as:

$$\hat{n}_A = \frac{\hat{\delta}}{3} - \frac{\Lambda\pi^2\hat{\delta}^2}{90\sqrt{2(2n+1)}} + \Lambda\sqrt{\frac{2}{2n+1}}\tau \qquad (159)$$

To obtained the above equation, an approximation used in chromatography, which is due to Vermeulen [268], is applied during the integration:

$$\sqrt{1-\exp(-x)} \cong 1 - \frac{6}{\pi^2}\sum_{n=1}^{\infty}\frac{\exp(-n^2x)}{n^2} \qquad (160)$$

Equation-(159) is valid for the transient state. For $\tau > \tau_s$ it simply becomes:

$$\hat{n}_A = \frac{\hat{\delta}_S}{3} - \frac{\Lambda\pi^2\hat{\delta}_S{}^2}{90\sqrt{2(2n+1)}} + \Lambda\sqrt{\frac{2}{2n+1}}\tau_S + \Lambda\sqrt{\frac{2}{n+1}}(\tau-\tau_S) \qquad (161)$$

All the equations above are formed from elementary functions and they are relatively simple to evaluate. When compared to HAA, the accuracy is quite good. A demonstration is given by Figure 35.

When calculating the uptake rates with HAA, the following equation is used:

$$\hat{n}_{A_{HAA}} = \left(\frac{2\Lambda^2}{n+1}\tau + \frac{1}{2}\right)\mathrm{erf}\left(\Lambda\sqrt{\frac{2\tau}{n+1}}\right) + \Lambda\sqrt{\frac{2\tau}{\pi(n+1)}}\exp\left(-\frac{2\Lambda^2}{n+1}\tau\right) \qquad (162)$$

This is the result obtained from time integration of Equation-(99).

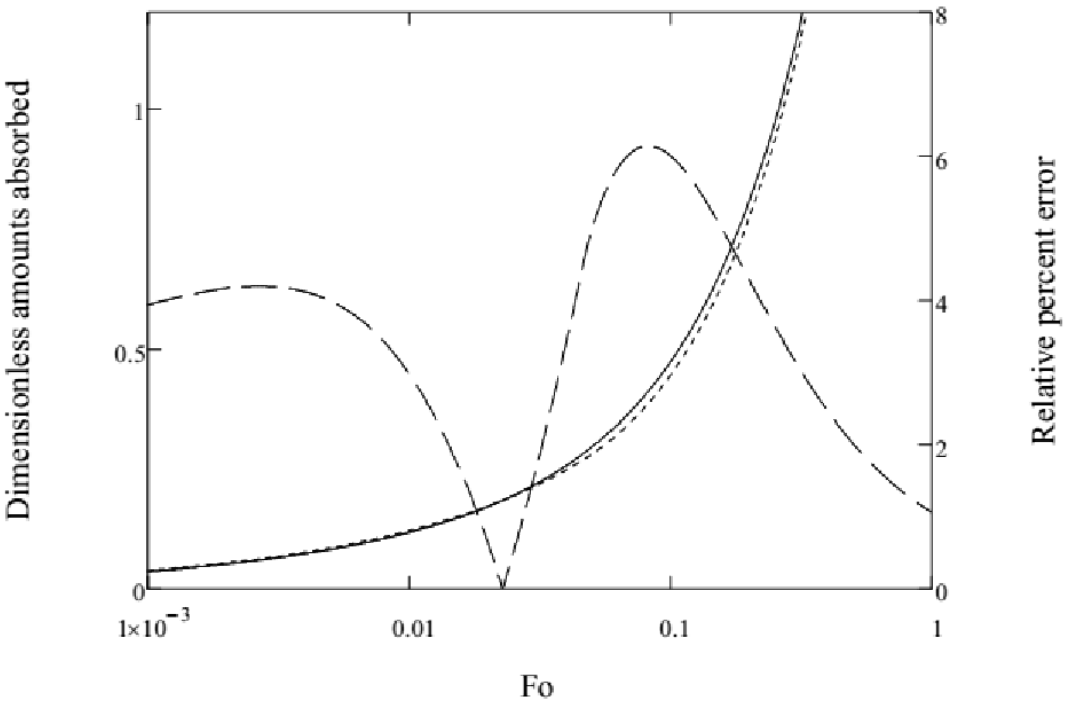

Figure 35. Comparison of HAA with Equation-(161) forn = 2 and $\Lambda = 4$. Straight line: HAA, dotted line: Equation-(161), dashed line: relative percent error when compared to HAA.

4.1.4.2. Velocity Fields

Now, functions other than unity can be substituted in place of f(ξ). Assuming it to be a general quadratic polynomial,

$$f(\xi) = a_0 - a_1\xi - a_2\xi^2 \tag{163}$$

the integral can be evaluated:

$$\int_0^{\hat{\delta}} (a_0 - a_1\xi - a_2\xi^2)\left(1 - \frac{\xi}{\hat{\delta}}\right)^2 d\xi = \frac{a_0}{3} - \frac{a_1}{6}\hat{\delta} - \frac{a_2}{10}\hat{\delta}^2 \tag{164}$$

Then the regular analysis of AIBM can be resumed. Solving the ODE yields:

$$\tau = \frac{a_1\hat{\delta}}{12\lambda^2} + \frac{a_2\hat{\delta}^2}{40\lambda^2} + \frac{5a_1\lambda - 10a_0\lambda^2 + 3a_2}{120\lambda^4}\ln\left(1 - \lambda^2\hat{\delta}^2\right) - \frac{a_1\hat{\delta}}{12\lambda^3}\ln\left(1 + \lambda\hat{\delta}\right) \tag{165}$$

λ was defined in Equation-(155). Although the expression in implicit in $\hat{\delta}$, it will allow further investigation. For example, substituting $\hat{\delta} = 1$ would yield τ_r like in the plug flow case. For τ_S, the same approach used for plug flow can be applied. The

velocity field can indeed be represented by higher order polynomials or by other functions. Still, the ODE of the IMBE can be integrated analytically for many cases. However, a general form of the integration does not seem to be derivable. Such a generalization is accomplished for diffusion with heterogeneous reaction in Section 4.2.2.

To find the amounts absorbed, integrating the IMBE is integrated in time:

$$\int_0^\tau -\frac{du}{d\xi}\Big|_{\xi=0} d\tau = \int_0^\tau \frac{2}{\hat{\delta}} d\tau = \int_0^\tau \left(\Lambda^2 \int_0^{\hat{\delta}} u^n d\xi + \frac{d}{dt}\int_0^{\hat{\delta}} f(\xi) u \, d\xi \right) d\tau$$

$$= \frac{\Lambda^2}{2n+1}\int_0^\tau \hat{\delta} d\tau + \int_0^{\hat{\delta}} f(\xi) u \, d\xi \qquad (166)$$

Note that the second integral is already evaluated before, therefore:

$$\hat{n}_a = \frac{\Lambda^2}{2n+1}\int_0^\tau \hat{\delta} d\tau + \frac{a_0}{3} - \frac{a_1}{6}\hat{\delta} - \frac{a_2}{10}\hat{\delta}^2 \qquad (167)$$

By inverting the remaining integral, one obtains:

$$\hat{n}_a = \frac{\Lambda^2}{2n+1}\left(\hat{\delta}\tau - \int_0^{\hat{\delta}} \tau d\hat{\delta} \right) + \frac{a_0}{3} - \frac{a_1}{6}\hat{\delta} - \frac{a_2}{10}\hat{\delta}^2 \qquad (168)$$

If specific value is wanted, one must solve for $\hat{\delta}$ from its implicit definition first and then apply the equations above. However, obtaining the general trend is simple. Since the above equation applies until $\tau = \tau_S$, and since at that time $\hat{\delta} = \hat{\delta}_S$ for all fields; one may then form a set for the dimensionless penetration thickness as $[0, \hat{\delta}_S]$ in order to plot $\hat{n}_A$ versus τ, which is also a function of $\hat{\delta}$.

The example treated in the beginning of section 4.1.2.2 is reprised here to show the deficiency of HAA and the proficiency of the new solution. The film flow with counter-current shear case is solved again, but this time with much higher shear: $S = -0.6$. The shear flow profile yields $a_0 = 0.4$, $a_1 = -0.6$, $a_2 = 1$. The calculation of $\hat{n}_A$ is then straightforward. The results of AIBM and HAA are compared with the MOL solution of the problem and relative percent errors are displayed in Figure 36. AIBM is especially successful and its errors are less than 10%. But on the other hand, HAA leads to larger and consistent errors.

This AIBM solution can be regarded as general solution to mass transfer with fast pseudo n^{th} order reaction. It can apply to many other problems, such as Graetz problems [208] or some more delinquent ones like membrane assisted gas-liquid microcontactors [209]. In both cases, the velocity is zero on the interface where the solute is released into the stream. The AIBM solution should adapt to these cases well.

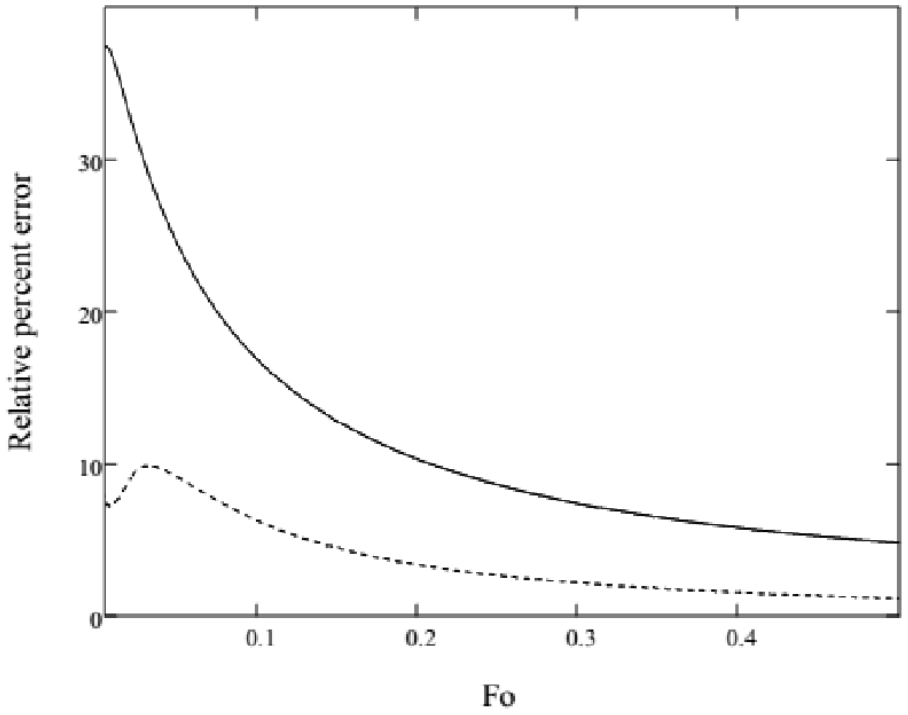

Figure 36. Comparison of AIBM and HAA with numerical solutions for the countercurrent shear flow case, $S = -0.6$, $n = 2$ and $\Lambda = 4$. Dotted line: AIBM, straight line: HAA.

Finally, one can now find the enhancement factor, by dividing Equation-(168) by the PT expression for amounts absorbed in dimensionless form:

$$\hat{n}_{aPT} = 2\sqrt{\frac{\tau}{\pi}} \qquad (169)$$

where for τ is already given by Equation-(165) for $\tau < \tau_S$.

4.1.4.3. The Finite Film

AIBM can be applied to a finite film also. Mathematically, the finite film solution will complement the semi-infinite solution, which gets terminated at τ_r. Thus for $\tau > \tau_r$, the problem has a new boundary condition:

$$\text{at } \xi = 1, \qquad u = u_w \tag{170}$$

where u_w is the time-dependent wall concentration. In this period, the time dependent penetration thickness vanishes and it equals to one. The quadratic equation which satisfies the boundary conditions is:

$$u = 1 + (1 - u_w)(\xi^2 - 2\xi) \tag{171}$$

The rest of the analysis is straightforward, but only if the reaction is of first order. For other orders (except zero) the problem becomes analytically intractable. One may try to linearize this terms, but both first order Taylor series expansion and error integral linearization failed to yield accurate results. Therefore, this case solved for the first order case only, with the same general quadratic velocity field given by Equation-(163). The wall concentration can be found explicitly as:

$$u_w = \frac{6 - \Lambda^2}{2 + 2\Lambda^2}\left\{1 - \exp\left[-\frac{6 + 2\Lambda^2}{3\vartheta}(\tau - \tau_r)\right]\right\} \tag{172}$$

Note that for $u_w > 0$, $\Lambda^2 < 6$, which conforms to the criterion given by Equation-(156).

ϑ is the modifier for the velocity field:

$$\vartheta = \frac{2a_0}{3} - \frac{5a_1}{12} - \frac{3a_2}{10} \tag{173}$$

The rest of the quantities can be obtained simply, for example flux:

$$-\frac{du}{d\xi}\bigg|_{\xi=0} = 2(1 - u_w) \tag{174}$$

For the amounts absorbed, the above equation can be integrated from τ_r to τ. The amounts absorbed up to τ_r can be found from Equation-(168), where $\hat{\delta} = 1$.

The solution is however still flexible, and it can provide various information. For example one may investigate the effect of wall slip or gas shear on mass transfer

rates by finding the derivatives with respect to the flow parameters investigated and then by comparing them. In addition, the solution is general for many flow fields, and when compared with available the exact solutions comprising special functions and implicit eigenvalue equations, it is relatively simple to handle.

4.1.4.4. Summary: Mass Transfer with Homogeneous Reaction

From the previous developments it has been shown quantitatively that penetration formulations can be used for fast reactions in flowing films with good accuracy, if the interfacial velocity is the maximum velocity in the film. PT is also valid for slow reactions if contact times are sufficiently short. Furthermore, it has been shown that microcontactors are efficient only when they do not saturate or deplete.

The new solution presented via AIBM can treat the velocity fields that HAA cannot handle. The finite solution also provides an explicit solution to investigate the effect of velocity profile of mass transfer for times after the molecules started to accumulate at the wall. For slow reactions, AIBM can provide the solution for long times, albeit for first order only. The unused film concept is punctuated, since a general limit is provided by the new solution. During pseudo order reactions, this would implement a constraint on liquid flow rate for more efficient production. Note that, when a pseudo or direct n^{th} order reaction is considered, for $n \geq 0$, Equation-(111) suggests that the effectiveness factor go to 1 as Λ goes to zero. Thus, decreasing the film thickness and conserving this over large numbers of contacting microunits will theoretically yield the highest amount of production. In other words, films may saturate to the highest degree when there is a pseudo order reaction, and film thickness may be decreased as much as it is possible. Although this would be limited by the flow rate requirements for complete wetting, in would also be limited to the applicability of pseudo-order reaction assumption for bimolecular reactions. In addition, there would be serious evaporation, when films are very thin. Normally the gas is saturated with the vapor of the liquid before sending it to the contactor, to prevent liquid loss [210]. But with slight disturbances like temperature evolution on the surface during absorption, evaporation may be a serious issue for very thin films.

Therefore, considering fast reactions, microreactors should be efficient. This is because they can contact large amounts of phases in short times due to their large interfacial areas. For slow reactions, they should also work well, since they may remove diffusional resistances to a large extent for such cases. The batch reactor limit of the second order reaction is an example. Since the provided interfacial area per unit volume is also large in stacked microreactors, this may mean also a significant reduction in total unit volume when total production amounts are compared.

Interfacial resistance is neglected through the whole section of 4.1. If the time constant for saturation is much smaller than the one of diffusion, then neglecting interfacial resistance is appropriate. Details for interfacial resistance are given in Appendix-E.

4.2. Gas-Liquid-Solid Systems

4.2.1. Fischer-Tropsch Synthesis and Unsteady-State Operation in a Conceptual Microreactor

As from this section, heterogeneous reactions in liquid films will be treated. The physics will involve the physical absorption of gaseous reactants in the liquid film, which is then followed by diffusion towards a catalytic wall. Usually these walls are monolithic or PDMS based supports which are washcoated with a catalyst [16, 163]. The diffusion of reactants is finally confronted by a complex surface reaction mechanism, which usually involves various adsorption, desorption, bond breaking-formation and surface diffusion steps. Low temperature Fischer-Tropsch synthesis on a ruthenium or cobalt catalyst will be considered.

4.2.1.1. Reactant Fluxes and Transportation through the Wax Film

First, one may check the magnitudes of absorption flux at gas-wax interface for hydrogen and carbonmonoxide. This should be important, since it may provide clues on the relative amounts of the feed gases transported to the catalyst surface. The poisoning effects of species then may be controlled via adjusting either the film thickness or interfacial concentrations by reactor operation.

In order to present a numerical comparision, one needs the solubility and diffusivity data. For solubility, the data of Albal et. al. [211] is used. Their data are correlated from their experimentation range to yield:

$$C^*_{H_2} = 2.281 \cdot 10^{-5}\, T^{1.204}\, P$$
$$C^*_{CO} = 2.615 \cdot 10^{-3}\, T^{0.484}\, P \qquad (175)$$

These expressions yield in terms of kmol/m^3. It is important to note that solubilities of the reactants in the paraffinic wax increase with temperature. On the other hand, the ratio of solubilities decreases with temperature. Their data covers the pressure range 1 to 3 MPa and a temperature range from 348 to 523 K. This range covers the low temperature operation range of FTS.

For diffusivities, the data of Erkey et. al. [212] is used. At 1.4 MPa, their results for temperatures between 475 and 536 K are fitted to yield:

$$\begin{aligned} D_{H_2} \cdot 10^9 &= 0.35862\,T - 133.44483 \\ D_{CO} \cdot 10^9 &= 8.60644 \cdot 10^{-8}\,T^{3.07722} \end{aligned} \tag{176}$$

Now for very short times of contact, one may resort to penetration model for the fluxes. The model suggests:

$$N_i = C_i^* \sqrt{\frac{D_i}{\pi t}} \tag{177}$$

describing the instantaneous surface flux for species "i". For long times, one may use the simple equations of the film model, with an instantaneous reaction rate:

$$N_i = \frac{D_i}{\delta} C_i^* \tag{178}$$

The instantaneous reaction rate means a zero concentration at the catalyst surface, which necessitates a very active catalyst with high loading or high dispersion. This formula shows that in a diffusion controlled scenario, hydrogen gradually enhances the advantage of being a better diffusant, as it approaches the surface.

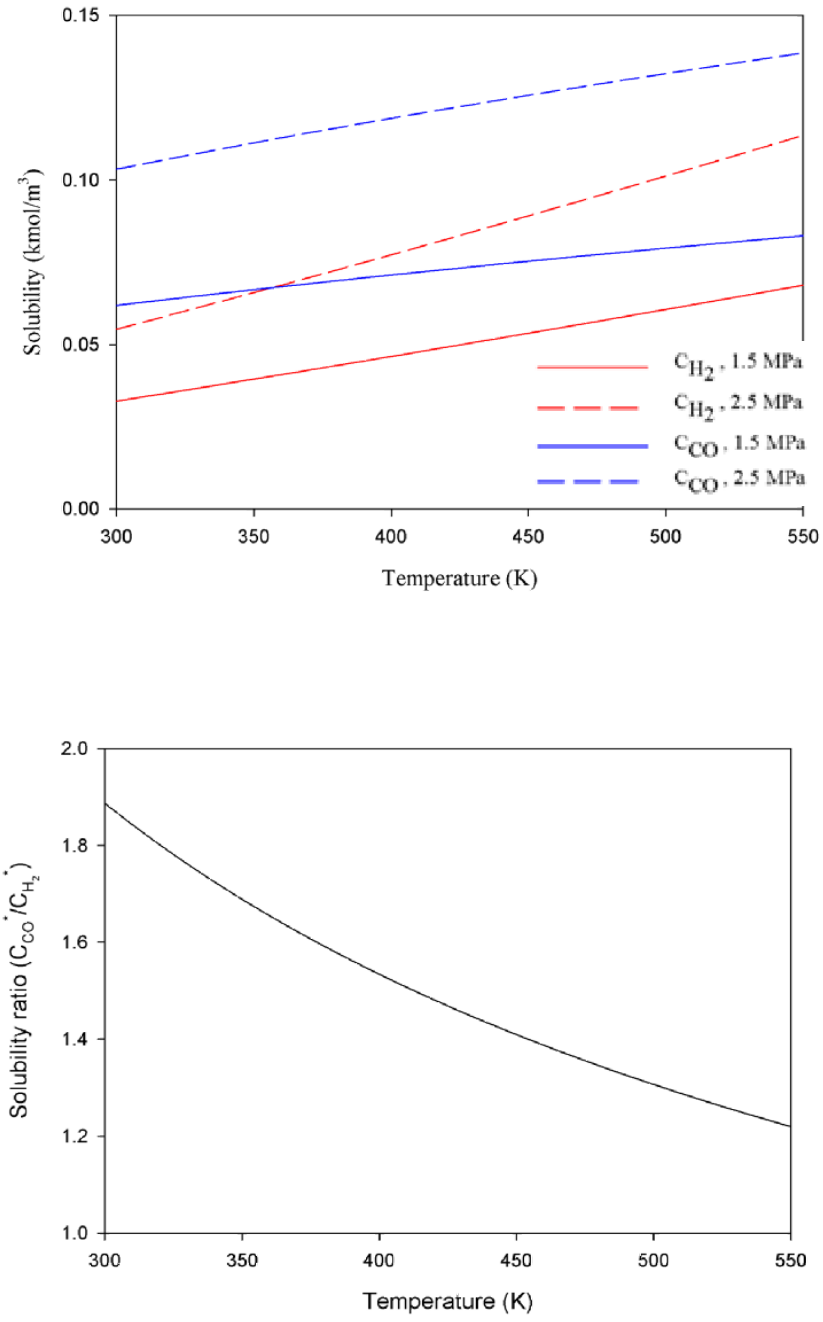

Figure 37. Variation of solubilities with temperature and pressure and the solubility ratio at 1.5 MPa. The ratio does not change much with pressure.

The reason is that the exponent of D, described as n below in Figure 39 increases from 0.5 and finally reaches 1, which represents the film model. Actually, this is the unification brought by the film-penetration model.

Figure 39 presents that the flux of hydrogen increases as it reaches the surface, comperatively to carbonmonoxide. A clearer way to picture this is to plot the fluxes predicted by both models and for both species at different temperatures. These are given in Figure 40.

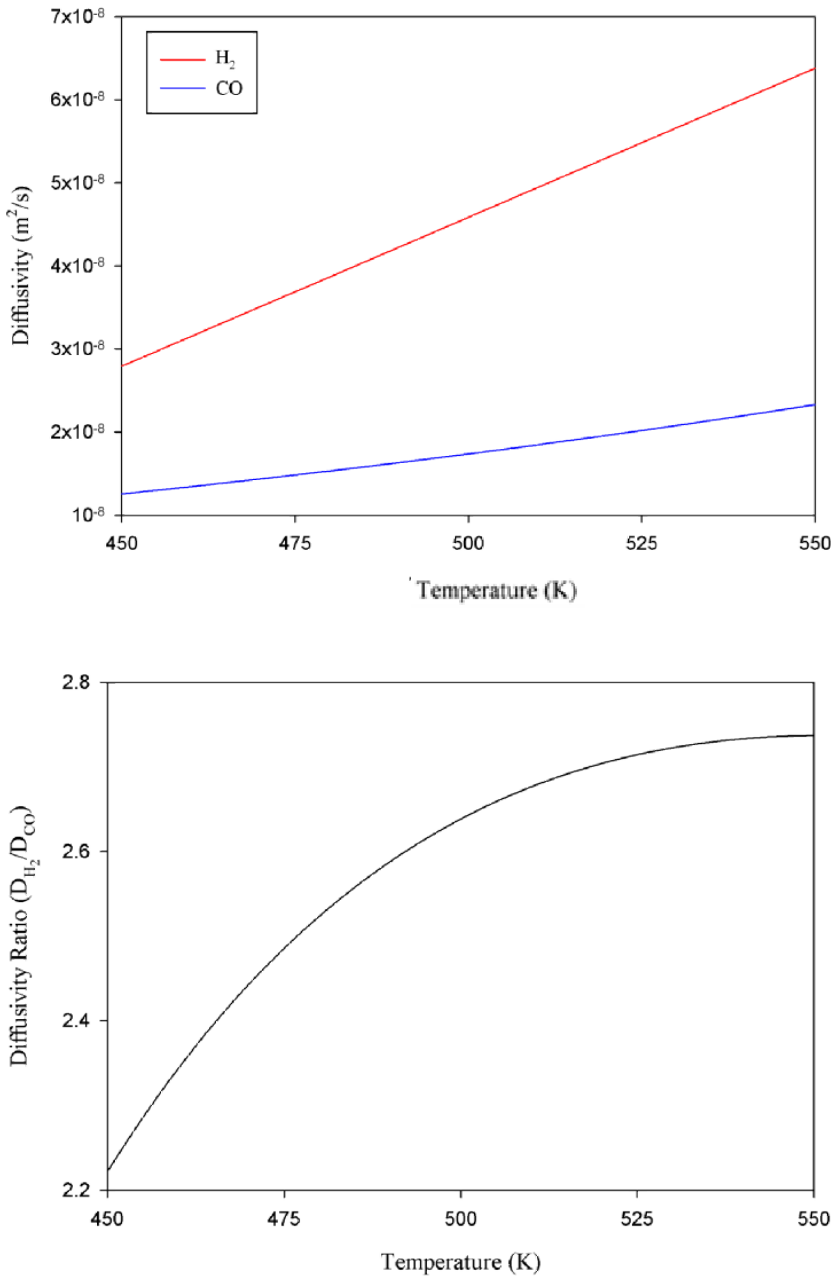

Figure 38. Diffusivities and diffusivity ratios of FTS reactants at 1.5 MPa.

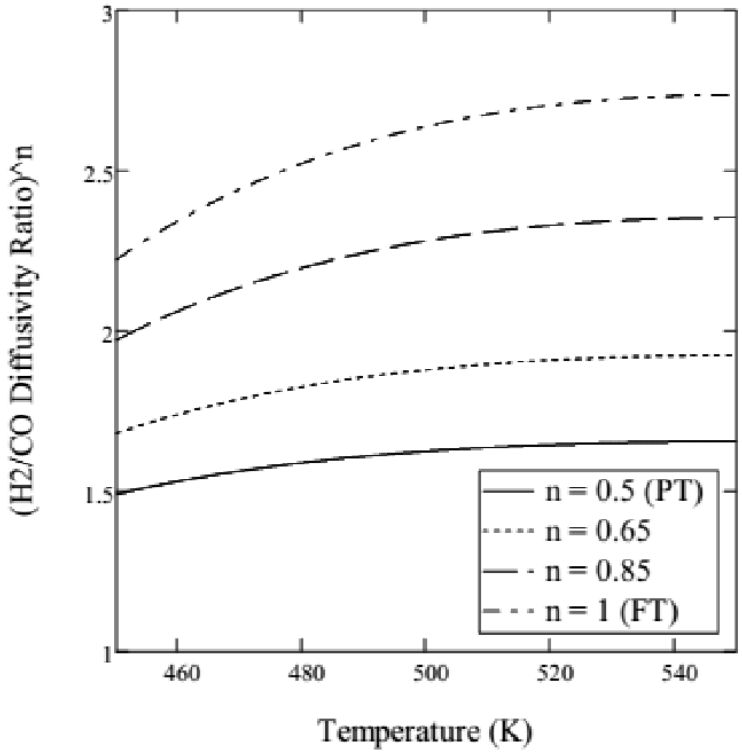

Figure 39. H_2 to CO diffusivity ratios as H_2 accumulates on the surface (as n increases).

Figure 40 shows that at 450 K, the initial surface fluxes of both species are almost the same. But at higher temperatures, for example at 550 K, significantly more hydrogen is transported through the wax. The reason is, the slopes for both the diffusivity and solubility of hydrogen are steeper and more sensitive to temperature, than the slopes of carbon monoxide. At long contact times, the transport rate of carbon monoxide decreases much more than the rate of hydrogen, in scenario of diffusional control. Hence hydrogen diffuses much faster than carbon monoxide does in almost any case, so if their relative flux is to be controlled, the feed, thus interfacial concentrations should be manipulated. That is, to adjust the ratio of adsorbed hydrogen and carbon monoxide on the surface, the ratio of their amounts in the gas phase must be modified accordingly.

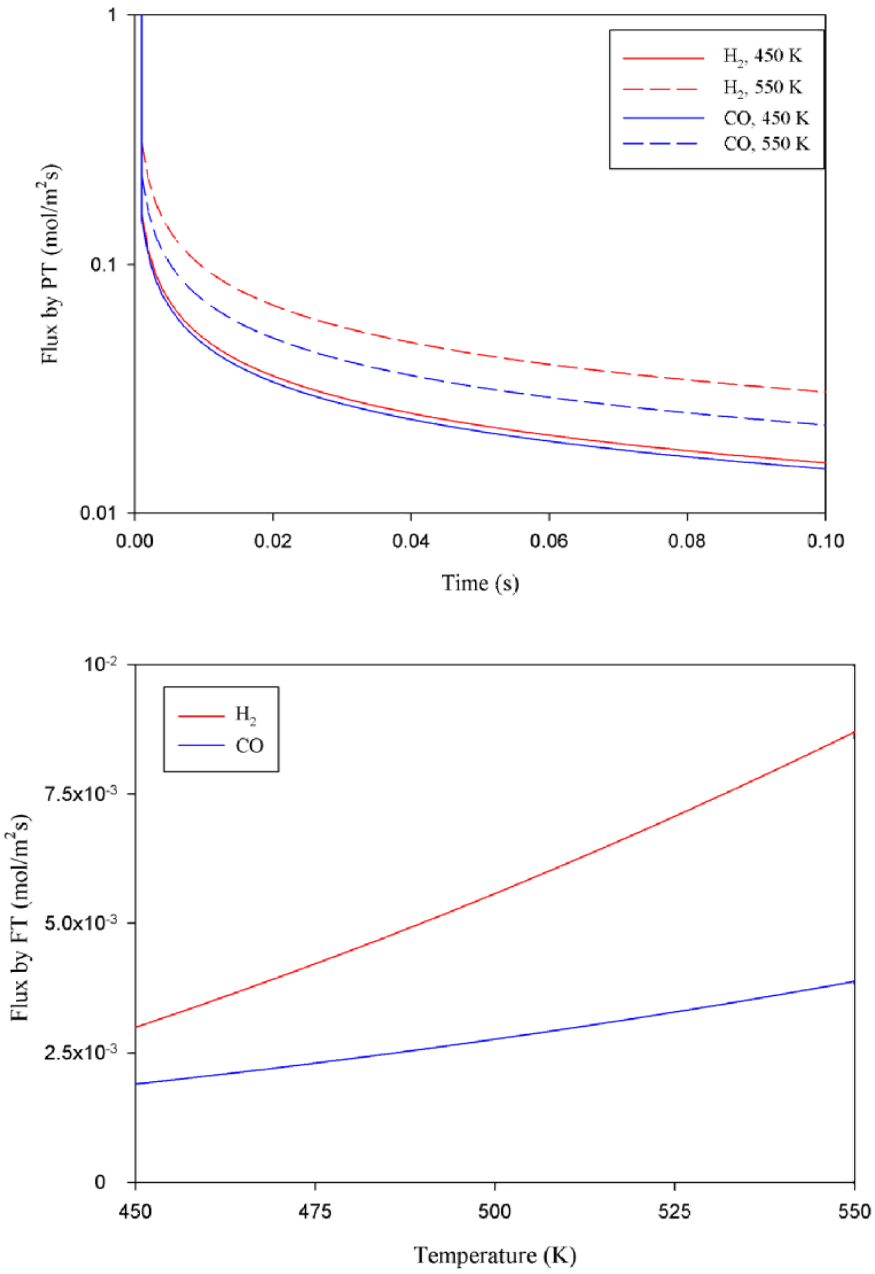

Figure 40. Reactant fluxes. Top: Penetration theory, bottom: film theory. Blue describes CO and red describes H_2.

4.2.1.2. Steady-State Effectiveness Factors for Bimolecular Power-Law Surface Reactions

Unlike homogeneous reactions considered before, a unique steady-state may not exist for surface reactions. This can occur even in isothermal systems, due to the highly nonlinear reaction rate expressions. Here, steady-state distributions and possible multiplicities will be demonstrated.

Inside a wax film, which is dilute in terms of the diffusants, one can write the species transport equations for hydrogen and carbon monoxide at steady state:

$$\frac{d^2C_{CO}}{dx^2} = 0, \qquad \frac{d^2C_{H_2}}{dx^2} = 0 \tag{179}$$

Since the reaction occurs at the boundary, reaction term is included in the boundary conditions:

$$\begin{aligned} &\text{at } x = 0, && C_{CO} = C_{CO}^{*} \text{ and } C_{H_2} = C_{H_2}^{*} \\ &\text{at } x = \delta, && -D_{H_2}\frac{dC_{H_2}}{dx} = k''C_{H_2}{}^{a}C_{CO}{}^{b} \\ &\text{at } x = \delta, && -D_{CO}\frac{dC_{CO}}{dx} = \nu k''C_{H_2}{}^{a}C_{CO}{}^{b} \end{aligned} \tag{180}$$

where k'' is the surface reaction rate. Here, a general power law kinetic expression is used. It is also shown that general power law relations can easily represent various forms of LHHW kinetics, if the applied pressure range is not more than an order of magnitude [213, 214]. The stoichiometric coefficient, ν, can be obtained from the general form of the Fischer-Tropsch reaction:

$$(2n+1)\,H_2 + n\,CO \rightarrow C_nH_{2n+2} + n\,H_2O \tag{71}$$

Upon unitizing the coefficient of hydrogen, the stoichiometric coefficient for carbon monoxide, for paraffin formation only, would be:

$$\nu = \frac{n}{2n+1} \tag{181}$$

Sole methane formation is usually not desired, therefore $n \neq 1$. For $n = 2$, $\nu = 0.4$ and for large n, ν approaches 0.5. When n is around 20, $\nu \cong 0.48$. This value will be used for the stoichiometric coefficient. For sole olefin production, $\nu = 0.5$ for carbon chains of any length. Equations-(179) and (180) can now written as:

$$D_{H_2}\frac{C^*_{H_2}-C_{H_{2S}}}{\delta}=k^{"}C_{H_2S}{}^{a}C_{CO_S}{}^{b}$$
$$D_{CO}\frac{C^*_{CO}-C_{CO_S}}{\delta}=\nu k^{"}C_{H_2S}{}^{a}C_{CO_S}{}^{b} \quad (182)$$

Subscript "s" stands for surface concentration. The number of parameters in the equations above can be reduced by using the second Damköhler number for species "i":

$$Da^{II}{}_i=\frac{k^{"}\delta}{D_i} \quad (183)$$

The use of the Damköhler number is not for non-dimensionalization, but for parameter lumping only. Also, one may define the diffusivity ratio as:

$$\frac{Da^{II}{}_{CO}}{Da^{II}{}_{H_2}}=\frac{D_{H_2}}{D_{CO}}=\gamma \quad (184)$$

Now, the Equations-(182) become:

$$f_1\left(C_{H_2S},C_{CO_S}\right)=Da^{II}{}_{H_2}\,C_{H_2S}{}^{a}C_{CO_S}{}^{b}-\left(C^*_{H_2}-C_{H_2S}\right)=0$$
$$f_2\left(C_{H_2S},C_{CO_S}\right)=\nu\gamma Da^{II}{}_{H_2}\,C_{H_2S}{}^{a}C_{CO_S}{}^{b}-\left(C^*_{CO}-C_{CO_S}\right)=0 \quad (185)$$

At 500 K, numerical values for equilibrium concentrations and the diffusivity ratio can be substituted into Equations- (185). Then, they can be solved for any $Da^{II}{}_{H_2}$. The algebraic Equations- (185) are mostly nonlinear for various values of a and b. They can be solved for species' surface concentrations with a code using Newton-Raphson (NR) root solving algorithm and combined L-U decomposition. The resulting surface concentrations will yield the effectiveness factor, which can be defined as:

$$\eta=\frac{\text{reaction rate at the surface}}{\text{reaction rate with interfacial conditions}}$$

$$\eta=\frac{k^{"}C_{H_{2S}}{}^{a}C_{CO_S}{}^{b}}{k^{"}C^*_{H_2}{}^{a}C^*_{CO}{}^{b}}=\left(\frac{C_{H_{2S}}}{C^*_{H_2}}\right)^{a}\left(\frac{C_{CO_S}}{C^*_{CO}}\right)^{b} \quad (186)$$

$Da^{II}{}_{H_2}$ is varied between 10^{-6} to 10^{3}. For low $Da^{II}{}_{H_2}$, the physics represents almost physical absorption and saturation in the film is inevitable, since the reaction is very slow. High $Da^{II}{}_{H_2}$ should mean very fast reactions and therefore the reaction is

diffusion controlled. The results for effectiveness factor are plotted in Figure 41. A more conditioned solver is necessary to resolve cases with negative orders, due to the existence of multiple roots, even at isothermal conditions.

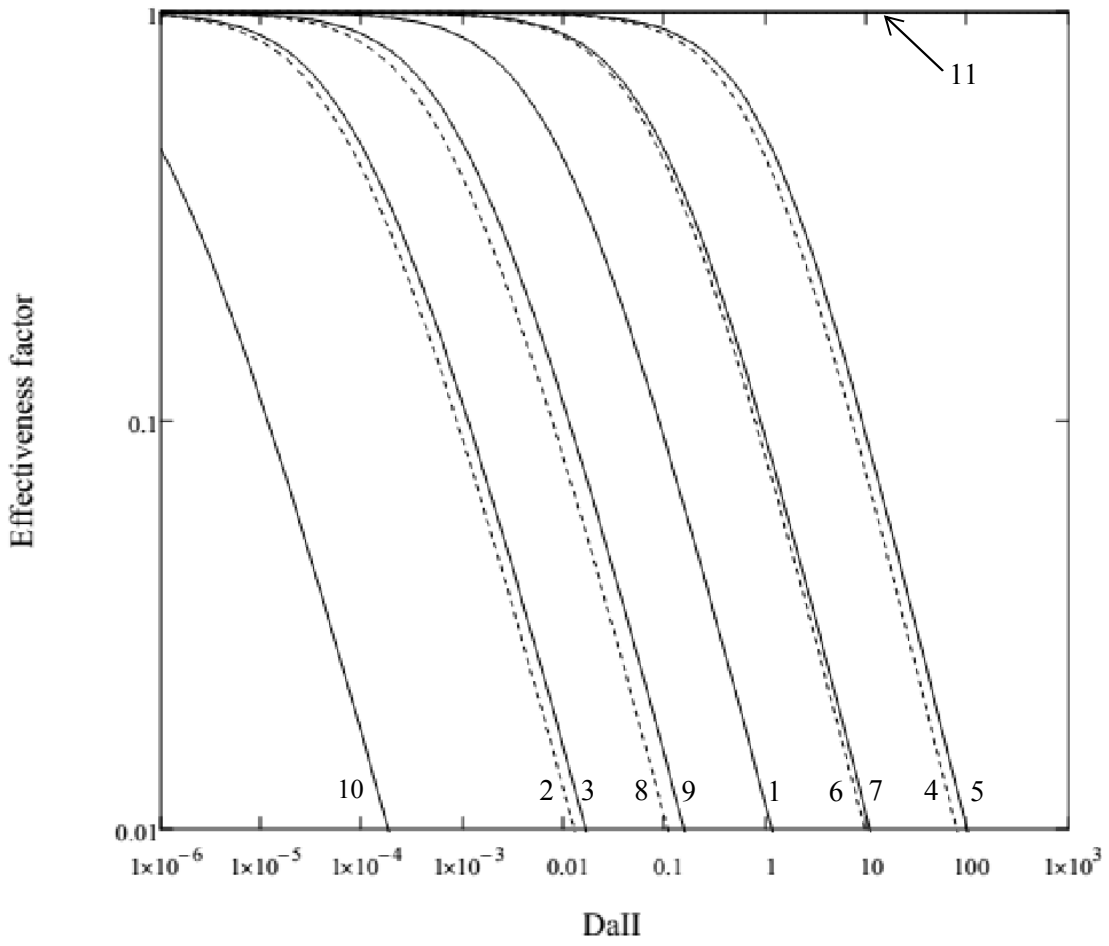

case	1	2	3	4	5	6	7	8	9	10	11
a	1	1	2	1	0	0.5	1	0.5	2	2	0
b	1	2	1	0	1	1	0.5	2	0.5	2	0

Figure 41. Effectiveness factors for various reaction orders. a: order of H_2, b: order of CO.

Since CO is a poisoning species, its order must be negative, similar to the literature data given in Table 5. For $a = 1$ and $b < 0$, effectiveness factors may take values higher than 1 at some $Da^{II}_{H_2}$ values. This is shown on Figure 42 below. Such a behavior was also shown by Roberts and Satterfield [215, 216] in isothermal LHHW

kinetics and by Rajadhyaksha et. al. [217] in nonisothermal LHHW and general power law kinetics, both for homogeneous reactions. The possible multiplicity regions will be shown exactly, since these regions are not displayed clearly by the authors.

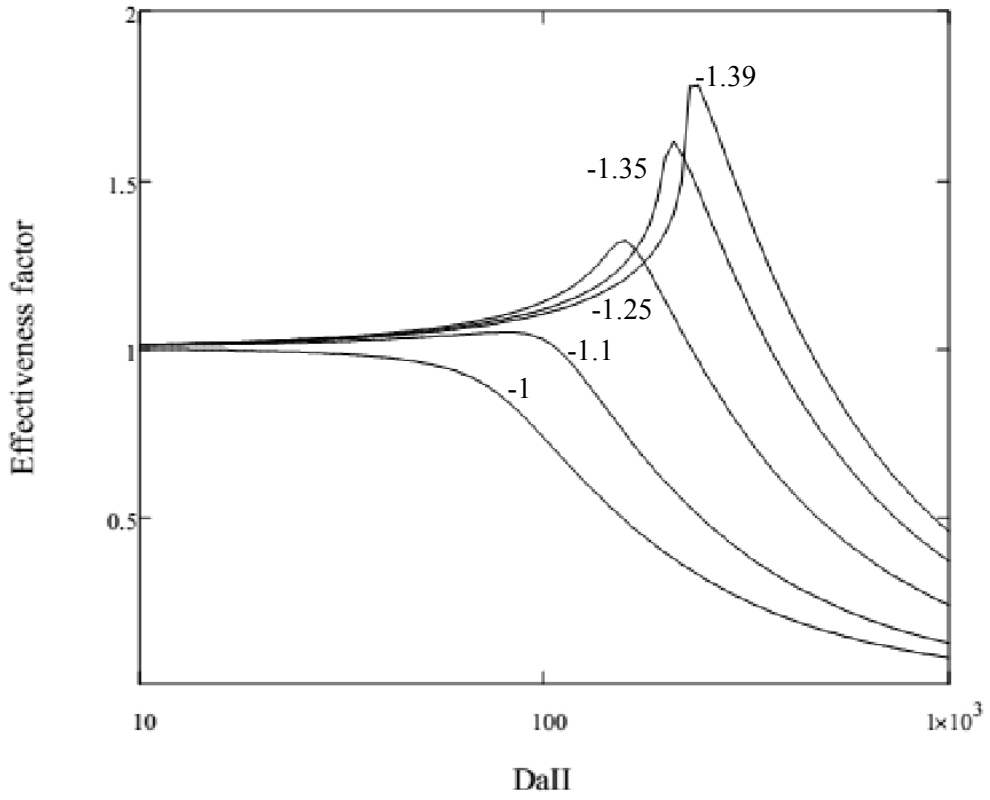

Figure 42. The formation of the peak in effectiveness factor and transition into multiple steady-states. Numbers define the order of CO, i.e. b.

As b decreases, the peak in the effectiveness factor vs $Da^{II}_{H_2}$ plot gets curved backwards. In this case, multiple steady states occur, and their formation depends on initial conditions [218]. The roots of the multiplicity cases above were found by reducing the system into a single equation:

$$f\left(C_{H_2S}\right) = \nu\gamma\left(C^*_{H_2} - C_{H_2S}\right) - \left[C^*_{CO} - \left(\frac{C^*_{H_2} - C_{H_2S}}{{Da^{II}}_{H_2} {C_{H_2S}}^{a}}\right)^{\frac{1}{b}}\right] = 0 \qquad (187)$$

with

$$C_{CO_S} = \left(\frac{C^*_{H_2} - C_{H_2S}}{Da^{II}{}_{H_2} C_{H_2S}{}^{a}} \right)^{\frac{1}{b}} \tag{188}$$

Then a bracketed NR method is used to find the first root, $C_{H_2S}{}^{1}$. After that, the found root is eliminated by employing:

$$g\left(C_{H_2S}\right) = \frac{f\left(C_{H_2S}\right)}{C_{H_2S} - C_{H_2S}{}^{1}} \tag{189}$$

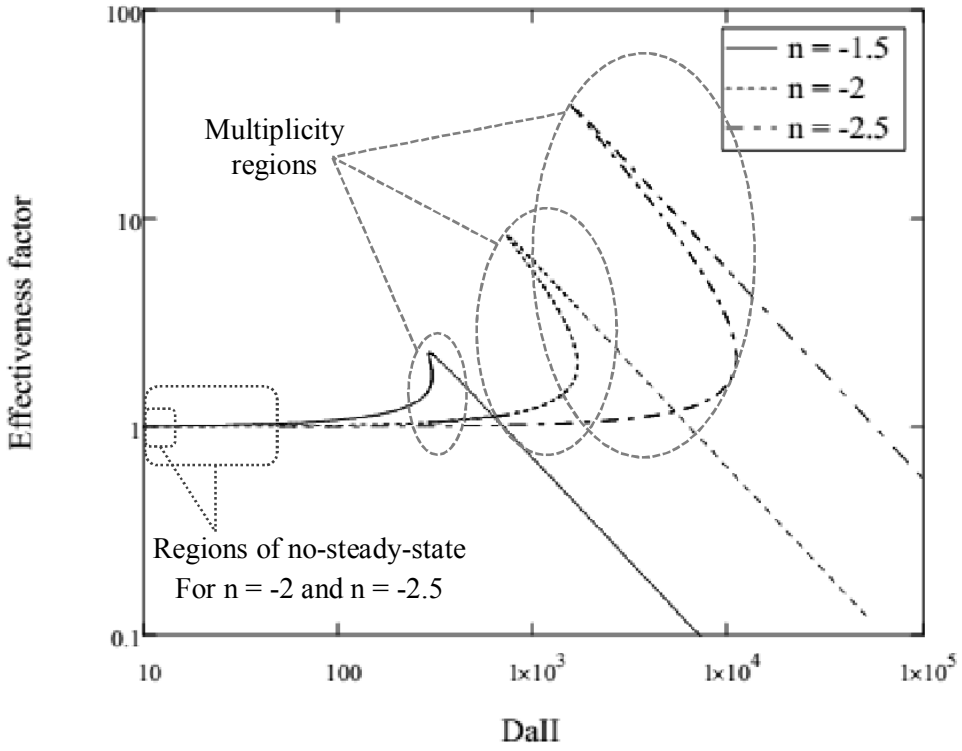

Figure 43. Effectiveness factors with negative orders.

This is followed by using an open NR formalism to find the second root. The same procedure is again applied in finding the third root. The code for this program is given in Appendix-F. The results are given on Figure 43. Multiplicities, according to the situation when the physical constants, i.e. $Da^{II}{}_{H_2}$, are known, are marked with oval circles. From the perspective of experimentation with unknown kinetic data, $\eta > 1$ would directly mean multiplicity, since the effectiveness factor can be experimentally obtained.

It should also be noted that there occurs to be a limiting $Da^{II}_{H_2}$ for each negative b value where a steady-state condition does not exist below it. The exact boundaries of this region may be overshadowed by the tolerances set in the NR algorithm. Nevertheless, the regions for $b = -2$ and -2.5 are roughly displayed in Figure 43. Such behavior may indirectly mean oscillatory kinetics.

4.2.1.3. Step 1: Conceptual Periodic Operation with General Negative Order Kinetics

Moving on from the steady-state solutions and effectiveness factors of a general power-law surface reaction in a film, one may suggest employing high Da^{II} numbers to bring effectiveness up to values larger than one. From the definition of Da^{II}, one may suggest thicker liquid films, but it is logical to keep the film thickness small as possible for a fast reaction, since large films would lead to higher diffusional resistances and therefore higher residence times. This is due to an increase in times spent by the molecules to reach the catalyst. So, thinner films should lead to smaller reactors with short residence times. This is valid as long as there is no recycle, in accordance with the hypothesis of microreactors.

At this instance, a special case of a surface reaction can be investigated, which approximately represents the FTS. With the knowledge that CO poisons the catalyst surface, CO should have a negative degree in the reaction rate expression. Similar to the previously given rate expressions, one may assume:

$$r_{H_2} = k'' \frac{C_{H_2 S}}{C_{CO_S}^{\ 2}} \tag{190}$$

This forecasts that rates can be enhanced, when CO is kept at low concentrations near the surface. This may be accomplished by operating the reactor in unsteady-state, since steady-state rates would be rather low. An option is to feed H_2 and CO in a sequential and periodic manner. With a predefined switching period, t_{sw}, a realistic description of such an operation would be a smoothed square wave for interfacial concentrations. This means a frequency of $2t_{sw}$. The corners of the square wave are

smoothed by a logistic function, which has an s-shaped sigmoid geometry. The width of the smoothed region is selected as $t_{sw}/2$. For H_2, the mathematical translation is:

$$f_{wave,H_2}(t) = \begin{cases} \dfrac{1}{1+e^{-(8e/t_{sw})t}}, & \text{for } 0 < t < t_{sw}/4 \\ 1, & \text{for } t_{sw}/4 < t < 3t_{sw}/4 \\ 1 - \dfrac{1}{1+e^{-(8e/t_{sw})t}}, & \text{for } 3t_{sw}/4 < t < 5t_{sw}/4 \\ 0, & \text{for } 5t_{sw}/4 < t < 7t_{sw}/4 \\ \dfrac{1}{1+e^{-(8e/t_{sw})t}}, & \text{for } 7t_{sw}/4 < t < 2t_{sw} \end{cases} \quad (191)$$

and $f_{wave}(t + 2t_{sw}) = f_{wave}(t)$, since $2t_{sw}$ is the period of the wave. For CO:

$$f_{wave,CO}(t) = \begin{cases} \dfrac{1}{1+e^{-(8e/t_{sw})t}}, & \text{for } 0 < t < t_{sw}/4 \\ 1, & \text{for } t_{sw}/4 < t < 3t_{sw}/2 \\ f_{wave,H_2}(t - t_{sw}), & \text{for } 3t_{sw}/2 < t \end{cases} \quad (192)$$

An example is given in Figure 44. A smoothed function is also need for attaining convergence in the numerical solutions that follow. Now for both species, the problem can be defined as:

$$D_i \frac{d^2C_i}{dx^2} = \frac{dC_i}{dt}, \qquad \begin{array}{ll} \text{at } x = 0, & C_i = f_{wave,i}(t)C_i^* \\ \text{at } x = \delta, & -D_i \dfrac{dC_i}{dx} = r_i \\ \text{at } t = 0, & C_i = C_{i_0} \end{array} \quad (193)$$

where $f_{wave,i}(t)C_i^*$ represents the time dependent fluctuating interfacial concentrations. As numerical values, δ is taken as 50μm, $C_{H_{2_0}} = C_{CO_0} = 5\ \text{mol/m}^3$. Diffusivities and solubilities are calculated at $T = 500$ K and $P = 1.5$ MPa. The values of γ and ν are kept as the same. The reaction rate constant is taken as 1 $\text{mol/m}^2\text{s}$, which leads to $Da^{II}_{H_2} = 1090$. In steady-state, the system is clearly in the multiplicity region, as can be seen from Figure 43.

The physics may be considered to represent annular flow. When clock time is replaced with exposure time, the interfacial concentrations change as hydrogen and carbon monoxide are periodically blown through the gas core. If the core is fast and concentrated with hydrogen and carbon monoxide, one may assume that interfacial concentrations switch according to the wave function all along the contact line. The

velocity field in the wax film is omitted since the aim is to demonstrate rate enhancements only qualitatively. For further analysis, a 2D model may be employed.

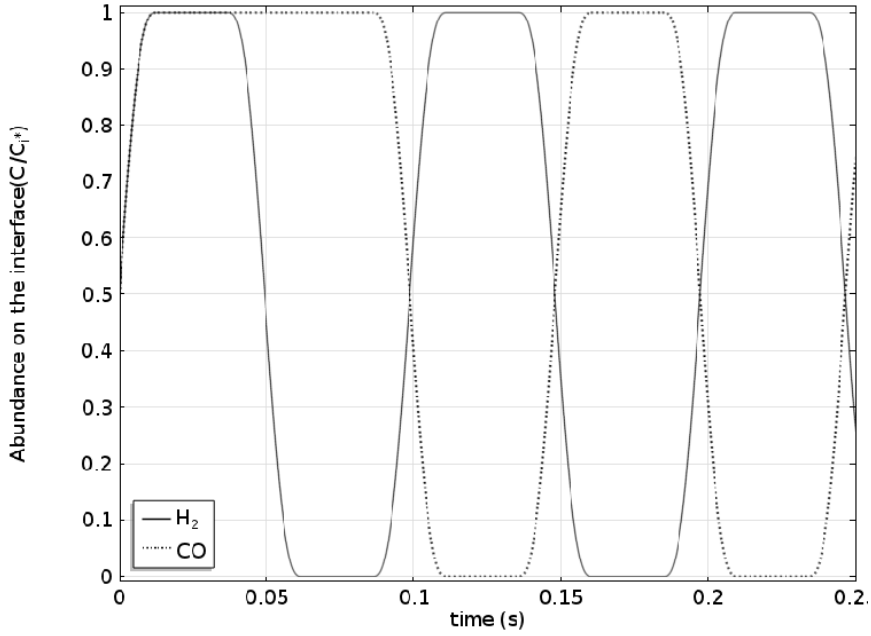

Figure 44. Smooth variations of H_2 and CO with t_{sw} = 0.05 s. Both species are fed in the first time period, and then H_2 feed is interrupted.

The problem numerically solved with COMSOL (version 4.3b). The solution is obtained by taking fixed time steps. This is done since freely taken time steps lead to numerical errors in this problem since there are sharp changes in the reaction rate. Free time steps lead to a large number of dents on the time trends of the reaction rate.

The eventual steady-state depends on the initial concentrations. In Figure 45, they are shown by points 1, 2 and 3 for the selected $Da^{II}_{H_2}$ It is observed that for high $C_{H_2 0}$ and very low C_{CO_0} the system tends to state 3, and as C_{CO_0} increases, the system tends to state 2 and then to state 1.

For $t_{sw} = 0.05, 0.1, 0.2$ s, the unsteady case given by Equation-(193) is solved. The time trend of reaction rate is given in Figure 46 and concentrations above the surface for a single switching period is given on Figure 47.

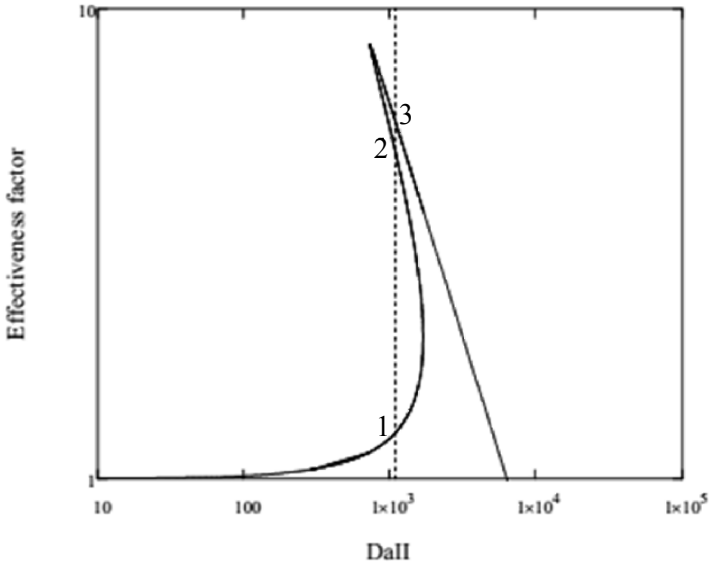

Figure 45. Multiplicity at $Da^{II}_{H_2} = 1090$.

Figure 46 shows that 1000 fold rate enhancements are possible. The dents in this figure are due to numerical errors coming from faulty time stepping, which are not completely prevented by taking fixed time steps. But these errors neither change the characteristics, nor the accuracy of the results that come after them. As demonstrated by Figure 47, there are secondary peaks of H_2 on the surface. The reason may be attributed to multiplicity, since the system may tend quickly to another state (akin to Figure 45), thereby giving an additional response.

By calculating the area below the time trend curves, one can obtain the total amounts reacted. The total amounts reacted between time periods t_1 and t_2 ,

$$n_{H_2} = \int_{t_1}^{t_2} r_{H_2}\, dt \qquad (194)$$

can provide a better quantitative judgment on the improvement of reaction rate. These results are shown by Figure 48. The figure shows that an optimal switching time with respect to the magnitudes of the reaction rate constant and the total exposure time must exist. Upon determining it, significant rate enhancements may be obtained.

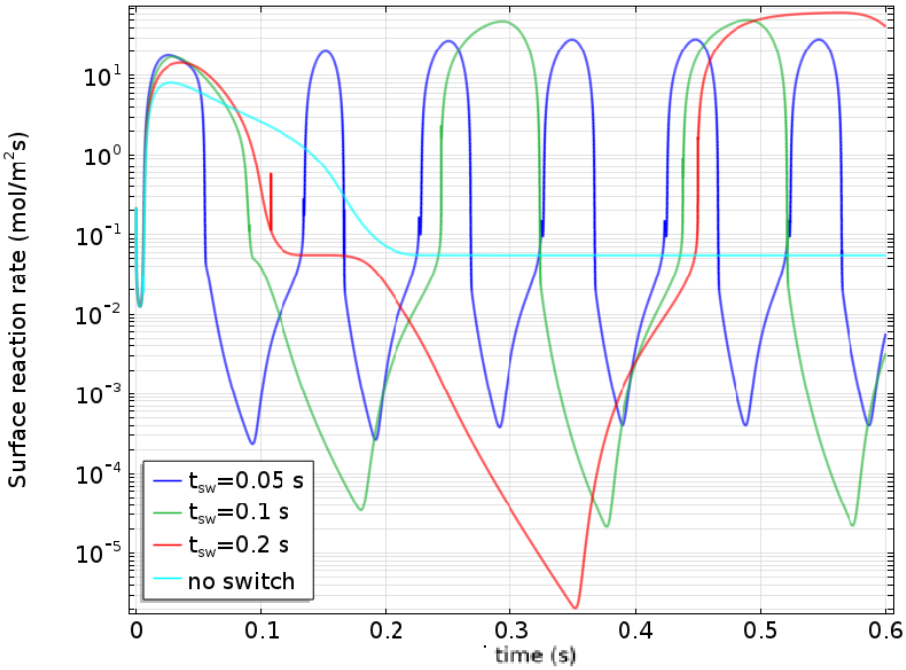

Figure 46. Time trend of reaction rate with different switching periods.

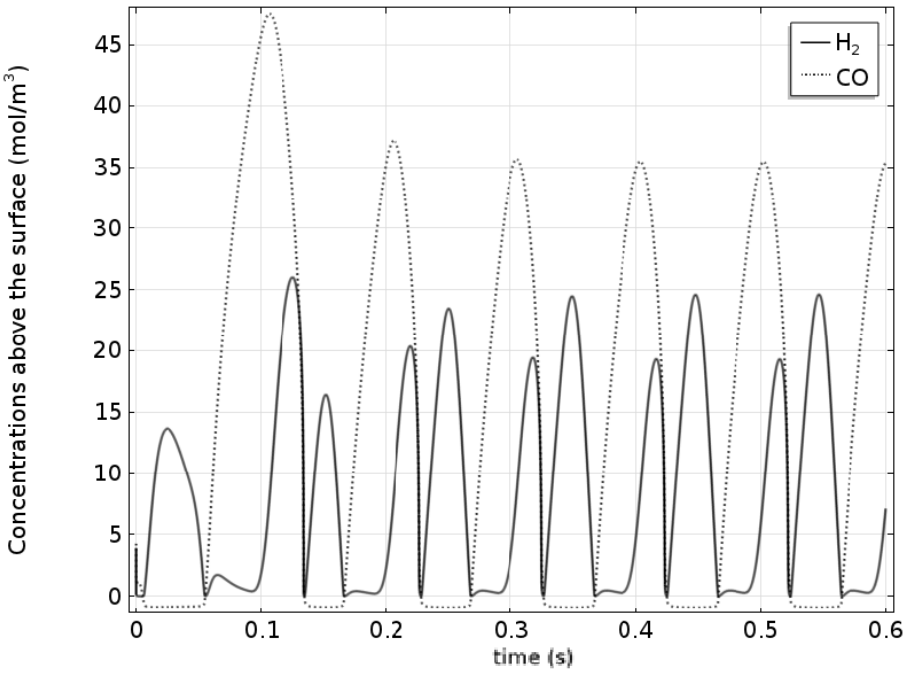

Figure 47. Concentrations above the surface for $t_{sw} = 0.05$ s.

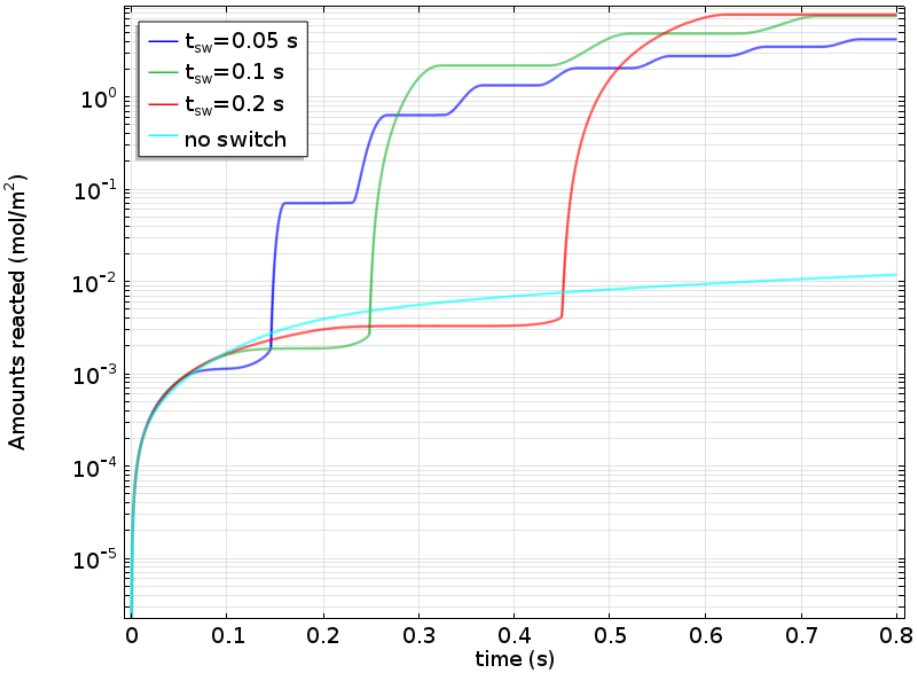

Figure 48. Total amounts of H_2 reacted over time with different switching periods.

The reaction rates are adjusted to prevent the occurrence of negative concentrations and almost infinitely fast rates. This is done by assuming the reaction rate as zero when the CO concentrations are less than $0.01C_{CO}^{*}$. Decreasing this limiting value tends the system to negative concentrations, thus smaller time steps are needed. It has been observed that selecting the limiting value does not change the physics much. For smaller limiting values, reaction rate peaks become sharper and have higher values, otherwise they get broader and their maximum decreases. However the total amounts reacted do not change much, and the general characteristics is preserved. One may also provide the average rates for different switching times. For t_{sw} equal to 0.05, 0.1 and 0.2 s, the average rates (in mol/m^2) become 6.702, 13.350 and 19.612 respectively, where the unmodified steady-state rate is 0.055 mol/m^2 only.

The order of CO was selected as -2 for this section to demonstrate the behavior vividly. The rate enhancements are expected to be still prevalent, when the order of CO is smaller than -1.

4.2.1.4. Step 2: Periodic Operation with Realistic Kinetics and No Diffusion

In this section, now realistic kinetics will be employed to demonstrate the rate enhancements in a semi-batch setup without any effects diffusion. The mechanism of Kellner and Bell [162] is used by Uner [219] to explain the effects of alkali promoters on the selectivity of FTS products. In this work, pseudo equilibrium expressions of methane formation rates are given. When the reaction product is mostly methane:

$$r_{C_1} = \left\{k_{10}K_2{K_3}^2K_7K_8K_9\left[k_4\left(K_3P_{H_2}\right)^{0.5} + k_6K_1P_{CO}\right]/{K_1}^3\right\}^{0.5}\frac{P_{H_2}}{{P_{CO}}^{1.5}} \qquad (195)$$

Although there are many rate and equilibrium constants, they can be lumped to get:

$$r_{C_1} = k_0\left({P_{H_2}}^{0.5} + \gamma P_{CO}\right)^{0.5}\frac{P_{H_2}}{{P_{CO}}^{1.5}} \qquad (196)$$

where

$$k_0 = \left(\frac{k_{10}k_4K_2{K_3}^{2.5}K_7K_8K_9}{{K_1}^3}\right)^{1/2}, \qquad \gamma = \frac{k_6K_1}{k_4{K_3}^{0.5}} \qquad (197)$$

γ shows the relative rates of CO_2 and H_2O formation. Higher γ means that CO_2 formation dominates and vice versa. The value of γ depends on the nature of the catalyst. First, methane formation is considered, so from reaction stoichiometry:

$$r_{H_2} = -3r_{C_1} = r_{CO} \qquad (198)$$

When longer hydrocarbons dominate, methane formation rates take the form:

$$r_{C_1} = k_{10}\left\{(1-\alpha){K_2K_3}^{3.5}K_7K_8{K_9}^2\left[k_4\left(K_3P_{H_2}\right)^{0.5} + k_6K_1P_{CO}\right]/k_p{K_1}^5\right\}^{1/3}\frac{{P_{H_2}}^{7/6}}{{P_{CO}}^{5/3}} \qquad (199)$$

Lumping results in:

$$r_{C_1} = k_{0_{HC}}(1-\alpha)^{1/3}\left({P_{H_2}}^{0.5} + \gamma P_{CO}\right)^{1/3}\frac{{P_{H_2}}^{7/6}}{{P_{CO}}^{5/3}} \qquad (200)$$

with

$$k_{0_{HC}} = k_{10}\left(\frac{k_4K_2{K_3}^{2.833}K_7K_8{K_9}^2}{k_p{K_1}^5}\right)^{1/3} \qquad (201)$$

The chain growth probability is given in implicit form:

$$\frac{(1-\alpha)^{4/3}}{\alpha}$$

$$= \frac{k_{to} + k_{tp}\left(K_3 P_{H_2}\right)^{1/2}}{\left\{k_p{}^2 K_1 K_2 K_3{}^{0.5} K_7 K_8 K_9{}^{-1}\left[k_4\left(K_3 P_{H_2}\right)^{0.5} + k_6 K_1 P_{CO}\right]/k_p K_1{}^5\right\}^{1/3}} \frac{1}{P_{H_2}{}^{1/6} P_{CO}{}^{1/3}} \quad (202)$$

It can be simplified by neglecting k_{to} and lumping parameters:

$$\frac{(1-\alpha)^{4/3}}{\alpha} = k_\alpha \frac{P_{H_2}{}^{1/3}}{\left(P_{H_2}{}^{0.5} + \gamma P_{CO}\right)^{1/3} P_{CO}{}^{1/3}} \quad (203)$$

Here:

$$k_\alpha = \left(\frac{k_{tp} K_1{}^5 K_9}{k_p k_4 K_1 K_2 K_3{}^{0.5} K_7 K_8}\right) \quad (204)$$

Hence, α is solved for each P_{H_2} and P_{CO} to get the reaction rate at that instant.

Without considering diffusion, the stoichiometric consumption of CO and H_2 is investigated, in order to see if the behavior is the same with the previous section. Thus, a semi-batch reactor is selected, where again the reactants are fed periodically. For H_2, one may give the equation to be solved:

$$\frac{dP_{H_2}}{dt} = r_{H_2} + pf(t_{sw}, t) \quad (205)$$

The pf (periodic forcing) function is the periodic feed function, which is time dependent. The function is a smoothed square wave, similar to the one presented in the previous subsection, but this time, the feed is based on stoichiometric ratios given by Equation-(198). It is presented by Figure 49.

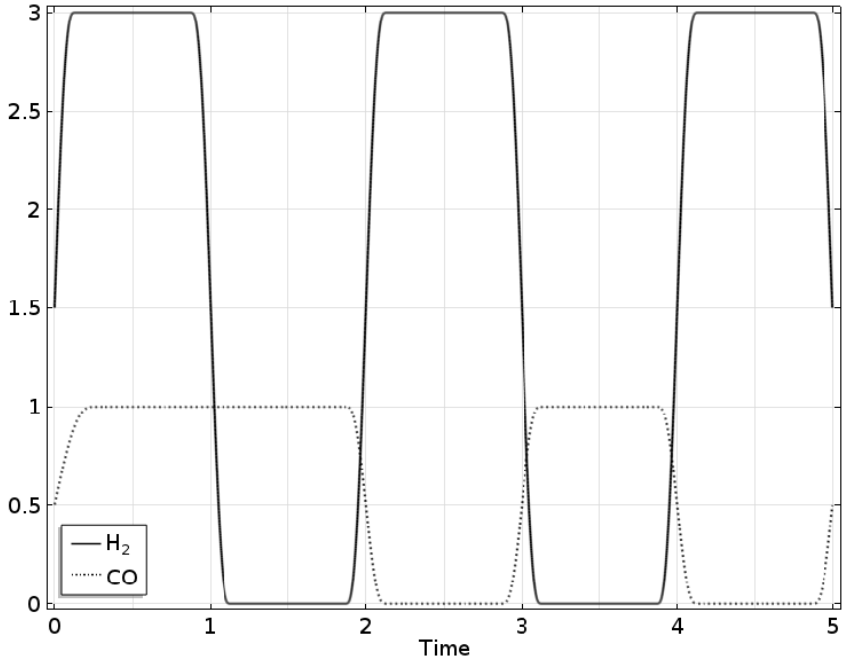

Figure 49. Square wave with stoichiometric ratios.

Note that when the relative domination of CO_2 and H_2O formation is predefined, there are two rate constants for longer hydrocarbon formation. The first one, $k_{0_{HC}}$, can always be compounded with time as a Damköhler number: $Da = k_{0_{HC}}t$. This means that if k_α is known, which is to be found from experiments, one may run an analysis based on the dimensionless time described by Da and see the response of kinetics. The speed and behavior of the response will then be quantified with respect to the relative speed of kinetics and the amount of periodic feed.

Here, the rate constants are taken as 1. Thus, time has also taken as a unitless quantity. Chain growth probability is solved with an NR algorithm at each time step. The oscillations in partial pressures and reaction rates are given in Figure 50 and Figure 51.

The main result from simulations is that Figure 50 and Figure 51 show a similar trend with Figure 46 and Figure 47. A steady-state rate for comparison is not possible in this case. In addition, the simulations show that the H_2/CO ratio should be smaller than 3. In the simulations, CO started to accumulate and reaction rates started to fall. Therefore the CO partial pressure was limited to 1, only then a periodic steady-state

in reaction rate was obtained. Variation of k_α might give the H_2/CO ratios according to chain propagation probability.

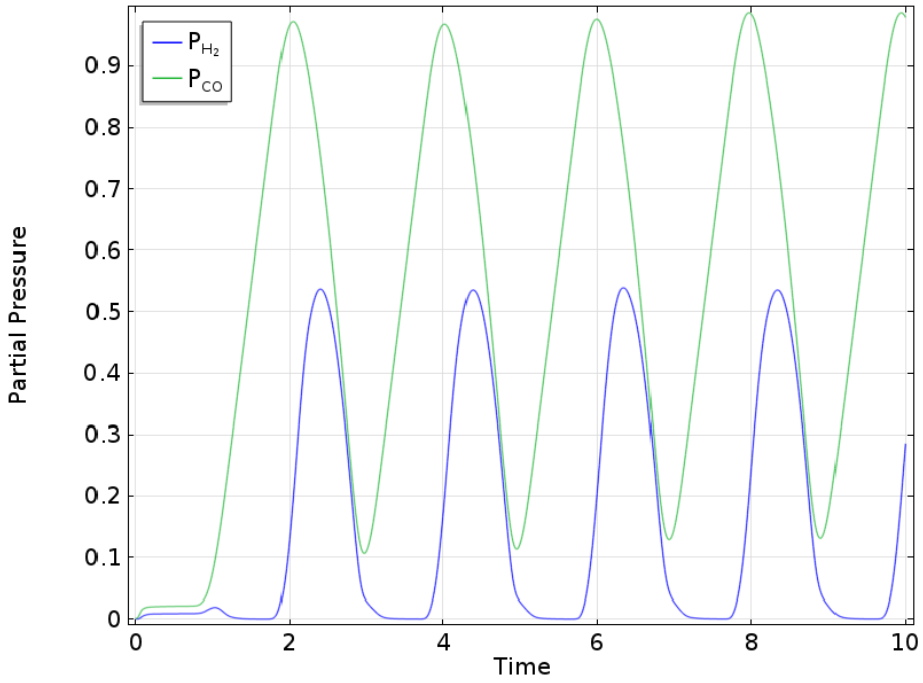

Figure 50. Oscillations in partial pressures.

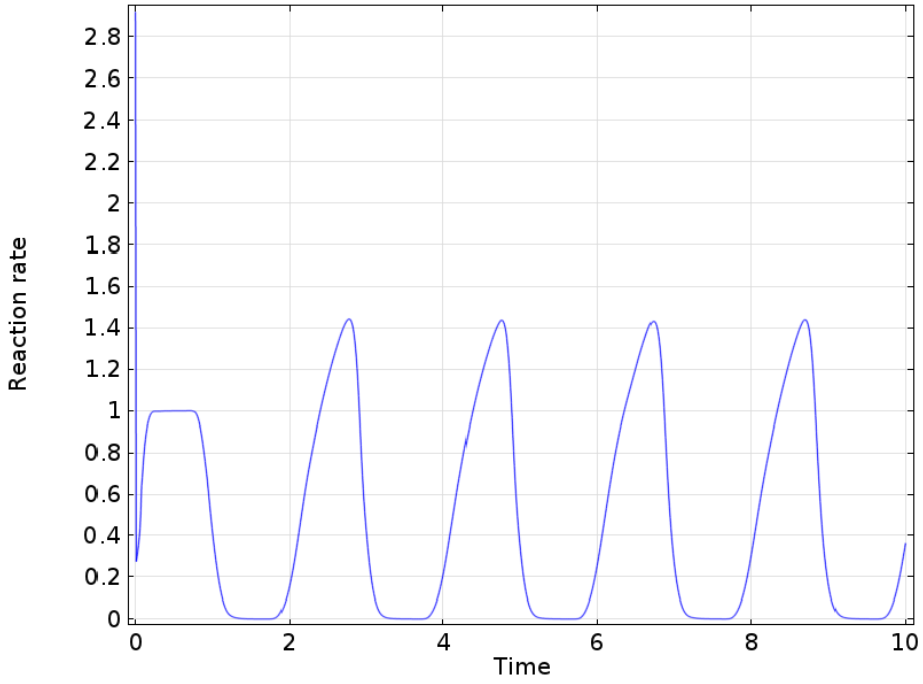

Figure 51. Oscillations in reaction rate.

4.2.1.5. Step 3: A Compartment Model of Taylor Flow for FTS

In the previous sections, periodic operation of FTS was investigated first by solving the diffusion-reaction problem with negative order power law kinetics and then by solving the more realistic rate equations in a batch system without diffusion. Now the methodology can be compounded into a more realistic setup.

This part will implement FTS into Taylor flow with help of a conceptual model. Since Taylor flow is naturally periodic, its coupling with FTS seems quite interesting. Although the feasibility and possibility is not known, it will be assumed that sequential bubbles of almost pure hydrogen and carbon dioxide are fed to the microchannel. The feed gases for FTS in conventional reactors are usually mixed as syngas. If the flow parameters of Taylor flow, like film thickness, bubble length, bubble velocity and liquid slug size, can be tuned, one may increase the selectivity and/or conversion of the process. The flow parameters depend on the geometry of the gas-liquid micro-contactor, the gas holdup and physical properties of the gas and liquid.

Since coupling multiphase flow fields with reactions involving many species is very laborious in CFD simulations, one may only run multiphase flow simulations with where hydrogen and carbon monoxide are fed into liquid paraffinic wax. This would give the flow parameters, like bubble and liquid slug lengths for example. In addition, CFD may mark out the region of feed velocities where Taylor flow reigns, akin to Figure 2. However, to resolve the film thickness in numerical simulations, a very dense mesh with aspect ratios close to unity is needed. It is also important to note that microchannels with non-circular cross-sections lead to different bubble shapes, lengths and film thicknesses.

Assuming that the flow and kinetic data is available, one may create a relatively simple model for Taylor flow. A representative scheme for a circular channel is given in Figure 52. The model is discrete in space and time. Compartments are defined to encapsulate the bubble and the liquid slug. The compartments are like unit cells that are lined up along the flow direction. Each comprises the film surrounding the bubble, the front cap of the bubble, the liquid slug and the rear cap of the bubble ahead. The bubble length is taken as the film length, L_B, and the slug length also

comprises the length of two bubble caps, which are assumed as spherical. It is given as L_S. So, length of each compartment would be $L_{cell} = L_B + L_S$. L_B and L_S can be obtained from CFD simulations.

Next, an important simplification is made on discretizing the time. Although the model is transient, time is divided into periods in which the bubbles and liquid slugs are assumed as stationary and confined to the compartment. After each period, they leave their compartment and move into the next one. As bubbles leave their previous compartments, they shrink instantly due to gases absorbed by the wax. The period for switching compartments is given as $t_p = L_{cell}/v_B$. v_B is the translational velocity of the bubbles. The velocity of the bubbles is assumed as constant throughout the compartments. The velocity and the lengths of the bubbles may vary slightly for bubbles of hydrogen and carbon monoxide. Therefore bubble collision and coalescence may occur for various gas holdups and channel lengths in reality. Such phenomena are neglected.

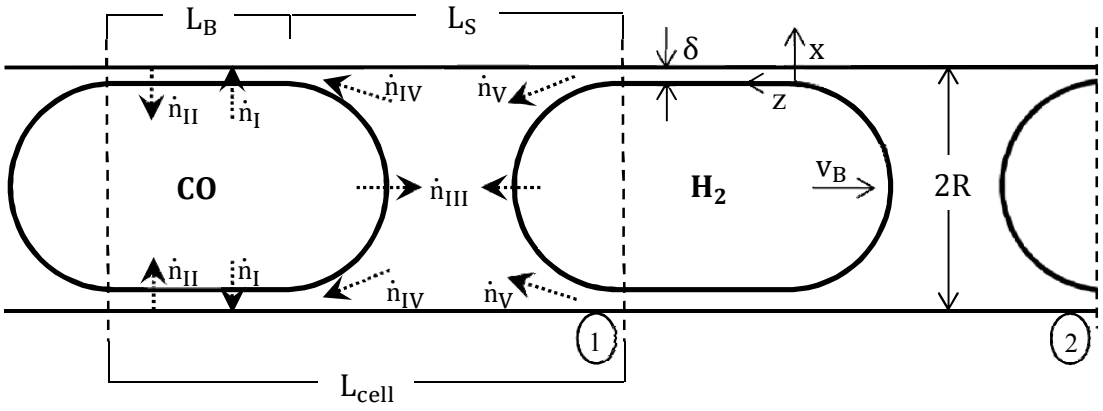

Figure 52. The compartment model of Taylor flow

In each compartment there are three regions: the film, the bubble and the liquid slug. These interact with each other by exchanging mass by diffusion and convection. According to the mass fluxes indicated by dotted arrows in Figure 52, the film is fed via reactants that are dissolved from the bubble ($\dot{n}_I$) and loses volatile products to the bubble ($\dot{n}_{II}$). It is also fed by the wax coming from the liquid slug in front of the bubble ($\dot{n}_{IV}$) and loses it to the slug behind ($\dot{n}_V$). For the bubble, additional mass

transport occurs via the front and rear caps, in addition to the dissolution-vaporization dynamics that occur on the film interface. The reactants also dissolves from the caps ($\dot{n}_{III}$) and join the contents of the liquid slug. Considering the liquid slug, it is fed by the wax leaving the film that surrounds the bubble ahead of it ($\dot{n}_V$); and loses its contents to the film behind ($\dot{n}_{IV}$). In addition, the slug is enriched in terms of the reactants that dissolve from bubble caps ($\dot{n}_{III}$).

Now that the formulation is almost complete, one may write the equations to be solved. During the start-up of Taylor flow, only a single compartment exists. The dissolution and reaction that occur during bubble formation is neglected. Let "i" denote the reactants, "j" denote the products and "k" denotes both for simplicity. Subscripts F,B and S denote film, bubble and slug. Superscripts denote the compartment number. So for the time period $0 < t < t_p$, the equations for the film can be given as:

$$\frac{\partial C_{F_k}^I}{\partial t} + v_i\left(1 - \frac{x}{\delta}\right)\frac{\partial C_{F_k}^I}{\partial z} = D_k \frac{\partial^2 C_{F_k}^I}{\partial x^2}$$

$$\begin{aligned} &\text{at } x = 0, && C_{F_i}^I = {C_{F_i}^I}^* \\ &\text{at } x = \delta, && -D_k \frac{\partial C_{F_k}^I}{\partial x} = r_k \\ &\text{at } z = 0, && C_{F_k}^I = 0 \\ &\text{at } t = 0, && C_{F_k}^I = 0 \end{aligned} \qquad (206)$$

Assume that the first bubble is filled with hydrogen. The velocity profile is taken as Couette flow, and a plug flow assumption is not made since in Section 4.2.2.5 it will be shown to be important for the diffusion to the catalytic wall. The interfacial velocity and the exact shape of the velocity profile are to be determined from CFD simulations. The boundary condition at the wall corresponds to the surface reaction rate. This may be bulk kinetics or it may be defined a microkinetic model, which brings its own set of ODEs along. Note that the boundary condition on the interface is given for reactants only. For products, it becomes:

$$\text{at } x = 0, \qquad -D_j \frac{\partial C_{F_j}^I}{\partial x} = k_B\left({C_{F_j}^I}^* - C_{B_j}^I\right) \qquad (207)$$

k_B is the mass transfer coefficient to the vaporization of volatile products. It is not yet known, but ways of estimating it are available. One may solve the area averaged form of the diffusion equation for evaporation into the bubble. In order to solve the equation, the velocity field in the bubble has to be known. For many flow fields, a simple solution is possible for the average concentration in the bubble [220]. Note that the interfacial concentrations are actually functions of the species' concentration inside the bubble. For the reactants, simple solubility data can be correlated and used, as done with Equations (175) and (176). But for the volatile products, the dynamics are governed by the thermodynamics of liquid-vapor equilibria, which induce some complexity. The last boundary condition denotes that the liquid phase is initially free of reactants.

For the bubble, one can write an equation analogous to the transient stirred tank:

$$V_B \frac{dC_{B_i}^I}{dt} = -2A_s {C_{F_i}^I}^* \sqrt{\frac{D_i}{\pi t}} - 2\pi(R-\delta)\int_0^{L_B}\left(-D_i \frac{\partial C_{F_i}^I}{\partial x}\bigg|_{x=0}\right)dz \qquad (208)$$

The first and the second terms on the right hand side denote the loss through dissolution from the caps and the lateral surface respectively. V_B is the volume of the bubble:

$$V_B = \frac{\pi h_s}{3}\left[3(R-\delta)^2 + {h_s}^2\right] + \pi(R-\delta)^2 L_B \qquad (209)$$

and A_s is the surface area of the caps:

$$A_s = 2\pi(R-\delta)h_s \qquad (210)$$

h_s is the length of the sphere cap. It depends on surface tension and the amount of liquid flow. h_s may be determined from CFD results or approximated from Bretherton's lubrication solution [221].

For the products, the equation for the bubble can be given as:

$$V_B \frac{dC_{B_j}^I}{dt} = 2\pi(R-\delta)k_B\left({C_{F_j}^I}^* - C_{B_j}^I\right) \qquad (211)$$

The re-dissolution from caps is neglected and the above equation is considered as to be indicating the net change. At $t = 0$, $C_{B_j}^I = 0$ where $C_{B_i}^I = C_{B_{i_0}}^I$, the initial concentration of the reactant inside the bubble.

And finally, one can write the equations for the liquid slug, in a similar fashion:

$$V_S \frac{dC_{S_i}^I}{dt} = A_s C_{F_i}^I * \sqrt{\frac{D_i}{\pi t}} - 2\pi v_i (R-\delta)^2 C_{S_i}^I \qquad (212)$$

with $C_{S_i}^I = 0$ at $t = 0$. V_s is the volume of the liquid slug:

$$V_S = \pi R^2 L_S - \frac{\pi h_s}{3}\left[3(R-\delta)^2 + {h_s}^2\right] \qquad (213)$$

The size of the liquid slug in front of the first bubble is actually much larger that its periodic value. However, bounds are kept as it is defined before. It would not affect the long time solution of this problem, when the duct is filled with bubbles and liquid slugs.

Note that both the bubble and the liquid slug are represented as well mixed systems. Such behavior is expected due to the possible circulations in both phases. At the same time, it is a necessary modification to simplify the model.

So now the problem consists a PDE and 2 ODE's for each species. For further periods of time, the ducts will be full of bubbles and number of equations will then be multiplied with number of compartments too. At first sight, the number of compartments may be found from L/L_{cell}. However, L_{cell} will be shown to be changing when bubbles shrink. Furthermore, number of compartments will not be equal to an integer, but for ducts that are long enough to contain few bubbles, the production rates should be proportioned well enough.

For the next time period, $t_p < t < 2t_p$, the equations for the bubble and the liquid slug evolve slightly, so as the boundary conditions. For the first compartment, the initially zero concentrations of the film and liquid slug will be non-zero. This is because of the products of the film and the dissolved reactants from rear sphere cap of the previous bubble will be present in the film and in the slug. Here, another perfect mixing assumption is made. The new initial values at $t = t_p$ will be the average of the amounts of species that are lost from the film and from the back of the bubble during $0 < t < t_p$:

$$C^{I}_{F_k} = C^{I}_{S_k} = \frac{\int_0^{t_p} A_s C^{I}_{F_i} * \sqrt{\frac{D_i}{\pi t}}\,dt + \int_0^{t_p} \frac{2\pi(R-\delta)^2 v_i}{\delta} \int_0^{\delta} \left(1 - \frac{x}{\delta}\right) C^{I}_{F_k}\big|_{z=L_B}\,dx\,dt}{V_F + V_S} \qquad (214)$$

$V_F = 2\pi R \delta L_B$ is the volume of the film.

For the film, the equations are the same, but the initial concentration changes since the new bubble is now full of carbon monoxide. For the bubble, the equations are also the same. But for the liquid slug, there is a slight change, since now there is a bubble ahead in compartment 2:

$$V_S \frac{dC^{I}_{S_i}}{dt} = A_s C^{I}_{F_i} * \sqrt{\frac{D_i}{\pi t}} + A_s{}^{II} C^{II}_{F\,i} * \sqrt{\frac{D_i}{\pi t}} - 2\pi v_i (R-\delta)^2 C^{I}_{S_i} + \frac{2\pi(R-\delta)^2 v_i}{\delta} \int_0^{\delta} \left(1 - \frac{x}{\delta}\right) C^{II}_{F\,i}\big|_{z=L_B}\,dx \qquad (215)$$

For the products:

$$V_S \frac{dC^{I}_{S_j}}{dt} = -2\pi v_i (R-\delta)^2 C^{I}_{S_j} + \frac{2\pi(R-\delta)^2 v_i}{\delta} \int_0^{\delta} \left(1 - \frac{x}{\delta}\right) C^{II}_{F\,j}\big|_{z=L_B}\,dx \qquad (216)$$

$A_s{}^{II}$ is the area of the rear cap of the bubble ahead. This is an important point, since the bubble in compartment 2 has now shrinked. The size can be taken as proportional to contents:

$$\frac{L_{B_{new}}}{L_{B_{old}}} = \frac{\delta_{new}}{\delta_{old}} = \frac{\sum_k C^{I}_{B_k}\big|_{t\,=\,n\,t_p}}{\sum_k C^{I}_{B_k}\big|_{t\,=\,(n-1)\,t_p}} \qquad (217)$$

n and n-1 denotes the beginning and end of time periods

From now on, one needs to solve the above equations. Starting from the first bubble, the simulation must tend to a periodic steady-state in terms of production after the duct has been filled with bubbles. With different flow characteristics, one should track the changes in overall reaction rate. By using n as the compartment number:

$$\text{total rate} = 2\pi R \sum_n \int_0^{L_B{}^n} \text{rate}^n\,dz \qquad (218)$$

Solving the rigorously coupled equations, one needs programming as well as PDE-ODE solvers. A possible tool is the joint COMSOL-Matlab platform, where the

solvers of COMSOL can be programmed with Matlab. Thereby, the outputs of each compartment may be fed as initial values and their data can be collected as desired.

4.2.2. Diffusion into a Flowing Liquid Film With Reaction on Solid Surface

In this section, the AIBM will be applied to heterogeneous reaction-diffusion problems. The aim is to obtain a formulation for arbitrary surface kinetics involving the diffusion and reaction of a single species in an arbitrary velocity field. This would imply a general resolution for the reaction-diffusion dynamics in thin flowing films, which may constitute a gas-liquid-solid or a liquid-liquid-solid system. The general formulation is then expected to cover a large class of microfluidic mass transfer cases, coupled with heterogeneous reactions.

In presence of homogeneous reactions, flow fields were found to be of minor importance in Section 4.1.2.2. However, in heterogeneous reactions there exists an initial period that involves the diffusion of absorbed species to the catalytic wall. This period is purely physical absorption. The sensitivity of physical absorption rates to different flow fields has been demonstrated in Section 4.1.2.1.

Since the general treatment is analytical, in addition to providing quantitative and qualitative predictions, it would also present ease in solving inverse problems (parameter estimation) or in optimization. At least, it can be a precursor or an initiator before running rigorous numerical analysis on these subjects. Besides, it will be shown that the AIBM solution also presents some extra results which cannot be obtained from standard analytical or numerical methods explicitly.

In this section, like the ones before, it is assumed that the resistance lies in the liquid phase. Unlike gas-liquid systems, this seems to be a very stringent condition for liquid-liquid synthesis. For a gas-liquid-solid system, Taylor flow in a wall coated monolith can be given as an example [222]. It will be seen that the general problem is very similar to the cases solved in Section 4.1.4. Here, only a single species is treated again. Such a model would be applicable to problems where the adsorption step of the modelled species is rate determining, which is abundant in the field of heterogeneous reactions, from ammonia synthesis to CVD operations [213].

4.2.2.1. Plug Flow: Zero and First Order Reaction

Starting from the first order reaction, the problem can be described as

$$\frac{\partial C}{\partial t} = D\frac{\partial^2 C}{\partial x^2} \qquad \begin{array}{c} \text{at } t = 0,\ C = 0 \\ \text{at } x = 0,\ C = C^* \\ \text{at } x = \delta,\ \dfrac{\partial C}{\partial x} = -\dfrac{k}{D}C \end{array} \qquad (219)$$

Since the film is in plug flow, $t = z/v_0$. This linear problem is analyzed first, since it is one of the rare cases with an exact solution. Steady state solution is:

$$\frac{C_\infty}{C^*} = \frac{1}{1+Da^{II}}\left[1 + Da^{II}\left(1 - \frac{x}{\delta}\right)\right] \qquad (220)$$

with $Da^{II} = k\delta/D = k/k_L$ [33]. As $Da^{II} \to \infty$ the solution tends to $C_\infty/C^* = 1 - x/\delta$ as expected; infinitely fast reactions lead to zero wall concentration. On the other hand for $Da^{II} \to 0$ the profile becomes flat: $C_\infty/C^* = 1$. The transient solution can be obtained via separation of variables:

$$\frac{C_\infty}{C^*} = \frac{1}{1+Da^{II}}\left\{1 + Da^{II}\left(1 - \frac{x}{\delta}\right) - \sum_{n=1}^{\infty} B_n \exp\left(-{\lambda_n}^2 \frac{Dt}{\delta^2}\right)\sin\left(\lambda_n \frac{x}{\delta}\right)\right\} \qquad (221)$$

where

$$B_n = \frac{(1+Da^{II})\int_0^1 \sin(\lambda_n \xi)d\xi - Da^{II}\int_0^1 \xi\sin(\lambda_n \xi)d\xi}{\int_0^1 \sin^2(\lambda_n \xi)d\xi} \qquad (222)$$

with eigenvalues obtained from $Da^{II} = -\lambda_n \cot(\lambda_n)$. Moving on to AIBM, one should note that the PT solution can be used up to a certain time for physical absorption, before which one can assume that the wall concentration is approximately zero. After that, chemical reaction takes place at the wall, and the profile is given by the AIBM. This is time to reach to the wall, t_r, the same given in the penetration thickness concept. From Equation-(21), one may expect $t_r = \delta^2/16$. But not only this value is devised on a pre-determined dimensionless concentration; it will also not work for films flowing with velocity profiles different than plug flow.

[33] Similar to Part-C, Da^{II} is taken as a grouping parameter. Hence it is not always dimensionless, for example for an n^{th} order reactions. This would provide simplicity during reactions of arbitrary type.

To obtain the IMBE, the PDE is integrated, but this time from 0 to δ, with δ as the constant film thickness. In the following equation, wall concentration, C_w, is time dependent. This leads to:

$$\frac{d}{dt}\int_0^{\delta} C\,dx = D\frac{\partial C}{\partial x}\bigg|_{x=\delta} - D\frac{\partial C}{\partial x}\bigg|_{x=0} = -kC_w - D\frac{\partial C}{\partial x}\bigg|_{x=0} \qquad (223)$$

A second order polynomial is chosen and the boundary conditions given in Equation-(219) are applied, along with the boundary condition at $x = \delta, C = C_w$. C_w is the concentration above the catalytic wall. The profile becomes:

$$C = C^* + (C^* - C_w)\left[\left(\frac{x}{\delta}\right)^2 - 2\frac{x}{\delta}\right] + \frac{k}{D}C_w\left(x - \frac{x^2}{\delta}\right) \qquad (224)$$

and the surface flux:

$$N = 2D\frac{(C^* - C_w)}{\delta} - kC_w \qquad (225)$$

After substituting the profile into the integral balance, an ODE for C_w is obtained:

$$C^* - C_w(1 + Da^{II}) = \frac{\delta^2}{12D}(4 + Da^{II})\frac{dC_w}{dt} \qquad (226)$$

This equation is to be integrated. But the time at when the concentration front reaches the wall is needed for the integration. Note that the factor in front of the bracket of the right hand side describes time. For now, this factor will be taken as the time to reach the surface arbitrarily:

$$t_r = \frac{\delta^2}{12D} \qquad (227)$$

The solution of this linear ODE is simple, with $C_w(t_r) = 0$, it yields:

$$C_w = \frac{C^*}{(1 + Da^{II})}\left\{1 - \exp\left[-\frac{(1 + Da^{II})}{(4 + Da^{II})}\left(\frac{t}{t_r} - 1\right)\right]\right\} \qquad (228)$$

Comparison with the exact solution (Figure 53) shows that the solution has good accuracy, especially near the interface. Furthermore, as $t \to \infty$, the quadratic profile gets a linear form and tends to the exact steady state solution. The accuracy of the AIBM solution decreases as Da decreases. However the error in surface flux expressions does not usually exceed 20%, before approximately reaching the steady-state. There seems to be a hump of error near steady-state, but this can be avoided if

steady-state fluxes are used when steady-state is near. Hence, an approximate time to reach steady state may be necessary, and it will be provided. For $Da^{II} > 1$, the solution is very accurate, especially in terms of surface flux.

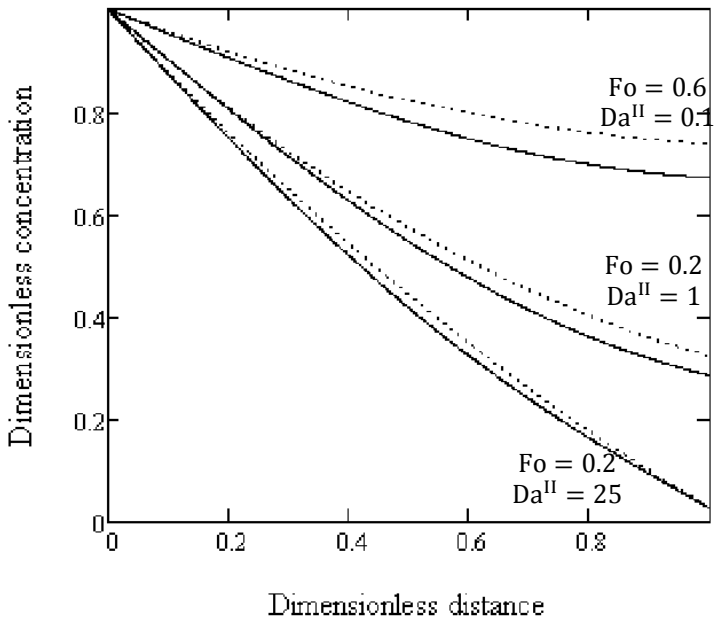

Figure 53. Exact versus AIBM comparison for the concentration profiles of a first order surface reaction.

From Equation-(220), one can see that for $Da^{II} < 0.01$, $C_w/C^* > 0.99$; thus the film gets almost saturated. If the contact times are not very short, then one may use simple batch reactor expressions in such a case, since concentration gradients vanish rapidly.

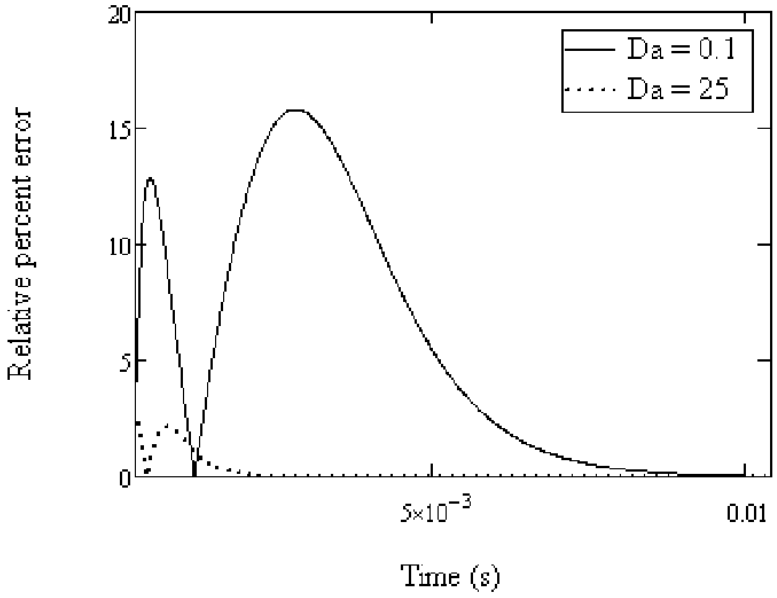

Figure 54. Relative percent error in surface flux predicted by AIBM for a first order reaction.

An immediate advantage of the AIBM solution is that it can handle a zero order surface reaction. A zero order reaction is actually an asymptote of Langmuir kinetics, in the case of complete kinetic control. Analytically and numerically, implementing the zero order surface reaction is difficult, since the BC becomes:

$$\text{at } x = \delta, \quad \frac{\partial C}{\partial x} = -k\Phi(C) \tag{229}$$

where Φ is the Heaviside step function. This renders analytical solutions impossible, and negative concentrations arise at initial contact times when Φ is not used. In numerical calculations, the step function is smoothed (as in Section 4.2.1) for ease in convergence. Physically, the step function should always be smooth since zero order reactions are never exactly zero order. An initial n^{th} order regime must prevail at sufficiently low concentrations. Thus, smoothing is not just a mathematical adjustment. Nevertheless, this ensures additional complication and needs additional verification in numerical calculations.

On the AIBM side, these difficulties vanish, since the initial sole diffusional period is not solved. Following the steps of the previous problem, one obtains the profile as:

$$C = C^* + (C^* - C_w)\left[\left(\frac{x}{\delta}\right)^2 - 2\frac{x}{\delta}\right] + Da^{II}\left[\frac{x}{\delta} - \left(\frac{x}{\delta}\right)^2\right] \tag{230}$$

and the wall concentration comes out as:

$$C_w = (C^* - Da^{II})\left\{1 - \exp\left[-\frac{1}{4}\left(\frac{t}{t_r} - 1\right)\right]\right\} \qquad (231)$$

Note that as $t \to \infty$, $C_w = C^* - Da^{II}$, which is exact.

4.2.2.2. Arbitrary Surface Reaction

In this case, the third boundary condition is replaced with

$$\text{at } x = \delta, \quad \frac{\partial C}{\partial x} = -\frac{k}{D} r(C_w) \qquad (232)$$

This converts the PDE into a formidable nonlinear problem. Similar problems are also encountered in radiative heat transfer coupled with conduction. One may apply Laplace transform [223], but this would lead to singular Volterra integral equations, which are quite difficult to solve, even numerically. Moreover one can apply the theory of integral transforms [224, 225], but the visual form of the solution does not tell anything about the physics of the problem and one needs many numerical implementations for solving the integrals.

The general profile can be written as:

$$C = C^* + (C^* - C_w)\left[\left(\frac{x}{\delta}\right)^2 - 2\frac{x}{\delta}\right] + Da^{II} r(C_w)\left[\frac{x}{\delta} - \left(\frac{x}{\delta}\right)^2\right] \qquad (233)$$

For a higher order polynomial, one cannot derive additional boundary conditions for this problem, in contrast to diffusion and diffusion with homogenous reaction problems. Hence, one may use moment equations of the type [226]:

$$\int_0^\delta x^j (DC_{xx} - C_t)dx = 0\ , \qquad j = 0,1,\cdots,n-1 \qquad (234)$$

$$\int_0^\delta C(x,0)dx = \int_0^\delta x^j\, g(x)dx = 0\ , \qquad j = 0,1,\cdots,n-1 \qquad (235)$$

Although non-uniform initial distributions are allowed and a significant improvement in accuracy is possible always guaranteed, the application of the moment equations (i.e. the method of moments) may lead to intractable ODE's for surface

concentrations.[34] Therefore, one may resume the analysis by using Equation-(233) in Equation-(223). The ODE generated by the AIBM can be partially integrated. The integral is not simple, but the result can be presented in a separable form. Therefore, it is implicit with respect to C_w:

$$I(C_w) = \int_0^{C_w} \frac{4 + Da^{II}(dr/dC'_w)}{C^* - C'_w - Da^{II} r(C'_w)} dC'_w = {}^{t}/_{t_r} - 1 \qquad (236)$$

Equation-(236) actually describes time inversely, in terms of surface concentration. In brief:

$$t = t_r[I(C_w) + 1] \qquad (237)$$

For a non-zero initial condition, Equation-(236) takes the form:

$$\int_{C_0}^{C_w} \frac{4 + Da^{II}(dr/dC'_w)}{C^* - C'_w - Da^{II} r(C'_w)} dC'_w = {}^{t}/_{t_r} \qquad (238)$$

In this case, t_r loses its physical meaning. The analysis in this part will be focused on fresh films with zero initial amounts of the reactant. So back to Equation-(236), instead of solving for C_w for each time, one may numerically solve the integral $I(C_w)$ up to the steady-state concentration, C_w^∞, which is found from:

$$(C^* - C_w^\infty) = Da^{II} r(C_w^\infty) \qquad (239)$$

then inversely plot the values found for time to get the evolution of surface concentration. For a CAS, like Mathcad, this is a very easy task, and actually even a spreadsheet can handle it. Thus, the number of roots to be solved is decreased to one. Solving Equation-(239) for C_w is usually a very simple task.

Note that both the first two terms and the last term of the denominator approach to the steady-state surface flux as time progress. Thus, the denominator tends to zero. This means an infinite time to the get the exact steady state wall concentration, which is physically and mathematically sound. At different Da^{II}, surface concentration are given for Freundlich and Langmuir type surface reaction rates:

$$r_F(C_w) = {C_w}^n, \qquad 0 < n < 1 \qquad (240)$$

[34] AIBM is related with the method of moments. Method of moments is actually a limited version of method of weighted residuals, which is also a subset of FEM. Hence, AIBM can also be seen as a single grid overly simple finite element application.

$$r_L(C_w) = \frac{C_w}{1 + KC_w} \tag{241}$$

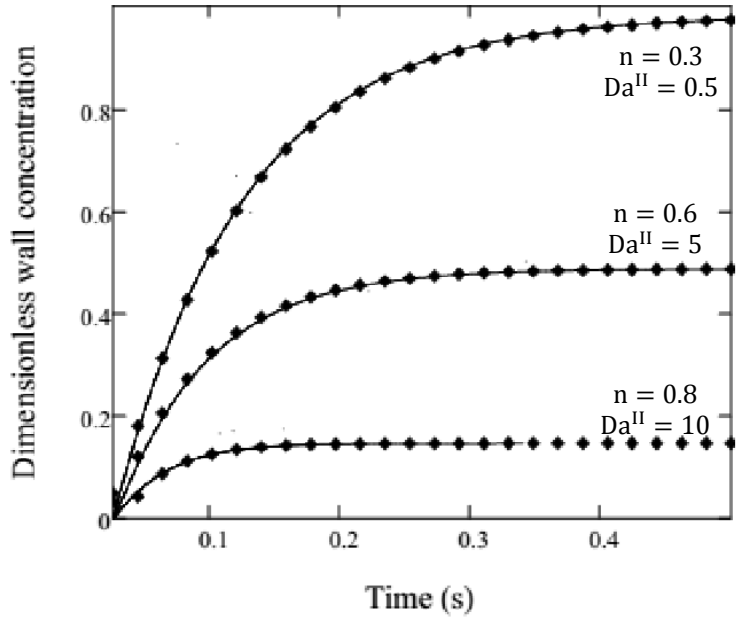

Figure 55. Dimensionless concentrations on the wall for Freundlich type reaction rate for different orders. Straight lines: AIBM, dots: numerical solution.

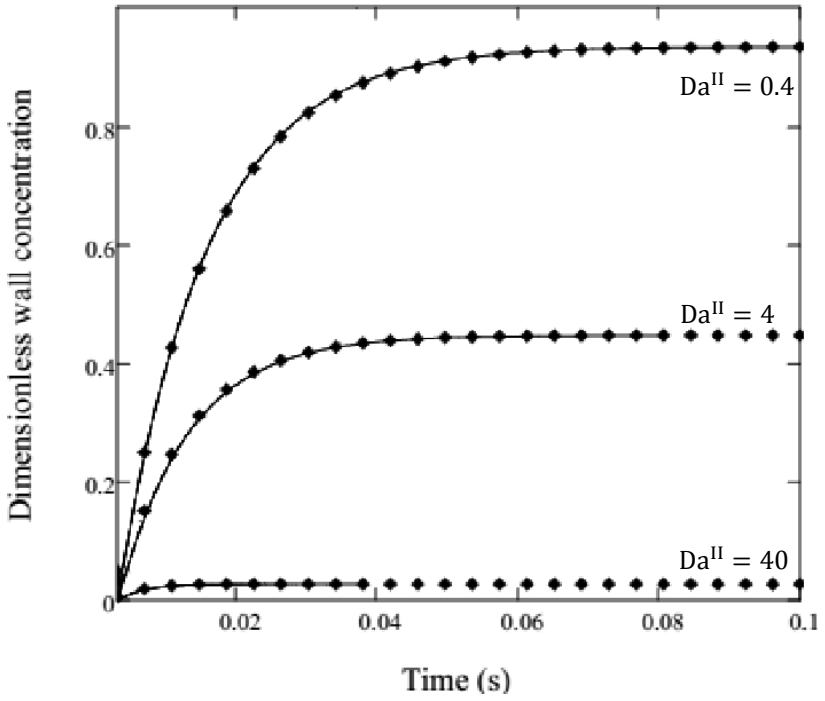

Figure 56. Dimensionless concentrations on the wall for Langmuir type reaction rate (K = 0.05). Straight lines: AIBM, dots: numerical solution.

In Figure 55 and Figure 56, the AIBM solutions are drawn up to a point where the steady-state is almost exactly reached.

4.2.2.3. Times to Reach Steady State

One advantage of this approximate analytical solution is the possibility to extract an explicit time to reach steady state. To accomplish this aim, the integral in Equation-(236) must be resolved approximately. Since the denominator tends to zero, one may first choose a near steady state value for surface concentration, $C_w^{\bullet}$. This would be the upper limit in evaluating $I(C_w)$. $C_w^{\bullet}$ may be assumed as the point when difference between the first two and the third terms of the denominator decrease to 1% of the steady state surface flux, i.e. $0.01(C^* - C_w^{\bullet})$. Furthermore, it is a fact that quantities in linear parabolic and elliptic diffusion problems decay exponentially if a stable steady-state exists[35]. Thus, one may find the average of the denominator over the interval 0 to $C_w^{\bullet}$, then take it out of the integral. Since the denominator is equal to C^* at $t = 0$ and defined to be equal to $0.01(C^* - C_w^{\bullet})$ at $t = t_{st}$, one may assume it as having the form:

$$De = C^* \exp(-\alpha t) \tag{242}$$

where α is an unknown decaying parameter. At the assumed steady-state, $t = t_{st}$, one may isolate αt_{st}:

$$\alpha t_{st} = \ln\left(\frac{100\, C^*}{C^* - C_w^{\bullet}}\right) \tag{243}$$

On the other hand, time averaging of the denominator gives:

$$\overline{De} = \frac{1}{t_{st}} \int_0^{t_{st}} C^* \exp(-\alpha t)\, dt = \frac{C^*}{\alpha t_{st}} [1 - \exp(-\alpha t_{st})] \tag{244}$$

After substituting the value of αt_{st} from Equation-(243):

$$\overline{De} = \frac{C^*}{\ln\left(\frac{100\, C^*}{C^* - C_w^{\bullet}}\right)} \left(1 - \frac{C^* - C_w^{\bullet}}{100\, C^*}\right) \cong \frac{C^*}{\ln\left(\frac{100\, C^*}{C^* - C_w^{\bullet}}\right)} \tag{245}$$

[35] This is evident in linear problems, where usual solutions obtained from classical methods like separation of variables have decaying exponential factors.

The behavior of the denominator is given Figure 57. As $C_w^{\bullet} \to C^*$ the actual denominator tends to zero, and the averaged denominator $\overline{De}$ also shows this characteristic.

Now since the denominator is a constant, and can be eliminated from the integral, Equation-(236) reduces to:

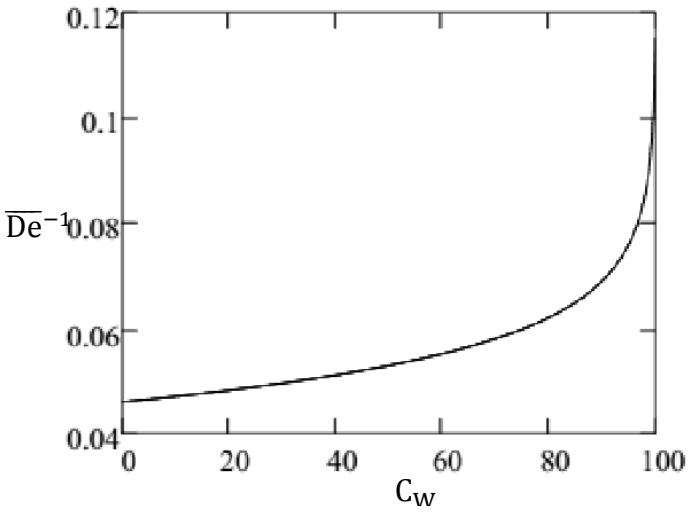

Figure 57. $\overline{De}^{-1}$ as a function of C_w.

$$I(C_w) \cong \frac{1}{\overline{De}} \int_0^{C_w} 4 + Da^{II}(dr/dC_w')dC_w' \cong {}^{t}/_{t_r} - 1 \qquad (246)$$

However to evaluate it, one needs to specify $C_w^{\bullet}$. A rough approximation should be enough. For Freundlich type surface rates, one may use the following formulas obtained via successive substitution:

$$C_w^{\bullet} = \left[\frac{C^* - (C^*/Da^{II})^{1/n}}{Da^{II}}\right]^{1/n}, \qquad \text{for } C^{*(1-n)/n^2} < Da^{II} \qquad (247)$$

$$C_w^{\bullet} = C^* - Da^{II}\left(C^* - Da^{II}C^{*n}\right)^n, \qquad \text{otherwise.} \qquad (248)$$

For Langmuir, one may utilize its zero and first order asymptotes respectively:

$$C_w^{\bullet} = C^* - Da^{II}/K\,, \qquad \text{for } K > 5 \qquad (249)$$

$$C_w^{\bullet} = C^*/(1 + Da^{II})\,, \qquad \text{for } K < 0.1 \qquad (250)$$

or just go for Equation-(239). Thus, the approximate times to reach steady state for Freundlich and Langmuir type reactions can be given respectively as:

$$t_{st} = t_r \left[\frac{1}{De} (4C_w^{\bullet} + Da^{II} C_w^{\bullet\, n}) + 1 \right] \tag{251}$$

$$t_{st} = t_r \left[\frac{1}{De} \left(4C_w^{\bullet} + \frac{Da^{II} C_w^{\bullet}}{1 + KC_w^{\bullet}} \right) + 1 \right] \tag{252}$$

or simply in general:

$$t_{st} = t_r \left[\frac{1}{De} \left(4C_w^{\bullet} + Da^{II} r(C_w^{\bullet}) \right) + 1 \right] \tag{253}$$

Equations (251) and (252) are applied for Freundlich and Langmuir expressions and results are presented in Figure 58. The intersecting linear lines are Equations (251) and (252), where curves are plotted from Equation-(236). The intersection point is the approximate steady-state.

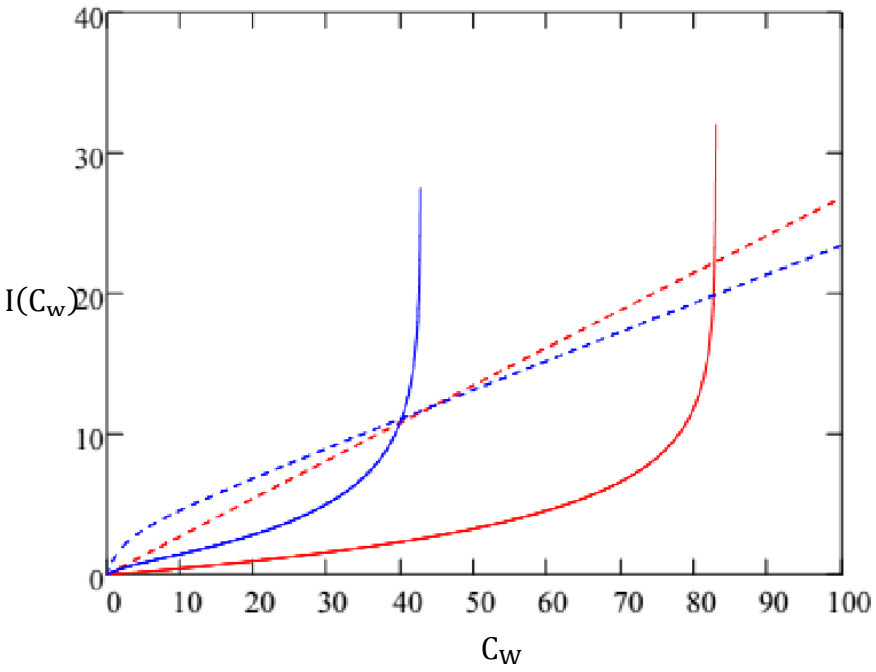

Figure 58. Finding approximate times to reach steady state. $C^* = 100$. Blue: Langmuir ($K = 0.5, Da = 30$), red: Freundlich ($n = 0.8, Da = 0.5$). Straight: Equation-(236), dotted: Equations (251) and (252).

It is observed that for Langmuir rates, the formulation underpredicts, and for Freundlich, the formulation overpredicts. For the test case presented above, Equations (251) and (252) yields the steady state time as 0.58 and 0.23 s for

Freundlich and Langmuir respectively. The values exactly predicted by Equation-(236) are 0.42 and 0.32. Although errors can be high as 50%, the formulation gives correct-to-the-order-of-magnitude results. The different behavior with respect to reaction rate expression comes from the simplifications done on the denominator term, whereby the characteristic of the rate expression is completely neglected.

Nevertheless, one may add that as Da^{II} decreases, $C_w^{\bullet}$ increases. This suggests, when $Da^{II} \ll 4C^*/r(C^*)$, Equation-(253) would simply reduce to:

$$t_{st} = t_r\left(\frac{4C_w^{\bullet}}{De} + 1\right) \tag{254}$$

Numerical experiments show that, this is quite valid when Da^{II} is around 50 times smaller than $4C^*/r(C^*)$.

4.2.2.4. Fluxes and the Amounts Absorbed

Using the general profile leads to the following equations:

$$\begin{aligned} -D\frac{\partial C}{\partial x}\Big|_{x=0} &= C^*\sqrt{\frac{D}{\pi t}}, \qquad \text{for } t < t_r \\ -D\frac{\partial C}{\partial x}\Big|_{x=0} &= \frac{2D}{\delta}(C^* - C_w) - kr(C_w), \qquad \text{for } t > t_r \end{aligned} \tag{255}$$

$$\begin{aligned} n_a &= 2C^*\sqrt{\frac{Dt}{\pi}}, \qquad \text{for } t < t_r \text{ ; otherwise:} \\ n_a &= \int_0^t -D\frac{\partial C}{\partial x}\Big|_{x=0} dt = 2C^*\sqrt{\frac{Dt_r}{\pi}} + \frac{2DC^*}{\delta}(t - t_r) - \frac{2D}{\delta}\int_{t_r}^{t} C_w\, dt - k\int_{t_r}^{t} r(C_w)\, dt \end{aligned} \tag{256}$$

Alternatively, by using Equation-(237) with $I(C_w)$ given by Equation-(236) and by applying the theory of inverse functions, the integrals of Equations-(256) can be inverted. This removes the necessity to solve $I(C_w)$ for C_w at each time. Such root finding operations would be costly. Especially near steady state, good guesses would be necessary for convergence. Therefore, for $t > t_r$, the following equation is simpler to use:

$$n_a = 2C^* \sqrt{\frac{Dt_r}{\pi}} + \frac{2DC^*}{\delta}(t - t_r) - \frac{2D}{\delta}\left[tC_w - \int_0^{C_w} t\, dC_w\right]$$

$$- k\left[tr(C_w) - \int_0^{C_w} t\left(\frac{dr}{dC_w}\right) dC_w\right] \qquad (257)$$

A sample result for the surface flux and the amount absorbed is provided in Figure 58. The accuracy is quite good for both quantities.

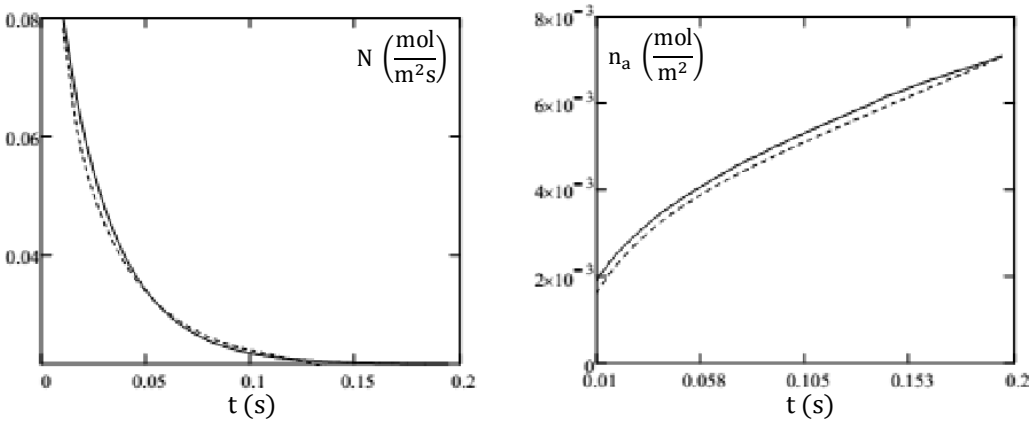

Figure 59. Left: surface fluxes, right: amounts absorbed. Straight line: AIBM, dotted line: numerical solution. The plots are given for Freundlich type reaction rate with $n = 0.8, Da = 2.5$

4.2.2.5. Arbitrary Velocity Field

All the analysis above was for plug flow, which is not always realistic for laminar microflows. In this part of the analysis, a stationary velocity field will be assumed:

$$v(x) = v_0\left[a_0 + a_1\frac{x}{\delta} + a_2\left(\frac{x}{\delta}\right)^2 + \cdots\right] = v_i f(x) \qquad (258)$$

Now the inspected PDE becomes,

$$f(x)\frac{\partial C}{\partial t} = D\frac{\partial^2 C}{\partial x^2} \qquad (259)$$

subject to the first two boundary conditions of Equation-(219) and to Equation-(232). As before, v_i has vanished according to the substitution $t = z/v_0$. To

use in kinetic studies, this problem was investigated and solved by Katz [227] in tubular geometry for arbitrary kinetics and velocity profile. Here, it will be shown that the AIBM solution is much simpler, more straightforward and much more general. Here, the function f(x) is considered as a polynomial, actually a general power series representation:

$$f(x) = \sum_{n=0}^{\infty} a_n \left(\frac{x}{\delta}\right)^n \tag{260}$$

Since power series are known for their capability for representing many functions, f(x) encompasses a relatively large family of velocity fields. The AIBM suggests the following integral "I_v" to be evaluated:

$$\int_0^{\delta} f(x) \frac{\partial C}{\partial t} dx = \frac{d}{dt} \int_0^{\delta} f(x)\, C\, dx = \frac{dI_v}{dt} \tag{261}$$

For all kinds of polynomial f(x), the integral on the right can be evaluated via integration by parts. But for a generally valid plug-it-in formula, one may pursue further analysis. The integral can be expressed as successive integrations by parts in indefinite form [228]:

$$I_v = f \int C dx - \frac{df}{dx} \iint C dx^2 + \frac{d^2 f}{dx^2} \iiint C\, dx^3 - \cdots \tag{262}$$

Each derivative of f(x) and each integral, considering "m" as the integration order of C, can be evaluated by using Equation-(260). Then, their multiplications can be evaluated at 0 and δ. This leads to constant multipliers for the terms obtained in the previous problem. The integral can be solved in a general form as:

$$I = \gamma_1 C^* \delta - \gamma_2 (C^* - C_w)\delta + \gamma_3 \frac{kr(C_w)}{D} \delta^2 \tag{263}$$

Since the time derivative in Equation-(261) will eliminate the first term above, it is not necessary to calculate γ_1. The ODE of the AIBM comes out as:

$$C^* - C_w - Da^{II} r(C_w) = \frac{\gamma_3 \delta^2}{2D} \left(\frac{\gamma_2}{\gamma_3} + Da^{II} \frac{dr}{dC_w}\right) \frac{dC_w}{dt} \tag{264}$$

Note that, under any velocity field, time to reach the surface is predicted by: $t_r = \gamma_3 \delta^2 / 2D$. Naturally, considering a finite sum of N elements to describe f(x), the modifiers γ_2 and γ_3 can be given as:

$$\gamma_2 = \frac{2}{3}\sum_{n=0}^{N} a_n - 2\sum_{m=2}^{N+1}\left[\frac{(-1)^m(m+1)}{(m+2)!}h(m)\right]$$

$$\gamma_3 = \frac{1}{6}\sum_{n=0}^{N} a_n - \sum_{m=2}^{N+1}\left[\frac{(-1)^m m}{(m+2)!}h(m)\right] \qquad (265)$$

$$h(m) = \sum_{n=m-1}^{N} a_n\left[\prod_{i=0}^{m-2}(n-i)\right]$$

These can be implemented into a CAS system with ease. As an example, Nusselt film flow profile can be used:

$$f(x) = 1 - \left(\frac{x}{\delta}\right)^2 \qquad (266)$$

which yields $\mathbf{a} = [1, 0, -1]$**.** Using these parameters one obtains $\gamma_2 = 11/30$ and $\gamma_3 = 7/60$. When compared to plug flow, the first term in the parenthesis of Equation-(264) becomes $22/7$ instead of 4, and the first factor on the right hand side, which is t_r, becomes $7\delta^2/120D$ instead of $\delta^2/12D$. This decrease in t_r is physically correct. Since flow gets slower near the wall, molecules reach it in shorter times, or in other words, in shorter axial distances. This behavior of t_r and the accuracy of the solution show that the method is self-sufficient and no rigorous exact solution is necessary to model the initial diffusion stage of the reactant in an arbitrary flow field. Since such solutions are overly complex and needs treating the corresponding Graetz problems [208] or numerical implementations, the approximate formulation is quite easy to use. The wall concentrations for the film flow case are provided in Figure 60. Film flow solutions are compared with the plug flow solution, which is scaled to have the same average velocity. For low Da^{II}, velocity profile becomes more effective.

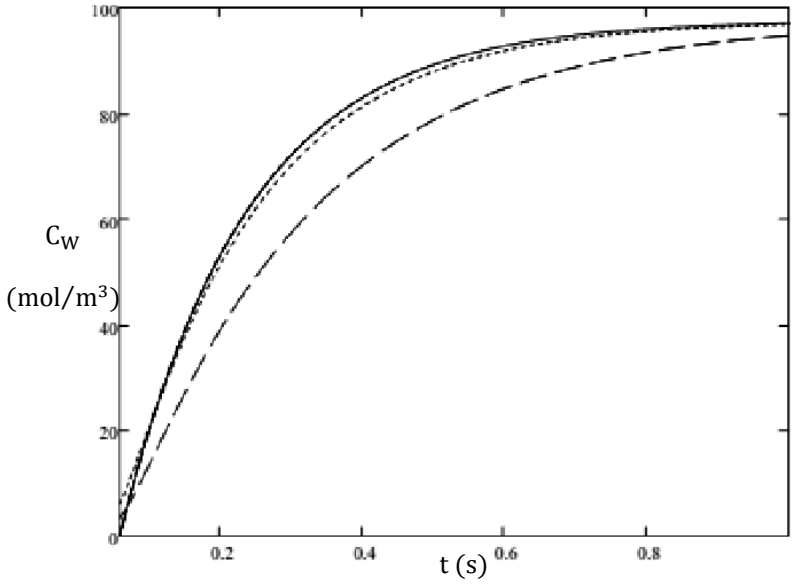

Figure 60. Wall concentration for a Freundlich type reaction($n = 0.6, Da = 0.01$) in film flow. Straight line: AIBM, dotted line: numerical solution, dashed line: numerical plug flow solution.

Due to the power law formulation, many types of steady flow fields can be incorporated into the AIBM solution. To show possible applications of the theory, various velocity profiles are given in Appendix-D.

The general form

$$t_r = \gamma_3 \delta^2 / 2D \tag{267}$$

bestows an important criterion. Pohorecki's discussion [103] on the existence of a minimum Fourier number for heterogeneous reactions (especially slow ones) can be enhanced. Pohorecki suggested $Fo \gg 1$ for heterogeneous reactions. This condition can be made more to the point by using the definition of t_r to express the minimum Fourier number Fo_{min}, since t_r is accepted by AIBM as the time that reaction starts on the wall:

$$Fo_{min} = \frac{t_r D}{\delta^2} = \frac{\gamma_3}{2} \tag{268}$$

Thus, for feasible synthesis:

$$Fo > \gamma_3 / 2 \tag{269}$$

where γ_3 introduces the effects of the velocity field. So, considering the Taylor model described in section 4.2.1.5, the above criterion must be satisfied for significant amounts of production. This is critical since the regime of gas-liquid superficial velocities that allow Taylor flow is quite large, as can be seen from Figure 2.

4.2.2.6. Time Dependent Velocity Fields and Moving Boundaries

The solution provided by AIBM to diffusion with heterogeneous reaction can be extended to suit many more problems. It can also handle time-dependent flow fields to a certain extent. For such a field, the integral in Equation-(261) can be simplified if function f is separable in terms of x and t:

$$\int_0^{\delta} f(x,t)\frac{\partial C}{\partial t}dx = \int_0^{\delta} g(x)h(t)\frac{\partial C}{\partial t}dx = h(t)\frac{d}{dt}\int_0^{\delta} g(x)C\,dx \quad (270)$$

Physically, this can correspond to many types of flow fields. One of the exact matches is oscillatory flow fields, whose long time solutions[36] are exactly of the form $f(x,t) = g(x)h(t)$ [229]. The integral can be treated as before, as long as power series expansions are valid. Using Equation-(263), integration leads to:

$$I(C_w) = \int_0^{C_w} \frac{(\gamma_2/\gamma_3) + Da^{II}(dr/dC'_w)}{C^* - C'_w - Da^{II}r(C'_w)}dC'_w = \int_{t_r}^{t} \frac{dt'}{t_r h(t)} \quad (271)$$

Usually $h(t)$ only a trigonometric function, it most likely involves sine and e^{iwt} type functions. These can be integrated with ease, and time can usually be expressed in explicit form as before. Therefore, oscillating flow fields can theoretically incorporated into analysis. Some difficulties may occur with $g(x)$ since it may involve trigonometric functions also. Trigonometric functions have economized power series [230], which are accurate over a defined region. For example on$[-1,1]$:

$$\sin\left(\frac{1}{2}\pi x\right) = 1.5706268x - 0.6432292x^3 + 0.0727102x^5 \quad (272)$$

which has an error lower than 0.1%.

[36] i.e. the periodic steady-state, initial transients are neglected.

A more general situation would be developing flows. Since their solutions are derived from classical Sturm-Liouville theory, they will be expressed as series. Each term of the series is separable in terms of time and space; however multiple terms render the middle integral in Equation-(261) intractable. As discussed in the Theory section under boundary layer theory, in liquid films velocity fields will develop much faster than concentration fields in liquids. This is determined by the Schmidt number, $Sc = \nu/D$. In liquids, $\nu \sim 10^{-3}$ and $D \sim 10^{-8} - 10^{-9}$, thus $Sc \sim 10^{5} - 10^{6}$. Nevertheless, in an extreme case, the first term of the series solution can be used. But for gaseous transport this is not possible since $Sc \sim 1$. Therefore different paths of analysis must be followed, an example is provided by Lopes et.al. [231] for heterogeneous reactions in microchannels, albeit only for first order.

And lastly, slightly non-flat geometries can also by treated with AIBM. As an example one may give the example of a thinning film, or a loosely corrugated wall. This resembles the quasi-steady state approximation in moving boundary problems, but in a general sense, it resembles the lubrication approximation [232]. So in such a case, one may denote:

$$t_r = \gamma_3 \delta(t)^2 / 2D \qquad (273)$$

where the thickness of the film slightly changes with exposure time.

Although many further extensions and applications to AIBM analysis seem to be possible, their importance is vague.

4.2.2.7. Summary: Mass Transfer with Heterogeneous Reaction

With Equation-(269), an important constraint for the effective use of a microfluidic film in heterogeneous synthesis is introduced. In addition, the AIBM formulation is shown to be quite general.

To compute the amounts absorbed in general, Equations (255) and (256) should be modified with respect to the velocity fields, since they were given for plug flow. Although the surface flux expression for $t > t_r$ will remain as the same in any velocity field, now for $t < t_r$, the expressions for flux and the amounts absorbed will

not be available, since the expressions for physical absorption are not known. One may similarly use AIBM for pure physical absorption, but it is known from Part-B that a general encapsulation of velocity fields is not possible for moving concentration fronts. However, this does not seem to be of utmost importance, and does not hinder the construction of the general equation for the enhancement factor. Equation-(256) must be modified for the initial period pf physical absorption. One may directly integrate the concentration profile (Equation-(233)) over the film at $t = t_r$. Since $C_w = r(C_w) = 0$ at that time,

$$\int_0^{\delta} C dx = \frac{C^* \delta}{3} = 2C^* \sqrt{\frac{Dt_r}{\pi}} \sqrt{\frac{\pi}{18\gamma_3}} \tag{274}$$

Where the last term square root is inferred Equation-(267) and serves as a correction factor to PT. Now Equation-(256) becomes:

$$n_a = 2C^* \sqrt{\frac{Dt_r}{\pi}} \sqrt{\frac{\pi}{18\gamma_3}} + \frac{2DC^*}{\delta}(t - t_r) - \frac{2D}{\delta}\left[tC_w - \int_0^{C_w} t\, dC_w\right] - k\left[tr(C_w) - \int_0^{C_w} t\left(\frac{dr}{dC_w}\right) dC_w\right] \tag{275}$$

Like the results presented in Section 4.1.4, the integrals can be evaluated with a CAS.

CHAPTER 5

SUMMARY, CONCLUSIONS AND RECOMMENDATIONS

5.1. Summary

In this study, the absorption of NO in aqueous solutions was experimentally studied in a novel contactor first. Then, the validity of penetration theory in microflow conditions was tested on mathematical grounds. Saturation of thin liquid films during physical absorption was demonstrated and the depletion limits in case of a second order bimolecular reaction was discussed. This was followed by the development of a general reaction-diffusion solution that describes mass transfer accompanied with homogeneous chemical reaction. These steps formed the first part of this thesis on gas-liquid systems. In the second part, dealing with gas-liquid-solid systems, Fischer-Tropsch synthesis in microreactors was investigated conceptually. A novel operation strategy was proposed and its implementation into Taylor flow was elaborated with a mathematical model. Finally, a general solution for mass transfer with heterogeneous reaction, which is applicable to microreactor scenarios, was presented.

5.2. Conclusions

In NO experiments, it was seen that the chemicals added for mass transfer intensification had led to an additional resistance, called as surface poisoning akin to heterogeneous reactions, on the interface of unmixed liquid layers; thereby decreasing uptake rates. This phenomenon may be attributed to Marangoni-like effects due to the changes in composition and/or temperature. Another explanation would be the surfactant-like behavior of reaction products or ions. In macrocontactors with active or passive mixing, this drawback of gas absorption accompanied by reactions may be concealed. However, in contactors with stable streamline flows, this effect may render chemical absorption attempts as useless. Since microreactors are ideal tools of such regular laminar flows, their proficiency in chemical absorption may not be as good as it is thought to be.

The analysis done on the validity of penetration theory proposes that theory leads to significant errors for physical absorption into finite flowing films and may be considered roughly to be valid for $Fo < 0.3$. However the theory is valid for all contact times if $\Lambda \gtrapprox 1$ in presence of a positive pseudo n^{th} order reaction, as long as the maximum velocity occurs on the gas-liquid interface. Furthermore, it has been observed that when approximately $\Lambda < 0.7$, the system can be well described by physical absorption, up to $Fo \sim 0.3$. The validity and constraints of coupling heat effects into the species transport equation are discussed. Considering saturation in thin films, the relevant magnitude of Fo with respect to certain flow fields is given. The depletion Fo has been provided via an implicit equation. The new solution obtained for diffusion into a flowing film with homogeneous reaction via approximate integral balance method covers a wide range of scenarios. It is shown to be accurate at least in terms of determining surface fluxes. A constraint on the maximum liquid flow rate has been provided. The solution can explain the interconnection of various flow fields with nonlinear reaction terms in an analytical way.

It has been demonstrated that manipulating the reactant mass fluxes of Fischer-Tropsch synthesis via changing hydrodynamic conditions is not likely. Therefore a periodic operation scheme of the synthesis suitable for microreactors has been shown

to be appropriate and effective, by numerical solutions. 1000 fold of rate enhancements are predicted with the new operation strategy. In addition, the behavior of effectiveness factors for general power law kinetics in presence of surface poisoning species is demonstrated. The regions of multiplicity and their effect on reaction-diffusion dynamics are displayed. A relatively simple model of Taylor flow accompanied by mass transfer and heterogeneous reactions is presented. Finally, a general solution for diffusion into flowing films with surface reaction is given, again by using the approximate integral balance method. The solution is shown to be accurate for various flow fields and nonlinear heterogeneous rate forms. An explicit criterion is derived for the times necessary for the initiation of the surface reaction after the initial diffusion period. This phenomenon is discussed on Taylor flow, considering it as a gas-liquid-solid synthesis system.

5.3. Recommendations

In order to show the existence of surface poisoning during gas absorption with chemical reaction into unmixed liquid films in microreactors, further experimentation with smaller contactors is necessary.

The mathematical analysis on penetration theory and diffusion-reaction in thin flowing films has been made by considering the film as isothermal. Coupling heat transfer with mass transfer and reaction would be a good multiphysics study, if temperature dependent data for physical and chemical properties are used. This would show the importance of heat transfer in microfluidic mass transfer cases.

The periodic operation of an heterogeneous reaction with poisoning species should be also demonstrated experimentally. The optimum switching time with respect to the given rate constant and reaction rate expression may be extracted by further analysis.

The model of Taylor flow can be simulated and it should be validated by experiments. Such models would be useful if they could attain predictive capabilities since complete numerical solutions have been discussed to be burdensome.

REFERENCES

[1] W. Chu, L.-N. Wang and P. A. Chernavskii, "Glow-Discharge Plasma-Assisted Design of Cobalt Catalysts for Fischer–Tropsch Synthesis," *Angew. Chem. Int. Ed.,* pp. 5052-5055, 2008.

[2] M. Dudukovic, "Challenges and innovations in reaction engineering," *Chem. Eng. Comm.,* vol. 196, pp. 252-266, 2009.

[3] R. Feynman, "There's plenty of room at the bottom," *Engineering and Science,* vol. 23, pp. 22-26, 1960.

[4] A. Manz and H. Becker, Microsystem Technologies in Chemistry and Life Science, Springer, 1998.

[5] A. Cybulski, A. Stankiewicz, R. E. Albers and J. Moulijn, "Monolithic reactors for fine chemicals industries: a comparative analysis of a monolithic reactor and a mechanically agitated slurry reactor," *Chem. Eng. Sci.,* vol. 54, pp. 2351-2358, 1999.

[6] I. Mazzarino and A. Barresi, "Catalytic combustion of VOC mixtures in a monolithic reactor," *Catal. Today,* vol. 17, pp. 335-347, 1993.

[7] Fraunhofer USA, 2008. [Online]. Available: http://www.fhcmi.org/LSE/Projects/08.html. [Accessed 11 08 2014].

[8] K. Jensen, "Microreaction engineering - is small better?," *Chem. Eng. Sci.,* vol. 56, pp. 293-303, 2001.

[9] J. Brandt and T. Wirth, "Controlling hazardous chemicals in microreactors: Synthesis with iodine azide," *Beilstein Journal of Organic Chemistry,* vol. 5, p. No. 30, 2009.

[10] T. Floyd, M. Losey, S. Firebaugh, K. Jensen and M. Schmidt, "Novel liquid phase microreactors for safe production of hazardous specialty chemicals," in *Microreaction Technology: Industrial Prospects*, Springer, 2000, pp. 171-180.

[11] DSM Corparation, "Pharma Chemical Brochure: Micro Reactor Technology," 2011.

[12] D. Roberge, B. Zimmerman, F. Rainone, M. Gottsponer, M. Eyholzer and N.

Kockmann, "Microreactor technology: a revolution for the fine chemical and pharmaceutical industries?," *Org. Process Res. Dev.,* vol. 12, pp. 905-910, 2008.

[13] D. Figeys and D. Pinto, "Lab-on-a-chip: A revolution in biological and medical sciences," *Anal. Chem.,* vol. 72, pp. 330-335, 2000.

[14] H. Sahoo, J. Kralj and K. Jensen, "Multistep continuous-flow microchemical synthesis involving multiple reactions and separations," *Angew. Chem.,* vol. 119, pp. 5806-5810, 2007.

[15] J. Kobayashi, Y. Mori and S. Kobayashi, "Multiphase organic synthesis in microchannel reactors," *Chem. Asian. J.,* Vols. 1-2, pp. 22-35, 2006.

[16] J. Kobayashi, Y. Mori, K. Okamoto, R. Akiyama, M. Ueno, T. Kitamori and S. Kobayashi, "A microfluidic device for conducting gas-liquid-solid hydrogenation reactions," *Science,* vol. 304, pp. 1305-1308, 2004.

[17] R. Masel, S. Gold and Z. Ni, "Microreactors and microreaction engineering," in *Encyclopedia of Chemical Processing*, Taylor & Francis, 2006, pp. 1643-1661.

[18] P. Sobieszuk, R. Pohorecki, P. Cyganski, M. Kraut and F. Olschewski, "Hydrodynamics and mass transfer in gas-liquid flows in microreactors," *Chem. Eng. Jour.,* vol. 35, pp. 1346-1358, 2012.

[19] Institut für Mikrotechnik Mainz, "FFMR Product Brochure," 2011.

[20] J. Yue, G. Chen, Q. Yuan, L. Luo and Y. Gonthier, "Hydrodynamics and mass transfer characteristics in gas–liquid flow through a rectangular microchannel," *Chem. Eng. Sci.,* vol. 62, p. 2096–2108, 2007.

[21] M. Kreutzer, F. Kapteijn, J. Moulijn, C. Kleijn and J. Heiszwolf, "Inertial and interfacial effects on pressure drop of Taylor flow in capillaries," *AIChE J.,* vol. 51, pp. 2428-2440, 2005.

[22] G. Taylor, "Deposition of a viscous fluid on the wall of a tube," *J. Fluid Mech.,* vol. 10, pp. 161-165, 1961.

[23] M. Al-Rawashdeh, F. Yue, G. Narendra, T. H. V. Nijhuis, J. Schouten and E. Rebrov, "Designing flow and temperature uniformities in parallel microchannels reactor," *AIChE J.,* vol. 60, pp. 1941-1952, 2014.

[24] H. Zhang, G. Chen, J. Yue and Q. Yuan, "Hydrodynamics and mass transfer of gas–liquid flow in a falling film microreactor," *AIChE J.,* vol. 55, pp. 1110-

1120, 2009.

[25] Z. M., A. Gavriilidis, C. Wille and V. Hessel, "Carbon dioxide absorption in a falling film microstructured reactor: Experiments and modeling," *Ind. Eng. Chem. Res.,* vol. 44, pp. 1742-1751, 2005.

[26] B. Vankayala, P. Löb, V. Hessel, G. Menges, C. Hofmann, D. Metzke, U. Krtschil and H. Kost, "Scale-up of process intensifying falling film microreactors to pilot production scale," *Int. J. Chem. React. Eng.,* vol. 5, p. A91, 2007.

[27] P. Danckwerts, "The absorption of gases in liquids," *Pure Appl. Chem. ,* vol. 10, pp. 625-642, 1965.

[28] M. Kashid, A. Renken and L. Kiwi-Minsker, "Gas-liquid and liquid-liquid mass transfer in microstructured reactors," *Chem. Eng. Sci.,* vol. 66, pp. 3876-3897, 2011.

[29] M. Dudukovic, "Frontiers in reactor engineering," *Science,* vol. 325, pp. 698-700, 2009.

[30] W. Whitman, "The two-film theory of gas absorption (re-print of the orijinal in Chem. Met. Eng., 29:146-148, 1923)," *Int. J. Heat Mass Transfer,* vol. 5, pp. 429-433, 1962.

[31] T. Sherwood, "A review of the development of mass transfer theory," *Chem. Eng. Edu,* no. 3, pp. 204-213, 1974.

[32] C. Geankoplis, Transport Processes and Separation Process Principles, 4th Ed., Prentice-Hall, 2003.

[33] T. Sherwood and K. Gordon, "A note on the additivity of diffusional resistances," *AIChE J.,* vol. 1, p. 129, 1955.

[34] W. Whitman and W. Lewis, "Principles of gas absorption," *Ind. Eng. Chem.,* vol. 16, pp. 1215-1220, 1924.

[35] H. Becker, "Mechanism of soluble gases in water," *Ind. Eng. Chem.,* vol. 16, pp. 1220-1224, 1924.

[36] R. Haslam, R. Hershey and R. Keen, "Effect of gas velocity and temperature on rate of absorption," *Ind. Eng. Chem.,* vol. 16, pp. 1224-1230, 1924.

[37] S. Hatta, "On the absorption velocity of gases by liquids," *Technol. Repts.*

Tôhoku Imp. Univ., vol. 10, pp. 613-622, 1932.

[38] D. van Krevelen and P. Hoftijzer, "Kinetics of gas-liquid reactions part I - General theory," *Recueil des Travaux Chimiques des Pays-Bas,* vol. 67, p. 563–586, 1948.

[39] O. Levenspiel and J. Godfrey, "A gradientless contactor for experimental study of interphase mass transfer with/without reaction," *Chem. Eng. Sci.,* vol. 29, pp. 1723-1730, 1974.

[40] W. Whitman and D. Davis, "Comparative absorption rates for various gases," *Ind. Eng. Chem.,* vol. 16, pp. 1233-1237, 1924.

[41] H. Hikita, S. Asai, H. Ishikawa and S. Hirano, "Kinetics of absorption of nitric oxide in aqueous acidic solutions of ferrous sulfate," *J. Chem. Eng. Jpn.,* vol. 10, pp. 120-124, 1977.

[42] E. Sada, H. Kumazawa, N. Tsuboi, I. Kudo and T. Kondo, "Absorption of nitric oxide in aqueous ferrous sulfate solutions," *Ind. Eng. Chem. Process Des. Dev.,* vol. 17, pp. 321-324, 1978.

[43] E. Sada, H. Kumazawa, I. Kudo and T. Kondo, "Absorption of NO in aqueous solutions of NaClO2 and NaOH," *Chem. Eng. Sci.,* vol. 33, pp. 315-318, 1978.

[44] J. Davies, A. Kilner and G. Ratcliff, "The effect of diffusivities and surface films on rates of gas absorption," *Chem. Eng. Sci.,* vol. 19, pp. 583-590, 1964.

[45] A. Beitel and W. Heideger, "Surfactant effects on mass transfer from drops subject to interfacial instability," *Chem. Eng. Sci.,* vol. 26, pp. 711-717, 1971.

[46] A. Tamir and J. Merchuk, "Effect of diffusivity on gas-side mass transfer coefficient," *Chem. Eng. Sci.,* vol. 33, pp. 1371-1374, 1978.

[47] M. Al-Dahhan and C. Wicks, "Modified contactor for experimental studies of mass transfer and chemical reaction across a liquid-liquid interface," *Ind. Eng. Chem. Res.,* vol. 35, pp. 3812-3816, 1996.

[48] L. Doraiswamy, Organic Synthesis Engineering, Oxford University Press, 2001.

[49] E. Cussler, Diffusion : mass transfer in fluid systems, 3rd Ed., Cambridge: Cambridge University Press, 2009.

[50] W. Nusselt, "Die Oberflaechenkondensation des Wasserdampfes (The surface condensation of water)," *Zetrschr. Ver. Deutch. Ing.,* vol. 60, pp. 541-546,

1916.

[51] R. Higbie, "The rate of absorption of a pure gas into still liquid during short periods of exposure," *Trans. Am. Inst. Chem. Eng.,* vol. 31, p. 365, 1935.

[52] L. Doraiswamy and D. Üner, Chemical Reaction Engineering: Beyond The Fundamentals, CRC Press, 2013.

[53] I. Tosun, Modeling in Transport Phenomena: A Conceptual Approach 2nd Edition, Elsevier Science, 2007.

[54] H. Weymann, "Finite speed of propagation in heat conduction, diffusion and viscous shear motion," *Am J Phys,* vol. 35, pp. 488-496, 1967.

[55] H. Johnstone and R. Pigford, "Distillation in a wetted-wall column," *Trans. Am. Inst. Chem. Eng.,* vol. 38, p. 25, 1942.

[56] M. Gad-el-Hak, "The fluid mechanics of microdevices - The Freeman Scholar Lecture," *J. Fluids Eng.,* vol. 121, pp. 5-33, 1999.

[57] P. Danckwerts, "Absorption by simultaneous diffusion and chemical reaction," *Trans. Far. Soc.,* vol. 46, p. 300, 1950.

[58] T. Sherwood, "The mechanism of mass transfer of solutes across liquid-liquid interfaces," *Chem. Eng. Sci.,* vol. 4, pp. 290-291, 1955.

[59] J. Lewis, "In reply to Professor Sherwood," *Chem. Eng. Sci.,* vol. 4, pp. 291-292, 1955.

[60] S. Komori, R. Nagaosa, Y. Murakami, S. Chiba, K. Ishii and K. Kuwahara, "Direct numerical simulation of three-dimensional open-channel flow with zero-shear gas–liquid interface," *Phys. Fluids A,* vol. 5, pp. 115-125, 1993.

[61] P. Danckwerts, "Significance of liquid-film coefficients in gas absorption," *Ind.& Eng. Chem.,* vol. 43, p. 1460, 1951.

[62] H. Toor and J. Marchello, "Film-penetration model for mass and heat transfer," *AIChE J.,* vol. 4, p. 97, 1958.

[63] P. Harriott, "A random eddy modification of the penetration theory," *Chem. Eng. Sci.,* vol. 17, pp. 149-154, 1962.

[64] C. Huang and C. Kuo, "General mathematical model for mass transfer accompanied by chemical reaction," *AIChE J.,* vol. 9, p. 161, 1963.

[65] H. Brusset, D. Depeyre and T. Le Quang, "An estimation of the film-penetration model parameters," *Chem. Eng. Sci.,* vol. 28, p. 31, 1973.

[66] E. Lightfoot, "Steady state absorption of a sparingly soluble gas in an agitated tank with simulataneous irreversible first-order reaction," *AIChE J.,* vol. 4, pp. 499-500, 1958.

[67] E. Lightfoot, "Gas absorption with simultaneous irreversible first-order reaction," *AIChE J.,* vol. 8, pp. 710-712, 1962.

[68] W. Gill and R. Nunge, "A note on unsteady gas absorption with chemical reaction," *Chem. Eng. Sci.,* vol. 17, pp. 683-688, 1962.

[69] J. Estrin and E. Schmidt, "Penetration theory applied to unsteady gas absorption with irreversible first-order reaction," *AIChE J.,* vol. 14, pp. 678-681, 1968.

[70] P. Danckwerts, "Gas absorption accompanied by chemical reaction," *AIChE J,* vol. 1, p. 456–463, 1955.

[71] E. Alper, "Physical absorption of a gas in laboratory models of a packed column," *AIChE J.,* vol. 25, pp. 545-547, 1979.

[72] D. Perlmutter, "Surface-renewal models in mass transfer," *Chem. Eng. Sci.,* vol. 16, pp. 287-296, 1961.

[73] T. Zwietering, "The degree of mixing in continuous flow systems," *Chem. Eng. Sci.,* vol. 11, pp. 1-15, 1959.

[74] P. Danckwerts, "Kinetics of the absorption of carbon dioxide in water," *Research,* vol. 2, p. 494, 1949.

[75] S. Miyamoto, "A theory of the rate of solution of gas into liquid," *Bull. Chem. Soc. Jpn.,* vol. 7, pp. 8-17, 1932.

[76] S. Miyamoto, "A theory of the rate of solution of gas into liquid II - A kinetic derivation of the distribution law," *Bull. Chem. Soc. Jpn.,* vol. 7, pp. 388-398., 1932.

[77] H. Toor, "Averaging of Mass Transfer Rates," *AIChE J.,* vol. 2, p. 578–10D, 1956.

[78] L. Scriven and R. Pigford, "Absorption into an accelerating film," *AIChE J.,* vol. 2, pp. 382-10s, 1958.

[79] L. Scriven and R. Pigford, "On phase equilibrium at the gas-liquid interface during absorption," *AIChE J.,* vol. 4, pp. 439-444, 1958.

[80] H. Toor and P. Raimondi, "Interfacial resistance in gas absorption," *AIChE J.,* vol. 5, p. 86–92, 1959.

[81] W. Thomas, S. Ismail and E. Palmer, "Interferometric studies of interfacial mass transfer in a liquid-liquid system," *Chem. Eng. Comm.,* vol. 2, pp. 87-101, 1976.

[82] R. Lessard and S. Zieminski, "Bubble coalescence and gas transfer in aqueous electrolytic solutions," *Ind. Eng. Chem.,* vol. 10, pp. 260-269, 1971.

[83] R. Coughlin, "Surface resistance in transport from vapor to liquid," *Chem. Eng. Sci.,* vol. 25, pp. 1503-1511, 1967.

[84] I. Eames, J. Marr and H. Sabir, "The evaporation coefficient of water: a review," *Int. J. Heat Mass Transfer,* vol. 40, pp. 2963-2973, 1997.

[85] C. Ward, "The rate of gas absorption at a liquid interface," *J. Chem. Phys.,* vol. 67, pp. 229-235., 1977.

[86] C. Ward, R. Findlay and M. Rizk, "Statistical rate theory of interfacial transport I - Theoretical development," *J. Chem. Phys.,* vol. 76, pp. 5599-5605., 1982.

[87] C. Ward, M. Rizk and A. Tucker, "Statistical Rate Theory of interfacial transport II - Rate of isothermal bubble evolution in a liquid–gas solution," *J. Chem. Phys.,* vol. 76, pp. 5606-5614, 1982.

[88] C. Ward and R. Findlay, "Statistical rate theory of interfacial transport III - Predicted Rate of Nondissociative Adsorption," *J. Chem. Phys.,* vol. 76, pp. 5615-5623, 1982.

[89] R. Findlay and C. Ward, "Statistical rate theory of interfacial transport IV - Predicted rate of dissociative adsorption," *J. Chem. Phys.,* vol. 76, pp. 5624-5631, 1982.

[90] L. Tao, "Gaseous absorption in a liquid," *Acta Mechanica,* vol. 49, pp. 33-47, 1983.

[91] R. Gupta and T. Sridhar, "Effect of interfacial resistance on quiescent gas-liquid absorption," *Chem. Eng. Sci.,* vol. 39, pp. 471-477, 1984.

[92] E. Harvey and W. Smith, "The absorption of carbon dioxide by a quiescent liquid," *Chem. Eng. Sci.,* vol. 10, pp. 274-280, 1959.

[93] H. Schlichting and K. Gersten, Boundary-layer theory, 8th Enlarged Ed., Springer, 2000.

[94] A. Acrivos and P. Chambre, "Laminar Boundary Layer Flows with Surface Reactions," *Ind. Eng. Chem.,* vol. 49, p. 1025–1029, 1957.

[95] J. Goddard and A. Acrivos, "An Analysis Of Laminar Forced-Convection Mass Transfer With Homogeneous Chemical Reaction," *Q. J. Mechanics Appl. Math.,* vol. 20, pp. 471-497, 1967.

[96] R. Bird, W. Stewart and E. Lightfoot, Transport Phenoemena 2nd Ed., Wiley & Sons, 2007.

[97] T. Akiyama, "The equivalence of the penetration and boundary layer theories," *Chem. Eng. Sci.,* vol. 27 , pp. 161-163, 1972.

[98] S. Sideman, "The equivalence of penetration and potential flow theories," *Ind. Eng. Chem.,* vol. 58, pp. 54-58, 1966.

[99] R. Emmett and R. Pigford, "Interfacial resistance - a study of gas absorption in falling liquid films," *Chem. Engng. Prog.,* vol. 50, pp. 87-93, 1954.

[100] S. Haase, R. Langsch, M. Weiss and R. Lange, "Hydrodynamics, mass transfer, and scale-up of miniaturised and structured fixed-bed reactors for gas-liquid-solid reactions," in *WCCE 9*, Korea, 2013.

[101] J. van Baten and R. Krishna, "CFD simulations of mass transfer from Taylor bubbles rising in circular capillaries," *Chem. Eng. Sci.,* vol. 59, pp. 2535-2545, 2004.

[102] C. Vandu, H. Liu and R. Krishna, "Mass transfer from Taylor bubbles rising in single capillaries," *Chem. Eng. Sci.,* vol. 60, p. 6430 – 6437, 2005.

[103] R. Pohorecki, "Effectiveness of interfacial area for mass transfer in two-phase flow in microreactors.," *Chem. Eng. Sci.,* vol. 62, pp. 6495-6498, 2007.

[104] E. van Elk, M. Knaap and G. Versteeg, "Application of the penetration theory for gas-liquid mass transfer without liquid bulk," *Chem. Eng. Res. Des.,* vol. 85, pp. 516-524, 2007.

[105] J. Yue, E. Rebrov and J. Schouten, "Enhancement factor for gas absorption in a finite liquid layer. Part 2: First-and second-order reactions in a liquid in plug

flow," *Chem. Eng. Technol.,* vol. 35, pp. 859-869, 2012.

[106] S. Kuhn and K. Jensen, "A pH-sensitive laser-induced fluorescence technique to monitor mass transfer in multiphase flows in microfluidic devices," *Ind. Eng. Chem. Res.,* vol. 51, p. 8999–9006, 2012.

[107] Y. Su, Y. Zhao, G. Chen and Q. Yuan, "Liquid–liquid two-phase flow and mass transfer characteristics in packed microchannels," *Chem. Eng. Sci.,* vol. 65, pp. 3947-3956, 2010.

[108] N. Mhiri, H. Monnier and H. Falk, "Intensification of the G/L absorption in microstructured falling film application to the treatment of chlorinated VOC's. Part III: Influence of gas thickness channel on mass transfer," *Chem. Eng. Sci.,* vol. 66, pp. 5989-6001, 2011.

[109] H. Hikita and S. Asai, "Gas absorption with (m,n)-th order irreversible chemical reaction," *Int. Chem. Eng,* vol. 4, pp. 332-340, 1964.

[110] S. Asai, "Linearization of Diffusion Equations with Chemical Reaction: Generalization of Hikita-Asai Approximation," *Can. J. Chem. Eng.,* vol. 68, pp. 284-291, 1990.

[111] W. Krückels, "On gradient dependent diffusivity," *Chem. Eng. Sci.,* vol. 28, pp. 1565-1576, 1973.

[112] E. Thiele, "Relation between Catalytic Activity and Size of Particle," *Ind. Eng. Chem.,* vol. 31, p. 916–920, 1939.

[113] H. Fogler, Elements of chemical reaction engineering, 4th Ed., Prentice Hall, 2005.

[114] B. Kulkarni and L. Doraiswamy, "Effectiveness factors in gas-liquid reactions," *AIChE J.,* vol. 21, pp. 501-506, 1975.

[115] K. Bischoff, "Effectiveness factors for general reaction rate forms," *AIChE J.,* vol. 11, p. 351–355, 1965.

[116] J. Yue, E. Rebrov and J. Schouten, "Enhancement factor for gas absorption in a finite liquid layer. Part 1: Instantaneous reaction in a liquid layer in plug flow," *Chem. Eng. Technol.,* vol. 35, pp. 679-692, 2012.

[117] J. Yue, E. Rebrov and J. Schouten, "Enhancement factor for gas absorption in a finite liquid layer. Part 3: Instantaneous and second-order reactions in a liquid in laminar flow," *Chem. Eng. Technol.,* vol. 35, pp. 1473-1485, 2012.

[118] "Enhancement factor for gas absorption in a finite liquid layer. Part 4: Influence of gas-phase mass transfer during a second-order reaction in a liquid in laminar flow," *Chem. Eng. Technol.,* vol. 36, pp. 611-626, 2013.

[119] P. Danckwerts, "Unsteady-state diffusion or heat-conduction with moving boundary," *Trans. Faraday Soc.,* vol. 46, pp. 701-712, 1950.

[120] E. Alper, Mass Transfer with Chemical Reaction: Lecture Notes (in Turkish), Ankara: Hacettepe University, 2001.

[121] R. Perry and R. Pigford, "Kinetics of gas-liquid reactions: simultaneous absorption and chemical reaction," *Ind. Eng. Chem.,* vol. 45, pp. 1247-1253, 1953.

[122] P. Brian, J. Hurley and E. Hasseltine, "Penetration theory for gas absorption accompanied by a second order chemical reaction," *AIChE J.,* vol. 7, pp. 226-231, 1961.

[123] P. Brian, "Gas absorption accompanied by an irreversible reaction of general order," *AIChE J.,* vol. 10, pp. 5-10, 1964.

[124] O. Levenspiel, Chemical reaction engineering, New York: Wiley, 1999.

[125] P. Danckwerts, Gas-liquid reactions, McGraw-Hill, 1970.

[126] R. Subramanian and R. Balasubramaniam, The Motion of Bubbles and Drops in Reduced Gravity, Cambridge University Press, 2001.

[127] C. Yih, "Instability due to viscosity stratification," *J. Fluid Mech.,* vol. 27, pp. 337-352, 1967.

[128] S. Chandrasekhar, Hydrodynamic and Hydromagnetic Stability, Oxford: Oxford University Press, 1981.

[129] A. Günther and K. Jensen, "Multiphase microfluidics: from flow characteristics to chemical and materials synthesis," *Lab Chip,* vol. 6, pp. 1487-1503, 2006.

[130] E. Davis, "Interfacial shear measurement for two-phase gas-liquid flow by means of Preston tubes," *Ind. Eng. Chem. Fundam.,* vol. 8, pp. 153-159, 1969.

[131] N. Brauner and D. Moalem-Maron, "The role of interfacial shear modelling in predicting the stability of stratified two-phase flow," *Chem. Eng. Sci.,* vol. 48, pp. 2867-2879, 1993.

[132] E. Davis, "An analysis of the falling-film gas-liquid reactor," *Chem. Eng. Sci.,* vol. 34, pp. 539-550, 1979.

[133] B. Azzopardi, H. Morvan, R. F. Mudde, Y. Yan, D. Zhao and S. Lo, Hydrodynamics of gas-liquid reactors : normal operation and upset conditions, New York: Wiley, 2011.

[134] H. Zhang, J. Yue, G. Chen and Q. Yuan, "Flow pattern and break-up of liquid film in single-channel falling film microreactors," *Chem. Eng. J.,* vol. 163, pp. 126-132, 2010.

[135] E. Lauga, M. Brenner and H. Stone, "Microfluidics: The No-Slip Boundary Condition," in *Springer Handbook of Experimental Fluid Mechanics*, Springer, 2007, pp. 1219-1240 .

[136] D. Morris, L. Hannon and A. Garcia, "Slip length in a dilute gas," *Phys. Rev. A,* vol. 46, pp. 5279-5281, 1992.

[137] P. Thompson and S. Troian, "A general boundary condition for liquid flow at solid surfaces," *Phys. Rev. Lett.,* vol. 63, pp. 766-769, 1997.

[138] T. Kitamori, T. Tsukahara and K. Mawatari, Extended-nanofluidic Systems for Chemistry and Biotechnology, London: Imperial College Press, 2012.

[139] P. Tsai, A. Peters, C. Pirat, M. Wessling, R. Lammertink and D. Lohse, "Quantifying effective slip length over micropatterned hydrophobic surfaces," *Phys. Fluid.,* vol. 21, p. 112002, 2009.

[140] R. Daniello, N. Waterhouse and J. Rothstein, "Drag reduction in turbulent flows over superhydrophobic surfaces," *Phys. Fluids,* vol. 21, p. 085103, 2009.

[141] L. Schwartz, H. Princen and A. Kiss, "On the motion of bubbles in capillary tubes," *J. Fluid. Mech.,* vol. 172, pp. 259-275, 1986.

[142] T. Sweeney and S. Calvert, "Gas absorption in a fin-wall conduit," *AIChE J.,* vol. 11, pp. 785-789, 1965.

[143] E. Rebrov, T. Duisters, P. Löb, J. Meuldijk and V. Hessel, "Enhancement of the liquid-side mass transfer in a falling film catalytic microreactor by in-channel mixing structures," *Ind. Eng. Chem. Res.,* vol. 51, pp. 8719-8725, 2012.

[144] S. Jayanti and G. Hewitt, "Hydrodynamics and heat transfer of wavy thin film flow," *Int. J. Heat Mass Transfer,* vol. 40, pp. 179-190, 1997.

[145] M. Miya, D. Woodmansee and T. Hanratty, "A model for roll waves in gas-liquid flow," *Chem. Eng. Sci.,* vol. 26, pp. 1915-1931, 1971.

[146] K. Triplett, S. Ghiaasiaan, S. Abdel-Khalik and D. Sadowski, "Gas-liquid two-phase flow in microchannels. Part I: two-phase flow patterns," *Int. J. Multiphase Flow,* vol. 25, pp. 377-394, 1999.

[147] R. Seban and A. Faghri, "Wave effects on the transport to falling laminar liquid films," *J. Heat Transfer ,* vol. 100, pp. 143-147, 1978.

[148] E. Ruckenstein, "A generalized penetration theory for unsteady-convective mass transfer," *Chem. Eng. Sci.,* vol. 23, pp. 363-371, 1968.

[149] K. Javdani, "Mass transfer in wavy liquid films," *Chem. Eng. Sci.,* vol. 29, pp. 61-69, 1974.

[150] K. Ishimi, S. Koroyasu and H. Hikita, "Effect of progressive waves on a liquid surface upon gas absorption in unsteady state," *J. Chem. Eng. Jpn.,* vol. 30, pp. 154-158, 1997.

[151] D. Howard and E. Lightfoot, "Mass transfer to falling films: Part I. Application of the surface stretch model to uniform wave motion," *AIChE J.,* vol. 14, pp. 458-467, 1968.

[152] K. Asokan, Mass Transfer Concepts, CRC Press, 2011.

[153] C. Ho, H. Chang, H. Chen, C. Chang, H. Li and Y. Chang, "CFD simulation of the two-phase flow for a falling film microreactor," *Int. J. Heat Mass Transfer,* vol. 54, pp. 3740-3748, 2011.

[154] R. Gupta, D. Fletcher and B. Haynes, "On the CFD modelling of Taylor flow in microchannels," *Chem. Eng. Sci.,* vol. 64, pp. 2941-2950, 2009.

[155] C. Albert, H. Marschall and D. Bothe, "Direct Numerical Simulation of interfacial mass transfer into falling films," *Int. J. Heat Mass Transfer,* vol. 69, pp. 343-357, 2014.

[156] K. Deshpande and W. Zimmerman, "Simulation of interfacial mass transfer by droplet dynamics using the level set method," *Chem. Eng. Sci.,* vol. 61, pp. 6486-6498, 2006.

[157] Y. Haroun, L. Raynal and D. Legendre, "Mass transfer and liquid hold-up determination in structured packing by CFD," *Chem. Eng. Sci.,* vol. 75, pp. 342-348, 2012.

[158] T. Taha and Z. Cui, "CFD modelling of slug flow in vertical tubes," *Chem. Eng. Sci.,* vol. 61, pp. 676-687, 2006.

[159] N. Shao, A. Gavriilidis and P. Angeli, "Mass transfer during Taylor flow in microchannels with and without chemical reaction," *Chem. Eng. J.,* vol. 160, pp. 873-881, 2010.

[160] G. Sisoev, O. Matar and C. Lawrence, "Absorption of gas into a wavy falling film," *Chem. Eng. Sci.,* vol. 60, pp. 827-838, 2005.

[161] M. Wörner, "Numerical modeling of multiphase flows in microfluidics and micro process engineering: a review of methods and applications," *Microfluid Nanofluid,* vol. 12, p. 841–886, 2012.

[162] C. Kellner and A. Bell, "The kinetics and mechanism of carbon monoxide hydrogenation over alumina-supported ruthenium," *J. Catal.,* vol. 70, pp. 418-432, 1981.

[163] R. Deugd, F. Kapteijn and J. Moulijn, "Trends in Fischer-Tropsch reactor technology: Opportunities for structured reactors," *Top. Catal.,* vol. 26, pp. 29-39, 2003.

[164] M. Post, A. van't Hoog, J. Minderhoud and S. Sie, "Diffusion limitations in Fischer-Tropsch catalysts," *AIChE J.,* vol. 35, pp. 1107-1114, 1989.

[165] R. Guettel and T. Turek, "Comparison of different reactor types for low temperature Fischer-Tropsch synthesis: A simulation study," *Chem. Eng. Sci.,* vol. 64, pp. 955-964, 2009.

[166] I. Yates and S. C.N., "Intrinsic Kinetics of the Fischer-Tropsch Synthesis on a Cobalt Catalyst," *Energy Fuels,* vol. 5, pp. 168-173, 1991.

[167] R. Dixit and L. Tavlarides, "Kinetics of the Fischer-Tropsch Synthesis," *Ind. Eng. Chem. Process Des. Dev.,* vol. 22, pp. 1-9, 1983.

[168] R. Deugd, R. Chougule, M. Kreutzer, F. Meeuse, J. Grievink, F. Kapteijn and J. Moulijn, "Is a monolithic loop reactor a viable option for Fischer–Tropsch synthesis," *Chem. Eng. Sci.,* vol. 58, p. 583–591, 2003.

[169] W. Zimmerman and D. Bukur, "Reaction kinetics over iron catalysts used for the Fischer-Tropsch synthesis," *Can. J. Chem. Eng.,* vol. 68, pp. 292-301, 1990.

[170] R. Dalla Betta, A. Piken and M. Shelef, "Heterogeneous methanation: initial rate of CO hydrogenation on supported ruthenium and nickel," *J. Catal.,* vol.

35, pp. 54-60, 1974.

[171] M. Vannice, "The catalytic synthesis of hydrocarbons from H2CO mixtures over the group VIII metals: I & II," *J.Catal.,* Vols. 449-473, p. 37, 1975.

[172] J. Ekerdt and A. Bell, "Synthesis of hydrocarbons from CO and H2 over silica-supported Ru: Reaction rate measurements and infrared spectra of adsorbed species," *J. Catal.,* vol. 58, pp. 170-187, 1979.

[173] İ. Bayar, Photocatalytic oxidation of NOx over TiO2 containing cement based materials, Ms. Thesis, Ankara: Middle East Technical University, 2013.

[174] K. Pohlhausen, "Zur näherungsweisen Integration der Differentialgleichung der Iaminaren Grenzschicht," *Z. Angew. Math. Mech.,* vol. 1, pp. 252-290, 1921.

[175] M. Özışık and D. Hahn, Heat Conduction 3rd Ed., Wiley & Sons, 2012.

[176] V. Volkov and V. Li-Orlov, "A refinement of the integral method in solving the heat conduction equation," *Heat Transfer - Soviet Research,* vol. 2, pp. 41-47, 1970.

[177] K. Papadopoulos, "Linear unsteady transport problems when there is an initial steady state," *Chem. Eng. Edu.,* vol. 1998, no. 3, pp. 260-261, 1998.

[178] W. Schiesser, The Numerical Method of Lines: Integration of Partial Differential Equations, San Diego, California: Academic Press, 1991.

[179] S. Wieder, Introduction to Mathcad for Scientists ad Engineers, McGraw-Hill, 1993.

[180] B. Fornberg, "Generation of finite difference formulas on arbitrarily spaced grids," *Math. Comp.,* vol. 51, pp. 699-706, 1988.

[181] C. Chan Man Fong, D. De Kee and P. Kaloni, Advanced Mathematics for Engineering and Science, Singapore: World Scientific, 2003.

[182] S. Chapra and R. Canale, Numerical Methods for Engineers, 5th Ed., New York: McGraw Hill, 2006.

[183] COMSOL AB, COMSOL Multiphysics Reference Guide v4.0a, 2010.

[184] K. Kustin, I. Taub and E. Weinstock, "A kinetic study of the formation of the ferrous-nitric oxide complex," *Inorg. Chem.,* vol. 5, p. 1079–1082, 1966.

[185] E. Sada, H. Kumazawa, I. Kudo and T. Kondo, "Individual and simultaneous absorption of dilute NO and SO2 in aqueous slurries of MgSO3 with Fe(II)-EDTA," *Ind. Eng. Chem. Process Dev.,* vol. 19, pp. 377-382, 1980.

[186] P. Danckwerts, "Surface instability during the absorption of CO2 by monoethanolamine solutions," *Chem. Eng. Sci.,* vol. 22, pp. 1513-1514, 1967.

[187] J. Buzek, J. Podkanski and K. Warmuzinski, "The enhancement of the rate of absorption of CO2 in amine solutions due to the Marangoni effect," *Energy Convers. Mgmt.,* vol. 38, pp. S69-S74, 1997.

[188] P. Brian, J. Vivian and D. Matiatos, "Interfacial turbulence during the absorption of carbon dioxide into monoethanolamine," *AIChE J.,* vol. 13, pp. 28-36, 1967.

[189] E. Sada, H. Kumazawa, M. Butt and J. Lozano, "Interfacial turbulence accompanying chemical absorption," *Can. J. Chem. Eng.,* vol. 55, p. 293–296, 1977.

[190] P. Brian, "Marangoni instability in vertical falling films versus horizontal stagnant liquid layers," *Chem. Eng. Sci.,* vol. 23, pp. 1513-1514, 1968.

[191] P. Sobieszuk, R. Pohorecki, P. Cyganski, M. Kraut and F. Olschewski, "Marangoni effect in a falling film microreactor," *Chem. Eng. J.,* vol. 164, pp. 10-15, 2010.

[192] J. Yue, E. Rebrov and J. Schouten, "Enhancement factor for gas absorption in a finite liquid layer. Part 2: First-and second-order reactions in a liquid in plug flow," *Chem. Eng. Tech.,* vol. 35, pp. 859-869, 2012.

[193] L. Doraiswamy and M. Sharma, Heterogeneous reactions : analysis, examples, and reactor design, vol.2, New York: Wiley-Interscience, 1984.

[194] J. Gottifredi, A. Yeremian and J. Ronco, "On the effect of flow patterns on the rate of mass transfer with chemical reaction," *Chem. Eng. Sci.,* vol. 25, pp. 1239-1242, 1970.

[195] B. Mehta and R. Aris, "A note on a form of the Emden-Fowler equation," *J. Math. Anal. Appl.,* vol. 36, pp. 611-621, 1971.

[196] B. Kulkarni and L. Doraiswamy, "Effectiveness factors in gas-liquid reactions: The general nth order case," *AIChE J.,* vol. 22, pp. 597-600, 1976.

[197] R. York, K. Bratlie, L. Hile and L. Jang, "Dead zones in porous catalysts: Concentration profiles ans efficiency factors," *Catal. Today,* vol. 160, pp. 204-

121, 2011.

[198] E. Thiele, "Relation between catalytic activity and size of particle," *Ind. Eng. Chem.,* vol. 31, p. 916–920, 1939.

[199] B. Mehta and R. Aris, "Communications on the theory of diffusion and reaction—VII The isothermal pth order reaction," *Chem. Eng. Sci.,* vol. 26, pp. 1699-1712, 1971.

[200] A. Cook and E. Moore, "Gas absorption with a first order chemical reaction and large heat effect," *Chem. Eng. Sci.,* vol. 27, pp. 605-613, 1972.

[201] B. Finlayson, Nonlinear analysis in chemical engineering, New York: McGraw-Hill, 1980.

[202] R. Mann and G. Clegg, "Gas absorption with an unusual chemical reaction: the chlorination of toluene," *Chem. Eng. Sci.,* vol. 30, pp. 97-101, 1975.

[203] S. Asai, "Linearization of diffusion equations with chemical reaction: generalization of Hikita-Asai approximation," *Can. J. Chem. Eng.,* vol. 68, pp. 284-291, 1990.

[204] H. Hlaváček, M. Kubiček and M. Marek, "Analysis of nonstationary heat and mass transfer in a porous catalyst particle I," *J. Catal.,* vol. 15, pp. 17-30, 1969.

[205] E. Tavera, "Analytical expression for the non-isothermal effectiveness factor: the nth-order reaction in a slab geometry," *Chem. Eng. Sci.,* vol. 60, pp. 907-916, 2005.

[206] P. Danckwerts, "Absorption by simultaneous diffusion and chemical reaction into particles of various shapes and into falling drops," *Trans. Faraday Soc.,* vol. 47, pp. 1014-1023, 1951.

[207] D. Tarzia, "A variant of the heat balance integral method and a new proof of the exponentially fast asymptotic behavior of the solutions in heat conduction problems with absorption," *Int. J. Engng. Sci.,* vol. 12, pp. 1253-1259, 1990.

[208] E. Davis, "Exact solutions for a class of heat and mass transfer problems," *Can. J. Chem.,* vol. 51, p. 562–572, 1973.

[209] J. De Jong, R. Lammertink and M. Wessling, "Membranes and microfluidics: a review," *Lab Chip,* vol. 6, pp. 1125-1139, 2006.

[210] M. Sato and M. Goto, "Gas absorption in water with microchannel devices,"

Separ. Sci. Technol., vol. 39, pp. 3163-3167, 2004.

[211] R. Albal, Y. Shah, N. Carr and A. Bell, "Mass transfer coefficients and solubilities for hydrogen and carbonmonoxide under Fischer-Tropsch conditions," *Chem. Eng. Sci.,* vol. 39, pp. 905-907, 1984.

[212] C. Erkey, J. Rodden and A. Akgerman, "Diffusivities of synthesis gas and n-alkanes in Fischer-Tropsch wax," *Energy Fuels,* vol. 4, pp. 275-276, 1990.

[213] M. Boudart, "Kinetics on ideal and real surfaces," *AIChE J.,* vol. 2, pp. 62-64, 1956.

[214] S. Weller, "Analysis of kinetic data for heterogeneous reactions," *AIChE J.,* vol. 2, pp. 59-62, 1956.

[215] G. Roberts and C. Satterfield, "Effectiveness factor for porous catalysts: Langmuir-Hinshelwood kinetic expressions," *Ind. End. Chem. Fundam.,* vol. 4, pp. 289-293, 1965.

[216] G. Roberts and C. Satterfield, "Effectiveness factor for porous catalysts: Langmuir-Hinshelwood kinetic expressions for bimolecular surface reactions," *Ind. Eng. Chem. Fundam.,* vol. 5, pp. 317-325, 1966.

[217] R. Rajadhyaksha, K. Vasudeva and L. Doraiswamy, "Effectiveness factors in Langmuir-Hinshelwood and general order kinetics," *J. Catal.,* vol. 41, pp. 61-71, 1976.

[218] J. Hartman, G. Roberts and C. Satterfield, "Effects of initial conditions on the steady-state activity of catalyst particles," *Ind. Eng. Chem. Fundam.,* vol. 6, pp. 80-83, 1967.

[219] D. Uner, "A sensible mechanism of alkali promotion in Fischer-Tropsch synthesis: Adsorbate mobilities," *Ind. Eng. Chem. Res.,* vol. 37, pp. 2239-2245, 1998.

[220] M. Dalgıç, Solutions of The Equations of Change By The Averaging Technique, Ms. Thesis, Ankara: Middle East Technical University, 2008.

[221] F. Bretherton, "The motion of long bubbles in tubes," *J. Fluid Mech.,* vol. 10, pp. 166-188, 1961.

[222] S. Roy, T. Bauer, M. Al-Dahhan, P. Lehner and T. Turek, "Monoliths as multiphase reactors: A review," *AIChE J.,* vol. 50, pp. 2918-2938, 2004.

[223] P. Chambré, "Nonlinear Heat Transfer Problem," *J. Appl. Phys.,* vol. 30, pp. 1683-1689, 1959.

[224] R. Cotta and M. Mihailov, Heat conduction: lumped analysis, integral transforms, symbolic computation, New York: Wiley, 1997.

[225] R. Grau, M. Cabrera and A. Cassano, "The laminar flow tubular reactor with homogeneous and heterogeneous reactions I. Integral equations for diverse reaction rate regimes," *Chem. Eng. Comm.,* vol. 184, pp. 229-257, 2001.

[226] H. Bengston and F. Kreith, "Approximate solution of heat-conduction problems in systems with nonuniform initial temperature distribution," *J. Heat Transfer,* vol. 92, pp. 182-184, 1970.

[227] S. Katz, "Chemical reactions catalysed on a tube wall," *Chem. Eng. Sci.,* vol. 10, pp. 202-211, 1959.

[228] M. Spiegel, Mathematical Handbook of Formulas and Tables, McGraw-Hill, 1968.

[229] L. Landau and E. Lifshitz, Fluid mechanics, 2nd Ed., New York: Pergamon Press, 1982.

[230] C. Hastings, Approximations for Digital Computers, Princeton, New Jersey: Princeton University Press, 1955.

[231] J. Lopes, A. Rodrigues and S. Cardoso, "approximate calculation of conversion with kinetic normalization for finite reaction rates in wall-coated microchannels," *AIChE J.,* vol. 57, pp. 2870-2887, 2011.

[232] L. Leal, Laminar Flow and Convective Transport Processes, Butterworth-Heinemann, 1992.

[233] W. Olbrich and J. Wild, "Diffusion from the free surface into a liquid film in laminar flow over defined shapes," *Chem. Eng. Sci.,* vol. 24, pp. 25-32, 1969.

[234] O. Vallaee and M. Soares, Airy functions and applications to physics, Hackensack, New Jersey: World Scientific, 2010.

[235] A. Apelblat, "Mass transfer with a chemical reaction of the first order: Analytical solutions," *Chem. Eng. J.,* vol. 19, pp. 19-37, 1980.

[236] A. Flores and J. Gottifredi, "A simple analysis of mass transfer with chemical reaction at a mobile interface," *Lett. Heat Mass Transfer,* vol. 9, pp. 141-149,

1982.

[237] E. Davis and T. Cooper, "Thermal entrance effects in stratified gas-liquid flow: experimental investigation," *Chem. Eng. Sci.,* vol. 24, pp. 509-520, 1969.

[238] S. Qian, S. Joo, Y. Jiang and M. Cheney, "Free-surface problems in electrokinetic micro- and nanofluidics," *Mech. Res. Commun.,* vol. 36, pp. 82-91, 2009.

[239] W. Choi, A. Sharma, S. Qian, G. Lim and S. Joo, "Is free surface free in micro-scale electrokinetic flows?," *J. Colloid Interface Sci.,* vol. 347, pp. 153-155, 2010.

[240] H. Carslaw and J. Jaeger, Conduction of Heat in Solids 2nd Ed., Oxford: Clarendon Press, 1959.

[241] L. Peters, Solutions of diffusion problem associated with a nonlinear boundary condition at a liquid-gas interface. Msc. Thesis, University of Toronto, 1972.

[242] T. Zien, "Approximate calculation of transient heat conduction," *AIAA J.,* vol. 14, pp. 404-406, 1976.

[243] T. Goodman, "The heat-balance integral - further considerations and refinements," *J. Heat Transfer,* vol. 83c, pp. 83-85, 1961.

[244] D. Moalem-Maron and Y. Meinhardt, "Solutions of the diffusion equation by Picard's iteration procedure," *Lett. Heat Mass Transfer,* vol. 5, pp. 269-277, 1978.

[245] H. Landahl, "An approximation method for the solution of diffusion and related problems," *Bull. Math. Biophys.,* vol. 15, pp. 49-61, 1953.

[246] T. Myers, "Optimizing the exponent in the heat balance and refined integral methods," *Int. J. Heat Mass Transfer,* vol. 36, pp. 143-147, 2009.

[247] M. Mantelli and W. Braga, "Temperature profiles for diffusion problem: precise solutions using heat balance integral method," *J. Thermophys. Heat Transfer,* vol. 25, pp. 443-449, 2011.

[248] D. Langford, "The heat balance integral," *Int. J. Heat Mass Transfer,* vol. 16, pp. 2424-2428, 1973.

[249] J. Hristov, "The heat-balance integral method by a parabolic profile with unspecified exponent: Analysis and benchmark exercises," *Thermal Science,*

vol. 13, pp. 27-48, 2009.

[250] S. Mitchell and T. Myers, "Improving the accuracy of heat balance integral methods applied to thermal problems with time dependent boundary conditions," *Int. J. Heat Mass Transfer,* vol. 53, p. 3540–3551, 2010.

[251] J. Hristov, "The heat-balance integral: 1. How to calibrate the parabolic profile," *C.R. Mecanique,* vol. 340, pp. 485-492, 2012.

[252] R. Thorsen and F. Landis, "Integral methods in transient heat conduction problems with non-uniform initial conditions," *Int. J. Heat Mass Transfer,* vol. 8, pp. 189-192, 1965.

[253] T. Goodman, "Application of integral methods to transient nonlinear heat transfer," in *Advances in Heat Transfer Vol.1 (Eds. T.F. Irvine and J.P. Hartnett)*, New York, Academic Press, 1964, pp. 51-122.

[254] B. Baudouy, "Heat-balance integral method for heat transfer in superfluid helium," *Thermal Science,* vol. 13, pp. 121-132, 2009.

[255] F. Mohamed, "The energy-integral method: application to linear hyperbolic heat-conduction problems," *App. Sci. Res.,* vol. 50, pp. 107-128, 1993.

[256] V. Ugrozov, A. Filippov, C. Paraskeva, G. Constantinides and V. Starov, "Diffusive dissolution of a drop in a capillary," *Colloids Surf., A,* vol. 239, pp. 129-133, 2004.

[257] M. Abramowitz and I. Stegun, Handbook of mathematical functions with formulas, graphs, and mathematical tables, U.S. Govt. Print. Off., 1964.

[258] P. Ball, "Engineering shark skin and other solutions," *Nature,* vol. 400, pp. 507-509, 1999.

[259] R. de Deugd, R. Chougule, M. Kreutzer, F. Meeuse, J. Grievink, F. Kapteijn and J. Moulijn, "Is a monolithic loop reactor a viable option for Fischer–Tropsch synthesis?," *Chem. Eng. Sci.,* vol. 58, pp. 583-591, 2003.

[260] M. Bradford, M. Te and A. Pollack, "Monolith loop catalytic membrane reactor for Fischer–Tropsch synthesis," *Appl. Catal., A.,* vol. 283, pp. 39-46, 2005.

[261] K. Pangarkar, T. Schildhauer, J. van Ommen, J. Nijenhuis, J. Moulijn and F. Kapteijn, "Experimental and numerical comparison of structured packings with a randomly packed bed reactor for Fischer–Tropsch synthesis," *Catal. Today.,*

vol. 147S, pp. S2-S9, 2009.

[262] D. Vervloet, K. Kamali, J. Gillissen, J. Nijenhuis, H. van den Akker, F. Kapteijn and J. van Ommen, "Intensification of co-current gas–liquid reactors using structured catalytic packings - A multiscale approach," *Catal. Today.,* vol. 147S, pp. S138-S143, 2009.

[263] C. Cao, J. Hu, S. Li, W. Wilcox and Y. Wang, "Intensified Fischer–Tropsch synthesis process with microchannel catalytic reactors," *Catal. Today,* vol. 140, pp. 149-156, 2009.

[264] C. Visconti, E. Tronconi, G. Groppia, L. Lietti, M. Iovane, S. Rossini and R. Zennaro, "Monolithic catalysts with high thermal conductivity for the Fischer–Tropsch synthesis in tubular reactors," *Chem. Eng. J.,* vol. 171, 2011.

[265] N. Hooshyar, D. Vervloet, F. Kapteijn, P. Hamersma, R. Mudde and J. van Ommen, " Intensifying the Fischer–Tropsch Synthesis by reactor structuring – A model study," *Chem. Eng. J.,* Vols. 207-208, p. 865–870, 2012.

[266] M. Hösükoğlu, M. Karakaya and A. Avcı, "Modeling and Simulation of Hydrocracking of Fischer−Tropsch Hydrocarbons in a Catalytic Microchannel Reactor," *Ind. Eng. Chem. Res.,* vol. 51, p. 8913−8921, 2012.

[267] G. Gümüşlü and A. Avcı, "Parametric Analysis of Fischer-Tropsch Synthesis in a Catalytic Microchannel Reactor," *AIChE J.,* vol. 58, pp. 227-235, 2012.

[268] D. Vervloet, F. Kapteijn, J. Nijenhuis and J. van Ommen, "A convection-based single-parameter model for heat transport in multiphase tubular reactors packed with closed cross flow structures," *Chem. Eng. J.,* vol. 233, pp. 265-273, 2013.

[269] L. A. Pellegrini, S. Bonomi, S. Gamba, V. Calemma and D. Molinari, "The “all components hydrocracking model”," *Chem. Eng. Sci.,* vol. 62, pp. 5013-5020, 2007.

[270] Y. Wang, W. Ma, Y. Lu, J. Yang, Y. Xu, H. Xiang, Y. Li, Y. Zhao and B. Zhang, "Kinetics modelling of Fischer–Tropsch synthesis over an industrial Fe–Cu–K catalyst," *Fuel,* vol. 82, pp. 195-213, 2003.

[271] T. Vermeulen, "Theory for irreversible and constant-pattern solid diffusion," *Ind. Eng. Chem.,* vol. 45, pp. 1664-1670, 1953.

APPENDIX A

DIFFUSION INTO FLOWING FILMS

The dimensionless solution to Equation-(94) under plug flow or quiescent conditions is:

$$u = 1 - \frac{4}{\pi}\sum_{n=0}^{\infty}\frac{1}{(2n+1)}\exp\left[-\left(\frac{2n+1}{2}\right)^2\pi^2\tau\right]\sin\left[\frac{2n+1}{2}\pi\xi\right] \quad \text{(A1)}$$

τ is exactly the same with Fo. Dimensionless surface flux can be given as[37]:

$$F_{plug} = \frac{N\delta}{DC^*} = 2\sum_{n=0}^{\infty}\exp\left[-\left(\frac{2n+1}{2}\right)^2\pi^2\tau\right] \quad \text{(A2)}$$

Integrating with respect to time yields the dimensionless amounts absorbed:

$$\hat{n}_{a_{plug}} = 2\sum_{n=0}^{\infty}\frac{\left\{1-\exp\left[-\left(\frac{2n+1}{2}\right)^2\pi^2\tau\right]\right\}}{\left(\frac{2n+1}{2}\right)^2\pi^2} \quad \text{(A3)}$$

For diffusion into laminar film flow, the surface flux expression expressed generally, such as:

$$F_{lam} = \sum_{n=1}^{\infty}A_n\exp(-\lambda_n\tau) \quad \text{(A4)}$$

where A_n are the series coefficients and λ_n are the eigenvalues. Up to $n = 10$, these values are provided by Olbrich and Wild [233] and given in Table 9. As in plug flow, integration with respect to time yields:

[37] For $\tau = Fo > 0.2$, a first term approximation in the series is satisfactory, the error is less than 2%.

$$\hat{n}_{a_{lam}} = \sum_{n=1}^{\infty} \frac{A_n}{\lambda_n}\left[1 - \exp(-\lambda_n \tau)\right] \tag{A5}$$

For generalized Couette flow, the PDE becomes:

$$(1 - a\xi)\frac{\partial C}{\partial \tau} = D\frac{\partial^2 C}{\partial \xi^2} \qquad \begin{array}{ll} \text{at } \tau = 0, & u = 0 \\ \text{at } \xi = 0, & u = 1 \\ \text{at } \xi = 1, & \partial u/\partial \xi = 0 \end{array} \tag{A6}$$

The PDE is linear, thus one may apply superposition to shift the non-homogeneity to the initial condition and then separation of variables can be used. One of the ODE's that appear after separation of variables is:

$$\frac{d^2 G}{d\xi^2} + {\lambda_n}^2 G - {\lambda_n}^2 a\xi G = 0 \tag{A7}$$

The solution can be obtained in terms of Airy functions[38] [234].

$$G = c_1 \mathrm{Ai}\left[\left(\frac{\lambda_n}{a}\right)^{2/3}(a\xi - 1)\right] + c_1 \mathrm{Bi}\left[\left(\frac{\lambda_n}{a}\right)^{2/3}(a\xi - 1)\right] \tag{A8}$$

Upon solving for the constants and superposing the solutions, the general solution is obtained as:

$$u = 1 - \sum_{n=1}^{\infty} C_n \exp\left(-{\lambda_n}^2 \tau\right)\left\{\mathrm{Ai}\left[\left(\frac{\lambda_n}{a}\right)^{2/3}(a\xi - 1)\right] + \vartheta\, \mathrm{Bi}\left[\left(\frac{\lambda_n}{a}\right)^{2/3}(a\xi - 1)\right]\right\} \tag{A9}$$

Eigenvalues are found from:

$$D\mathrm{Ai}\left[\left(\frac{\lambda_n}{a}\right)^{2/3}(a - 1)\right] - \vartheta\, D\mathrm{Bi}\left[\left(\frac{\lambda_n}{a}\right)^{2/3}(a - 1)\right] = 0 \tag{A10}$$

where

$$\vartheta = \frac{\mathrm{Ai}\left[-\left(\frac{\lambda_n}{a}\right)^{2/3}\right]}{\mathrm{Bi}\left[-\left(\frac{\lambda_n}{a}\right)^{2/3}\right]} \tag{A11}$$

and DAi and DBi are derivatives of Airy functions. Airy functions and their derivatives are well implemented into various CAS. The series coefficients are solved from:

[38] Airy functions are related to Bessel functions [2], but such a transformation seems to be more complicated.

$$C_n = \frac{\int_0^1 (1 - a\xi) f(\xi) d\xi}{\int_0^1 (1 - a\xi)\, f(\xi)^2 d\xi} \tag{A12}$$

$f(\xi)$ is the function given in the braces of Equation-(A9). In Table 9 the first 15 values for series coefficients and eigenvalues are provided for $a = 0.2, 0.5$ and 1. The surface flux can be given as:

$$F_{co} = \sum_{n=1}^{\infty} a^{1/3} {\lambda_n}^{2/3} C_n \exp\left(-{\lambda_n}^2 \tau\right) \left\{ \mathrm{DAi}\left[-\left(\frac{\lambda_n}{a}\right)^{2/3}\right] - \vartheta\, \mathrm{DBi}\left[-\left(\frac{\lambda_n}{a}\right)^{2/3}\right] \right\} \tag{A13}$$

All the equations related to generalized Couette flow is rather complicated. But the above equation surface flux equation can be presented in the form of Equation-(A4), thereby simplifying it as:

$$F_{co} = \sum_{n=1}^{\infty} S_n \exp\left(-{\lambda_n}^2 \tau\right) \tag{A14}$$

The first 15 values of S_n are given in Table 9 for $a = 0.2, 0.5$ and 1. Integration in time yields:

$$\hat{n}_{a_{co}} = \sum_{n=1}^{\infty} \frac{S_n}{{\lambda_n}^2} \left[1 - \exp\left(-{\lambda_n}^2 \tau\right)\right] \tag{A15}$$

Now Equations (A2), (A4) and (A14) can be compared with the dimensionless amounts absorbed predicted by PT via the equation:

$$F_{PT} = 2\sqrt{\frac{\tau}{\pi}} \tag{A16}$$

The error

$$\mathrm{Err} = \frac{F_{PT} - F_{exact}}{F_{exact}} \cdot 100 \tag{A17}$$

where F_{exact} denotes numerical plug, film or Couette flow solutions, is plotted on Figure 28.

Table 9. Series coefficients and eigenvalues for film and generalized Couette flows.

	Film Flow [1]		Generalized Coeutte Flow								
			a = 1		a = 0.5		a = 0.2		a = 1	a = 0.5	a = 0.2
n	A_n	λ_n	C_n	λ_n	C_n	λ_n	C_n	λ_n	S_n	S_n	S_n
1	2.69639	5.12166	1.93787	2.79953	2.48098	1.94729	-3.05946	1.69412	3	2.234	2.06972
2	2.57148	39.66083	-0.85964	7.48178	0.30576	5.51910	-0.14296	4.98286	3	2.3033	2.10433
3	2.55661	106.24923	0.57294	12.18640	-0.66867	9.14425	0.82934	8.29092	3	2.3136	2.10748
4	2.55201	204.85606	-0.43649	16.89527	-0.28481	12.78015	0.11769	11.60193	3	2.3168	2.10835
5	2.54999	335.47320	0.35564	21.60566	0.34696	16.41992	-0.50042	14.91392	3	2.31819	2.10871
6	2.54892	498.09708	-0.30175	26.31677	0.27919	20.06149	-0.11929	18.22637	3	2.31891	2.1089
7	2.54828	692.72580	0.26306	31.02826	-0.18577	23.70406	0.35877	21.53906	3	2.31931	2.109
8	2.54787	919.35817	-0.23383	35.73998	-0.2634	27.34723	0.12214	24.85190	3	2.31958	2.10907
9	2.54759	1177.99343	0.21091	40.45187	0.07969	30.99079	-0.27648	28.16483	3	2.31975	2.10912
10	2.54738	1468.63100	-0.19241	45.16385	0.2375	34.63462	-0.12435	31.47782	3	2.31988	2.10915
11			0.17713	49.87591	-0.00312	38.27864	0.2209	34.79086	3	2.31997	2.10916
12			-0.1643	54.58803	-0.20341	41.92280	0.12571	38.10394	3	2.32004	2.10918
13			0.15335	59.3002	-0.05278	45.56707	-0.17975	41.41704	3	2.32008	2.1092
14			-0.14388	64.01239	0.1635	49.21143	-0.12622	44.73016	3	2.32012	2.10921
15			0.13561	68.72461	0.09173	52.85585	0.14738	48.04330	3	2.32017	2.10922

APPENDIX B

SOLUTIONS OF THE STEADY-STATE REACTION-DIFFUSION EQUATIONS

B.1. Aris' Problem

Aris' treatment [195] will be reprised here with additions of critical Thiele moduli. One should solve the equation:

$$\frac{d^2u}{d\xi^2} = \Lambda^2 u^n \tag{B1}$$

with boundary conditions:

$$\begin{aligned} \text{at } \xi = 1, \quad & u = 1 \\ \text{at } \xi = 0, \quad & du/d\xi = 1 \end{aligned} \tag{B2}$$

When $n \neq 1$ or $n \neq 0$ the above equation is nonlinear. Therefore instead of a solution for the concentration profile in closed form, an expression for Λ is aimed. Multiplication of Equation-(B1) with $2(du/d\xi)$, then integrating from 0 to ξ gives:

$$\left(\frac{du}{d\xi}\right)^2 = \Lambda^2 \frac{2}{n+1}(1 - {u_0}^{n+1}) \tag{B3}$$

Taking the square root of the above equation, then separation and integration results in:

$$\Lambda\xi = \sqrt{\frac{2}{n+1}} \int_{u_0}^{u} (u^{n+1} - {u_0}^{n+1})^{-1/2}\, du \qquad \text{(B4)}$$

Since $u = 1$ at $\xi = 1$,

$$\Lambda = \sqrt{\frac{2}{n+1}} \int_{u_0}^{1} (u^{n+1} - {u_0}^{n+1})^{-1/2}\, du \qquad \text{(B5)}$$

The integral can be put in a valuable form by letting $z = 1 - (u_0/u)^{n+1}$ and substituting it to get an incomplete beta function. The incomplete beta function can also be expressed as a Gauss hypergeometric function, which allows easier analysis and computation.

$$B_x(p, q) = \int_0^x t^{p-1}(1-t)^{q-1} dt = \frac{x^p}{p} F(p, 1-q; p+1; x) \qquad \text{(B6)}$$

The Gauss hypergeometric function[39] is given as:

$$F(a, b; c; x) = \sum_{n=0}^{\infty} \frac{(a)_n (b)_n}{(c)_n} \frac{x^n}{n!} \qquad \text{(B7)}$$

with the Pochhammer symbol $(q)_n$:

$$(q)_n = \begin{cases} 1 & , \quad \text{for } n = 0 \\ q(q+1) \ldots (q+n-1) & , \quad \text{for } n > 0 \end{cases} \qquad \text{(B8)}$$

The hypergeometric function is always positive. The equation for Λ results in:

$$\Lambda = \sqrt{\frac{2}{n+1}}\, {u_0}^{-(n-1)/2}\, (1 - {u_0}^{n+1})^{0.5}\, F(0.5\,, 0.5 + q\,; 1.5\,; 1 - {u_0}^{n+1}) \qquad \text{(B9)}$$

with $q = 1/n + 1$. This expression is valid for $n \geq 1$, and it has to be modified for $-1 < n \leq 1$. One may apply the identity,

$$F(a, b; c; x) = (1-x)^{c-a-b}\, F(c-a, c-b; c; x) \qquad \text{(B10)}$$

which converges at $x = 1$ only when $\mathrm{Re}(c - a - b) > 0$. Thus, Equation- (B9) becomes,

$$\Lambda = \sqrt{\frac{2}{n+1}}\, (1 - {u_0}^{n+1})^{0.5}\, F(1\,, 1-q\,; 1.5\,; 1 - {u_0}^{n+1}) \qquad \text{(B11)}$$

[39] Also shown as ${}_2F_1(a, b; c; x)$.

Mehta and Aris also give solutions for $n = -1$ and $n < -1$, for these are not provided here, since they are assumed to be irrelevant for gas-liquid reactions.

B.2. The Unused Film

As discussed in section 4.1.2.3, the wall concentration for $-1 < n < 1$ does not tend to infinity as Λ increases, and it also does not go to zero like reactions with $n < -1$. This indicates that beyond certain Λ, there exists a dead region. In catalysts, the equivalent phenomenon is recently analyzed by York. et al. [197]. For the pseudo order reaction in a falling film, similar analysis can be provided for quantitative results. By considering no reaction at the wall, i.e. $u_0 \to 0$, Equation-(B11) can be simplified into:

$$\Lambda = \sqrt{\frac{2}{n+1}}\ \ F(1\ ,1-q\ ;1.5\ ;1) \qquad \text{(B12)}$$

By using the property:

$$F(a,b;c;1) = \frac{\Gamma(c)\Gamma(c-a-b)}{\Gamma(c-a)\Gamma(c-b)} \qquad \text{(B13)}$$

and some relations attributed to the gamma function Γ:

$$\Gamma(1/2) = \sqrt{\pi}, \qquad \Gamma(3/2) = \frac{\sqrt{\pi}}{2}, \qquad \Gamma(m+1) = m\Gamma(m) \qquad \text{(B14)}$$

Equation-(B12) leads to:

$$\Lambda_0 = \frac{1+n}{1-n}\sqrt{\frac{2}{n+1}} \qquad \text{(B15)}$$

Now Equation-(B15) can be used to obtain an exact penetration thickness, ξ_0, by integrating Equation-(B3) from ξ_0 to 1.

$$\Lambda(1-\xi_0) = \Lambda_0 \qquad \text{(B16)}$$

Via translating the coordinates to the ones used in section 4.1.2.3, one may find the condition for the existence of an unused liquid layer near the wall:

$$\xi_0 = \frac{\delta_p}{\delta} = \frac{\Lambda_0}{\Lambda} < 1 \tag{B17}$$

which means

$$\Lambda > \frac{1+n}{1-n}\sqrt{\frac{2}{n+1}} \tag{B18}$$

If the above criterion is satisfied for $-1 < n < 1$, then an exactly unused liquid film appears. In dimensional form, the result can be expressed as:

$$\frac{2(n+1)D}{(1-n)^2 k \delta^2 C_A^{0\,n-1}} < 1 \tag{B19}$$

B.3. Standard solutions for zero and first order reaction:

The zero order form or Equation-(B1) can be solved simply to give:

$$u = 1 + \frac{\Lambda^2}{2}(\xi^2 - 1) \tag{B20}$$

At $\xi = 0$:

$$u_0 = 1 - \frac{\Lambda^2}{2} \tag{B21}$$

which leads to:

$$\Lambda_c = \sqrt{2(1-u_0)} \tag{B22}$$

For a prescribed error, u_0 can be found from Equation-(108), and then Λ_c can be found from the equation above. For 5% error, $\Lambda_c = 1.347$. It exactly matches with the curve given in Figure 30.

For a first order reaction, solution can also be easily obtained as:

$$u = \frac{\cosh(\Lambda\xi)}{\cosh(\Lambda)} \tag{B23}$$

Similarly,

$$u_0 = \frac{1}{\cosh(\Lambda)} \tag{B24}$$

$$\Lambda_c = \operatorname{acosh}(u_0{}^{-1}) \tag{B25}$$

For 5 % error, $\Lambda_c = 1.856$. This value also matches exactly with Figure 30.

APPENDIX C

THE DUHAMEL SOLUTION

The problem described by Equations (127), (128) and (132) can be restated as:

$$\frac{\partial p}{\partial t} = D\frac{\partial^2 p}{\partial x^2}\,, \qquad \begin{aligned} &\text{at } x = 0,\ \ p = C_{B_0}\exp\left(-zkC_A^{*^m}t\right) - zC_A^* \\ &\text{at } x = \delta,\ \ \frac{dp}{dx} = 0 \\ &\text{at } t = 0,\ \ p = C_{B_0} \end{aligned} \tag{C1}$$

By convention, shift the nonhomogeneity in the initial condition to the boundary by letting:

$$\hat{p} = \frac{C_B - zC_A}{C_{B_0}} - 1 \tag{C2}$$

Now the new problem becomes:

$$\frac{\partial \hat{p}}{\partial t} = D\frac{\partial^2 \hat{p}}{\partial x^2}\,, \qquad \begin{aligned} &\text{at } x = 0,\ \ \hat{p} = \exp\left(-zkC_A^{*^m}t\right) - \frac{E_i}{E_i - 1} = f(t) \\ &\text{at } x = \delta,\ \ \frac{dp}{dx} = 0 \\ &\text{at } t = 0,\ \ p = 0 \end{aligned} \tag{C3}$$

This solution to Equation set (C3) is given by Duhamel's integral as [175]:

$$\hat{p} = f(0)\theta(x,t) + \int_0^{\tau} \theta(x,t)\frac{df(\tau)}{d\tau}d\tau \tag{C4}$$

$\theta(x,t)$ is called as the auxiliary problem. This is the solution for the case of diffusion into a finite layer subjected to a unit step concentration at one of the boundaries. The

solution is already given in Appendix-A by Equation- (A1). Evaluating Equation-(C4) gives the solution as:

$$\hat{p} = \frac{-1}{E_i - 1}\theta(x,t) - 1 + \exp\left(-{\Lambda_s}^2 Fo\right) + \frac{4}{\pi}\sum_{n=0}^{\infty}\frac{1}{(2n+1)}\frac{\sin\left(\lambda_n \frac{x}{\delta}\right)}{1 - {\lambda_n}^2/{\Lambda_s}^2}\left[\exp\left(-{\lambda_n}^2 Fo\right) - \exp\left(-{\Lambda_s}^2 Fo\right)\right] \quad (C5)$$

The eigenvalues are given as $\lambda_n = [\pi(2n+1)/2]$. The value of $\hat{p}$ at the wall can be found by setting $x = \delta$. Then according to the regimes dictated by Λ_s, as given in Table 8, one may set p as p_{wall}. Thus, Equation-(C5) reduces to:

$$\frac{\pi}{4}\varphi = \frac{1}{E_i - 1}\sum_{n=0}^{\infty}\frac{(-1)^n}{(2n+1)}\exp\left(-{\lambda_n}^2 Fo_D\right) + \sum_{n=0}^{\infty}\frac{(-1)^n}{(2n+1)}\frac{\exp\left(-{\lambda_n}^2 Fo_D\right)}{1 - {\lambda_n}^2/{\Lambda_s}^2} + \exp\left(-{\Lambda_s}^2 Fo_D\right)\left[\frac{\pi}{4} - \sum_{n=0}^{\infty}\frac{(-1)^n}{(2n+1)}\frac{1}{1 - {\lambda_n}^2/{\Lambda_s}^2}\right] \quad (C6)$$

One may now simplify the series. We are expecting to solve for Fo_D, and it is certain that Fo_D will be large for the case of depletion of B. This is true for any regime, since for all regimes, C_A is expected to accumulate near the wall up to a significant degree. This argument gets invalidated when B diffuses much faster than A, but here, only equal diffusivities are considered. Therefore, the first term of the first series can be taken and the rest can be disregarded with quite good accuracy (see footnote 37 in Appendix A).

$$\sum_{n=0}^{\infty}\frac{(-1)^n}{(2n+1)}\exp\left(-{\lambda_n}^2 Fo_D\right) \cong \exp\left(-\frac{\pi^2}{4}Fo_D\right) \quad (C7)$$

For $\Lambda_s \ll \pi^2/4$, the second series can be approximated as:

$$\sum_{n=0}^{\infty}\frac{(-1)^n}{(2n+1)}\frac{\exp\left(-{\lambda_n}^2 Fo_D\right)}{1 - {\lambda_n}^2/{\Lambda_s}^2} \approx -{\Lambda_s}^2\sum_{n=0}^{\infty}\frac{(-1)^n}{(2n+1)}\frac{\exp\left(-{\lambda_n}^2 Fo_D\right)}{{\lambda_n}^2} \quad (C8)$$

For $\Lambda_s \gg \pi^2/4$,

$$\sum_{n=0}^{\infty}\frac{(-1)^n}{(2n+1)}\frac{\exp\left(-{\lambda_n}^2 Fo_D\right)}{1 - {\lambda_n}^2/{\Lambda_s}^2} \approx \exp\left(-\frac{\pi^2}{4}Fo_D\right) \quad (C9)$$

One may use both, according to the magnitude of Λ_s. However, it is observed by numerical experimentation that the use of Equation-(C9) for all Λ_s is suitable, and does not induce significant error in calculations. In addition, low Λ_s values make the series sum usually very small, such that it can be discarded in many cases. Therefore Equation-(C9) is a good approximation.

The third term goes to zero if Λ_s is very large, due to the exponential term in front of the square brackets. Thus, considering small Λ_s, the third series can be simplified as:

$$\sum_{n=0}^{\infty} \frac{(-1)^n}{(2n+1)} \frac{1}{1-{\lambda_n}^2/{\Lambda_s}^2} \cong \frac{4{\Lambda_s}^2}{\pi^2} \underbrace{\sum_{n=0}^{\infty} \frac{(-1)^n}{(2n+1)}}_{\cong 0.969} \cong \frac{3.876{\Lambda_s}^2}{\pi^2} \quad \text{(C10)}$$

Hereby, by using Equations (C7), (C9) and (C10), Equation-(135) is obtained:

$$\frac{\pi}{4}\varphi = \frac{E_i}{E_i - 1} \exp\left(-\frac{\pi^2}{4} Fo_D\right) + \exp\left(-{\Lambda_s}^2 Fo_D\right)\left(\frac{\pi}{4} - \frac{3.876{\Lambda_s}^2}{\pi^2}\right) \quad \text{(C11)}$$

APPENDIX D

STEADY VELOCITY FIELDS FOR FILMS WITH A FREE SURFACE

D.1. Generalized Couette Flow:

$$v(x) = v_0\left(1 - a\frac{x}{\delta}\right) \qquad \text{(D1)}$$

This may be a simplification for many flows, when mean velocity is $v_0(1 - a/2)$. v_0 is the interfacial velocity. The parameter "a" can be a fitting parameter or may signify wall slip. It lies between 0 and 1. As $a \to 0$, plug flow is approached, as $a \to 1$ simple Couette flow is obtained. When penetration thickness is small, using such a flow field is called as the Leveque approximation [235]. It also represents a mobile interface, which can occur if one of the flowing phases is almost stagnant, and the other flowing fluid phase drags the interface [236, 237].

D.2. Falling Film (Nusselt):

$$v(x) = \frac{\rho g \delta^2}{2\mu}\left[1 - \left(\frac{x}{\delta}\right)^2\right] \qquad \text{(D2)}$$

This profile is the source of the expression given by Equation-(60).

D.3. Falling Film with Interfacial Shear:

$$v(x) = \frac{\rho g \delta^2}{2\mu}\left[1 - \left(\frac{x}{\delta}\right)^2\right] + \frac{\tau_i \delta}{\mu}\left(1 - \frac{x}{\delta}\right) \qquad \text{(D3)}$$

τ_i is the interfacial shear, for $\tau_i > 0$ the flow is relatively cocurrent, for $\tau_i < 0$ the flow is relatively countercurrent.

D.4. Falling Film with Wall Slip:

$$v(x) = \frac{\rho g \delta^2}{2\mu}\left[1 - \frac{2b_s}{\delta} - \left(\frac{x}{\delta}\right)^2\right] \qquad \text{(D4)}$$

b_s is the slip length.

D.5. Falling Film with Wall Slip and Interfacial Shear:

$$v(x) = \frac{\rho g \delta^2}{2\mu}\left[1 - \frac{2b_s}{\delta} - \left(\frac{x}{\delta}\right)^2\right] + \frac{\tau_i \delta}{\mu}\left(1 - \frac{b_s}{\delta} - \frac{x}{\delta}\right) \qquad \text{(D5)}$$

The following two profiles are given to show the capability of a power series expression:

D.6. Non-isothermal Falling Film (or an evaporating component under a linear temperature gradient) [96]

$$v(x) = \frac{\rho g \delta^2}{\mu_0}\left[e^{\alpha}\left(\frac{1}{\alpha} - \frac{1}{\alpha^2}\right) - e^{\alpha x/\delta}\left(\frac{x}{\alpha\delta} - \frac{1}{\alpha^2}\right)\right] \qquad \text{(D6)}$$

The viscosity is temperature dependent: $\mu = \mu_0 e^{-\alpha x/\delta}$. The exponential term can be expanded, yielding:

$$v(x) = \frac{\rho g \delta^2}{\mu_0}\left[e^{\alpha}\left(\frac{1}{\alpha} - \frac{1}{\alpha^2}\right) + \frac{1}{\alpha^2} - \frac{1}{2}\left(\frac{x}{\delta}\right)^2 - \frac{1}{6}\left(\frac{x}{\delta}\right)^3 - \cdots\right] \quad \text{(D7)}$$

D.7. Power-Law Falling Film [96]

$$v(x) = \left(\frac{\rho g \delta^2}{\mu}\right)^{1/n} \frac{\delta}{1/n+1}\left[1 - \left(\frac{x}{\delta}\right)^{1/n+1}\right] \quad \text{(D8)}$$

where the fluid is pseudoplastic for $0 < n < 1$ and dilatant for $n > 1$. By using a CAS, the fractional order can be expanded around δ, the result can be simplified and terms can be collected. For n>0.45, a five term expansion is enough.

$$v(x) = \left(\frac{\rho g \delta^2}{\mu}\right)^{1/n} \frac{\delta}{1/n+1}\left[a_0 + a_1\left(\frac{x}{\delta}\right) + a_2\left(\frac{x}{\delta}\right)^2 + a_3\left(\frac{x}{\delta}\right)^3 + a_4\left(\frac{x}{\delta}\right)^4\right] \quad \text{(D9)}$$

with

$$a_0 = 1 + \frac{6n^3 - 11n^2 - 24n + 6}{24n^4}, \qquad a_1 = \frac{20n^3 - 24n^4 + 20n^2 - 20n + 4}{24n^4}$$

$$a_2 = -\frac{36n^3 + 6n^2 - 24n + 6}{24n^4}, \qquad a_3 = -\frac{4n^2 - 12n^3 + 12n - 4}{24n^4},$$

$$a_4 = \frac{n^2 - 2n^3 + 2n - 1}{24n^4} \quad \text{(D10)}$$

The following microfluidic flows are not seem to be used in mass transfer cases yet, but since they are interesting and they can also be incorporated into the AIBM solutions for heterogeneous reactions, they are included here.

D.8. Electroosmotic Flow with a Free Surface [238]**:**

$$v(x) = E_0\left[1 - \exp\left(-\frac{\delta - x}{De}\right) - \frac{\delta - x}{De}e^{-1/De}\right] \quad \text{(D11)}$$

$$E_0 = \frac{\varepsilon E_{el} \zeta \delta}{\rho \nu^2} \quad \text{(D12)}$$

E_0 is the electroosmotic number. ε is the dielectric constant, E_{el} is the external velocity field, ζ is the zeta potential and De is the Debye number, which shows the ratio of the Debye screening length[40] and film thickness. The exponential term can be expanded easily.

D.9. Electrokinetic Flow with a Free Surface [239]**:**

$$v(x) = E_0 \left[\cosh\left(\frac{\delta - x}{De}\right) + \frac{\zeta - \text{coshh}(1/De)}{\sinh(1/De)} \sinh\left(\frac{\delta - x}{De}\right) \right] \quad \text{(D13)}$$

The hyperbolic functions can simply be expanded similarly.

[40] Shows the effective layer thickness, in which electrostatic effects persist.

APPENDIX E

NOTES ON INTERFACIAL RESISTANCE

Since the Statistical Rate Theory of Ward [85] is mathematically complicated (singular and nonlinear BC), one may try to extract some information by comparing it with the linear resistance case. The approximate solution provided by Gupta and Sridhar [91] (Equation-(37)) would be useful. When the resistance is described by the linear boundary condition given by Equation-(33), one obtains the following result for surface concentration [240] :

$$\frac{C_i}{C^*} = 1 - \exp(\beta'^2)\mathrm{erfc}(\beta') \qquad \text{(E1)}$$

with $\beta' = k_S\sqrt{t/D}$. The similarities between Equations-(37) and (E1); and the β- β' groups are intriguing. To predict the same saturation times with the nonlinear model, the interfacial resistance coefficient k_S must approximately be equal to $2K_s/C^*$. With this modification, $\beta' = 2\beta$. The modified and unmodified predictions of the linear model given by Equation-(E1) are plotted below, with the results given by Equation-(37). Although the modified linear and nonlinear models meet sufficiently early, the unmodified linear model is very different for both short and long times, it tends to C^* very slowly.

The proportion between ω′ and ω can be verified by evaluating the integral squared error[41]:

$$E = \int_1^U \left\{\sqrt{1 - \exp(\beta^2)\mathrm{erfc}(\beta)} - 1 + \exp[(n\beta)^2]\mathrm{erfc}(n\beta)\right\}^2 d\beta \qquad \text{(E2)}$$

1 is the lower limit at which saturation is about 75%, as can be seen in Figure 61.U is the higher limit for β. Taking it as 6 as in the previous figure yields Figure 62, showing that the error is zero around 2. The exact value is 2.016.

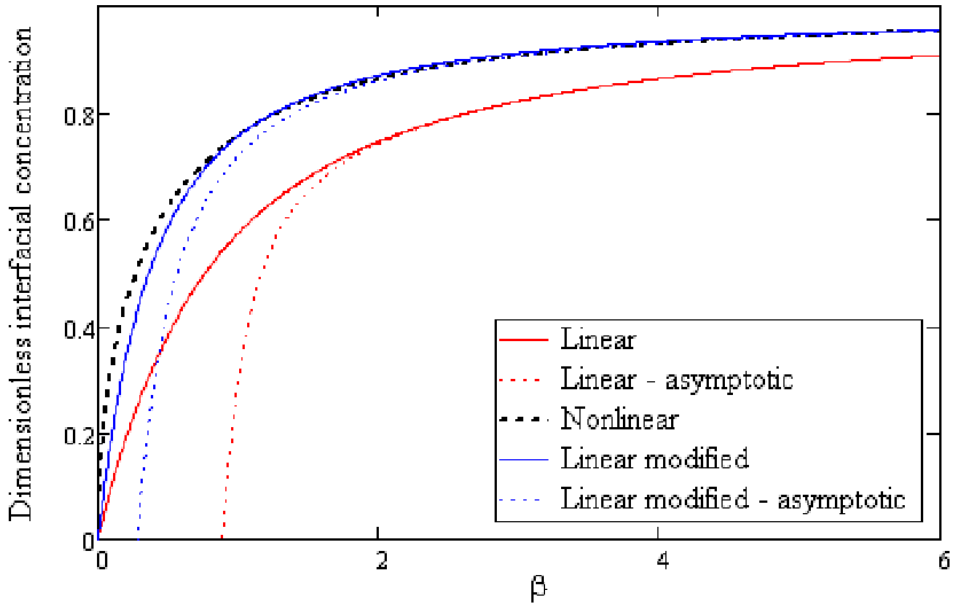

Figure 61. Saturation of the interface with respect to ω predicted by different equations.

Such a relation gives a good estimate for the linear Fickian resistance k_s in terms of known quantities K_s and C^* only. The estimate may gain more importance as it gives an approximate value for the Sherwood number for interfacial resistance, $Sh_i = k_s\delta/D \cong 2\,K_s\delta/C^*D$, which is used regularly for analyzing many problems of mass transfer.

[41] In principle, the relation is equivalent to one given by Equation-(G6), but this time surface concentration and a time integral is used.

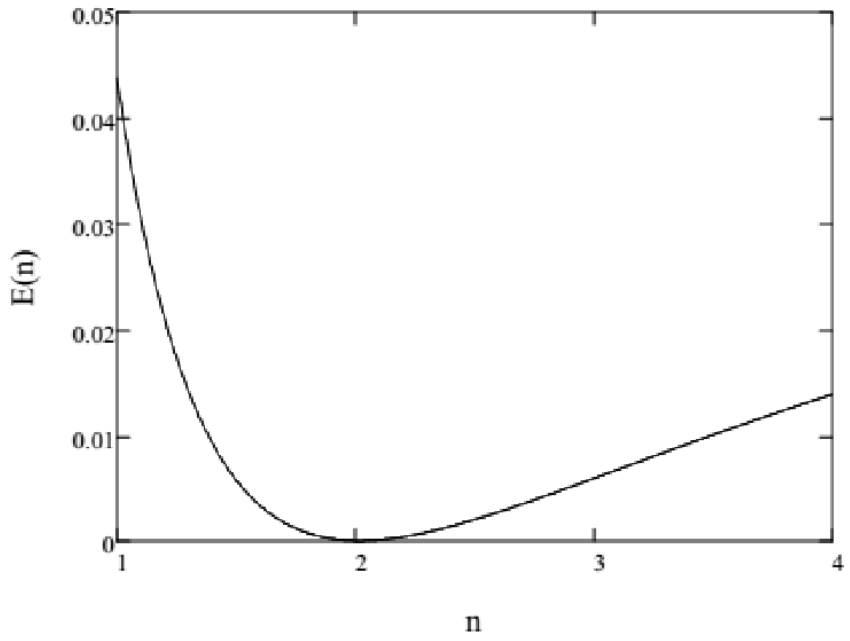

Figure 62. Variation of error with the linear proportionality constant.

The asymptotic formulas given in Figure 61 are series expansions for the exponential and error functions [240].

$$\frac{C_i}{C^*} = 1 - \frac{1}{\sqrt{\pi}}\left(\frac{1}{\beta} - \frac{1}{2\beta^3} + \frac{1 \cdot 3}{2^2\beta^5} - \cdots\right) \qquad \text{(E3)}$$

The asymptotical formula for the modified linear case may be truncated to its first term (given by the blue dotted line), to deduce an explicit saturation time[42].

$$\frac{C_i}{C^*} = 1 - \frac{1}{2\beta\sqrt{\pi}} \qquad \text{(E4)}$$

With the percent interfacial saturation $s° = C_i/C^*$, the time for saturation can be given as:

$$t_S^* = \frac{{C^*}^2 D}{4\pi(1 - s°){K_S}^2} \qquad \text{(E5)}$$

Equation-(E5) provides a simple way of calculating saturation times, explicitly and accurately. It is valid for saturation percentages higher than 75%. For $\beta = 1$, its error

[42] Expanding Equation-(37) in square brackets and then taking the first term yields to much higher errors (15%) in predicting the saturation time.

is less than 5% than decays rapidly zero around $\beta = 2$. By using an order of magnitude approach, $C^* \sim 10$, $K \sim 10^{-3}$ [91] and $D \sim 10^{-9}$, time for 90% saturation is ~ 0.1 s.

Equation-(E5) can also be considered as the time constant for interfacial saturation. In absorption into very thin films (or in very short contact times), one should compare it with the time constant of diffusion [52]:

$$t_D = \frac{\delta^2}{D} = \frac{D}{\bar{k}_L'^2} \tag{E6}$$

as a check whether Equation-(E5) is applicable or not. Since all the expressions are derived on a semi-infinite medium, the diffusion fronts should not reach the wall significantly before saturation. This indicates the condition: $t_D > t_S^*$.

When there is reaction in the fluid, one should solve the transient nonlinear problem with a source term, in order to get the interfacial concentration vs. time trend. Even numerically, this is difficult, due to the singularity of the nonlinear BC at zero concentration. Special integral transform techniques may be necessary [241] and it is avoided. But solving the steady state problem can give final value of the interfacial concentration. This is valid for any flowing finite film as long the reaction proceeds.

One may solve:

$$D\frac{d^2C}{dx^2} - kC = 0, \qquad \begin{matrix} \text{at } x = 0, & -D\dfrac{dC}{dx} = K_S\left(\dfrac{C^*}{C} - \dfrac{C}{C^*}\right) \\ \text{at } x = \delta, & \dfrac{dC}{dx} = 0 \end{matrix} \tag{E7}$$

to get:

$$C_i = \frac{C^*}{\sqrt{\dfrac{C^*\sqrt{kD}}{K_S}\tanh(\Lambda) + 1}} \tag{E8}$$

Note that the factor in the denominator is a new dimensionless group. It gives the ratio of reaction rate to interfacial saturation rate:

$$\frac{C^{*}\sqrt{kD}}{K_S} = \frac{\sqrt{Da}}{\beta} = \gamma_S \qquad \text{(E9)}$$

For low Thiele modulus, $\tanh(\Lambda) \to 0$, giving the expected result :$C_i \cong C^{*}$. For large Λ, , $\tanh(\Lambda) \to 1$, yielding:

$$C_i = \frac{C^{*}}{\sqrt{\gamma_S + 1}} \qquad \text{(E10)}$$

The presence of a very fast chemical reaction prevents the use of $\beta' = 2\beta$ equivalency of the linear and nonlinear BCs. This can be further proved by solving Equation-(E8) with the linear resistance BC for the surface concentration. For low γ_S or low Λ, the $\beta' = 2\beta$ relation is valid.

Similar to γ_S in Equation-(E9), one may write down the time constant for diffusion with reaction, in order to compare the relative effects of interfacial saturation and reaction:

$$t_{D/R} = \frac{D}{E^2 \bar{k}_L'^{\,2}} \qquad \text{(E11)}$$

For $t_{D/R} \gg t_S^{*}$, the effects of interfacial saturation can be neglected.

APPENDIX F

COMPUTER CODE FOR SOLVING NONLINEAR ALGEBRAIC EQUATIONS WITH MULTIPLE ROOTS

A code is written on Mathcad to solve for the roots of Equation- (187). This is not a straightforward task since negative reaction orders may lead to very separate multiple steady states, or in other words, distant roots. A general solution methodology to highly nonlinear algebraic equations with multiple roots still does not seem to be well developed. Solving systems is much harder and more case specific. Therefore, this code is specific to this equation only, and also it depends on the values of parameters in Equation-(187). For example, solubilities and diffusivities are calculated from Equations (175) and (176) at 500 K and 1.5 MPa. The ratio of hydrogen to carbon monoxide diffusivities, γ, is taken as 2.638 and ν is used as 0.48. The lowest Da^{II} for which a root exists, is found manually for given reaction orders and parameters. Similarly the highest Da^{II} is decided, where η is almost zero. Then a set is created between these values. The solver has predefined modifiers to enhance convergence for solving 2^{nd} and 3^{rd} roots. The limits of the region of multiplicity are also manually and roughly distinguished. In this region, a denser set of Da^{II} values is selected to provide a fine resolution when plotting the data. When roots are extracted, a sorting algorithm (or a kind of a path finding algorithm) is employed to plot the data.

The main program is given by Figure 63. The program solves the three sets of reaction orders, which are given on Figure 43. The output of the program is a three

dimensional matrix, where rows correspond to the number of data points. Columns are comprised of three vectors of effectiveness factors which are calculated via the extracted roots, and another vector for the values of the Da^{II} set. Each three dimensional layer is for a given set of reaction orders.

When the matrix is obtained, the sorting algorithm (given by Figure 64) then can process each layer of the matrix, where it arranges the effectiveness factors in such a path, like from point 1 to point 2 and then to point 3 of Figure 45.

$$
\begin{aligned}
&\text{Nonlinneg}\left(f, Da_{matrix}, degree\right) := \\
&\quad v \leftarrow \text{length}\left(degree^{\langle 1\rangle}\right) \\
&\quad \text{for } m \in 1..v \\
&\qquad \begin{pmatrix} a \\ b \end{pmatrix} \leftarrow \left(degree^{T}\right)^{\langle m\rangle} \\
&\qquad Da_{series} \leftarrow Da_{matrix_m}{}^{T} \\
&\qquad end \leftarrow \text{length}\left(Da_{series}\right) \\
&\qquad C_{H2lim} \leftarrow C_{H2int} - 0.001 \\
&\qquad \text{for } n \in 1..end \\
&\qquad\quad Da \leftarrow \left(Da_{series}\right)_n \\
&\qquad\quad r1 \leftarrow \text{root}\left(f\left(C_{H2s}, Da, a, b\right), C_{H2s}, 10^{-3}, C_{H2lim}\right) \\
&\qquad\quad eta_1 \leftarrow \left(\frac{r1}{C_{H2int}}\right)^{a} \cdot \left[\frac{\left(\frac{C_{H2int} - r1}{Da \cdot r1^{a}}\right)^{\frac{1}{b}}}{C_{COint}}\right]^{b} \\
&\qquad\quad g\left(C_{H2s}, Da, a, b\right) \leftarrow \frac{f\left(C_{H2s}, Da, a, b\right)}{\left(r1 - C_{H2s}\right)} \\
&\qquad\quad guess \leftarrow \frac{r1}{1.5} \\
&\qquad\quad r2 \leftarrow \left| \begin{array}{l} value \leftarrow i \quad \text{on error } \text{root}(g(guess, Da, a, b), guess) \\ \text{if}(\text{Im}(value) \neq 0, i, value) \end{array} \right. \\
&\qquad\quad \text{if } \text{Im}(r2) = 0 \\
&\qquad\qquad eta_2 \leftarrow \left(\frac{r2}{C_{H2int}}\right)^{a} \cdot \left[\frac{\left(\frac{C_{H2int} - r2}{Da \cdot r2^{a}}\right)^{\frac{1}{b}}}{C_{COint}}\right]^{b} \\
&\qquad\qquad h\left(C_{H2s}, Da, a, b\right) \leftarrow \frac{g\left(C_{H2s}, Da, a, b\right)}{\left(r2 - C_{H2s}\right)}
\end{aligned}
$$

Figure 63. Mathcad code to solve Equation- (187) for multiple roots.

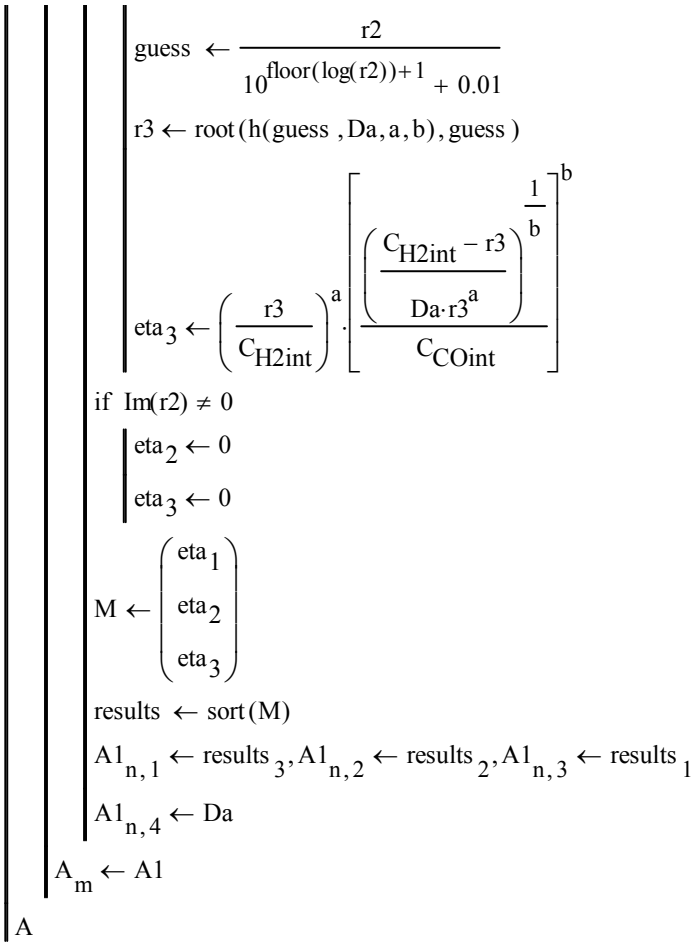

Figure 63 cont'd. Mathcad code to solve Equation- (187) for multiple roots.

```
Sort(eta) := | m ← length(eta^⟨1⟩)
             | n ← 1
             | while eta_{n,3} = 0
             |     E_{n,1} ← eta_{n,1}
             |     E_{n,2} ← eta_{n,4}
             |     n ← n + 1
             | save ← n
             | while eta_{n,3} ≠ 0
             |     E_{n,1} ← eta_{n,3}
             |     E_{n,2} ← eta_{n,4}
             |     n ← n + 1
             | cont ← n
             | it ← cont
             | n ← n − 1
             | while n ≠ save − 1
             |     E_{it,1} ← eta_{n,2}
             |     E_{it,2} ← eta_{n,4}
             |     n ← n − 1
             |     it ← it + 1
             | for n ∈ save .. m
             |     E_{it,1} ← eta_{n,1}
             |     E_{it,2} ← eta_{n,4}
             |     it ← it + 1
             | E
```

Figure 64. Sorting algorithm

APPENDIX G

AIBM SOLUTION FOR PENETRATION THEORY AND NOTES ON ACCURACY

Continuing from Equation-(79), one may assume a second order polynomial for the concentration profile:

$$C = a + bx + cx^2 \tag{G1}$$

The constants can be found by applying the following boundary conditions:

$$\begin{aligned} &\text{at } x = 0, && C = C^* \\ &\text{at } x = \delta_p(t), && C \cong 0 \\ &\text{at } x = \delta_p(t), && \partial C/\partial x \cong 0 \end{aligned} \tag{G2}$$

resulting in:

$$\begin{gathered} a = C^*, \qquad b = -\frac{2C^*}{\delta_p}, \qquad c = \frac{C^*}{{\delta_p}^2} \\ \frac{C}{C^*} = \left(1 - \frac{x}{\delta_p}\right)^2 \end{gathered} \tag{G3}$$

The concentration profile can be substituted into the IMBE, Equation-(79), to obtain:

$$\delta_p \frac{d\delta}{dt} = 6D \tag{G4}$$

This ODE has the initial condition $\delta(0) = 0$. Solving δ yields:

$$\delta_p = \sqrt{12Dt} \qquad \text{(G5)}$$

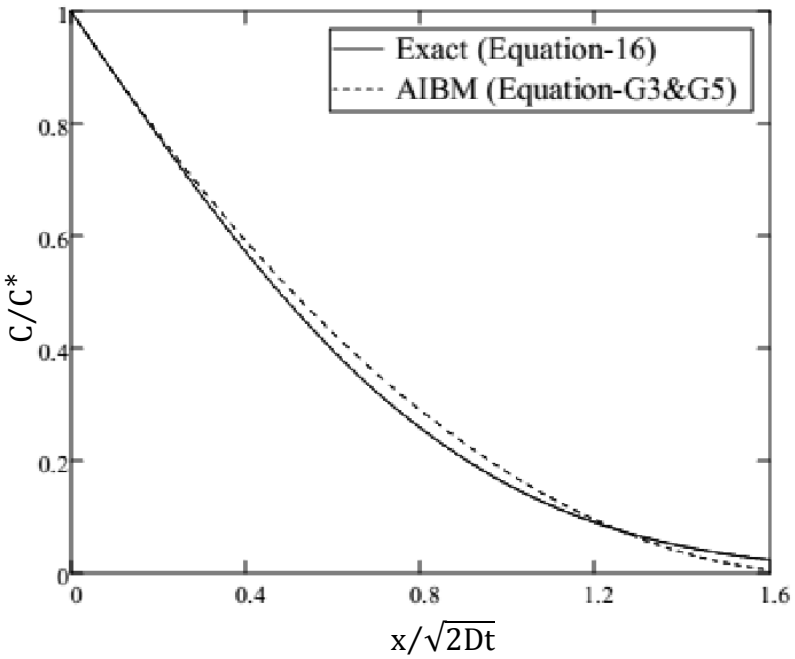

Figure 65. Comparison of the exact and the approximate solution

Note that this expression is very similar to the penetration thickness expression given by Equation-(21). One may increase the accuracy by assuming a different trial function, for example a higher order polynomial or an exponential function [242]. This would indeed require additional boundary conditions. An option is to use a smoothing boundary condition, $\partial^2 C/\partial x^2 = 0$ on the penetration front. Higher order smoothing conditions, i.e. higher derivatives, can also be used for higher order polynomials. But as Goodman states [243], increasing the order (or the exponent in collapsible forms) of polynomial solutions does not guarantee an increase in accuracy. He punctuates that accuracy would be improved only if the additional condition is created on the boundary with the lower derivative. This would imply new derived boundary conditions on the fixed surface. For example, if the PDE treated above is evaluated at $x = 0$, the time derivative would be zero due to the Dirichlet boundary condition. This would leave $\partial^2 C/\partial x^2 = 0$ at $x = 0$. Like the smoothing condition, this derived condition can also be extended to higher orders. But its use may bring difficulties in evaluating the IMBE or solving the resulting ODE. The results obtained with different profiles for the problem above treated are

given in Table 10. Surface fluxes are compared with the exact solution given by Equation-(18). Note that the profile has an important impact on accuracy. This is a characteristic of such approximate solutions, where profiles are selected a priori [244].

Table 10. Errors in surface fluxes via different profiles

The Profile	Surface Flux: Percent Error
Linear [245]	-11.3 %
Exponential [245]	+25.4 %
Quadratic (Equations (G3) and (G5))	+2.3 %
Cubic – I [175]	-6.2 %
Cubic – II [175]	+8.3 %
Fourth Degree [175]	-3.0 %
Quadratic – DIM [176]	-2.3 %
Myers's Best Fit [246]	-4.1 %

Accuracy can be improved by other means. For example, one may match the approximate solution with arbitrary the exponent with a special exact case. Then one can determine the exponent according to this equality. Mantelli and Braga [247] applied this procedure for time dependent surface temperature and flux problems and obtained very good results. Langford [248] established a criterion to minimize the overall error. The criterion does not need an exact solution and described by the path difference integral:

$$\mathrm{Err}(t) = \int_0^{\delta_p(t)} (DC_{xx} - C_t)^2 dx \geq 0 \qquad \text{(G6)}$$

In is important to note that one generally tries to obtain a correct surface flux expression. However, Langford's criterion is based on matching the approximate solution to the exact one on the whole solution domain. The overall squared error as given by Equation-(G6) can be minimized analytically for simple PDEs [246], but

for problems involving physical parameters which cannot be exterminated via normalization, like reaction-diffusion, optimization cannot be done by analytical methods. The exponent may depend on those additional parameters or maybe also on time. A resolution might be obtained via nonlinear and/or multivariate regression, but this would be very costly. Optimization of AIBM solutions is currently under investigation [249, 250, 251].

Note that the method is applied to uniform initial conditions only. Nonuniform initial conditions can also be handled; such cases are solved by Thorsen and Landis [252] and Bengston and Kreith [226]. They use moment equations, which are given in section 4.2.2.1, and computations are heavy. At very short times, or for very rugged initial distributions, AIBM is quite erroneous.

It may also be useful to give some examples on the history and current uses of AIBM. The method was applied to biological diffusion problems first by Landahl [245].Then Goodman applied it to heat conduction problems with temperature dependent properties [243] and established its systematic use [253]. Nowadays the AIBM is actively used in solving fractional-subdiffusion equations [254], hyperbolic heat conduction [255] and moving boundary problems [256]. In the latter, numerical methods are harder to implement and exact solutions are very few. This renders the method as especially valuable and it is found to be quite accurate for such problems. For moving boundary problems one may give freezing, melting, ablation, shrinking core model of gas-solid reactions and dissolution of gas bubbles as examples.